Dissecting *Mla3–AVR-Rmo1* recognition and specificity

Diana Gómez De La Cruz

Thesis submitted to the University of East Anglia for the Degree of Doctor of Philosophy

March 2023

Abstract

The plant immune system heavily relies on immune receptors known as nucleotide binding leucine-rich repeat (NLR) proteins, which recognise pathogen-secreted effectors to trigger a robust immune response. In barley, resistance to powdery mildew caused by *Blumeria graminis* f. sp. *hordei* (*Bgh*) is conferred by the *Mildew locus a* (*Mla*), an NLR that exists as a highly expanded allelic series. Each *Mla* allele governs *Bgh* isolate-specific resistance by recognising a corresponding *AVR*$_a$ effector. In addition, different alleles can confer resistance against divergent fungal pathogens. This is the case of the *Mla3* allele, which not only recognises *AVR*$_{a3}$ from *Bgh,* but also confers resistance to the blast fungus *Magnaporthe oryzae*. In this thesis, I aimed to molecularly characterise *M. oryzae* recognition by *Mla3* and elucidate the principles governing multiple pathogen recognition by this NLR. I found that *PWL2,* an effector known to condition pathogenicity of *M. oryzae* towards weeping lovegrass, is the gene underlying *AVR-Rmo1,* the blast effector recognised by *Mla3*. Evidence indicates that barley and weeping lovegrass convergently evolved to recognise *PWL2* with conserved specificity. I established that the C-terminus of Mla3 defines specificity of Pwl2 recognition and protein structure predictions suggest that this region binds to Pwl2 by mimicking the binding interface of a Pwl2 host target. By assessing copy number variation and allelic diversity, I defined that *Mla3* functions in a dosage-dependent manner and postulate that polymorphisms reduce the sensitivity threshold to trigger an immune response upon effector recognition, abolishing the high dosage requirement for functional resistance. The identity of *AVR*$_{a3}$, the *Bgh* effector recognised by *Mla3,* remains unknown. However, Pwl2 belongs to the family of MAX effectors, which is absent in *Bgh,* hence suggesting that Mla3 recognises structurally unrelated effectors. Altogether, these findings lay the foundation for understanding the mechanisms that shaped multiple pathogen recognition by *Mla3*.

Table of Contents

List of Figures

List of Tables

Abbreviations

ABC	ATP-binding cassette
ADPr-ATP	ADP-ribosylated ATP.
ADR1	Activated disease resistance 1.
APAF-1	Apoptotic protease-activating factor 1
APR	Adult plant resistance.
ATR	*Arabidopsis thaliana*–recognised.
AVR	Avirulence.
BIC	Biotrophic interfacial complex.
Bgh	*Blumeria graminis* f. sp. *hordei*.
Bgt	*Blumeria graminis* f. sp. *tritici*
BLAST	Basic Local Alignment Search Tool
BOP	Bambusoideae, Oryzoideae, Pooideae
CC	Coiled-coil.
CC_R	RPW8-type coiled-coil.
CC_{G10}	G10-subclade coiled-coil.
CED-4	Cell death protein 4.
C-JID	C-terminal jelly-roll/Ig-like domain.
CNL	CC-NLR.
Co-IP	Co-immunoprecipitation.
Cryo-EM	Cryogenic electron microscopy
CSEP	Candidate secreted effector protein
DAMP	Damage associated molecular pattern.
dpi	Days post infiltration.
EDS1	Enhanced disease susceptibility 1.
EIHM	Extra-invasive hyphal membrane.
ETI	Effector triggered immunity.
FOLD	Fol dual-domain.
HD1	Helical domain 1.
HIPP	HMA-isoprenylated plant proteins.
HMA	Heavy metal-associated.
Hpa	*Hyaloperonospora arabidopsidis*.
HR	Hypersensitive response.
ID	Integrated domain.
LOV1	Locus orchestrating victorin effects 1
LRR	Leucine rich repeat.
LysM	Lysin motif.
MAMP	Microbe-associated molecular pattern.
MAPK	Mitogen-activated protein kinase.
MAX	*Magnaporthe* Avrs and ToxB-like.
MHD	Methionine-histidine-aspartate.
Mla	Mildew locus a.
NB	Nucleotide-binding.
NB-ARC	Nucleotide-binding adaptor shared by APAF-1, plant R proteins and CED4.
NLR	Nucleotide binding leucine-rich repeat.
NOD	Nucleotide-binding oligomerisation domain.
NRC	NLR required for cell death.
NRG1	N required gene 1.

PACMAD	Panicoideae, Arundinoideae, Chloridoideae, Micrairoideae, Aristidoideae, Danthonioideae
PAD4	Phytoalexin deficient 4.
PAMP	Pathogen-associated molecular pattern.
Pbr1	AvrPphB response 1.
PBS1	AvrPphB susceptible 1.
PCR	Polymerase chain reaction.
Pgt	*Puccinia graminis* f. sp. *tritici.*
Pik	*Pyricularia oryzae* resistance-k.
Pm3	Powdery mildew resistance 3.
pRib-ADP	2'-(5"-phosphoribosyl)-5'-adenosine diphosphate.
pRib-AMP	2'-(5"-phosphoribosyl)-5'-adenosine monophosphate.
PRR	Pattern recognition receptor.
Pst	*Puccinia striiformis* f. sp. *tritici*
PTI	Pattern triggered immunity.
PVX	Potato virus x.
PWL	Pathogenicity towards weeping lovegrass.
R gene	Resistance gene.
RALPH	RNAse-like protein expressed in haustoria.
RanGAP2	Ran GTPase Activating Protein 2.
RAR1	Required for Mla12 resistance 1.
RGA4/5	*R*-gene analog 4/5.
RGH	Resistance gene homologue.
RIN4	RPM1-interacting protein 4.
RK	Receptor kinase.
RLCK	Receptor-like cytoplasmic kinase.
RLK	Receptor-like kinase.
RLP	Receptor-like protein.
RNL	CC_R-NLR.
Rmo1	Resistance to *Magnaporthe oryzae* 1
ROQ1	Recognition of XopQ 1.
ROS	Reactive oxygen species.
RPM1	Resistance to *Pseudomonas syringae* pv. *macuolicola* 1.
RPP1	Recognition of *Peronospora parasitica* 1.
RPP13	Recognition of *Peronospora parasitica* 13.
RPS2	Resistance to *Pseudomonas syringae* 2.
RPS4	Resistance to *Pseudomonas syringae* 4.
RPS5	Resistance to *Pseudomonas syringae* 5.
RRS1	Resistance to *Ralstonia solanacearum* 1.
SAG101	Senescence-associated gene 101.
SD	Solanaceae domain.
SGT1	Suppressor of G2 allele of SKP1.
Sr	Stem rust resistance.
SS15	SPRYSEC15.
STAND	Signal transduction ATPases with numerous domains.
TIR	Toll-interleukin-1 receptor.
TNL	TIR-NLR.
WHD	Winged-helix domain.
XopQ	Xanthomonas outer protein Q.
ZAR1	HopZ-Activated Resistance 1.

Acknowledgements

I would like to acknowledge and thank everyone involved in my journey throughout my PhD. I am very grateful to Matthew Moscou for the opportunity of joining his group to grow as a scientist, for his supervision, mentorship, and encouragement. I would like to thank Nick Talbot for his insightful contributions, for his support over the course of my PhD, and for forging opportunities for my professional development. I would also like to express my gratitude to Sophien Kamoun, for his mentorship and valuable feedback. Thank you all for reshaping my view of what makes a great scientist.

I feel extremely privileged of being part of the Moscou Lab, for their warmth and support. I would like to thank Inma for her immense expertise and patience, for making sure everything runs smoothly in the lab and for her never-ending advice; Phon, for her outstanding organisation and greenhouse-managing skills; and all the present and past lab members, for being such great colleagues and making this journey a very enjoyable one. I am grateful to the Talbot Lab, who always made me feel part of their family. Thank you especially to Vincent Were, for contributing to this project and helping me along the way. Thank you to the Kamoun Lab, for providing invaluable feedback and creating such a stimulating environment. I have always felt part of the Kamounity—thank you for adopting me as an honorary member. I am grateful to Thorsten Langner for first seeing potential in me, for giving me the opportunity to join The Sainsbury Laboratory as a predoc and for being my first scientific mentor at TSL.

Thank you to *all* the people at TSL who have made this possible. Thank you to the support teams that work tirelessly to make sure the scientific output of TSL has a signature of outstanding quality. I feel incredibly lucky to have been able to work in such an exciting and stimulating working environment.

I am grateful to all the role models who have inspired me and have shaped the vision of the scientist I aspire to be. I would like to thank Adriana Bernal and Silvia Restrepo, for sharing their passion for molecular biology and plant–microbe interactions with me, and for their dedication to doing science in Colombia. I also want to thank Ola Białas, Erin Zess and Lida Derevnina for being an inspiration—you are empowering scientists I look up to. Thank you all for being passionate female role models in science.

I want to thank Molly Bergum, Daniel Lüdke, Andres Posbeyikian, Adeline Harant, Ola, and Mauricio Contreras for taking the time to provide helpful and insightful feedback to my thesis. Your input and contributions immensely helped to shape the final product.

Special thank you to Molly Mae for being the best lab mate and friend I could have wished for. Thank you for all the laughs, jokes, hikes, swims, coffee breaks, motivation, and endless joyful memories. Difficult times felt a lot lighter with your support, company, and encouragement.

Thank you to the incredible TSLytherin student community for making TSL a jovial and fun environment to work in—it has been a delight to learn from you all. Special thank you to past and present members of the first-floor student office for being part of my daily adventures. In particular, thanks to Kelly Robinson—the science queen that has been by my side since day one; to Cami Molinari for her support, friendship, and all the fun times in beautiful Lanzarote and numerous house parties; and to Anam Siddiqui, Marquitos Dräger and Nef, for making sure a day did not go by without a good laugh. I would also like to thank Andy, AmirAli Toghani, Daniel Lüdke and Sara Dorhmi for your friendship and support. To my virtual thesis-writing companion, Sophie Johnson, thank you for the weekly motivation and moral support throughout these past months—we did it together.

I am grateful for spending the past years in the fine city of Norwich. I would like to give a special thanks to Fede Alfano, a great housemate who always made sure pizza and Argentinian asado were never missing in the house. Thank you to Kofra for warming my heart with Colombian coffee; and thank you to the Bodypump classes that nourished my mental health and wellbeing.

Special thank you to Mau, for your company, constant support, and motivation, for all the insightful scientific discussions, and all the help and patience in the lab. Thank you for your care and laughter throughout my PhD, especially during the past months of writing.

Lastly, a big thank you to my family—I would not be here without your support and encouragement. Thank you to my parents, for your constant love, enthusiasm, and great contributions to make this dream possible. To my brothers, thank you for your company and fun times. I could not be a luckier daughter or sister—this is all thanks to you.

Chapter 1: General Introduction

1.1 Brief overview of the plant immune system

Plants, like any living organism, face the constant risk of pathogen attack. Pathogens, including viruses, bacteria, fungi, oomycetes, nematodes, insects, and parasitic plants have evolved intricate lifestyles to colonise, feed and reproduce on their hosts. However, it is rather evident that not all plants are susceptible to most existing pathogens, in part because pathogens are not adapted to invade all plants. Physical plant barriers such as the cuticle, trichomes and cell wall, as well as chemical defences such as antimicrobial compounds, provide a basal line of defence that most pathogens cannot breach (Hanley et al., 2007; Serrano et al., 2014; Berhin et al., 2022). In addition, plants have evolved an innate immune system to defend themselves against biotic stress. This system is based on a two-tiered model that mainly relies on two classes of immune receptors that perceive non-self-molecules or self-molecules derived from damage caused by pathogens (Jones and Dangl, 2006; Dodds and Rathjen, 2010).

The first tier corresponds to the surveillance of the extracellular space through perception of pathogen-derived molecules to avoid invasion. These molecules are known as microbe-associated molecular patterns (MAMPs), and can be conserved across species, such as fungal chitin and bacterial flagellin (Zipfel et al., 2004). In addition, extracellular surveillance also monitors the presence of endogenous damage-associated molecular patterns (DAMPs). Membrane-localized pattern recognition receptors (PRRs) perceive MAMPs or DAMPs and initiate the so-called pattern-triggered immunity (PTI) (Couto and Zipfel, 2016; Hou et al., 2019). Most PRRs are receptor-like kinases (RLKs) or receptor-like proteins (RLPs), possessing either a lysin-motif (LysM) or a leucine-rich repeat (LRR) extracellular domain in charge of ligand binding (Zipfel, 2014). RLKs have a cytoplasmic kinase domain, whereas RLPs require an adaptor receptor kinase (RK) to form a bipartite receptor for downstream signalling (Tang et al., 2017). Upon MAMP perception by the extracellular domain, PRRs form a complex with co-receptors that result in auto and trans-phosphorylation events (Macho and Zipfel, 2014). Most PRR complexes involve receptor-like cytoplasmic kinases (RLCKs) that when activated, act as executors of downstream signalling and launch signature responses of PTI (Boller and Felix, 2009; Hohmann et al., 2017). These responses mainly include production of apoplastic reactive oxygen species (ROS), cell wall strengthening by callose deposition, mitogen-activated protein kinase (MAPK) cascades, altered ion fluxes, transcriptional

reprogramming, and production of antimicrobial compounds (DeFalco and Zipfel, 2021).

Pathogens have evolved ways to circumvent PTI by secreting a repertoire of effector proteins into the plant apoplast or in the intracellular space to suppress immune responses, modulate host processes, and promote virulence (Hogenhout et al., 2009; Win et al., 2012). The second layer of plant immunity, known as effector-triggered immunity (ETI), involves recognition of effectors by intracellular immune receptors, the majority of which belong to the family of nucleotide binding leucine-rich repeat (NLR) receptors, and constitute the predominant class of resistance (*R*) genes in plants (Jones and Dangl, 2006). Upon effector recognition, NLRs undergo significant conformational changes that trigger a rapid immune response, often associated with a localised form of programmed cell death known as hypersensitive response (HR)—a robust response that arrests progression of disease (Dodds and Rathjen, 2010). Additional ETI outputs also include MAPK signalling cascades, ROS burst, calcium flux, major transcriptional changes and phytohormone signalling (Cui et al., 2015). Pathogen effectors that are recognised by immune receptors are usually termed avirulence—AVR—proteins, as their recognition by the host typically leads to effective pathogen restriction, and therefore results in an *avirulent* infection phenotype (Duxbury et al., 2016). Effector recognition by NLRs is specific, meaning that they usually act on a limited subset of pathogen races by recognising specific cognate effectors (Dodds and Rathjen, 2010).

Up until recently, PTI and ETI were studied and thought of as two distinct branches of the plant immune system. However, despite involving activation by two distinct types of immune receptors and the requirement of different early signalling components, both lead to similar and overlapping downstream responses, suggesting converging elements in the signalling cascades (Yuan et al., 2021a). Indeed, recent studies have shed light on the intricate interactions between PTI and ETI. Increasing evidence suggests the crosstalk between both branches, as they mutually potentiate each other, and both cell surface PRRs and intracellular NLRs act in concert to trigger responses that are functionally interdependent (Ngou et al., 2021; Tian et al., 2021; Yuan et al., 2021b). Nonetheless, the mechanistic insights on how both layers of immune signalling cooperate with each other remain elusive.

1.2 NLR immune receptors

NLR receptors are present across all kingdoms of life (Jones et al., 2016; Uehling et al., 2017; Gao et al., 2020; Gao et al., 2022) and belong to the signal transduction ATPases with numerous domains (STAND) superfamily. STAND proteins share a conserved tripartite architecture, with an N-terminal signalling domain, a central nucleotide-binding oligomerisation domain (NOD), and a C-terminal *sensor* domain that contains superstructure forming repeats (Lukasik and Takken, 2009). In the case of NLRs, the central nucleotide-binding domain is exclusively a nucleotide-binding adaptor shared by APAF-1, plant R proteins and CED-4 (NB-ARC) domain (Duxbury et al., 2021; Kourelis et al., 2021). The C-terminal domain is typically an LRR domain, and based on the type of the N-terminal signalling domain, NLRs in angiosperms can be clustered into one of three major monophyletic groups: the subclade of TIR-NLRs (or TNLs), which contain an N-terminal Toll-interleukin-1 receptor (TIR) domain; the subclade of CC-NLRs (or CNLs) with an N-terminal Rx-type coiled-coil (CC) domain; and the subclade of CC_R-NLRs (or RNLs), which contain an N-terminal RPW8-type CC domain. Noteworthy, TNLs have been largely lost in monocots (Shao et al., 2016) and even though NLRs also occur in nonflowering plants, they carry additional types of N-terminal domains (Andolfo et al., 2019).

The conserved domain architecture in STAND proteins across kingdoms highlight their dual role in immunity, as they perceive non-self or damage-derived molecules, and act as switches that turn on immune responses upon pathogen perception. Recent studies of plant and bacterial NLR and NOD-like activated receptor complexes have demonstrated striking mechanistic conservation with mammalian innate immune systems (Jones et al., 2016; Gao et al., 2020; Gao et al., 2022). Activation of metazoan NLRs is triggered by perception of PAMPs (pathogen-associated molecular patterns, similar to MAMPs) and results in the formation of inflammasomes, which are higher order wheel-like oligomerised complexes (Hu and Chai, 2016). As consequence of oligomerisation, the N-terminal signalling domain of individual subunits are assembled in close proximity and recruit caspases to initiate immune signal transduction (Lechtenberg et al., 2014; Kim et al., 2016). In the absence of pathogen perception, plant NLRs remain in an inactive state through intramolecular interactions (Förderer et al., 2022a). Upon recognition of cognate effectors by plant NLRs, the NB-ARC domain releases ADP and binds ATP (Maruta et al., 2022), thus inducing significant conformational changes that result in oligomerisation and formation of an

inflammasome-like structure called resistosome (Wang et al., 2019a; Wang et al., 2019b; Ma et al., 2020; Martin et al., 2020b; Förderer et al., 2022b; Zhao et al., 2022). Structural studies using Cryo-EM have shown that pathogen perception of the effector AvrAC leads to the formation of a pentameric homo-oligomer of the *Arabidopsis thaliana* CNL ZAR1 (HopZ-Activated Resistance 1) (Wang et al., 2019a). The same is true for the activated wheat CNL Sr35, which forms a pentameric resistosome upon binding of its corresponding effector AvrSr35 (Förderer et al., 2022b; Zhao et al., 2022), suggesting evolutionary conservation of pentameric structures triggered by activation of CNLs. The structure of two activated TNLs, ROQ1 (Recognition of XopQ 1) in *Nicothiana benthamiana* and RPP1 (Recognition of *Peronospora parasitica* 1) in *A. thaliana,* revealed that binding to their corresponding effectors triggers the formation of higher order tetramers in both cases (Ma et al., 2020; Martin et al., 2020b). In addition, the bacterial STAND proteins Avs3 from *Salmonella enterica* and Avs4 from *E. coli,* both of which are NOD-like receptors, form tetramers upon direct binding of the terminase subunit and the portal protein of tailed phages, respectively (Gao et al., 2022). In all studied instances across different kingdoms, NLR or STAND protein oligomerisation upon pathogen perception leads to and is required for cell death, highlighting its importance for the activation of immune responses.

1.2.1 NLR domain architecture

1.2.1.1 N-terminal TIR and CC domains

Depending on their N-terminal domain, plant NLRs can be broadly classified into TIR-NLRs or CC-NRLs. Within CC-NLRs, three further distinctions can be made between Rx-type CC-NLRs (CNLs), RPW8-type CC NRLs (RNLs) and a further monophyletic subclade that was recently proposed as the G10-subclade of NLRs (CC_{G10}-NLRs) (Shao et al., 2016; Andolfo et al., 2019). Unlike RNLs, CNLs carry a conserved characteristic EDVID motif in the CC domain (Bentham et al., 2018). Mutation of the EDVID motif in the barley CNL Mla10 (Mildew locus a 10) rendered the full-length receptor unable to trigger cell death, highlighting the importance of this motif in immune signalling (Bai et al., 2012). Other studies have proposed that the EDVID motif in Rx, a CNL in potato conferring resistance against PVX (potato virus x), is rather involved in mediating intramolecular interactions between the CC domain and other NLR domains (Rairdan et al., 2008). The group of RNLs largely consists of helper NLRs from the ADR1 (Activated Disease Resistance 1) and NRG1 (N Required Gene 1) family, which

are required for signalling downstream of other NLRs (Feehan et al., 2020). The ADR1 family has been found to assist signalling in both CNL and TNL-mediated immunity, whereas NRG1 family members have been reported to act downstream of TNL but not CNL-activation(Bonardi et al., 2011; Qi et al., 2018; Castel et al., 2019; Wu et al., 2019). TNLs have been completely lost in monocot plant species, and not surprisingly, the NRG1 family is largely absent in this group too, reflecting the functional connection between TNLs and NRG1 (Collier et al., 2011; Shao et al., 2016; Baggs et al., 2020; Duxbury et al., 2021).

Overall, both TIR and CC domains have been implicated as modules required for downstream signal transduction, self-association, or cofactor association (Bentham et al., 2018). Several studies have shown that expression of the N-termini of plant NLRs on their own—either TIR or CC domains alone and in the absence of effectors—is often sufficient to trigger a constitutive immune response (usually HR), highlighting them as minimal subunits required for effective immune activation (Swiderski et al., 2009; Krasileva et al., 2010a; Bai et al., 2012; Cesari et al., 2016). This suggests that other NLR domains play a role in autoinhibition and maintaining an inactivated (*off*) state of the full-length protein. In addition, reports indicate that N-termini oligomerise, and this is required for downstream cell death immune signalling (Williams et al., 2014; Casey et al., 2016; Duxbury et al., 2020). Upon NLR effector recognition, oligomerisation mediated by the exchange of ADP to ATP in the NB-ARC domain of individual NLR protomers promotes association between the N-terminal domain of different subunits (Wang et al., 2020; Maruta et al., 2022). The CC and RPW8-type CC domain in CNLs and RNLs, respectively, form an α-helix bundle. Upon oligomerisation, the α1-helices of the CNL ZAR1 and the RNLs NRG1 and ADR1 have been shown to form a cation channel that promotes Ca^{2+} influx and subsequent cell death, which requires the presence of conserved negatively charged N-terminal residues (Bi et al., 2021; Jacob et al., 2021). In the case of TNLs, NLR oligomerisation promotes specific assembly of individual protomers that form a dimer of TIR domain dimers with NAD^+ cleaving (NADase) activity (Wan et al., 2019; Ma et al., 2020; Martin et al., 2020b), leading to the production of small signalling molecules required for activation of subsequent components of the TNL signalling pathway (Huang et al., 2022; Jia et al., 2022). Mutations in the NADase active site of TIR domains of TNLs such as RPS4 (Resistance to *Pseudomonas syringae* 4) in *A. thaliana,* ROQ1 and RPP1 compromised cell death activity, suggesting its key role in plant defence activation (Wan et al., 2019; Ma et al., 2020; Martin et al., 2020b).

A significant difference between the immune signalling triggered by TNLs and CNLs resides in the NADase enzymatic activity by TIR domains. CC domains have no known enzymatic activity; however, the pentameric structure of the CNL ZAR1 resistosome revealed that the N-terminal α1-helix of the CC domain of each individual subunit undergoes a conformational switch upon oligomerisation, forming an exposed funnel-shaped structure that will then constitute the cation permeable channel required for cell death (Wang et al., 2019a). A random truncation screen established that the 29 N-terminal amino acids of the *N. benthamiana* CNL NRC4 (NLR required for cell death 4) constitute the conserved minimal region within the α1-helix of the CC-domain that is required for cell death (Adachi et al., 2019b. This region is defined by a motif with the consensus sequence MADAxVSFxVxKLxxLLxxEx, also coined as "MADA" motif. This motif, also present in ZAR1, is conserved not only in sequence, but also in function in 20% of all angiosperm CNLs. Mutations in conserved residues within the MADA motif lead to loss of cell death activity without compromising oligomerisation (Adachi et al., 2019b). A recent report established the presence of a subfamily of CC domains that is specific to non-flowering plant lineages and carries the MAEPL motif, which is functionally similar to the angiosperm MADA motif (Chia et al., 2022). Interestingly, the MADA motif is absent in CNLs that require helper NLRs to function, likely due to functional degeneration over evolutionary time. These specialised *sensor* NLRs rely on other NLRs to relay immune activation and therefore do not trigger cell death on their own (Adachi et al., 2019b). Noteworthy, RNLs also lack the MADA motif. It remains to be established whether the wealth of CC-NRLs missing the MADA motif carry additional conserved motifs with fundamental functional differences.

Additionally, the CC domain of some CNLs has been shown to associate with proteins distinct to NLRs. A region comprising the EDVID motif of the CC domain of Rx interacts with RanGAP2 (Ran GTPase Activating Protein 2), a protein required for Rx-mediated resistance (Sacco et al., 2007). The *A. thaliana* CNL RPM1 (Resistance to *Pseudomonas syringae* pv. *macuolicola* 1) perceives the bacterial effectors AvrRpm1 and AvrB via monitoring of the small host protein RIN4 (RPM1-interacting protein 4) (Mackey et al., 2002). All domains of RPM1, including the CC domain, have been shown to play a role in interaction with RIN4 and thus activation of immune signalling (El Kasmi et al., 2017). The CNL RPS5 (Resistance to *Pseudomonas syringae* 5) requires and forms a complex with the *A. thaliana* protein kinase PBS1 (AvrPphB susceptible 1) to effectively recognise the effector AvrPphB (Ade et al., 2007). Formation of this complex is mediated by the

CC N-terminal domain of RPS5 (Qi et al., 2012). Interestingly, the CC domains of Rx, RPM1 and RPS5 do not induce cell death independently (Moffett et al., 2002; Ade et al., 2007; El Kasmi et al., 2017), suggesting a different immune signalling mechanism from CNLs containing a MADA motif that do not require additional proteins to recognise their corresponding effectors.

1.2.1.2 NB-ARC domain

The NB-ARC domain (also known as the nucleotide binding oligomerisation domain—NOD) (Bentham et al., 2017), is highly conserved across NLRs at the sequence and structural level. For this reason, it is often used to make phylogenetic inferences in NLR evolutionary studies. It is positioned in the middle, in between the N-terminal domain and the LRR domain, and contains three subdomains: the nucleotide binding domain (NB), the ARC1 domain with a four-helix bundle (also known as the helical domain 1—HD1), and the ARC2 domain with a winged helix fold (also known as the winged-helix domain—WHD) (Duxbury et al., 2021). The NB domain contains the Walker A or P-loop motif (GxxxxGK[T/S]), important for nucleotide binding, and the Walker B motif (hhhDD/E), required for Mg^{2+} coordination and hydrolysis of ATP (Bonardi et al., 2012). The ARC2 domain or WHD contains the methionine-histidine-aspartate (MHD) motif important for ADP binding (Takken et al., 2006). Most of these conserved motifs are located at the intramolecular binding interface of the three NB-ARC subdomains and form a nucleotide binding pocket that is crucial for NLR activation (Slootweg et al., 2013).

The NB-ARC domain acts as a molecular switch that modulates significant structural changes that lead to and are required for NLR oligomerisation and activation (Maruta et al., 2022). The ADP-bound form of the NB-ARC domain maintains NLRs in an inactive state. In this inactive state, intramolecular interactions maintain the nucleotide binding pocket formed by the NB, HD1 and WHD regions, in a closed state (Burdett et al., 2019). Upon pathogen perception, these interactions are disrupted allowing the exchange of ADP for ATP at the interface formed by the NB and the HD1 domains, while the WHD is displaced and moved away from the nucleotide binding site (Maruta et al., 2022). In the case of the ROQ1 resistosome, the ATP molecule is stabilised at the nucleotide binding pocket by the P-loop motif, which recognises the β-phosphate group of the ATP molecule, and the β- and γ-phosphates are coordinated with the Mg^{2+} ion in close proximity to the Walker B motif (Martin et al., 2020b). The rotation of the WHD

domain displaces the ADP-specific MHD motif, thereby exposing and stabilising the oligomerisation interfaces. This allows for the NB-HD1 surface of one protomer to intercalate with the NB-WHD surface of another protomer. Mutations in these surfaces resulted in disruption of NLR oligomerisation and therefore loss of cell death response (Martin et al., 2020b).

The importance of the nucleotide binding sites of the NB-ARC domain is reflected by the fact that mutations in the conserved motifs of the different subdomains lead to either loss of function or autoactivity in cell death signalling (Baudin et al., 2017). For example, an aspartate-to-valine mutation in the MHD motif of several plant NLRs has resulted in auto-inducing cell death activity (Bendahmane et al., 2002). In the case of the flax M NLR protein, this mutation was corelated with increased ATP binding that favours an active state in the absence of the corresponding effector (Williams et al., 2011). On the other hand, a lysine-to-arginine substitution in the P-loop motif of the NB domain of multiple NLRs abrogated ATP-binding affinity and led to complete loss of immune signalling (Tameling et al., 2006) (Tameling et al., 2002; Williams et al., 2011; Bai et al., 2012). Nonetheless, these rules do not apply to all cases. The rice CNL RGA5 (R-gene analog 5), for instance, does not require an intact P-loop motif to function (Césari et al., 2014). RGA5 requires the helper CNL RGA4 (R-gene analog 4) to recognise the effectors AVR1-CO39 and AVR-Pia from the fungal pathogen *Magnaporthe oryzae* (Cesari et al., 2013). In addition, mutations of the MHD motif of RGA5 did not lead to constitutive cell death activity, nor did they impact the ability of RGA5 to function (Césari et al., 2014). This suggests that the mechanism of activation of NLRs that require helper NLRs to function differs from the current resistosome model inferred by the structures of activated ZAR1, Sr35 (Stem rust resistance 35), ROQ1 and RPP1.

Interestingly, pathogens have evolved mechanisms to interfere with NLR signalling by targeting the NB-ARC domain. One such case is the potato cyst nematode *Globodera rostochiensis* that secretes the effector SPRYSEC15 (SS15) to suppress signalling mediated by the *N. benthamiana* helper CNLs NRC2 and NRC3 (NLR required for cell death 2/3) (Derevnina et al., 2021). A recent study demonstrated that SS15 blocks NRC2 oligomerisation by binding to the NB-ARC domain. SS15 binds to a loop that acts like a hinge by connecting the NB domain with the HD1 and the WHD and allowing conformational changes upon NLR activation. It is hypothesised that SS15 prevents NRC2 oligomerisation by locking this hinge, thus preventing structural changes required for oligomerisation. Interestingly, mutation of single residues in the HD1 domain that

are within the binding interface with SS15 lead to escape of suppression by the effector (Contreras et al., 2023).

1.2.1.3 LRR domain

The leucine rich repat (LRR) domain is present across a large number of protein families from all kingdoms and is known to have protein-ligand interaction motifs (Ng and Xavier, 2011). Each repeat within the LRR domain has an eleven-residue motif, LxxLxLxxN/CxL, that forms a β-strand and adjacent loop regions, followed by a variable sequence (Kobe and Kajava, 2001). A single LRR domain can contain between 2 to 45 repeats that fold into a horseshoe shape, in which the parallel β-strands of each repeat are located in the concave face, whereas the adjacent loops and α-helices from the variable regions are located in the convex face (Enkhbayar et al., 2004; Ng and Xavier, 2011).

In NLRs, the LRR domain often functions as a regulatory unit in charge of receptor autoinhibition through intramolecular interactions with other domains (Padmanabhan et al., 2009). In the absence of pathogen recognition, the LRR region tightly interacts with the NB-ARC domain to keep the nucleotide binding pocket in a closed state (Tameling et al., 2006). Some NLRs become constitutively active when their LRR domain is removed, highlighting its role in maintaining an inactive state (Bai et al., 2012). In addition, the LRR domain plays a key role in pathogen recognition either by direct binding of effectors or additional host proteins required for pathogen perception. Ligand binding to the LRR releases the NB-ARC domain due to steric clash and allows the exchange of ADP for ATP, thus inducing NLR oligomerisation (Burdett et al., 2019) (Maruta et al., 2022). Multiple studies have shown the active involvement of the LRR domain in pathogen perception. In all the resistosome structures solved by Cryo-EM, the LRR domain plays a key role by directly binding to the effector, like in the case of the CNL Sr35 and the TNLs ROQ1 and RPP1 (Ma et al., 2020; Martin et al., 2020b; Förderer et al., 2022b; Zhao et al., 2022), or through host ligand binding as in the case of ZAR1 (Wang et al., 2019a). The surface-exposed residues in the LRR domain provide an extended interaction interface for pathogen recognition, and the low sequence conservation (Padmanabhan et al., 2009) of each repeat suggests that they can accommodate the acquisition of polymorphisms that promote the evolution of new recognition specificities, as in the case of the Mla allelic series in barley (Seeholzer et al., 2010; Prigozhin and Krasileva, 2021).

In addition, some TNLs have been found to have a post-LRR domain, also known as C-terminal jelly-roll/Ig-like domain (C-JID), which has a crucial role in effector binding. In the case of ROQ1 and RPP1, direct effector recognition by the LRR domain is assisted primarily by the C-JID domain (Ma et al., 2020; Martin et al., 2020b).

1.2.1.4 Unconventional integrated domains (IDs)

Approximately 10% of the NLRs within a given plant species have an unconventional architecture that includes an additional noncanonical NLR domain, usually referred to as an integrated domain (ID) (Kroj et al., 2016; Sarris et al., 2016). Several studies have shown that these IDs often belong to protein families that are targeted by pathogen effectors. Therefore, IDs are hypothesised to have evolved from the integration of effector host targets within different locations of canonical NLRs, aiding in effector recognition (Marchal et al., 2022b). However, this has only been rigorously confirmed in the few cases of NLRs with IDs in which their corresponding effectors are known (Tasset et al., 2010; Maqbool et al., 2015; Zhang et al., 2017; Guo et al., 2018b; Mukhi et al., 2021). The activity of the majority of IDs is associated with protein kinases, DNA-binding, protein-protein interactions, redox reactions, and hormone signalling (Sarris et al., 2016). Because NLR-IDs are present across the genomes of most flowering plants, it has been proposed that most plants share a mechanism of NLR evolution through gene fusions (Bailey et al., 2018b; Grund et al., 2019).

1.3 Effector recognition by NLRs

Even though the mode of recognition has not been established for most NLRs, in general, they recognise effectors through two main mechanisms: directly, through NLR-effector binding, or indirectly, through NLR monitoring of host proteins that are modified by their cognate effectors (van der Hoorn and Kamoun, 2008; Cesari, 2018; Kourelis and van der Hoorn, 2018; Duxbury et al., 2021)

1.3.1 Direct recognition

Direct perception of effectors follows a model of receptor-ligand recognition of non-self, meaning that one NLR directly binds one effector molecule (Baggs et al., 2017). The number of confirmed examples of direct recognition is limited. The rice CNL Pi-ta is known to directly bind AvrPita from the blast fungus *Magnaporthe oryzae* (Jia et al., 2000). Other examples include the flax TNL alleles L5/6/7, and the M TNL, which recognise Avr567 and AvrM from the flax rust fungus *Melampsora lini*, respectively (Dodds et al.,

2006; Catanzariti et al., 2010); the Arabidopsis TNL RPP1, which recognises the effector ATR1 from the oomycete *Hyaloperonospora arabidopsidis* (*Hpa*) (Krasileva et al., 2010b; Ma et al., 2020); the *N. benthamiana* TNL ROQ1, which directly binds its cognate *Xanthomonas* effector XopQ (Schultink et al., 2017; Martin et al., 2020b); some alleles of the barley CNL Mla, which were recently shown to directly interact with their corresponding AVR_a effectors from *Blumeria graminis* f. sp. *hordei* (*Bgh*) (Saur et al., 2019; Bauer et al., 2021); the rye Mla homologue Sr50, which binds to AvrSr50 from *Puccinia graminis* f. sp. *tritici* (Chen et al., 2017) (*Pgt*); the wheat CNL Sr35, which confers resistance against *Pgt* through direct interaction with the effector AvrSr35 (Förderer et al., 2022b; Zhao et al., 2022); and the tomato CNL Sw-5b, which directly recognizes the movement protein NSm from different tospoviruses (Zhu et al., 2017). In most cases of physical binding, the LRR domain executes effector perception and plays a key role in specificity of recognition, as polymorphisms in this region amongst alleles or paralogues of these NLRs result in different or even expanded recognition specificities (Dodds et al., 2001; Brunner et al., 2010; Seeholzer et al., 2010). Noteworthy, in the case of Sw-5b, an additional domain other than the LRR region also mediates interaction with the NSm viral protein. The SD (Solanaceae domain) in Sw-5b is an extended N-terminal domain, located before the CC domain, that directly interacts with NSm and is critical for the induction of HR, as it enhances the ability of Sw-5b to detect low levels of the viral protein (Li et al., 2019).

It is not surprising that further instances of direct NLR-effector interaction have not yet been reported. Pathogens are under strong selective pressure to alter effectors that escape recognition by their hosts, and similarly, plants are under pressure to diversify and maintain recognition of fast evolving pathogens(Dangl and McDowell, 2006). However, the longer life cycle of plants in comparison to pathogens imposes an evolutionary disadvantage in the former, limiting the speed of NLR diversification (Baggs et al., 2017).

1.3.2 Indirect recognition

Different effectors and effector families have evolved to manipulate similar host processes and often, even the same proteins to promote disease (Sánchez-Vallet et al., 2018). This provides an efficient framework through which NLRs have evolved to recognise effectors by monitoring the molecular status of their targets. If the monitored effector target is functional and is itself involved in a particular cellular process, it is also known as a guardee. Alternatively, if the perturbed protein mimics an effector target, is

not functional and serves solely as bait, it is called a decoy (van der Hoorn and Kamoun, 2008; Kourelis and van der Hoorn, 2018; Adachi et al., 2019a). As consequence, multiple unrelated effectors can be indirectly recognised by a few NLRs through common host targets. One example is the recognition of the bacterial effectors AvrRpm1, AvrB and AvrRpt2 that target the *A. thaliana* protein RIN4, which is guarded by two different NLRs, RPM1 and RPS2 (Resistance to *Pseudomonas syringae* 2). AvrRpm1 and AvrB induce phosphorylation of RIN4, which triggers immune activation by RPM1, whereas AvrRpt2 cleaves RIN4, activating RPS2-mediated immune signalling (Mackey et al., 2002; Axtell and Staskawicz, 2003). Another example is the recognition of the *Pseudomonas* effector AvrPphB, which cleaves several receptor-like cytoplasmic kinases (RLCKs), including PBS1, triggering recognition by the CNL RPS5. PBS1 forms a pre-recognition complex with RPS5, which becomes activated upon cleavage of PBS1 by AvrPphB (Swiderski and Innes, 2001; Ade et al., 2007). The unrelated *Pseudomonas* effectors AvrPto and AvrPtoB are recognised by the CNL Prf, which forms a complex with the protein kinase Pto. Binding of Pto by AvrPto and AvrPtoB then triggers Prf-immune signalling (Kim et al., 2002). The CNL ZAR1 recognises the effectors HopZ1a and HopF2a from *P. syringae,* and AvrAC from *Xanthomonas campestris* by guarding RLCKs. The acetyltransferase activity of HopZ1a on the pseudokinase ZED1 is perceived by ZAR1, activating an immune response. AvrAC uridylates the RLCK PBL2, which is sensed by ZAR1 in complex with the RLCK RKS1, triggering resistosome formation (Lewis et al., 2010; Lewis et al., 2013; Wang et al., 2015; Baudin et al., 2017; Seto et al., 2017; Wang et al., 2019a).

Interestingly, there is a limited number of documented cases of fungal effectors indirectly recognised by NLRs. One such case is recognition of the *M. oryzae* effector AVR-Pii by the rice receptor pair Pii. AVR-Pii binds to the allelic OsExo70-F2 and OsExo70-F3 proteins, which are subunits of the octomeric exocyst complex (Fujisaki et al., 2015; De la Concepcion et al., 2022). This interaction is sensed by Pii, via an integrated RIN4/NOI domain (Fujisaki et al., 2017). Another case is the recognition of the host-selective toxin victorin, secreted by the necrotrophic fungus *Bipolaris victoriae,* by the *A. thaliana* CNL LOV1 (Locus orchestrating victorin effects 1). Victorin binds the host thioredoxin AtTRX-h5, thus triggering LOV1-activated cell death (Lorang et al., 2004; Sweat and Wolpert, 2007; Lorang et al., 2012). In this case, however, recognition of victorin triggers susceptibility rather than resistance, as the cell death response is of benefit for this necrotrophic pathogen (Lorang et al., 2007).

1.3.3 Recognition by NLR-IDs

The origin of IDs within NLRs likely stems from the duplication of effector targets and fusion within NLRs (Cesari et al., 2014). As such, it is though that, while mimicking effector targets, IDs act as baits that directly bind effectors or serve as substrate for their enzymatic activities (i.e. act as integrated guardees or decoys) (Marchal et al., 2022b). One example is the TNL RRS1 (Resistance to *Ralstonia solanacearum* 1), which has a C-terminal WRKY integrated domain (Le Roux et al., 2015; Huh et al., 2017a). In Arabidopsis, the effector PopP2 from the bacterial pathogen *Ralstonia solanacearum* targets WRKY transcription factors to facilitate infection, but also acetylates key lysine residues in the WRKY ID of RRS1, activating recognition (Tasset et al., 2010; Zhang et al., 2017). Although structurally distinct from PopP2, RRS1 also recognises the effector AvrRps4 from *Pseudomonas syringae* via interaction with the WRKY integrated domain, and an unknown effector from *Colletotrichum higginssianum* (Tasset et al., 2010; Le Roux et al., 2015; Sarris et al., 2015; Huh et al., 2017b; Ma et al., 2018). Noteworthy, AvrRps4 also targets WRKY transcription factors in *A. thaliana* and prevents their interaction with W-box DNA via steric blocking (Mukhi et al., 2021). Other two well-known cases of recognition via an integrated decoy are the rice CNLs RGA5 and Pik-1 (*Pyricularia oryzae* resistance-k 1), that contain a heavy metal-associated (HMA) domain integrated at the C-terminal or in between the CC and the NB domain, respectively (Maqbool et al., 2015; Guo et al., 2018a). Not surprisingly, the group of MAX effectors from the blast fungus *M. oryzae*, which are sequence-unrelated but structurally similar, are known to target HMA-isoprenylated plant proteins (HIPPs) (Maidment et al., 2021). Thus, the HMA domain in RGA5 serves as bait that physically binds to the effectors AVR1-CO39 and AVR-Pia, and the one in Pik-1 binds to AVR-Pik (Maqbool et al., 2015; Ortiz et al., 2017; Guo et al., 2018a).

All these three cases of NLRs with IDs that perceive pathogen effectors (i.e. sensor NLRs) require a genetically and physically linked NLR to relay the downstream immune signalling, also known as helper NLR. The genetic linkage of these sensor-helper NLR pairs, with head-to-head orientation and shared promoter, ensures their co-regulation and co-segregation. RRS1 is paired with the TNL RPS4 (Resistance to *Pseudomonas syringae* 4), and RGA5 and Pik-1 are paired with RGA4 and Pik-2, respectively (Césari et al., 2014; Le Roux et al., 2015; Maqbool et al., 2015; Huh et al., 2017b). This system of sensor-helper allows the tolerance of point mutations in the ID of sensor NLRs that increase the binding affinity to their cognate effectors, without affecting the NLR

immune signalling function (Baggs et al., 2017; Białas et al., 2018; Adachi et al., 2019a; Białas et al., 2021).

1.4 NLR signalling and activation

1.4.1 NLRs can work as singletons, pairs or networks

Increasing evidence has revealed insights into the principles that govern NLR-mediated immunity in plants. The original gene-for-gene model proposed by Flor implies the existence of one resistance gene per each recognised pathogen effector (Flor, 1971). As shown by several already described examples, many NLRs fall outside this model. Some NLRs indeed function as single genetic units that have the ability to sense effectors and trigger an immune response, and have therefore been defined as singleton NLRs (Adachi et al., 2019a). This is the case of some of the NLRs involved in direct effector recognition, such as Sr35 in wheat, Mla in barley and its ortholog Sr50 in rye, as well as other NLRs that guard effector targets, such as RPS5 or ZAR1 in *A. thaliana* (Ade et al., 2007; Qi et al., 2012; Cesari et al., 2016; Baudin et al., 2017; Chen et al., 2017; Wang et al., 2019a; Förderer et al., 2022b; Zhao et al., 2022). However, as previously described for the sensor-helper NLR pairs, some NLRs specialized in pathogen recognition (aka *sensors*) require a partner NLR that executes the downstream immune signalling (aka *helpers*). This is the case of all known NLRs with an ID, in which two genetically linked NLRs are required for effector recognition: the sensor, which has an ID to *sense* the pathogen, and the helper in charge of executing the immune response (Adachi et al., 2019a; Feehan et al., 2020).

Interestingly, not all cases of sensor NLRs that require a helper are genetically linked to the latter, nor are they connected in a one-to-one relationship. Some NLRs can form higher order signalling networks in which one sensor NLR genetically interacts with more than one helper, and similarly, a helper NLR serves in signalling transduction for more than one sensor (Kourelis and Adachi, 2022). In these cases, helper NLRs are not always genetically linked to sensors, and can be located elsewhere in the genome (Cesari, 2018; Adachi et al., 2019a). One example of a receptor network is the NRC (NLR required for cell death) network in Solanaceae plant species, in which a few helper NLRs called NRCs execute the immune signalling triggered by a larger series of sensor NLRs that perceive a wealth of pathogens, including insects, viruses, oomycetes, bacteria and nematodes (Wu et al., 2017). Both sensor and helper NLRs within the NRC network are

part of the well-supported phylogenetic NRC superclade in Solanaceae species, suggesting they most likely evolved from a sensor-helper NLR pair and underwent through subsequent diversification (Wu et al., 2017). Unlike NRCs, which carry the conserved MADA motif in the CC domain, sensor NLRs within the network appear to have lost it, probably due to functional degeneration as consequence of selection towards effector perception rather than immune signalling (Adachi et al., 2019b). This implies an asymmetrical evolutionary model in which sensor NLRs are "allowed" to experience expanded rates of diversification that extends the spectrum of pathogen perception, whereas the selective pressure on helper NLRs limits them to maintain their function in immune signalling—hence their reduced numbers in comparison to sensors (Adachi et al., 2019b). From an evolutionary and functional perspective, an NLR immune network provides several advantages such as enhanced evolvability due to specialisation, as well as robustness upon challenge by pathogens (Wu et al., 2017; Adachi et al., 2019a).

Although smaller than the NRC network, RNLs also act as helper NLRs in networks that aid the immune signalling of both, CNLs and TNLs (Feehan et al., 2020). RNLs from the ADR1 family are involved in both, CNL and TNL-activated immunity, whereas the NRG1 family uniquely assists TNLs (van Wersch et al., 2020; Duxbury et al., 2021). The responses derived from ADR1 signalling are thought to limit pathogen growth through transcriptional reprogramming, while NRG1 activation is thought trigger a cell death response. All TNLs rely on RNLs to execute an immune output (Bonardi et al., 2011; Lapin et al., 2019; Saile et al., 2020; Dongus and Parker, 2021; Sun et al., 2021).

1.4.2 NLR activation

Until not long ago, the NLR activation mechanisms and the events that followed effector recognition remained largely unknown. Recent biochemistry and structural studies have unveiled some of the principles that rule immune activation by NLRs and their similarities across kingdoms (Duxbury et al., 2021).

1.4.2.1 Activation of singleton CNLs

The resistosome structures solved by Cryo-EM of the CNLs ZAR1 from *A. thaliana* and Sr35 from wheat revealed the conserved pentameric wheel-like structure amongst these two NLRs (Wang et al., 2019a; Förderer et al., 2022b; Zhao et al., 2022), despite their differences in the mechanism of effector recognition. In its inactive state, ZAR1 forms a heterodimeric complex with the pseudokinase RKS1. Upon pathogen

challenge by *X. campestris,* the effector AvrAC uridylates the RLCK decoy protein PBL2, which subsequently binds to the ZAR1-RKS1 complex, opening the nucleotide binding pocket in the NB-ARC domain and promoting exchange of ADP for ATP. This then triggers oligomerisation of activated ZAR1 into a wheel-like structure formed by five protomers. Each single subunit includes one monomer of ZAR1, one of RKS1 and one of PBL2 in its uridylated state. ZAR1 oligomerisation brings together the N-terminal helix of the CC domain of each protomer—where the MADA motif resides (Adachi et al., 2019b)—forming an α-helical barrel that protrudes out of the pentameric structure, associates with the plasma membrane and forms a calcium-permeable cation channel that leads to cell death. Noteworthy, AvrAC is not part of the activated complex (Wang et al., 2019a; Wang et al., 2019b).

The wheat Sr35, on the other hand, directly recognises its cognate *Pgt* effector AvrSr35. The Sr35 resistosome, formed upon direct binding of AvrSr35 exclusively through the LRR domain, is also formed by five receptor protomers, each bound to one effector molecule. AvrSr35 was found to form dimers in solution; however, as the stoichiometric ratio between Sr35 and AvrSr35 is 1:1 in the resistosome structure, AvrSr35 dimers likely disassociate upon Sr35 recognition (Zhao et al., 2022). Like in the ZAR1 resistosome, effector perception releases the inhibitory intramolecular interactions, allowing the exchange of ADP for ATP at the nucleotide binding pocket, followed by NLR oligomerisation. In each protomer, AvrSr35 is tightly packed in the inner lateral side of the C-terminal part of the LRR domain by polar interactions, through charge and shape complementarity (Förderer et al., 2022b; Zhao et al., 2022). Interestingly, upon structure comparison, the AvrSr35 dimerization interface completely overlaps with the AvrSr35-Sr35 recognition interface, and AvrSr35 residues that participate in dimerization are also recognised by Sr35 (Zhao et al., 2022). Similar to the ZAR1 resistosome, the α1-helix of the CC domain of Sr35 also forms the funnel-shaped structure necessary for cell death, and truncation assays showed that mutants lacking the 20 N-terminal residues of Sr35 lost immune function but maintained resistosome assembly (Förderer et al., 2022b; Zhao et al., 2022). Overall, the similarities between ZAR1 and Sr35 resistosome structures demonstrate remarkable mechanistic conservation across distantly related CNLs.

1.4.2.2 Activation of paired NLRs

Two of the best characterised paired NLRs in plants are the RGA4-RGA5 pair and the Pik1-Pik2 pair, both from rice. Even though the exact mechanism that leads to activation of paired NLRs is still not well understood, it is known that not all pairs work according to the same principles. RGA4 and RGA5, for example, function through de-repression. When expressed on its own, the RGA4 helper triggers constitutive cell death. In the absence of Avr-Pia or AVR1-CO39, the RGA5 sensor acts as a negative regulator of RGA4 suppressing its autoactivity. Upon effector binding to the HMA domain of RGA5, RGA4 is released, thus triggering an immune response (Cesari et al., 2013; Césari et al., 2014; Guo et al., 2018a). On the other hand, Pik-1 and Pik-2 work through a model of cooperation in which neither trigger constitutive cell death, and both are required for signalling (Zdrzałek et al., 2020). However, the structural principles of paired NLR activation remain unknown. Whether they form resistosome structures, the involvement of sensor and helper in this higher-order molecular structures, the stoichiometry of such oligomers, and their role as potential calcium channels remain open questions.

1.4.2.3 Activation of the NRC network

Two recent studies on the mechanism of activation of the NRC network found that sensor NLRs activate helper NRCs and trigger their oligomerisation upon pathogen perception. As sensor NLRs do not oligomerise and are also not part of the NRC stable oligomer, a model of activation and release was proposed. In this model, sensor NLRs perceive pathogens, mediate oligomerisation of downstream helpers and remain in the cytoplasm, while oligomerised helper NRCs translocate to the plasma membrane where they form punctate structures that possibly correspond to calcium channels that trigger cell death (Ahn et al., 2022; Contreras et al., 2022). In contrast to hetero-complexes formed by activated paired NLRs in metazoan systems where both sensor and helper NLRs are part of the inflammasome (Vance, 2015), the model of NRC activation in Solanaceae plant species postulates a "helper only" resistosome structure (Ahn et al., 2022; Contreras et al., 2022).

1.4.2.4 Activation of TNL immune signalling

Unlike pentameric CNL resistosome structures, activated TNLs oligomerise into a tetrameric resistosome complex in which the TIR domains of each protomer are brought into proximity to form a dimer of asymmetric dimers with exposed NADase active sites, as shown by the cryo-EM structures of activated ROQ1 and RPP1 (Ma et al.,

2020; Martin et al., 2020b). The effectors ATR1 and XopQ are directly recognised by RPP1 and ROQ1, respectively, through the LRR region and the post LRR C-JID domain. Effector binding leads to the release of the NB-ARC domain by the LRR region, allowing a conformational switch to the ATP-bound form that promotes oligomerisation into a four-leave-clover structure (Ma et al., 2020; Martin et al., 2020b). Interestingly, the RPP1 resistosome was found to be in an ADP rather than an ATP-bound state (Ma et al., 2020). Each resistosome contains four TNL molecules and four effector molecules. The dimer of dimers of TIR domains with NADase activity formed upon oligomerisation forms a holoenzyme that catalyses the production of signalling molecules which then activate downstream immune modules (Ma et al., 2020; Martin et al., 2020b).

In general, plant TNLs require RNLs to execute immune responses (Feehan et al., 2020). The ADR1 and NRG1 RNLs serve as helper NLRs that execute immune signalling downstream of TNLs (Lapin et al., 2022). Activated TNLs require the lipase-like proteins EDS1 (enhanced disease susceptibility 1), PAD4 (phytoalexin deficient 4) and SAG101 (senescence-associated gene 101) to recruit and activate helper RNLs. PAD4 and SAG101 are exclusive partners of EDS1. In *A. thaliana,* the EDS1-PAD4 heterodimer cooperates with ADR1 to restrict pathogen growth, whereas the EDS1-SAG101 heterodimer cooperates with NRG1 to promote cell death (Wagner et al., 2013). It was hypothesised that the EDS1-PAD4 and EDS1-SAG101 complexes act as receptors of specific TIR-derived signals that trigger cooperation and activation of ADR1 and NRG1, respectively. Two recent studies identified the TIR-catalysed products—formed upon TNL holoenzyme activation—that induce subsequent selective activation of ADR1 and NRG1 (Huang et al., 2022; Jia et al., 2022). A crystal structure of the EDS1-PAD4 complex revealed that the small molecule 2'-(5"-phosphoribosyl)-5'-adenosine diphosphate (pRib-ADP) or monophosphate (pRib-AMP) binds to a conserved pocket between these two proteins. pRib-ADP and pRib-AMP are derived from the TIR catalytic activity of an activated TNL resistosome and strongly induce interaction of the EDS1-PAD4 heterodimer with ADR1, thereby activating ADR1-mediated immunity (Huang et al., 2022). On the other hand, a Cryo-EM structure of the TNL-activated EDS1-SAG101 heterodimer revealed that the NADase activity of the assembled TIR domains catalyses the production of ADP-ribosylated ATP (ADPr-ATP) and this molecule binds to EDS1-SAG101 in a similar pocket as pRib-ADP/AMP in EDS1-PAD4. ADPr-ATP binding to EDS1-SAG101 induces a conformational change in SAG101 that enables interaction with NRG1 in a similar fashion to the activation of

ADR1 by EDS1-PAD4. Interestingly, synthesis of pRib-ADP and pRib-AMP requires hydrolysis of ADPr-ATP, also catalysed by TIR enzymatic activity (Jia et al., 2022).

Noteworthy, expression of wild-type ADR1 or an NRG1 mutant in the MHD motif led to constitutive cell death activity in HeLa cells derived from calcium influx (Jacob et al., 2021). This indicates that like ZAR1, activated RNLs also act as calcium permeable cation channels. However, the exact activation mechanism of helper RNLs by the EDS1-PAD4 and EDS1-SAG101 complexes remains to be fully elucidated.

1.5 Multiple pathogen recognition

Flor first described host-pathogen interactions as a gene-for-gene model in which one plant resistance gene confers resistance to a matching pathogen *AVR* gene (Flor, 1971). This paradigm facilitated the understanding of the dynamics of plant-microbe interactions and the cloning of dozens of NLRs. Yet, in addition to the already described cases in which more than one NLR is required to recognise a cognate effector, there are a few reports of NLRs that confer resistance to multiple different pathogens. One example is the previously mentioned TNL pair RRS1 and RPS4, which forms an immune receptor complex required to recognise the effectors PopP2 from *R. solanacearum,* AvrRps4 from *P. syringae* and an unknown molecule from *C. higginisianum* (Narusaka et al., 2009; Ma et al., 2018). Two different alleles of RRS1 have been found: The RRS1-R allele that recognises both, AvrRps4 and PopP2, and carries a C-terminal extension after the WRKY domain, and the RRS1-S allele that only recognises AvrRps4 and has a truncated shorter C-terminal extension (Guo et al., 2020). Although structurally distinct, AvrRps4 and Pop2 interact with the same region of the WRKY domain in both RRS1 alleles (Mukhi et al., 2021). Pop2 acetylates lysine residues within the WRKYGQK motif of the WRKY domain, which promotes association of the C-terminal extension of the RRS1-R allele with its TIR domain, thereby relieving inhibition of the TIR domain of RPS4 and therefore triggering an immune response. The shorter C-terminal extension of RRS1-S is not sufficient for this de-repression to occur (Guo et al., 2020). AvrRps4, on the other hand, also interacts with the TIR domain of RRS1 to promote its association with the WRKY domain and C-terminal extension of both RRS1 alleles, thereby de-repressing RPS4 (Tasset et al., 2010; Le Roux et al., 2015; Sarris et al., 2015; Huh et al., 2017b; Ma et al., 2018; Mukhi et al., 2021) and activating resistance.

Another example of multiple pathogen recognition by a plant NLR is the tomato Mi-1.2 protein, which belongs to the NRC superclade, is part of the sensor NLRs in the

NRC network and requires the helper NLR NRC4 to function (Wu et al., 2017). Mi-1.2 has been widely deployed as a resistance gene and is known to confer resistance to the root-knot nematodes *Meloidogyne incognita, M. arenaria* and *M. javanica,* as well as to the aboveground potato aphid *Macrosiphum euphorbiae*, and to the whitefly *Bemisia tabaci* (Rossi et al., 1998; Vos et al., 1998; Nombela et al., 2003). Resistance to nematodes mediated by Mi-1.2 is associated with HR in the roots soon after feeding of infective juveniles (Rossi et al., 1998). Contrarily, resistance in aboveground tissue is manifested by a reduction of insect feeding, fecundity and survival. Mi-1.2 is expressed in both roots and leaves, but resistance in the former occurs right after germination, while resistance in leaves is not observed until the plants are at least five weeks old (Li et al., 2006). Mi-1.2 mediated resistance requires NRC4, is known to involve activation of MAPK signalling cascades and requires salicylic acid to function (Li et al., 2006). Nevertheless, the mechanism underlying Mi-1.2 recognition of various highly divergent pests remains unidentified.

ZAR1 in *A. thaliana* also confers resistance to *P. syringae* by recognising the effectors HopZ1a and HopF2a, and to *X. campestris* by recognising AvrAC. All cases require RLCK proteins for indirect effector recognition (Lewis et al., 2010; Lewis et al., 2013; Baudin et al., 2017; Seto et al., 2017; Wang et al., 2019a). ROQ1 confers resistance to *P. syringae, Xanthomonas* spp. and *Ralstonia* spp., by directly recognising the homologous effectors HopQ1, XopQ and RipB, respectively (Schultink et al., 2017; Thomas et al., 2020). Additionally, one Mla allele in barley—Mla8—was recently reported to confer resistance to the non-adapted pathogen wheat stripe rust (*Puccinia striiformis* f. sp. *tritici*—*Pst*), in addition to barley powdery mildew *Bgh*. Neither the *Pst* effector nor the *Bgh* AVR_{a8} recognised by Mla8 have been yet identified (Bettgenhaeuser et al., 2021). However, a direct model of effector recognition has been proposed for other Mla alleles and their corresponding AVR_a effectors from *Bgh* (Saur et al., 2019).

Finally, although not an NLR, Lr34 is an *R* gene that confers resistance to multiple rust pathogens in wheat. Lr34 is an ATP-binding cassette (ABC) transporter (Krattinger et al., 2011) that confers broad spectrum adult plant resistance (APR) to wheat leaf rust caused by *Puccinia triticina, Pst*, and wheat powdery mildew (*Blumeria graminis* f. sp. *tritici—Bgt*) in a non-specific manner (Dyck, 1987; Mcintosh, 1992; Spielmeyer et al., 2005; Morgounov et al., 2012; Spielmeyer et al., 2013). When Lr34 was transferred from wheat landraces into the domesticated wheat variety Thatcher, race specific resistance against stem rust (*P. graminis* f. sp. *tritici*) was also observed (Dyck and Samborski, 1979; Vanegas et al., 2008). Remarkably, introduction of *Lr34* in different

cereal species has also provided resistance against a wide variety of pathogens. When the wheat sequence of *Lr34* was introduced into barley, it conferred resistance against powdery mildew (*Bgh*) and barley leaf rust (*P. hordei*). However, a deleterious autoimmune phenotype was observed due to the constitutive expression of defence responses (Risk et al., 2013). Partial resistance to the blast fungus *M. oryzae* was observed when *Lr34* was introduced in rice (Krattinger et al., 2016). Transgenic sorghum plants expressing Lr34 from wheat had increased resistance against sorghum rust (*P. purpurea*) and anthracnose disease (*Colletotrichum sublineolum*) (Schnippenkoetter et al., 2017). Finally, maize *Lr34*-expressing maize were more resistant to the rust fungus *P. sorghi* and to the northern corn leaf blight disease (*Exserohilum turcicum*) (Sucher et al., 2017). In all cases, expression of Lr34 was linked to an early senescence-like phenotype known as leaf tip necrosis (Singh, 1992), suggesting that the molecular pathway providing broad-spectrum resistance is likely conserved in all the cereals tested. Recent studies have revealed that the Lr34 ABC transporter mediates redistribution of the plant hormone ABA, having an impact in the transcriptional response to this phytohormone and ABA-controlled processes such as dehydration tolerance and transpiration (Krattinger et al., 2019).

1.6 NLR evolution and genetic diversity

The number of NLRs greatly varies across species, ranging from less than a dozen in green algae, to a few in watermelon, maize, papaya and kiwi, to unusually high numbers in apple and hexaploid wheat (Baggs et al., 2017; Baggs et al., 2020). Lineage-specific NLR expansions and contractions have occurred mainly through series of tandem duplication events and prevalent deletions, respectively, that follow lineage-specific evolutionary trajectories influenced by transposon content and activity, plant lifestyles and adaptation to their environments, and particular events such as domestication bottlenecks (Baggs et al., 2017; Tamborski and Krasileva, 2020; Barragan and Weigel, 2021).

NLRs are not evenly located across genomes and are in fact commonly found as clusters (Meyers et al., 2003; Van de Weyer et al., 2019). These clusters exist as a result of tandem duplication, unequal crossing over and gene conversion events (Michelmore and Meyers, 1998). For this reason, some clusters can exhibit high structural variation within a species, resulting in suppressed meiotic recombination (Wei et al., 1999). The clustered arrangement of NLRs provides means for increasing functional NLR diversity through the so-called model of birth and death (Michelmore and Meyers, 1998). Intragenic and

intergenic recombination, as well as gene conversion events can generate chimeric LRRs that result in the birth of new full-length NLRs with novel pathogen recognition specificities (Tamborski and Krasileva, 2020). At the same time, unequal crossing over events can also result in the loss of existing functional genes or in truncated non-functional NLRs that might act as reservoirs for future evolution. A high NLR copy number within clusters also represents higher probabilities of acquiring mutations, some of which can be beneficial for expanded pathogen recognition (Barragan and Weigel, 2021).

Understanding the genetic basis of pathogen resistance has traditionally relied on genomic comparison of resistant vs. susceptible individuals. In some cases, differences in resistance can be explained by presence/absence variation of NLRs, rather than the existence of divergent functional and non-functional NLR alleles (Henk et al., 1999). The fact that some NLRs have not been fixed in the population and are absent in some individuals reflects that these NLRs might represent a fitness cost in the absence of the pathogen (Tian et al., 2003). Opposite to presence/absence variation, some NLRs exist as extensive allelic series, wherein different alleles are functional and confer resistance against different races of the same pathogen. This is exemplified by the *L* locus in flax, with 11 different alleles of the same TNL that recognise 10 distinct specificities of different races of the rust fungus *M. lini* (Ellis et al., 1999); the RPP13 CNL in *A. thaliana* has 19 different haplotypes that directly bind the polymorphic effector ATR13 from the oomycete *Hpa* (Bittner-Eddy et al., 2000); wheat *Pm3* encodes a CNL with 17 known alleles that confer isolate-specific resistance against the wheat powdery mildew pathogen *Blumeria graminis* f.sp. *tritici* (*Bgt*) by recognising different *AvrPm3* effectors (Srichumpa et al., 2005; Bhullar et al., 2010; Bourras et al., 2019); and in barley, the *Mildew locus A* (*Mla*) encodes a CNL with over 20 alleles that have distinct recognition specificities of *Bgh* AVR_a effectors (Wei et al., 1999; Saur et al., 2019; Bauer et al., 2021). In all these cases of NLR allelic series, differences in pathogen isolate recognition are attributed to the variation located mainly in the LRR region across alleles (Ellis et al., 1999; Bittner-Eddy et al., 2000; Seeholzer et al., 2010).

It has been hypothesised that expanded allelic series are signature of direct recognition of effectors from filamentous pathogens. Effectors that are under pressure of direct NLR recognition rapidly diversify and in turn drive diversification of their corresponding NLR in host populations, clearly exemplifying pathogen-host co-evolution (Saur et al., 2021). In some cases, the creation of new alleles with novel

recognition specificities also implies neofunctionalization. Different barley Mla alleles do not recognise allelic effectors from *Bgh*, but rather sequence-unrelated structurally similar AVR_a effectors (Lu et al., 2016; Saur et al., 2019; Bauer et al., 2021). Similarly, the different *Bgt* AvrPm3 effectors recognised by the wheat Pm3 allelic series also have low levels of sequence similarity but are predicted to share overall structural conservation (Bhullar et al., 2009; Bourras et al., 2015; Bourras et al., 2019). Interestingly, even though barley Mla and wheat Pm3 are phylogenetically unrelated, they evolved as expanded allelic series to recognise *Bgh* AVR_a effectors and *Bgt* AvrPm3 effectors, respectively, which are all predicted to share an RNAse-like fold. While direct recognition of AvrPm3 effectors by Pm3 has not been demonstrated, it is tempting to hypothesise a conserved model of recognition similar to AVR_a-Mla corresponding pairs, which has been shown to be direct (Saur et al., 2021).

1.7 *Mildew locus A* (*Mla*)

In barley (*Hordeum vulgare*), race-specific resistance to *Bgh* (causal agent of powdery mildew) is conferred by the *Mla* locus (Jørgensen and Wolfe, 1994), which is located on the short arm of chromosome 1H. The first sequenced haplotype was from the susceptible reference cultivar Morex, where it spans a region of 265 kb that includes eight genes derived from three families of CNLs, designated as Resistance gene homologues (*RGH1*, *RGH2*, and *RGH3*), and two nested regions of transposable elements (Wei et al., 1999; Wei et al., 2002). These three NLR families are highly divergent, sharing <43% interfamily sequence similarity (Seeholzer et al., 2010). The *Mla* locus has undergone rounds of multiple insertions, duplications and gene inversions that have led to drastic structural variation across haplotypes. For this reason, the locus experiences suppressed recombination between haplotypes, with little conservation towards the centre and partial sequence conservation limited to the proximal and distal ends of the locus (Wei et al., 1999; Wei et al., 2002).

Functional isolate-specific resistance to *Bgh* is attributed to over 30 variants of the *Mla* NLR gene which belongs to the *RGH1* family, where each *Mla* allele governs specific resistance to *Bgh* isolates by recognising its cognate avirulence AVR_a effector. Traditionally, different *Mla* resistance specificities have been identified through mapping populations with distinct resistance profiles against *Bgh* isolates carrying different AVR_a genes (Wei et al., 2002). Cloning and/or sequencing of over 20 *Mla* resistance specificities has revealed that they share >90% similarity and are closely related to *RGH1bcd,* a

truncated and non-functional NLR that belongs to the *RGH1* gene family in Morex (Seeholzer et al., 2010). Shared insertions and deletions across alleles indicate that they might have originated from a common ancestor, and further recombination events led to the generation of the breadth of alleles with distinct specificities (Wei et al., 2002).

Studies on *Mla* have contributed to the understanding of general NLR function. Expression of the CC domain of Mla10, and the CC domains of Sr33 and Sr50—Mla orthologues in wheat and rye, respectively—was sufficient to induce HR in *N. benthamiana,* delimiting this region as the minimal functional unit for cell death induction (Maekawa et al., 2011; Cesari et al., 2016). Structural and molecular studies have shown self-association of the CC domain of these NLRs and the importance of oligomerisation interfaces for cell death activity (Bai et al., 2012; Cesari et al., 2016). Purification of full-length Mla27 from insect cells indicated that this allele was bound to ADP, confirming that NLRs are bound to ADP rather than ATP in their inactive state (Maekawa et al., 2011). Reciprocal swaps confined in the LRR region between the Mla1 and Mla6 alleles resulted in changes in the specificity of effector recognition (Shen et al., 2003; Bauer et al., 2021). In addition, swap of the LRR region between Mla10 and Mla22 resulted in exchanged specificity of AVR_{a10} and AVR_{a22} recognition (Bauer et al., 2021). Not surprisingly, polymorphic sites in the LRR domain of *Mla* are under diversifying selection (Seeholzer et al., 2010; Maekawa et al., 2018) and are predicted to be located at solvent-exposed sites. In addition, some *Mla* alleles are known to be dependent on RAR1 and SGT1 to function (Shen et al., 2003). These two co-chaperones have been repeatedly shown to play a role in immunity and to positively control protein accumulation of some Mla alleles (Bieri et al., 2004). Remarkably, RAR1/SGT1 dependence in Mla is determined by a single amino acid in the LRR region (Halterman and Wise, 2004).

Several alleles of *Mla* activate cell death immune signalling when co-expressed with their corresponding *AVR_a Bgh* effectors in barley protoplasts and in the heterologous system *N. benthamiana* (Saur et al., 2019). The fact that expression of additional proteins was not required to elicit cell death in *N. benthamiana* highlights the ability of Mla to sense effectors and function independently as a singleton NLR. Cell death in this heterologous dicot system triggered by co-expression of Mla-AVR_a pairs could be explained either by direct effector recognition, or by the presence of a guardee or decoy sufficiently conserved between distantly related monocot and dicot plant species. However, association of Mla alleles and their cognate AVR_a effectors in yeast-

two-hybrid experiments and split luciferase assays most likely suggests a mechanism of direct effector binding (Saur et al., 2019; Bauer et al., 2021).

Most *AVR$_a$* effectors identified so far are sequence unrelated and are encoded in different locations in the genome of *Bgh* isolates (Lu et al., 2016; Saur et al., 2019; Bauer et al., 2021). They are predicted to be structurally similar, sharing an RNAse-like fold with no apparent RNAse activity (Bauer et al., 2021). The capacity of different, yet highly similar *Mla* alleles in barley to recognise sequence unrelated effectors from *Bgh* highlights the remarkable functional diversification within this NLR (Seeholzer et al., 2010; Lu et al., 2016; Saur et al., 2019). In addition, the *Mla* orthologues *Sr50* in rye and *Sr33* in wheat are known to confer resistance against wheat stem rust caused by *Puccinia graminis* f. sp. *tritici* (*Pgt*) (Periyannan et al., 2013; Mago et al., 2015; Chen et al., 2017), thus indicating that the *RGH1* gene family has the evolutionary capacity to recognise independently evolved effectors from highly divergent pathogens (*Bgh* is an Ascomycete and *Pgt* is Basidiomycete), and setting the precedent of multiple pathogen recognition by a single locus. Quite remarkably, it is now known that AvrSr50, the *Pgt* effector directly recognised by Sr50, does not have an RNAse-like fold, but rather has a novel structure amongst fungal effectors (Chen et al., 2017; Ortiz et al., 2022). Moreover, a recent study established that *Rps7*, a locus in barley that confers resistance against the non-adapted wheat stripe rust pathogen *Puccinia striiformis* f. sp. *tritici* (*Pst*), is in fact *Mla.* The *Mla8* allele is sufficient to confer resistance against *Pst* in barley transgenics (Bettgenhaeuser et al., 2021). This result established that a single *Mla* allele has the capacity to recognise highly divergent fungal lineages. The identity of *AVR$_{a8}$* from *Bgh* and the *Pst* effector recognised by *Mla8* remains to be established, and whether they are structurally similar or distinct as well. Furthermore, direct effector recognition is yet to be tested. Nonetheless, altogether the evidence highlights remarkable functional diversification in *Mla.*

1.8 *Resistance to Magnaporthe oryzae 1 (Rmo1)*

While barley exhibits considerable susceptibility to diverse host-specific linages of the blast fungus *Magnaporthe oryzae*, several accessions have been found to be resistant. Phenotypic screens and genetic analysis in barley have identified a few genes and quantitative trait loci (QTLs) involved in resistance against this pathogen (Sato et al., 2001; Aghnoum et al., 2019). A recent study involving a collection of elite European barley cultivars revealed that almost half of them are, to some extent, resistant to certain isolates of blast (Aghnoum et al., 2019). Elite barley cultivars represent a narrow genetic

population, therefore additional resistance genes are likely present in wild barley collections. Yaegashi (1988) identified *PHR-1*, the first reported locus in barley conferring resistance to M80-25, a rice-infecting isolate of *M. oryzae* (Yaegashi, 1988). Crosses between the resistant cultivars Daisen Gold and Miho Golden, both carrying PHR-1, did not produce any susceptible progeny, suggesting a dominant type of resistance (Yaegashi, 1988). No further mapping or cloning was carried out on *PHR-1*. The locus *Resistance to Magnaporthe oryzae* 2 (*Rmo2*) was identified by making crosses between barley cultivars that showed various patterns of resistance to blast, and the highly susceptible parent Nigrate. *Rmo2* was mapped to chromosome 7H and shown to confer resistance against a wide range of *M. oryzae* isolates from different hosts (i.e. rice, wheat, *Eleusine* spp. and *Setaria* spp.) (Nga et al., 2012). However, fine mapping of *Rmo2* is still required for the complete cloning and characterization of the gene underlying resistance.

The locus *Resistance to Magnaporthe oryzae 1* (Rmo1) was initially mapped in barley to the short arm of chromosome 1H using a doubled haploid mapping population (N=100) from a cross between the cultivars Baronesse and BCD47, which are resistant and susceptible to the rice-infecting *M. oryzae* isolate KEN54-20, respectively (Inukai et al., 2006). *Rmo1* was found to be co-segregating with the *Mla* locus from Baronesse (Inukai et al., 2006). Further fine mapping in a recent study established the complete coupling of these two resistance loci (Brabham, 2019). RNAseq data confirmed that all three *RGH* families within the *Mla* locus are expressed in the cultivar Baronesse, which carries *Mla3* as the *RGH1* allele. Leveraging natural variation across a panel of 40 different barley accessions, the barley cultivar Maritime was found to have identical *RGH2* and *RGH3* alleles to Baronesse, but a different *Mla* (*RGH1*) allele. Unlike Baronesse, Maritime is susceptible to the *M. oryzae* isolate KEN54-20, suggesting that neither *RGH2* nor *RGH3* from the *Mla* locus underlie *Rmo1*. Moreover, when transformed with *Mla3* (the *RGH1* allele of Baronesse), the susceptible barley accession Golden Promise gained resistance to *M. oryzae*, indicating that *Mla3* is *Rmo1* (Brabham, 2019). Remarkably, this constitutes yet another example of multiple pathogen recognition and functional diversification in *Mla*. In addition to conferring resistance against *Bgh* by recognising the cognate effector *AVR*$_{a3}$, *Mla3* also confers resistance against *M. oryzae,* likely by recognising the corresponding effector *AVR-Rmo1* (Brabham, 2019). Noteworthy, the identity of neither *AVR*$_{a3}$ from *Bgh* nor *AVR-Rmo1* from *M. oryzae* has been established, thus the mechanism of recognition of these effectors remains elusive.

1.9 Fungal pathogens recognised by *Mla3*

1.9.1 *Blumeria graminis* f. sp. *hordei* (*Bgh*)

Blumeria graminis is an ascomycete fungal species that comprises specialized forms (*forma speciales*) of obligate biotrophs that cause powdery mildew disease in the grasses, including several important cereal crops (Wyand and Brown, 2003). As an obligate biotroph, it entirely depends on living host cells to grow and complete its life cycle. When airborne conidiospores land on the plant surface, they germinate with a primary germ tube, form an appressorial germ tube that then penetrates the plant cell wall and grows to form haustoria, a structure surrounded by the plant plasma membrane that serves as interface for nutrient uptake and export of effector molecules (Thordal-Christensen et al., 2000). *B. graminis* f. sp. *hordei* (*Bgh*) is the specialized form that infects barley and causes barley powdery mildew. Different isolates of *Bgh* can be distinguished based on their virulence or avirulence phenotype on barley cultivars carrying different resistance genes, such as the *Mla* allelic series (Jørgensen and Wolfe, 1994). Genome sequencing of mildew isolates has predicted several genes encoding candidate secreted effector proteins (CSEPs) presumed to contribute to fungal virulence (Pedersen et al., 2012; Wicker et al., 2013). Interestingly, ~15% of CSEPs were predicted as RNAse-like proteins expressed in haustoria (RALPHs) (Pedersen et al., 2012; Spanu, 2017; Pennington et al., 2019). Most RALPHs share a single intron at a conserved position, suggesting a common origin from an ancestral protein with an RNAse-like fold, followed by diversification (Spanu, 2017). Transcriptome-wide association studies in *Bgh* have identified some of the avirulence effectors (*AVR*$_a$) that are recognised by their corresponding *Mla* alleles in barley (Lu et al., 2016; Saur et al., 2019; Bauer et al., 2021). Most of the *AVR*$_a$ effectors identified so far (*AVR*$_{a1}$, *AVR*$_{a6}$, *AVR*$_{a7}$, *AVR*$_{a9}$ and *AVR*$_{a13}$)—with the exception of the allelic *AVR*$_{a10}$ and *AVR*$_{a22}$—are sequence unrelated and yet recognized by highly similar Mla receptors (Saur et al., 2019). Structure predictions indicate that the identified *AVR*$_a$ effectors are RALPHs; however, they all lack residues that are critical for catalytic activity and have no RNAse activity (Bauer et al., 2021). Recent findings have suggested that *Bgh* populations actively maintain a pool of *AVR*$_a$ genes rather than selectively fixing a few of them (Saur et al., 2019) as a result of the co-evolutionary arms race with the matching barley *Mla* alleles. This process has likely contributed to the proliferation and diversification of RALPH effectors in *Bgh* (Saur et al., 2021).

1.9.2 *Magnaporthe oryzae*

Magnaporthe oryzae (teleomorph of *Pyricularia oryzae*) is an ascomycete fungus that causes blast disease on a wide range of grasses such as rice (*Oryzae sativa*), barley (*Hordeum vulgare*), wheat (*Triticum aestivum*), oat (*Avena sativa*), foxtail millet (*Setaria italica*), finger millet (*Eleusine coracana*), perennial ryegrass (*Lolium perenne*) and weeping lovegrass (*Eragrostis curvula*). However, host-specific subgroups within *M. oryzae* can only infect a limited set of grass species (Hyon et al., 2012). Infection by *M. oryzae* starts with the attachment of a three-cell conidia to the host surface, followed by development of a germ tube and formation of the appressorium, a specialized infection cell that melanises, generates high turgor pressure and breaks the leaf cuticle using a penetration peg that requires the formation of a septin ring. After penetration, the fungus invades the plant through primary and secondary invasive bulbous hyphae, which are enclosed by a plant-derived extra-invasive hyphal membrane (EIHM) (Galhano and Talbot, 2011). During infection, *M. oryzae* secretes several effectors to manipulate host processes and promote disease. Based on their localization in the host, effectors can be divided into cytoplasmic or apoplastic (Bai et al., 2012). Cytoplasmic effectors such as Pwl2 and Bas2 initially accumulate at the biotrophic interfacial complex (BIC)—a plant-derived structure at the tip of the primary invasive hyphae—and subsequently translocate into the host cytoplasm. Some cytoplasmic effectors like Pwl2 can move into uncolonized neighbouring cells, likely through plasmodesmata. On the other hand, apoplastic effectors like Bas4 and Slp1 do not accumulate at the BIC, but rather localise in the apoplastic space between invasive hyphae and the EIHM (Zhang and Xu, 2014). Cell-to-cell movement has not been reported for this type of effectors (Khang et al., 2010). After colonisation of the first plant cell by hyphal growth that rapidly fills the interior space, *M. oryzae* moves to neighbouring cells in a synchronous manner through pit fields where plasmodesmata accumulate. Fungal hyphae become swollen and then undergo constrictions at the rice cell junctions in a process that resembles the formation of an appressorium and a penetration peg. This structure important for cell-to-cell movement has been coined as transpressorium (Cruz-Mireles et al., 2021).

Phylogenetically divergent lineages of *M. oryzae* are preferentially associated with one or very limited host genera. Studies to define the factors delimiting host-species specificity have established that recognition of effectors by a few resistance genes is the major player that determines host range dynamics in *M. oryzae*. For instance, the *PWL* effector gene family conditions pathogenicity towards weeping lovegrass (*Eragrostis*

curvula) (Kang et al., 1995). Rice isolates of *M. oryzae* carrying *PWL2* and *Eleusine* isolates that have *PWL1* are restricted from infecting *E. curvula* (Kang et al., 1995; Sweigard et al., 1995). Likewise, the genes *PWT1* and *PWT2* are involved in conferring avirulence of *Setaria* and rice-infecting isolates on wheat. *Lolium* isolates are conditioned by *PWT3* from infecting wheat, and *Avena* isolates that carry *PWT3* and *PWT4* are also avirulent on this cereal (Murakami et al., 2000; Takabayashi et al., 2002; Tosa et al., 2006; Chuma et al., 2010; Inoue et al., 2017). This suggests that host species specificity in *M. oryzae* is mostly ruled by the gene-for-gene model of compatible and incompatible interactions (Takabayashi et al., 2002). Loss of virulence effectors has been shown to play a critical role in host jump events. This was the case of the devastating emergence of wheat blast, attributed to the deployment of wheat varieties lacking *Rwt3*—the resistance gene against *PWT3* present in *Lolium*-infecting isolates—which served as springboard for the host jump of *Lolium* isolates to wheat. *Lolium* isolates that were now virulent on *rwt3* wheat subsequently acquired loss-of-function alleles of *PWT3* and gained further pathogenicity in most wheat populations regardless of the presence of *Rwt3* (Inoue et al., 2017).

1.10 Plant pathogen effectors

Plant pathogens secrete effectors inside the intracellular plant space or in the apoplastic space to modulate the cell biology of the host, suppress plant immunity, promote host colonisation, and support pathogen growth (Win et al., 2012). Expression of effectors is usually tightly regulated according to different infection stages. Findings of a recent time course study in *M. oryzae* clearly illustrated this by showing that groups of effectors are temporally co-regulated during different infection stages (Yan et al., 2023). Most well-characterised effectors are cell-wall degrading enzymes, protease inhibitors, disruptors of hormone or immune signalling pathways, interactors of the ubiquitin-proteasome system, protectors from plant hydrolytic enzymes, transcriptional re-programmers among others (Hogenhout et al., 2009; Win et al., 2012; Sánchez-Vallet et al., 2018).

While being exposed to host recognition, effectors are in the battlefront of the evolutionary arms race between plants and pathogens. As a result, fluctuating positive and negative selective pressures on effectors lead to their rapid constant evolution. Host specialisation is greatly determined by the effector repertoire (Sánchez-Vallet et al., 2018). Pathogens are under the constant pressure to escape host recognition while maintaining virulence on a given host (Dong and Ma, 2021). This is achieved by constant effector

modification, deletion, alteration of expression and even gain of novel genes (Sánchez-Vallet et al., 2018). Several effectors within a species have been shown to be redundant and act on similar host processes (Win et al., 2012). Such redundancy plays a role in bet-hedging by pathogens and is mainly derived from gene duplication events (Ghosh and O'Connor, 2017). This guarantees that if a given effector becomes recognised by its host, losing it will not compromise the ability of the pathogen to cause disease (Birch et al., 2008; Thordal-Christensen et al., 2018).

Most effectors have low to no sequence similarity to known proteins or protein domains. Yet, increasing evidence shows the prevalence of unrelated effectors that share structural similarities, and the convergent evolution of unrelated effectors from distinct pathogens to target conserved host processes (Franceschetti et al., 2017). A recent study that modelled the structure of the secreted proteins from several agriculturally important fungal pathogens found common effector folds that are present across several fungal species, as well as lineage-specific structurally similar effector families that uniquely expanded in obligate biotrophs such as *Bgh*. Duplication events and rapid divergence were proposed as the main drivers of the emergence of groups of effectors with similar folds (Seong and Krasileva, 2023). One of the most common examples of sequence unrelated effectors that share a similar fold are the MAX (*Magnaporthe* Avrs and ToxB-like) effectors. Effectors within this group form a six-stranded β-sandwich with two antiparallel β-sheets (de Guillen et al., 2015). The family of MAX effectors is one of the most highly expanded in the fungal pathogens *M. oryzae* and *Venturia inequalis,* and is also present in *Colletotrichum* species (de Guillen et al., 2015; Rocafort et al., 2022; Seong and Krasileva, 2023). Interestingly, several *M. oryzae* MAX effectors such as AVR-Pik, AVR-Pia, AVR1-CO39, AVR-Mgk1 commonly bind proteins in rice containing an HMA domain (De la Concepcion et al., 2018; Guo et al., 2018a; Białas et al., 2021; Maidment et al., 2021; Sugihara et al., 2023). Other examples of effector families with common folds are the RNAse-like effector family highly expanded in *Bgh* (Pedersen et al., 2012; Spanu, 2017) and the Fol dual-domain (FOLD) effector family in *Fusarium oxysporum* f. sp. *lycopersici* (Yu et al., 2022).

As previously mentioned, effectors are under constant pressure to evade recognition by host immune receptors. As a consequence, some avirulence genes have high rates of polymorphic changes in key surface-exposed residues that might escape detection (Białas et al., 2018; Upson et al., 2018; Ortiz et al., 2022). This is the case of AVR-Pik, an effector that has evolved to escape recognition by the Pik NLR pair in rice.

Allelic variants of AVR-Pik have very few amino acid polymorphisms and all are located at the binding interface with the HMA ID of the Pik-1 sensor (De la Concepcion et al., 2018). In addition, effectors can also exhibit presence/absence variation that correlates with host specificity and adaptation (Fouché et al., 2018). This principle rules the host range dynamics of *M. oryzae,* as illustrated, for instance, by the absence of the effector AVR1-CO39 in the rice-infecting lineage of this pathogen, largely due to the presence of the corresponding Pi-CO39 resistance gene (also known as the RGA4-RGA5 NLR pair) in cultivated rice (Zheng et al., 2010; Cesari et al., 2013).

1.11 Aims of the thesis

In this study, I delve into the functional diversification of *Mla* in barley by focusing on the recognition of the highly divergent fungal pathogens *Bgh* and *M. oryzae* by the *Mla3* allele. The main objective of this thesis was to molecularly characterise *Mla3*-mediated resistance against blast as a means to shed light on this case of multiple pathogen recognition. In chapter 3, I aimed to identify the *M. oryzae* gene underlying *AVR-Rmo1,* the blast effector recognised by *Mla3*. A forward genetics screen on *M. oryzae* revealed that *AVR-Rmo1* is *PWL2,* a previously characterised effector that conditions pathogenicity of *M. oryzae* towards weeping lovegrass. Using a set of naturally occurring isolates representing *PWL2* natural variation, I established that *Mla3* in barley and an unknown *R* gene in weeping lovegrass recognise *PWL2* with conserved specificity. The lack of a clear *Mla* (*RGH1*) orthologue in weeping lovegrass suggests that both barley and weeping lovegrass convergently evolved to recognise the same effector from *M. oryzae*.

In chapter 4, I sought to define the principles governing specificity of *PWL2* recognition by *Mla3* by leveraging natural variation in *Mla*. I generated chimeric versions of *Mla3* based on the closest *Mla* allele that does not recognise *PWL2* in order to narrow down the region(s) that define specificity of recognition. I found that an eight amino acid window in the C-terminus of *Mla3* is required for *PWL2* recognition, and a basic residue within this region is critical to maintain effector recognition.

In chapter 5, I aimed to establish the molecular mechanism of *PWL2* recognition by *Mla3*. I used protein–protein interaction assays to address whether Mla3 directly recognises Pwl2, as suggested for other *Mla–AVR*$_a$ pairs, or indirectly, similar to recognition of multiple pathogens by the *Arabidopsis* NLR ZAR1. By testing binding in three different biological systems, I found that Mla3 interacts with Pwl2 through its C-

terminus, indicating direct effector recognition. Furthermore, using structure prediction tools, I modelled the structure of the C-terminus of Mla3 in complex with Pwl2 and found that it largely resembles the structure of Pwl2 bound to OsHIPP43, an HMA-containing protein in rice targeted by this MAX effector. These findings suggest that Mla3 evolved to recognise Pwl2 by mimicking the binding interface of a Pwl2 host target.

Finally, in chapter 6, I explored *Mla3* natural variation in barley to understand the principles of functional resistance against blast and powdery mildew conferred by *Mla3*. I found that *Mla3* copy number correlates with expression levels, and multiple copies are required for functional disease resistance. Based on allelic diversity, I hypothesised that polymorphisms in certain *Mla3*-related alleles overcome the requirement of high expression whilst maintaining effector recognition. I discuss the potential implications of these findings in *Mla3* function and evolution.

Overall, this work provides insights into the mechanisms that may have driven multiple pathogen recognition by *Mla3* and contributes to our understanding of the functional diversification of the *Mla* allelic series. Although the gene underlying AVR_{a3}—the *Bgh* effector recognised by *Mla3*—remains unknown, the findings of this work lay the foundation to formulate hypotheses for the speedy identification of this effector and advance the molecular disentanglement of recognition of unrelated effectors by *Mla3*.

Chapter 2: Materials and Methods

2.1 Plant material

Barley accessions used in this work (listed in **Table A.I.1**) were obtained from John Innes Centre (Norwich, UK), the United Stated Department of Agriculture Agricultural Research Service National Small Grains Collection (Aberdeen, ID, US), Oregon State University, (Corvallis, OR, US) and IPK Gene Bank Leibniz Institute (Gatersleben, Germany). *Eragrostis curvula* was obtained from Star Seed, Inc. (Kansas, USA). All seedlings used in infection assays and *Nicotiana benthamiana* plants used for agroinfiltration experiments were grown in a controlled environment at 25°C, under a 16/8 h light/dark cycle and 45-65% humidity, unless stated otherwise.

2.2 Propagation and growth of *Magnaporthe oryzae*

Magnaporthe oryzae isolates used in this study (listed in **Table A.I.2**) were obtained from the group of Ryohei Terauchi (Iwate Biotechnology Research Centre, Kitakami, Iwate, Japan). All isolates were grown on Complete Medium (CM) agar plates (10 g/L D-glucose, 2 g/L tryptone, 1 g/L yeast extract, 5% (v/v) nitrate salts, 0.1% trace elements (22 mg/L zinc sulphate heptahydrate, 11 mg/L boric acid, 5 mg/L manganese (II) chloride tetrahydrate, 5 mg/L iron (II) sulphate heptahydrate, 1.7 mg/L cobalt (II) chloride hexahydrate, 1.6 mg/L copper (II) sulphate pentahydrate, 1.5 mg/L sodium molybdate dehydrate, 50 mg/L ethylenediaminetra-acetic acid), 0.1 % (v/v) vitamin supplement (0.001 g/L biotin, 0.001 g/L pyridoxine, 0.001 g/L thiamine, 0.001 g/L riboflavin, 0.001 g/L, 0.001 g/L nicotinic acid), 1 g/L casamino acids, pH adjusted to 6.5 with NaOH, and 15 g/L agar). *Magnaporthe oryzae*-inoculated plates were incubated at 25°C under a 12 h light/dark cycle. For long term storage, isolates were grown over sterile Whatman filter paper (GE Healthcare Whatman™ Qualitative Filter Paper, Fisher Scientific UK) placed on top of CM agar plates. Filter papers were subsequently dehydrated and stored at -20°C.

2.3 Pathogenicity assays

2.3.1 Infection assays with *M. oryzae*

M. oryzae conidia were collected from mycelia grown on CM plates by adding 5 mL of distilled water to the surface and gently scraping with the bottom of a sterile 1.5 mL microcentrifuge tube. The suspension was filtered through sterile Miracloth™ and centrifuged at 5000x*g* for 10 min at room temperature. The supernatant was discarded, and the conidia pellet was resuspended in 5 mL of 0.2% (w/v) gelatin. Conidia concentration was determined using a haemocytometer and adjusted to $1x10^5$ conidia mL^{-1}. For leaf drop inoculations on barley, the first leaf of 7-day old seedlings was detached and placed on agar boxes (5 g/L agar-agar, 0.1 g/L benzimidazole). Each leaf was inoculated with 3 to 4 drops of 5 µL of the conidial suspension. Agar boxes with inoculated barley leaves were placed in a growth cabinet at 25°C and a 16/8 h light/dark cycle. Infection phenotypes were recorded 7 days post inoculation (dpi). For spray infections on *E. curvula,* 10-day old seedlings were evenly sprayed with the conidia suspension using an airbrush (Badger, USA). Infected seedlings were covered in polythene bags and kept in a growth cabinet at 25°C and a 16/8 h light/dark cycle. Infection phenotypes were recorded 7 days post inoculation (dpi).

2.3.2 Infection assays with *Blumeria graminis* f. sp. *hordei* (*Bgh*)

Bgh isolate BM20/1/11 (AVR_{a3}) was obtained from NIAB (Cambidge, UK). Barley seedlings for infection assays with *Bgh* were grown in a containment greenhouse with a day period of 16 h at 18°C, and a dark period of 8 h at 12°C. *Bgh* inoculum was maintained by iterative inoculations of the susceptible barley accession Manchuria. Inoculation of barley accessions of interest was done by gently shaking infected Manchuria plants on top of pots that were laying on their side with one-week old seedlings. The same procedure was done on the opposite side of the pots. Infected plants were kept in the containment greenhouse and phenotypes were recorded 7 dpi.

2.4 Molecular biology methods with *M. oryzae*

2.4.1 *M. oryzae* protoplast purification

Protoplast from *M. oryzae* were obtained as previously described (Talbot et al., 1993). Briefly, the region of active fungal growth was cut from the surface of a CM agar

plate, blended in 150 mL of CM liquid media, and incubated for 48 h at 25°C and 120 rpm. The liquid culture was filtered through sterile Miracloth™ and excess moisture was removed by pressing with sterile paper towel. Mycelium was transferred to a 50 mL centrifugation tube and gently resuspended and digested with 5 % Glucanex™ in 0.7 M NaCl (pH 5.5, filter sterilized). The mycelium suspension was incubated at 25°C for 3 h under gentle shaking at 75 rpm. The digested mycelium was filtered through sterile Miracloth™ and protoplasts were collected from the pellet after centrifugation for 10 min at 4°C and 3500x*g*.

2.4.2 *M. oryzae* high molecular weight genomic DNA extraction

High molecular weight genomic DNA extraction from protoplasts of *M. oryzae* was performed for Oxford Nanopore Technologies (ONT) DNA sequencing of the isolates KEN54-20 and Ina87T-156A. Extraction of high molecular weight DNA was carried out as previously described by (Schwessinger and Rathjen, 2017) with some modifications. Briefly, 10 mL of lysis buffer was prepared as follows: 2.5 mL of autoclaved buffer A (0.35M Sorbitol, 0.1M Tris-HCl, 5mM EDTA pH 8.0), 2.5 mL of autoclaved buffer B (0.2M Tris-HCL, 50mM EDTA pH8.0, 2M NaCl, 2% CTAB), 1 mL of filter-sterilized buffer C (5% Sarkosyl N-lauroylsarcosine sodium salt), 1 mL of 10% Polyvinylpyrrolidone 40, 1 mL of 10% Polyvinylpyrrolidone 10 and 10 uL of RNAse A (ThermoFisher Scientific). The pellet containing protoplasts was thoroughly resuspended in 10 mL of preheated lysis buffer and incubated under constant rotation for 30 min at room temperature. 250 uL of Proteinase K (New England BioLabs) was added to the sample and further incubated under permanent rotation for another 30 min, followed by 5 min on ice. The sample was mixed with 2 mL of 5M potassium acetate, incubated on ice for no longer than 5 min and centrifuged for 12 min at 4°C and 5000x*g*. The supernatant was transferred and mixed with 10 mL of phenol:chloroform:isoamyl alcohol (P:C:I) (25:24:1). After mixing by inversion for 2 min, the sample was centrifuged at 4°C and 4000x*g* for 10 min. The supernatant was recovered and mixed once more with 10 mL of P:C:I, followed by centrifugation at 4°C and 4000x*g* for another 10 min to separate the organic phase and remove proteins. The supernatant was mixed by inversion with 1 mL of 3M sodium acetate. One mL of isopropanol was added subsequently. The sample was incubated at room temperature for 5 min and centrifuged at 4°C and 8000x*g* for 30 min. The supernatant was discarded and the DNA, visible as a translucent pellet at the bottom, was washed with 70% ethanol and then centrifuged at 5000x*g* for 5 min. Four

more additional washing steps with 70% ethanol were performed, with the final two spins at 13000x*g*. The ethanol was discarded, and the DNA pellet was let to air-dry for 5 min. The DNA was resuspended in molecular grade water and let to dissolve at room temperature. The sample was treated with RNAse A (ThermoFisher Scientific) and column-purified using the Genomic DNA Clean and Concentrator Kit (Zymo Research) according to the manufacturer's instructions. DNA concentration was measured using the Qubit™ dsDNA HS Assay Kit (ThermoFisher Scientific).

2.4.3 Oxford Nanopore DNA sequencing

The high molecular weight gDNA library of the *M. oryzae* isolates KEN54-20 and Ina87T-156A was prepared without shearing to maximize sequencing read length. Short DNA fragments were removed with the Short Read Eliminator Kit (Circuloromics®) according to the manufacturer's instructions. DNA repair, end-prep, adapter ligation and clean-up were performed according to the 1D Lambda Control Experiment (SQK-LSK109) protocol provided by Oxford Nanopore Technologies (ONT). The libraries were loaded into R9.4.1 FLO-MIN106 flow cells and MinION sequencing was performed according to ONT guidelines using the ONT MinKNOW software.

2.4.4 *M. oryzae* DNA extraction for short read sequencing

For Illumina sequencing of genomic DNA, mycelia from one-week-old plates of *M. oryzae* isolates KEN54-20 and *avr-Rmo1* mutants were collected, ground with liquid nitrogen to a fine powder using a mortar and pestle, and transferred into 1.5 mL microcentrifuge tube until about two thirds full. 500 uL of preheated CTAB buffer (0.2 M Tris-HCl pH 7.5, 50 mM EDTA, 2 M NaCl, 2% (w/v) CTAB) pH 7.5 were added and samples were incubated at 65°C for 30 min, gently mixing every 10 min. Subsequently, 500 uL of chloroform:isoamyl alcohol (24:1) were added and samples were incubated for 30 min under constant shaking at 300 rpm, followed by centrifugation at 16000x*g* for 10 min. The supernatant was transferred into a new 1.5 mL microcentrifuge tube and 500 uL of chloroform:isoamyl alcohol (24:1) were added, mixed for 5 min, and then centrifuged at 16000x*g* for another 10 min. The top aqueous phase was transferred to a new tube and 1mL of ice-cold isopropanol was added and mixed. Samples were incubated at -20°C for 2 h and then centrifuged at 16000x*g* for 10 min. The supernatants were discarded. DNA pellets were allowed to drain for five min and were subsequently resuspended in 500uL of sterile water. 50 uL of 3 M NaOAc were added with 1 mL of

ice-cold 100% ethanol, followed by incubation at -20°C for one hour and centrifugation at 16000x*g* for 20 min. The supernatants were discarded and 400 uL of ice-cold 70% ethanol were added. The samples were centrifuged at 16000x*g* for 5 min, the supernatants were discarded, and the pellets were allowed to air-dry. DNA samples were resuspended in 100 uL of TE+RNAse A (ThermoFisher Scientific) and stored at 4°C. Concentration of DNA samples were measured using the Qubit™ dsDNA HS Assay Kit (Thermo FisherScientific). DNA samples were submitted for library preparation and whole genome sequencing by Illumina to Novogene. The isolate KEN54-20 was sequenced with paired end, 150 bp reads with libraries of 400 bp and 600 bp inserts, and KEN54-20 *avr-Rmo1* mutants were sequenced with paired end, 150 bp reads with libraries of 400 bp inserts.

2.4.5 *M. oryzae* protoplast transformation

Transformation of *M. oryzae avr-Rmo1* mutants was performed using protoplast as starting material as previously described (Talbot et al., 1993). The protoplasts pellet obtained as described in section 2.4.1 was gently washed with 50 mL of cold STC buffer (1.2 M sorbitol, 10 mM Tris-HCl pH 7.5, 10 mM $CaCl_2$), centrifuged at 3500x*g* for 10 min, resuspended in 150 μL of cold STC buffer and transferred to a 1.5 mL microcentrifuge tube. Transformation was performed by mixing the protoplasts with 4 μg of the vector pCB1532::*pPWL2:PWL2:tPWL2* (provided by Dr. Vincent Were from the Talbot lab), incubating at room temperature for 15 min, and subsequently adding 1 mL of PTC buffer (60% (v/v) PEG 4000, 10 mM Tris-HCl pH 7.5, 10 mM $CaCl_2$). The mix was let to stand for 5 min at room temperature and added to BDCM liquid medium (0.8 M sucrose, 1.7 g/L yeast nitrogen base without amino acids and ammonium sulphate, 2 g/L Ammonium nitrate, 1 g/L asparagine, 10 g/L glucose). The transformed protoplasts in the BDCM medium were let to recover by overnight incubation at 25°C and 120 rpm. The protoplast culture was added to molten BDCM agar and poured onto plates. Selective BDCM media (BDCM media lacking glucose) with 1% agar and sulfonylurea (150 μg/mL Chlorimuron ethyl) was added on top as overlay. Plates were incubated at 25°C for 7-10 days until transformed colonies emerged and started to grow. Individual colonies were transferred to BDCM agar plates with 100 μg/mL sulfonylurea and kept for confirmation by PCR and further assays. *PWL2*-transformed colonies were confirmed by PCR using the primers listed in **Table 2.1**.

Table 2.1 Primers used to confirm *PWL2* complementation of *avr-Rmo1 M. oryzae* mutants.

Primer name	Sequence	Purpose in this study	Source
PWL2ORF	*ATGAAATGCAACAACATCATCCTCCC*	Confirm *PWL2* complementation	Were, 2018
PWL2ORR	*ACATAATATTGCAGCCCTCTTCTCGC*	Confirm *PWL2* complementation	Were, 2018

2.5 Computational analysis for the identification of *AVR-Rmo1*

2.5.1 Genome assembly

Base calling of ONT sequencing data was performed with Guppy v3.2.2. Read quality assessment was performed using Pauvre (https://github.com/conchoecia/pauvre) and trimmed using NanoFilt (Li et al., 2009). The hybrid assembler MaSuRCA v3.3.3 (Zimin et al., 2013) was used with default parameters to assemble the reference genome of *M. oryzae* isolate KEN54-20 including ONT and Illumina data. Pilon (Walker et al., 2014) was used to improve the genome assembly. Alignment of Illumina reads to ONT data was performed using BWA (v0.7.12-r1039; http://bio-bwa.sourceforge.net/). Quality of the assembled and polished genome was assessed using the *k*-mer Analysis Toolkit (KAT; https://github.com/TGAC/KAT). *Ab initio* gene prediction was performed using Augustus (v3.3.2; https://github.com/Gaius-Augustus/Augustus) with the *M. oryzae* species gene model prediction. Genome assembly and annotation completeness were assessed with BUSCO v3 (Waterhouse et al., 2018). The *PWL2* region was investigated manually by aligning ONT reads to the reference genome using minimap2 (v2.17-r954-dirty). Illumina reads of *M. oryzae* KEN54-20 wild-type and *avr-Rmo1* mutants were aligned to the genome using BWA. Aligned reads were inspected using IGV (v2.5.3) (Robinson et al., 2011). A full set of commands are available on Github (https://github.com/matthewmoscou/AvrRmo1).

2.5.2 Identification of shared mutations in *M. oryzae avr-Rmo1* mutants

The *k*-mer analysis toolkit (KAT; v2.4.1) was used to scan the genome to identify *k*-mers (k=27) that were present in wild-type but absent in all *avr-Rmo1* mutants. A genome scan was performed by counting the number of *k*-mers present in wild-type and absent in all mutants within a window of 10 kb with step size 1 kb.

2.6 General molecular biology methods

2.6.1 Polymerase chain reaction (PCR) and PCR product purification

Amplification of DNA fragments through PCR was done using Phusion™ High-fidelity DNA polymerase (ThermoFisher Scientific) according to the manufacturer's instructions. Annealing temperatures were optimised for each reaction based on the primer combination and were calculated using the Tm calculator tool from ThermoFisher Scientific. The elongation time in each cycle was 30 s/kb. PCR products were run through a 1% (w/v) agarose gel in 1X Tris-borate EDTA (TBE) buffer (0.09 M Tris-borate, 2 mM EDTA) stained with ethidium bromide for visualisation under UV-light. Bands corresponding to the desired PCR products for cloning were excised from the agarose gel and purified using the NucleoSpin Gel and PCR Clean-up kit (Macherey-Nagel) according to the manufacturer's protocol.

2.6.2 Golden Gate cloning

All constructs generated in this work were assembled using Golden Gate cloning. The protocol implemented was modified from the literature (Weber et al., 2011). For level 0 constructs, the restriction-ligation reactions were prepared by mixing 100 ng of the PCR product of interest and the desired level 0 acceptor backbone, 2 U (units) of *BpiI* (ThermoFisher Scientific), 4 U of T4 DNA ligase (New England Biolabs), 1X T4 DNA ligase buffer (New England Biolabs), 1X BSA (New England Biolabs), and nuclease-free water up to a final volume of 15 μL. Level 1 assemblies were done by mixing 100 ng of the desired level 1 acceptor plasmid, 100 ng of each of the level 0 modules, 2 U of *BsaI*-HF (New England Biolabs), 4 U of T4 DNA ligase (New England Biolabs), 1X T4 DNA ligase buffer (New England Biolabs), 1X BSA (New England Biolabs), and nuclease-free water up to a final volume of 15 μL. The assembly reaction was incubated at 37°C for 20 s, followed by 26 cycles of 3 min at 37°C and 4 min at 16°C, then 5 min at 50°C, and a final step of 5 min at 80°C.

2.6.3 Bacterial transformation

Transformation of *E. coli* DH5α competent cells was done by mixing 50 μL of competent cells with 5 μL of the desired Golden Gate cloning reaction, followed by incubation on ice for 5 min and heat shock at 42°C for 30 s. The cells were immediately incubated on ice for 2 min, and mixed with 300 μL of lysogeny broth (LB) medium to

recover at 37°C and 190 rpm for 45 minutes. One third of the cells was plated on solid LB medium with the appropriate antibiotics (50 μg/mL kanamycin, 50 μg/mL spectinomycin, 100 μg/mL carbenicillin) and incubated overnight at 37°C. Blue-white screening for colony selection was performed by adding 1mM IPTG (isopropyl β-D-1-thiogalactopyranoside) and 50 μg/mL X-gal to LB agar plates when required. Co-transformation of *E. coli* SHuffle cells for recombinant protein production was performed by following a similar protocol, but adding 1 μL of each of the assembled pOPIN constructs containing the genes of interest.

Transformation of *Agrobacterium tumefaciens* GV3101::pMP90 was done by electroporation. Briefly, electrocompetent cells were mixed with the construct of interest and transferred to a prechilled electroporation cuvette of 1 mm width. The cuvette was then placed in an electroporator (BioRad) with the following settings: voltage = 1.8 kV, capacitance = 25 μF, resistance = 200 Ω. Following electroporation, 700 μL of LB medium were immediately added to the cells, which were then incubated for one hour at 28°C and 190 rpm. The cells were plated on solid LB medium with the appropriate antibiotics (100 μg/mL carbenicillin, 100 μg/mL rifampicin and 10 μg/mL gentamycin) and incubated for 48 h at 28°C.

2.6.4 Colony PCR and plasmid preparation

Colony PCR was performed with GoTaq® G2 DNA polymerase (Promega) using the 5X Green GoTaq® Reaction buffer following the manufacturer's instructions. Plasmid extraction was carried out using the NucleoSpin Plasmid kit (Macherey-Nagel) according to the manufacturer's protocol.

2.7 Molecular cloning

2.7.1 *Mla* alleles, mutant versions, and truncations

The CDS of *Mla3* (UZM07847.1) from the barley accession Baronesse previously established by the Moscou lab at The Sainsbury Laboratory (TSL) (Norwich, UK) (Brabham, 2019) was domesticated to remove internal *BsaI* and *BpiI* restriction sites, and synthesised by Twist Bioscience (San Francisco, CA, USA). The synthesised gene fragments had *BpiI* adaptors for Golden Gate assembly into the level 0 acceptor plasmid pICH41308 (TSL SynBio). The *Mla3* CDS was amplified using the primers listed in

Table 2.2 to clone it without a stop codon into the level 0 acceptor plasmid pICSL01005 (TSL SynBio) by Golden Gate assembly. The coding sequences of *Mla23*, *Mla34*, *Mla35* and *Mla39* (Seeholzer et al., 2010) were codon optimised for expression in *N. benthamiana*. These genes and the coding sequences of *Mla-WBDC233* and *Mla-WBDC221* were domesticated to remove internal *BsaI* and *BpiI* restriction sites, synthesised without stop a codon and cloned by Twist Bioscience (San Francisco, CA, USA). Synthesised genes were cloned in the pTwist_Kan_High_Copy cloning vector (Twist Bioscience) with flanking *BsaI* restriction sites for subsequent level 1 Golden Gate assemblies.

Mla3 truncations to clone single domains, combinations of domains or the C-terminus variants (Mla3_V874 and Mla3_V911) were amplified using the primers listed in **Table 2.2**. PCR fragments were purified and cloned into the level 0 acceptor plasmid pICSL01005 (TSL SynBio) using Golden Gate cloning.

Table 2.2 List of primers used to clone Mla3 wild type and Mla3 truncations.

Primer name	Sequence	Purpose in this study	Source
Mla3_fw	*AGAAGACAAAATGGATATTGTCACC GGTGCC*	Golden Gate cloning of Mla3	This study
Mla3_NS_rv	*AAGAAGACAACGAACCGAAATCAGT CCACTCCTC*	Golden Gate cloning of Mla3	This study
Mla3_CC_rv	*AAGAAGACAACGAACCCAAAGCTC GAAGGCAAGGGTC*	Golden Gate cloning of Mla3 truncation	This study
Mla3_NBARC_fw	*AAGAAGACAAAATGTATGCTGAAGC GACAGAGCTAG*	Golden Gate cloning of Mla3 truncation	This study
Mla3_NBARC_rv	*AAGAAGACAACGAACCAGGCCTGG CTTGATGATC*	Golden Gate cloning of Mla3 truncation	This study
Mla3_LRR_fw	*AAGAAGACAAAATGTTCACAGATAT CAAGAGTATG*	Golden Gate cloning of Mla3 truncation	This study
Mla3_V874_fw	*AAGAAGACAAAATGGTCCGGGTGG CTAAAGAGGATGG*	Golden Gate cloning of Mla3 truncation	This study
Mla3_V911_fw	*AAGAAGACAAAATGGTTGGTGAGGC CAAGGAGGCGGAGGCTG*	Golden Gate cloning of Mla3 truncation	This study

The Mla3 mutants $Mla3^{F99E}$, $Mla3^{H501Q}$, $Mla3^{H501G}$, and $Mla3^{D502V}$ were generated by site directed mutagenesis on Mla3 using fusion PCR to amplify and fuse one fragment upstream and one fragment downstream of the desired mutation using the primers listed in **Table 2.3**. The final PCR products containing the desired mutation were cloned into the level 0 acceptor plasmid pICSL01005 (TSL SynBio) using Golden Gate cloning. $Mla3^{L11E}$, Mla3Δ6 and Mla-HOR21599 were generated by doing site directed mutagenesis on Mla3 by inverse PCR using the primers listed in **Table 2.3**, followed by *BpiI* digestion and ligation using the Golden Gate protocol.

Table 2.3 List of primers for site directed mutagenesis of Mla3.

Primer name	Sequence	Purpose in this study	Source
Mla3_fw	*AGAAGACAAAATGGATATTGTCACC GGTGCC*	Golden Gate cloning of Mla3 mutants by fusion PCR	This study
Mla3_NS_rv	*AAGAAGACAACGAACCGAAATCAG TCCACTCCTC*	Golden Gate cloning of Mla3 mutants by fusion PCR	This study
Mla3_F99E_fw	*CTGATGATAACAACAACAAAGAGAA GGGGCTCATGAAGAGGAC*	$Mla3^{F99E}$ site directed mutagenesis by fusion PCR	This study
Mla3_F99E_rv	*GTCCTCTTCATGAGCCCCTTCTCTT TGTTGTTGTTATCATCAG*	$Mla3^{F99E}$ site directed mutagenesis by fusion PCR	This study
Mla3_H501Q_fw	*CATATGCTTGCCGTGTACAGGATAT GGTTCTGGACCTTAT*	$Mla3^{H501Q}$ site directed mutagenesis by fusion PCR	This study
Mla3_H501Q_rv	*ATAAGGTCCAGAACCATATCCTGTA CACGGCAAGCATATG*	$Mla3^{H501Q}$ site directed mutagenesis by fusion PCR	This study
Mla3_H501G_fw	*GCATATGCTTGCCGTGTAGGTGATA TGGTTCTGGACCTTAT*	$Mla3^{H501G}$ site directed mutagenesis by fusion PCR	This study
Mla3_H501G_rv	*ATAAGGTCCAGAACCATATCACCTA CACGGCAAGCATATGC*	$Mla3^{H501G}$ site directed mutagenesis by fusion PCR	This study
Mla3_D502V_fw	*CATATGCTTGCCGTGTACATGTAAT GGTTCTGGACCTTATCTG*	$Mla3^{D502V}$ site directed mutagenesis by fusion PCR	This study
Mla3_D502V_rv	*GTCCAGAACCATTACATGTACACG GCAAGCATATG*	$Mla3^{D502V}$ site directed mutagenesis by fusion PCR	This study
Mla3_L11E_fw	*AAGAAGACAACGAGATTCCCAAGT TGGGGGAGCT*	$Mla3^{L11E}$ site directed mutagenesis by inverse PCR	This study
Mla3_L11E_rv	*AAGAAGACAACTCGTTGGAAATGG CACCGGTGAC*	$Mla3^{L11E}$ site directed mutagenesis by inverse PCR	This study
Mla3delta6_L0_fw	*AAGAAGACAAGGCTTCAGTTGGTG TGTTGC*	Cloning of Mla3Δ6 by inverse PCR	This study
Mla3delta6_L0_rv	*AAGAAGACAAAGCCTGACAGCCAA CTAAATTTAG*	Cloning of Mla3Δ6 by inverse PCR	This study
Mla3_S671P_L0_rv	*AAGAAGACAACAGAGACACCAAGA TACCACTCAACACTTCTATGGATGT CAGATTTTGCAACACACCAACTGGA GGAACCACCTGACAGCCAAC*	Cloning of Mla-HOR21599 by inverse PCR	This study
Mla3_L710F_L0_fw	*AAGAAGACAATCTGAACATTATTGC ACAAGAGCTTGGCAACTTGAAAAG GCTGAGGGAGCTTAACATTTTCTTC AATGATGGTAGTTTGG*	Cloning of Mla-HOR21599 by inverse PCR	This study

The $Mla3^{no\ C\text{-}term}$, $Mla3^{Swap1}$, $Mla3^{Swap2}$, $Mla23^{with\ C\text{-}term}$, $Mla23^{Swap1}$, and $Mla23^{Swap2}$ chimeras were generated by PCR using the primers listed in **Table 2.4** and pICSL01005:*Mla3* and pTwist_Kan_high_copy:*Mla23* as templates when appropriate. Purified PCR products were cloned into the level 0 acceptor plasmid pICSL01005 (TSL SynBio) using Golden Gate assembly. All level 0 and level 1 constructs were verified by DNA sequencing.

Table 2.4 List of primers to clone Mla3 and Mla23 chimeras.

Primer name	Sequence	Purpose in this study	Source
Mla3_fw	*AGAAGACAAAATGGATATTGTCACC GGTGCC*	Golden Gate cloning of Mla3 chimeras	This study
Mla23_fw	*AAGAAGACAAAATGGACATAGTGA CAGGGGCC*	Golden Gate cloning of Mla23 chimeras	This study
Mla3_no_Cterm_rv	*AAGAAGACAACGAACCCAAATCGT CATCATGAGCAC*	Golden Gate cloning of Mla3$^{\text{no C-term}}$	This study
Mla3_S1_rv	*AAGAAGACAACGAACCGAAATCAG TCCACTCCTCACACAAATCGTCATC ATGAGCACCTTTTGCTATACGTGGC CTCATCTGAATGCTGATTTGCGGGT GGTTAGGGTGTGCGTCCAAGGCAC GCCTCACCACAGC*	Golden Gate cloning of Mla3$^{\text{Swap1}}$	This study
Mla3_S2_rv	*AAGAAGACAACGAACCGAAATCAG TCCACTCCTCACAGAGGTCATCGT CCTGGGCTCCCTCTGCAATCGGGG GATGCATGAAGATAGCAATATAATA TACGTGCGGGTCAGC*	Golden Gate cloning of Mla3$^{\text{Swap2}}$	This study
Mla23_w_Cterm_rv	*AAGAAGACAACGAACCGAAATCAG TCCACTCCTCACAGAGGTCATCGT CCTGGGCTC*	Golden Gate cloning of Mla23$^{\text{with C-term}}$	This study
Mla23_S1_rv	*AAGAAGACAACGAACCCATGAGGT CATCGTCCTGGGCTCCCTCTGCAA TCGGGGGATGCATGAAGATAGCAA TATAATATACGTGCGGGTCAGCTTT CAGTGCTCTTCTTACAACAGCCTC*	Golden Gate cloning of Mla23$^{\text{Swap1}}$	This study
Mla23_S2_rv	*AAGAAGACAACGAACCCATCAAAT CGTCATCATGAGCACCTTTTGCTAT ACGTGGCCTCATCTGAATGCTGATT TGCGGGTGGTTAGGGTGTGC*	Golden Gate cloning of Mla23$^{\text{Swap2}}$	This study

2.7.1.1 Molecular cloning for transient expression *in planta*

All *Mla* alleles, mutants and truncations were cloned with the same modules into the level 1 binary acceptor plasmid pICH47732 (Addgene no. 4800) for transient gene expression in *N. benthamiana*. Constructs were generated by Golden Gate assembly with pICH85281 (mannopine synthase + Ω promoter (Mas Ω), Addgene no. 50272), pICSL50009 (6xHA C-terminal tag, Addgene no. 50309), and pICSL60008 (Arabidopsis heat shock protein terminator (AtHSP18 terminator), TSL SynBio).

The following Mla mutant versions were generated by inverse PCR using the primers listed in **Table 2.5** and the corresponding level 1 assembly containing the Mla allele of interest as template: Mla3$^{\text{Swap1a}}$, Mla3$^{\text{Swap1b}}$, Mla23$^{\text{Swap1a}}$, Mla23$^{\text{Swap1b}}$, Mla3$^{\text{K926D}}$, Mla23$^{\text{D926K}}$, Mla3$^{\text{D928H}}$, Mla23$^{\text{H928D}}$, Mla3$^{\text{H930N}}$, Mla23$^{\text{N930H}}$, Mla3$^{\text{V931H}}$, Mla23$^{\text{H931V}}$, Mla3$^{\text{Y932P}}$, Mla23$^{\text{P932Y}}$, Mla3$^{\text{Y933Q}}$, Mla23$^{\text{Q933Y}}$, Mla34$^{\text{D926K}}$, Mla35$^{\text{D926K}}$, Mla39$^{\text{E926K}}$. The PCR products were circularised by *BsaI* digestion and ligation using the protocol for Golden Gate assembly.

Table 2.5 List of primers to generate Mla3 and Mla23 Swap1 mutations.

Primer name	Sequence	Purpose in this study	Source
Mla3_S1a_fw	*AAGGTCTCAGACGCACACCCTCA CGTATATTATATTAGCATTCAG*	Mla3^{Swap1a} cloning by inverse PCR	This study
Mla3_S1a_rv	*AAGGTCTCACGTCCAAGGCACGC CTCACCACAG*	Mla3^{Swap1a} cloning by inverse PCR	This study
Mla23_S1a_fw	*AAGGTCTCAAAAGCTGACCCGAA CCACCCGCAAATCGCTATC*	Mla23^{Swap1a} cloning by inverse PCR	This study
Mla23_S1a_rv	*AAGGTCTCACTTTCAGTGCTCTTC TTACAACAGC*	Mla23^{Swap1a} cloning by inverse PCR	This study
Mla3_S1b_fw	*AAGGTCTCAAACCACCCGCAAAT TAGCATTCAGATGAGGCCAC*	Mla3^{Swap1b} cloning by inverse PCR	This study
Mla3_S1b_rv	*AAGGTCTCAGGTTCGGGTCAGCT TTCAAGGC*	Mla3^{Swap1b} cloning by inverse PCR	This study
Mla23_S1b_fw	*AAGGTCTCACACGTATATTATATC GCTATCTTCATGCATCCC*	Mla23^{Swap1b} cloning by inverse PCR	This study
Mla23_S1b_rv	*AAGGTCTCACGTGAGGGTGTGCG TCCAGTG*	Mla23^{Swap1b} cloning by inverse PCR	This study
Mla23_D926K_fw	*AAGGTCTCAAAAGCACACCCTAA CCACCCGC*	Mla23^{D926K} site directed mutagenesis by inverse PCR	This study
Mla23_D926K_rv	*AAGGTCTCACTTTCAGTGCTCTTC TTACAACAGC*	Mla23^{D926K} site directed mutagenesis by inverse PCR	This study
Mla3_K926D_fw	*AAGGTCTCAGACGCTGACCCGCA CGTATATTATA*	Mla3^{K926D} site directed mutagenesis by inverse PCR	This study
Mla3_K926D_rv	*AAGGTCTCACGTCCAAGGCACGC CTCACCACAG*	Mla3^{K926D} site directed mutagenesis by inverse PCR	This study
Mla23_H928D_fw	*AAGGTCTCAGACCCTAACCACCC GCAAATCGC*	Mla23^{H928D} site directed mutagenesis by inverse PCR	This study
Mla23_H928D_rv	*AAGGTCTCAGGTCTGCGTCCAGT GCTCTTCTTAC*	Mla23^{H928D} site directed mutagenesis by inverse PCR	This study
Mla3_D928H_fw	*AAGGTCTCACACCCGCACGTATA TTATATTAGCATTC*	Mla3^{D928H} site directed mutagenesis by inverse PCR	This study
Mla3_D928H_rv	*AAGGTCTCAGGTGAGCTTTCAAG GCACGCCTCACCACAGCC*	Mla3^{D928H} site directed mutagenesis by inverse PCR	This study
Mla23_N930H_fw	*AAGGTCTCACACCACCCGCAAAT CGCTATCTTC*	Mla23^{N930H} site directed mutagenesis by inverse PCR	This study
Mla23_N930H_rv	*AAGGTCTCAGGTGAGGGTGTGCG TCCAGTGC*	Mla23^{N930H} site directed mutagenesis by inverse PCR	This study
Mla3_H930N_fw	*AAGGTCTCAAACGTATATTATATTA GCATTCAGATGAGGC*	Mla3^{H930N} site directed mutagenesis by inverse PCR	This study
Mla3_H930N_rv	*AAGGTCTCACGTTCGGGTCAGCT TTCAAGGC*	Mla3^{H930N} site directed mutagenesis by inverse PCR	This study
Mla23_H931V_fw	*AAGGTCTCAGTACCGCAAATCGC TATCTTCATG*	Mla23^{H931V} site directed mutagenesis by inverse PCR	This study
Mla23_H931V_rv	*AAGGTCTCAGTACGTTAGGGTGT GCGTCCAG*	Mla23^{H931V} site directed mutagenesis by inverse PCR	This study
Mla3_V931H_fw	*AAGGTCTCACACTATTATATTAGC ATTCAGATGAGGCC*	Mla3^{V931H} site directed mutagenesis by inverse PCR	This study

Table 2.5 List of primers to generate Mla3 and Mla23 Swap1 mutations (continued).

Primer name	Sequence	Purpose in this study	Source
Mla3_V931H_rv	*AAGGTCTCAAGTGGTGCGGGTCA GCTTTCAAG*	Mla3^{V931H} site directed mutagenesis by inverse PCR	This study
Mla23_P932Y_fw	*AAGGTCTCATATCAAATCGCTATC TTCATGCATCC*	Mla23^{P932Y} site directed mutagenesis by inverse PCR	This study
Mla23_P932Y_rv	*AAGGTCTCAGATAGTGGTTAGGG TGTGCGTC*	Mla23^{P932Y} site directed mutagenesis by inverse PCR	This study
Mla3_Y932P_fw	*AAGGTCTCACCGTATATTAGCATT CAGATGAGGCCACGTATAGC*	Mla3^{Y932P} site directed mutagenesis by inverse PCR	This study
Mla3_Y932P_rv	*AAGGTCTCAACGGTACGTGCGGG TCAGCTTTC*	Mla3^{Y932P} site directed mutagenesis by inverse PCR	This study
Mla23_Q933Y_fw	*AAGGTCTCATATATCGCTATCTTC ATGCATCCC*	Mla23^{Q933Y} site directed mutagenesis by inverse PCR	This study
Mla23_Q933Y_rv	*AAGGTCTCATATACGGGTGGTTA GGGTGTG*	Mla23^{Q933Y} site directed mutagenesis by inverse PCR	This study
Mla3_Y933Q_fw	*AAGGTCTCACAAATTAGCATTCAG ATGAGGCCACGTATAGC*	Mla3^{Y933Q} site directed mutagenesis by inverse PCR	This study
Mla3_Y933Q_rv	*AAGGTCTCATTTGATATACGTGCG GGTCAGCTTTC*	Mla3^{Y933Q} site directed mutagenesis by inverse PCR	This study
Mla34_D926K_fw	*AAGGTCTCAAAGGCCCATTCCAA TCACCCAG*	Mla34^{D926K} site directed mutagenesis by inverse PCR	This study
Mla34_D926K_rv	*AAGGTCTCACCTTCAGTGCATGT CTGACAGC*	Mla34^{D926K} site directed mutagenesis by inverse PCR	This study
Mla35_D926K_fw	*AAGGTCTCAAAGGCACACCCTAA TCACCCAC*	Mla35^{D926K} site directed mutagenesis by inverse PCR	This study
Mla35_D926K_rv	*AAGGTCTCACCTTAAGGGCGCGC CTTACGGC*	Mla35^{D926K} site directed mutagenesis by inverse PCR	This study
Mla39_E926K_fw	*AAGGTCTCAAAGGCTCACCCGTC ACACCCTC*	Mla39^{E926K} site directed mutagenesis by inverse PCR	This study
Mla39_E926K_rv	*AAGGTCTCACCTTCAAAGCTCTC CTAAGTGC*	Mla39^{E926K} site directed mutagenesis by inverse PCR	This study

Substitution of residue K926 in Mla3 for all possible 19 amino acids was done by annealing pairs of oligos listed in **Table 2.6** containing the corresponding K926 mutation with flanking *BsaI* restriction sites. Briefly, matching oligos were mixed in equimolar concentrations and incubated at 95°C for 2 min and gradually cooled down to 25°C over 45 min. In parallel, the Mla3 sequence outside the region covered by the oligos and embedded in the level 1 assembly for transient expression was amplified by inverse PCR using the primers listed in **Table 2.6**. The purified PCR product and each pair of annealed oligos was assembled by Golden Gated cloning using *BsaI*.

2.7.1.2 Molecular cloning for yeast-two-hybrid experiments

The level 0 modules containing Mla3 or Mla3 truncations were cloned into the pGBKT7 level 1 acceptor (TSL SynBio) by Golden Gate assembly. The module pICSL50028 (no stop to stop, TSL SynBio) was used to add a stop codon when appropriate.

Table 2.6 List of oligos to generate Mla3 K926 mutations.

Primer name	Sequence	Purpose in this study	Source
Mla3_K926_PCR_fw	*AAGGTCTCATATTATATTAGC ATTCAGATGAGGCCACG*	Golden Gate cloning of Mla3^{K926} substitutions	This study
Mla3_K926_PCR_rv	*AAGGTCTCACACAGCCTCCG CTTCCTTTG*	Golden Gate cloning of Mla3^{K926} substitutions	This study
Mla3_K926R_fw	*AAGGTCTCATGTGGTGAGGC GTGCCTTGCGTGCTGACCCG CACGTATATTAGAGACCAA*	Mla3^{K926R} mutation	This study
Mla3_K926R_rv	*TTGGTCTCTAATATACGTGCG GGTCAGCACGCAAGGCACG CCTCACCACATGAGACCTT*	Mla3^{K926R} mutation	This study
Mla3_K926H_fw	*AAGGTCTCATGTGGTGAGGC GTGCCTTGCACGCTGACCCG CACGTATATTAGAGACCAA*	Mla3^{K926H} mutation	This study
Mla3_K926H_rv	*TTGGTCTCTAATATACGTGCG GGTCAGCGTGCAAGGCACG CCTCACCACATGAGACCTT*	Mla3^{K926H} mutation	This study
Mla3_K926S_fw	*AAGGTCTCATGTGGTGAGGC GTGCCTTGAGCGCTGACCCG CACGTATATTAGAGACCAA*	Mla3^{K926S} mutation	This study
Mla3_K926S_rv	*TTGGTCTCTAATATACGTGCG GGTCAGCGCTCAAGGCACG CCTCACCACATGAGACCTT*	Mla3^{K926S} mutation	This study
Mla3_K926T_fw	*AAGGTCTCATGTGGTGAGGC GTGCCTTGACTGCTGACCCG CACGTATATTAGAGACCAA*	Mla3^{K926T} mutation	This study
Mla3_K926T_rv	*TTGGTCTCTAATATACGTGCG GGTCAGCAGTCAAGGCACGC CTCACCACATGAGACCTT*	Mla3^{K926T} mutation	This study
Mla3_K926N_fw	*AAGGTCTCATGTGGTGAGGC GTGCCTTGAACGCTGACCCG CACGTATATTAGAGACCAA*	Mla3^{K926N} mutation	This study
Mla3_K926N_rv	*TTGGTCTCTAATATACGTGCG GGTCAGCGTTCAAGGCACGC CTCACCACATGAGACCTT*	Mla3^{K926N} mutation	This study
Mla3_K926Q_fw	*AAGGTCTCATGTGGTGAGGC GTGCCTTGCAGGCTGACCCG CACGTATATTAGAGACCAA*	Mla3^{K926Q} mutation	This study
Mla3_K926Q_rv	*TTGGTCTCTAATATACGTGCG GGTCAGCCTGCAAGGCACG CCTCACCACATGAGACCTT*	Mla3^{K926Q} mutation	This study
Mla3_K926C_fw	*AAGGTCTCATGTGGTGAGGC GTGCCTTGTGTGCTGACCCG CACGTATATTAGAGACCAA*	Mla3^{K926C} mutation	This study
Mla3_K926C_rv	*TTGGTCTCTAATATACGTGCG GGTCAGCACACAAGGCACGC CTCACCACATGAGACCTT*	Mla3^{K926C} mutation	This study
Mla3_K926G_fw	*AAGGTCTCATGTGGTGAGGC GTGCCTTGGGAGCTGACCCG CACGTATATTAGAGACCAA*	Mla3^{K926G} mutation	This study
Mla3_K926G_rv	*TTGGTCTCTAATATACGTGCG GGTCAGCTCCCAAGGCACGC CTCACCACATGAGACCTT*	Mla3^{K926G} mutation	This study
Mla3_K926P_fw	*AAGGTCTCATGTGGTGAGGC GTGCCTTGCCTGCTGACCCG CACGTATATTAGAGACCAA*	Mla3^{K926P} mutation	This study
Mla3_K926P_rv	*TTGGTCTCTAATATACGTGCG GGTCAGCAGGCAAGGCACG CCTCACCACATGAGACCTT*	Mla3^{K926P} mutation	This study
Mla3_K926A_fw	*AAGGTCTCATGTGGTGAGGC GTGCCTTGGCCGCTGACCCG CACGTATATTAGAGACCAA*	Mla3^{K926A} mutation	This study
Mla3_K926A_rv	*TTGGTCTCTAATATACGTGCG GGTCAGCGGCCAAGGCACG CCTCACCACATGAGACCTT*	Mla3^{K926A} mutation	This study
Mla3_K926V_fw	*AAGGTCTCATGTGGTGAGGC GTGCCTTGGTTGCTGACCCG CACGTATATTAGAGACCAA*	Mla3^{K926V} mutation	This study

Table 2.6 List of oligos to generate Mla3 K926 mutations (continued).

Primer name	Sequence	Purpose in this study	Source
Mla3_K926V_rv	*TTGGTCTCTAATATACGTGCG GGTCAGCAACCAAGGCACGC CTCACCACATGAGACCTT*	Mla3^{K926V} mutation	This study
Mla3_K926I_fw	*AAGGTCTCATGTGGTGAGGC GTGCCTTGATAGCTGACCCG CACGTATATTAGAGACCAA*	Mla3^{K926I} mutation	This study
Mla3_K926I_rv	*TTGGTCTCTAATATACGTGCG GGTCAGCTATCAAGGCACGC CTCACCACATGAGACCTT*	Mla3^{K926I} mutation	This study
Mla3_K926L_fw	*AAGGTCTCATGTGGTGAGGC GTGCCTTGTTGGCTGACCCG CACGTATATTAGAGACCAA*	Mla3^{K926L} mutation	This study
Mla3_K926L_rv	*TTGGTCTCTAATATACGTGCG GGTCAGCCAACAAGGCACGC CTCACCACATGAGACCTT*	Mla3^{K926L} mutation	This study
Mla3_K926M_fw	*AAGGTCTCATGTGGTGAGGC GTGCCTTGATGGCTGACCCG CACGTATATTAGAGACCAA*	Mla3^{K926M} mutation	This study
Mla3_K926M_rv	*TTGGTCTCTAATATACGTGCG GGTCAGCCATCAAGGCACGC CTCACCACATGAGACCTT*	Mla3^{K926M} mutation	This study
Mla3_K926F_fw	*AAGGTCTCATGTGGTGAGGC GTGCCTTGTTCGCTGACCCG CACGTATATTAGAGACCAA*	Mla3^{K926F} mutation	This study
Mla3_K926F_rv	*TTGGTCTCTAATATACGTGCG GGTCAGCGAACAAGGCACG CCTCACCACATGAGACCTT*	Mla3^{K926F} mutation	This study
Mla3_K926Y_fw	*AAGGTCTCATGTGGTGAGGC GTGCCTTGTATGCTGACCCG CACGTATATTAGAGACCAA*	Mla3^{K926Y} mutation	This study
Mla3_K926Y_rv	*TTGGTCTCTAATATACGTGCG GGTCAGCATACAAGGCACGC CTCACCACATGAGACCTT*	Mla3^{K926Y} mutation	This study
Mla3_K926W_fw	*AAGGTCTCATGTGGTGAGGC GTGCCTTGTGGGCTGACCCG CACGTATATTAGAGACCAA*	Mla3^{K926W} mutation	This study
Mla3_K926W_rv	*TTGGTCTCTAATATACGTGCG GGTCAGCCCACAAGGCACG CCTCACCACATGAGACCTT*	Mla3^{K926W} mutation	This study
Mla3_K926E_fw	*AAGGTCTCATGTGGTGAGGC GTGCCTTGGAGGCTGACCCG CACGTATATTAGAGACCAA*	Mla3^{K926E} mutation	This study
Mla3_K926E_rv	*TTGGTCTCTAATATACGTGCG GGTCAGCCTCCAAGGCACGC CTCACCACATGAGACCTT*	Mla3^{K926E} mutation	This study

2.7.1.3 Molecular cloning for recombinant protein expression

The level 0 module containing the Mla3 C-terminus (Mla3_V874) was cloned into the pOPIN_F6_Kan level 1 acceptor (TSL SynBio) by Golden Gate assembly. The module pICSL50028 (no stop to stop, TSL SynBio) was also included to add a stop codon.

2.7.2 Fungal effectors

The coding sequences of *PWL2* (AAA91019.1) and *AVR$_{a10}$* (Saur et al., 2019) without signal peptide were synthesised and cloned by Twist Bioscience (San Francisco,

CA, USA) with codon optimisation for expression in *N. benthamiana* and domestication to remove *BpiI* and *BsaI* sites. The synthesised sequences were cloned in the pTwist_Kan_High_Copy cloning vector (Twist Bioscience) with flanking *BsaI* restriction sites for subsequent level 1 Golden Gate assemblies. The *pwl2-2* variant was generated by site directed mutagenesis on *PWL2* using fusion PCR to amplify and fuse one fragment upstream and one fragment downstream of the D90N mutation using the primers listed in **Table 2.7**. The final PCR product containing the desired mutation was cloned into the level 0 acceptor plasmid pICSL01005 (TSL SynBio) using Golden Gate cloning. The *pwl2-3* variant was cloned by amplifying the gene from the pGADT7:*pwl2-3* obtained from the Talbot lab at TSL (Norwich, UK) using the primers listed in **Table 2.7**. The purified PCR product was cloned into the level 0 acceptor plasmid pICSL01005 (TSL SynBio) by Golden Gate assembly. AVR-PikD, previously cloned by Białas et al. (2021) was amplified from the pTRBO:*AVR-PikD* construct using the primers listed in **Table 2.7** and cloned into the level 0 acceptor plasmid pICSL01005 (TSL SynBio) by Golden Gate cloning. All level 0 and level 1 constructs were verified by DNA sequencing.

Table 2.7 List of primers to clone pwl2-2, pwl2-3 and AVR-PikD

Primer name	Sequence	Purpose in this study	Source
Pwl2_fw	*AAGAAGACAAAATGGGCGGTGGATG GAC*	Golden Gate cloning of pwl2-2 and pwl2-3	This study
Pwl2-2_D90N_rv	*GCCTATCTGATTTATTTTCCTGGTGG*	Golden Gate cloning of pwl2-2 and pwl2-3	This study
Pwl2-2_D90N_fw	*CCACCAGGAAAATAAATCAGATAGGC*	Pwl2D90N site directed mutagenesis for pwl2-2	This study
Pwl2_NS_rv	*AAGAAGACAACGAACCCATAATATTG CAAC*	Pwl2D90N site directed mutagenesis for pwl2-2	This study
AvrPikD_L0_fw	*AAGAAGACAAAATGGAAACTGGTAAT AAATATATTG*	Golden Gate cloning of AVR-PikD	This study
AvrPikD_L0_rv	*AAGAAGACAACGAACCAAAACCTGGT CTTTTTTTACCC*	Golden Gate cloning of AVR-PikD	This study

2.7.2.1 Molecular cloning for transient expression *in planta*

Level 0 effector modules were cloned into the level 1 binary acceptor plasmid pICH47732 (Addgene no. 4800) for transient gene expression in *N. benthamiana*. Constructs were generated by Golden Gate assembly with pICH51266 (long 35S + Ω promoter, Addgene no. 50267), pICSL50007 (3xFLAG C-terminal tag, Addgene no. 50308), and pICH41414 (35S terminator, Addgene no. 50337).

2.7.2.2 Molecular cloning for yeast-two-hybrid experiments

The level 0 effector modules were cloned into the pGADT7 level 1 acceptor (TSL SynBio) by Golden Gate assembly. The module pICSL50028 (no stop to stop, TSL SynBio) was also included to add a stop codon.

2.7.2.3 Molecular cloning for recombinant protein expression

The level 0 module containing Pwl2 was cloned into de pOPIN_F5_Carb level 1 acceptor (TSL SynBio) with pICSL30019 (6xHis N-terminal tag, with 3C protease cleavage site, TSL SynBio) by Golden Gate assembly. The module pICSL50028 (no stop to stop, TSL SynBio) was also included to add a stop codon.

2.7.3 *OsHIPP43-HMA* and *AtTRXh5*

The coding sequence of AtTRXh5 (Q39241.1) was synthesised as gene fragment by Twist Bioscience (San Francisco, CA, USA) with codon optimisation for gene expression in *N. benthamiana* and domestication to remove *BsaI* and *BpiI* restriction sites. Flanking adapters with *BpiI* restriction sites were added for cloning into the pICSL01005 (TSL SynBio) acceptor plasmid using Golden Gate cloning. The coding sequence of OsHIPP43-HMA (LOC_Os01g32330.1) cloned into pICH41308 (TSL SynBio) was obtained from the Kamoun lab at TSL (Norwich, UK). All level 0 and level 1 constructs were verified by DNA sequencing.

2.7.3.1 Molecular cloning for transient expression *in planta*

The AtTRXh5 and OsHIPP43-HMA level 0 modules were cloned into the level 1 binary acceptor plasmid pICH47732 (Addgene no. 4800) for transient gene expression in *N. benthamiana*. Constructs were generated by Golden Gate assembly with pICSL13001 (long 35S CaMV promoter + 5' untranslated leader, Addgene no. 50265), pICSL30009 (4xMyc N-terminal tag, Addgene no. 50301), and pICH41414 (35S terminator, Addgene no. 50337). The module pICSL50028 (no stop to stop, TSL SynBio) was included to add a stop codon in the AtTRXh5 cloning reaction.

2.7.3.2 Molecular cloning for yeast-two-hybrid experiments

The construct pGBKT7:OsHIPP43-HMA was obtained from the Talbot lab at TSL (Norwich, UK).

2.8 Biochemistry methods

2.8.1 *In planta* protein expression

Transient gene expression in planta was carried out by delivering T-DNA constructs transformed in *A. tumefaciens* GV3101::pMP90 into leaves of 4-week old *N. benthamiana* plants as previously described (Win et al., 2011). Liquid cultures of LB medium inoculated with *A. tumefaciens* containing the constructs of interest were grown overnight at 28°C under constant agitation. The cultures were centrifuged at 5000x*g* for 10 min and cell pellets were resuspended in infiltration buffer (10 mM MES, 10 mM $MgCl_2$, and 150 μM acetosyringone). The OD_{600} of each *A. tumefaciens* suspension was measured and adjusted to a final working concentration as indicated in **Table 2.8**. For cell-death assays, the *A. tumefaciens* strains containing the expression vectors of interest were mixed accordingly to reach the required final concentration specified in **Table 2.8**, unless stated otherwise. The third and fourth upper leaves of 4-week old *N. benthamiana* plants were agroinfiltrated using a 1 mL disposable syringe. Leaves were collected 3 days after infiltration.

Table 2.8 List of constructs used for transient expression in *N. benthamiana*

Protein	Tag	Promoter	Terminator	Working OD_{600}	Purpose
Mla10	6xHA (C-term)	Mas + Ω	AtHSP18	0.1	Protein expression and cell death
Mla3 (wild type, mutants and chimeras)	6xHA (C-term)	Mas + Ω	AtHSP18	0.5	Protein expression, cell death and CoIP
$Mla3^{F99E}$	6xHA (C-term)	Mas + Ω	AtHSP18	0.25	Protein expression and cell death
$Mla3^{H501Q}$	6xHA (C-term)	Mas + Ω	AtHSP18	0.25	Protein expression and cell death
$Mla3^{H501G}$	6xHA (C-term)	Mas + Ω	AtHSP18	0.25	Protein expression and cell death
$Mla3^{D502V}$	6xHA (C-term)	Mas + Ω	AtHSP18	0.25	Protein expression and cell death
Mla3_CC	6xHA (C-term)	Mas + Ω	AtHSP18	0.25	Protein expression and cell death
$Mla3^{L11E}$_CC	6xHA (C-term)	Mas + Ω	AtHSP18	0.5	Protein expression and CoIP
Mla3_CC-NBARC	6xHA (C-term)	Mas + Ω	AtHSP18	0.5	Protein expression and CoIP
Mla3_NBARC	6xHA (C-term)	Mas + Ω	AtHSP18	0.8	Protein expression and CoIP
Mla3_NBARC-LRR	6xHA (C-term)	Mas + Ω	AtHSP18	0.5	Protein expression and CoIP

Table 2.8 List of constructs used for transient expression in *N. benthamiana* (continued).

Protein	Tag	Promoter	Terminator	Working OD_{600}	Purpose
Mla3_LRR	6xHA (C-term)	Mas + Ω	AtHSP18	0.5	Protein expression and CoIP
Mla_V874	6xHA (C-term)	Mas + Ω	AtHSP18	0.8	Protein expression and CoIP
Mla_V911	6xHA (C-term)	Mas + Ω	AtHSP18	0.8	Protein expression and CoIP
Mla23 (wild type, mutants and chimeras)	6xHA (C-term)	Mas + Ω	AtHSP18	0.5	Protein expression, cell death and CoIP
Mla34 (wild type and mutant)	6xHA (C-term)	Mas + Ω	AtHSP18	0.5	Protein expression and cell death
Mla35 (wild type and mutant)	6xHA (C-term)	Mas + Ω	AtHSP18	0.6	Protein expression and cell death
Mla39 (wild type and mutant)	6xHA (C-term)	Mas + Ω	AtHSP18	0.5	Protein expression and cell death
Mla3Δ6	6xHA (C-term)	Mas + Ω	AtHSP18	0.5	Protein expression and cell death
Mla-HOR21599	6xHA (C-term)	Mas + Ω	AtHSP18	0.5	Protein expression and cell death
Mla-WBDC233	6xHA (C-term)	Mas + Ω	AtHSP18	0.5	Protein expression and cell death
Mla-WBDC221	6xHA (C-term)	Mas + Ω	AtHSP18	0.5	Protein expression and cell death
Pwl2	3xFLAG (C-term)	Long 35S + Ω	35S	0.3	Protein expression, cell death and CoIP
pwl2-2	3xFLAG (C-term)	Long 35S + Ω	35S	0.3	Protein expression, cell death and CoIP
pwl2-3	3xFLAG (C-term)	Long 35S + Ω	35S	0.3	Protein expression, cell death and CoIP
pwl2-3	3xFLAG (C-term)	Long 35S + Ω	35S	0.5	CoIP
AVR-PikD	3xFLAG (C-term)	Long 35S + Ω	35S	0.5	Protein expression, cell death and CoIP
OsHIPP43	4xMyc (N-term)	Long 35S	35S	0.5	Protein expression
AtTRXh5	4xMyc (N-term)	Long 35S	35S	0.5	Protein expression

2.8.2 Plant protein extraction

Total plant protein extraction was performed as previously described (Win et al., 2011). For protein expression analyses, six 8 mm *N. benthamiana* leaf discs were collected in 2 mL microcentrifuge tubes with two 3 mm glass beads inside. For co-immunoprecipitation assays, two full leaves were collected and stored in 5 mL centrifuge tubes with two 5 mm zirconium oxide beads (Retsch). Samples were snap frozen in liquid nitrogen immediately after collection. Frozen tissue was ground for 30 s at 1500 rpm

using a Geno/Grinder® with frozen cryo-blocks to hold the sample tubes. Ground tissue samples were mixed with twice as much (w/v) ice-cold GTEN extraction buffer (10% (v/v) glycerol, 25 mM Tris-HCl pH 7.5, 1 mM EDTA, 300 mM NaCl) supplemented with 2% (w/v) PVPP, 10 mM dithiothreitol (DTT), 1% (v/v) protease inhibitor cocktail (Sigma), and 0.2% (v/v) IGEPAL® CA-630. Samples were incubated on ice for 10 min until the tissue was homogeneously mixed with the extraction buffer. Subsequently, samples were centrifuged at 5500x*g* for 20 min at 4°C, and the supernatant was transferred to a fresh tube and centrifuged under the same conditions for another 10 min. After centrifugation, the supernatant was filtered through a 0.45 μm syringe filter to obtain the final total protein extract. Samples were mixed in a 3:1 (v/v) ratio with 4X Laemmli sample buffer (BioRad) supplemented with 10 mM DTT and incubated at 90°C for 10 minutes prior SDS-PAGE electrophoresis.

2.8.3 Co-immunoprecipitation

Co-immunoprecipitation (co-IP) assays were performed as previously described (Win et al., 2011) using affinity chromatography with Anti-HA Affinity Matrix (Roche) or Anti-FLAG® M2 Affinity Gel (Sigma). 30 μL of beads were resuspended in 100 μL of IP buffer (GTEN with 0.2% (v/v) IGEPAL® CA-630) and mixed with 1 mL of total protein extract. The extract containing the beads was placed in a rotary mixer an incubated for 1.5 h at 4°C. Subsequently, the sample was centrifuged at 1000x*g* for 1 min at 4°C. The supernatant was carefully discarded, and the resin was resuspended in 1 mL of IP buffer followed by centrifugation at 1000x*g* for 1 min at 4°C. This washing step was repeated 4 more times, for a total of 5 rounds of washes. After the final washing step, the supernatant was discarded, and any remains were carefully removed using a needle and a 1 mL syringe. The beads were resuspended in 1X Laemmli sample buffer (BioRad) supplemented with 10 mM DTT and eluted by incubating at 80°C for 10 min. Samples were centrifuged at 8000x*g* before SDS-PAGE electrophoresis.

2.8.4 SDS-PAGE electrophoresis

For Western blot and protein purification analysis, SDS-PAGE electrophoresis was carried out running commercial 4-20% Mini-PROTEAN® TGX Precast gels (BioRad) in 1X Tris-glycine buffer (25 mM Tris, 250 mM glycine, 0.1% (w/v) SDS) for approximately 1.5 h at 100 V. The PageRuler™ Plus prestained protein ladder (ThermoFisher Scientific) was used as reference for approximate protein size.

2.8.5 Western blot analysis

Following SDS-PAGE electrophoresis, proteins were transferred from the polyacrylamide gel onto a PVDF (polyvinylidene difluoride) membrane using the Trans-Blot Turbo transfer system (BioRad) according to the manufacturer's protocol. After the transfer, the PVDF membrane was incubated for 45 min in 5% (w/v) milk in 1X TBST (Tris-buffered saline with 0.1% Tween®20) blocking solution. Next, the blocking solution was replaced by 5% (w/v) milk in 1X TBST buffer containing the appropriate antibody for probing. HA-tag detection was done in one step by using Anti-HA-Peroxidase, high affinity antibody (Roche) in a 1:5000 dilution. FLAG-tag detection was done in one step using ANTI-FLAG® M2-Peroxidase (HRP) antibody (Sigma) in a 1:5000 dilution. The membrane was incubated with the appropriate antibody for minimum 4 h (or overnight), followed by three washes of 10 min in 1X TBST buffer. Protein detection was done by adding Pierce™ ECL Western Blotting Substrate (Thermo Fisher Scientific) and SuperSignal™ West Femto Maximum Sensitivity Substrate (Thermo Fisher Scientific) in a 1:1 (v/v) ratio. Membrane imaging was performed using an Amersham ImageQuant 800 western blot imager system or an ImageQuant LAS 4000 luminescent imager (Cytiva). Equal protein loading was checked by staining the PVDF membrane with Ponceau S solution (Sigma).

2.8.6 Yeast-two-hybrid assay

Chemically competent *Saccharomyces cerevisiae* Y2HGold cells (Takara Bio) were co-transformed with pGBKT7 and pGADT7 constructs (TSL SynBio) containing the genes of interest (**Table A.I.5**), using the commercial kit Frozen-EZ Yeast Transformation II™ (Zymo Research) following the manufacturer's instructions. Co-transformed yeast cells were selected on SD solid medium not supplemented with leucine or tryptophane (SD-LW) after incubation at 28°C for three days. Single yeast colonies grown on SD-LW plates were used to inoculate liquid SD-LW medium and incubated overnight at 28°C and 190 rpm. Saturated cultures were adjusted to an OD_{600} of 1 and used for three tenfold serial dilutions (10^{-1}, 10^{-2} and 10^{-3}). 5 µL drops of the initial yeast suspensions and each dilution were placed on SD-LW agar plate, and on SD solid media not supplemented with leucine, tryptophane, histidine or adenine (SD-LWHA) containing X-α-gal. Yeast growth was documented after incubation at 28°C for four days.

2.8.7 Heterologous protein production and purification

For co-purification of Pwl2 with the C-terminus of Mla3, *E. coli* Shuffle cells were co-transformed with the expression vectors pOPINF5_His-Pwl2 and pOPINF6_Mla3_V874 and colonies were selected on LB agar plates with 50 μg/mL kanamycin and 100 μg/mL carbenicillin. Co-transformed cells were grown overnight as a starter culture in 100 mL of LB medium with the appropriate antibiotics at 37°C and constant shaking. The pre-culture was used to inoculate 1 L of auto-induction medium (AIM) (Studier, 2005) with the appropriate antibiotics to reach a starting OD_{600} of 0.1. The culture was grown at 30°C for 4-6 hours at 180 rpm until reaching an OD_{600} of 0.6-0.8 to then induce the cells at 18°C and constant agitation overnight. The cells were harvested by centrifuging at 5500x*g* for 10 min at 4°C and resuspended in A1 buffer (50 mM Tris-HCl pH 7.5, 5% (v/v) glycerol, 500 mM NaCl, 50 mM glycine, 20 mM imidazole, and cOmplete™ mini EDTA-free protease inhibitor cocktail (Roche)). Lysis was performed by sonicating the cells for 4 min in pulses (1 second on, 3 seconds off) followed by centrifugation at 18000x*g* for 30 min at 4°C. The lysate (supernatant) was used for protein tandem purification by immobilized metal affinity chromatography and size exclusion chromatography through gel filtration (IMAC-GF). The sample was injected into a 5 mL HisTrap™ Fast Flow (Ni^{2+}-NTA) column (Cytiva) connected to an ÄKTA pure™ protein purification system (Cytiva) and eluted in 4 mL fractions of A1 buffer supplemented with 500 mM imidazole). Fractions with highest absorbance at 280 nm containing His-tagged proteins were used for size exclusion chromatography by gel filtration through a Superdex 75 26/60 column (Cytiva), and eluted in A2 buffer (20 mM HEPES pH 7.5, 150 mM NaCl). Eluted fractions under the peak with highest absorbance at 280 nm were collected and the cleavable His tag in Pwl2 was removed by adding 3C-protease in a ratio of 10 μg 3C-protease/mg protein, and incubating overnight at 4°C. To capture the His-tag from the sample, the digested protein was passed through a 5 mL HisTrap™ Fast Flow (Ni^{2+}-NTA) column (Cytiva). The flow-through was fractionated by a final gel filtration through a Superdex 75 26/60 column (Cytiva) and eluted in A2 buffer. Samples were taken after each step of the purification process and mixed in a 3:1 (v/v) ratio with 4X Laemmli sample buffer (BioRad) supplemented with 10 mM DTT, followed by incubation at 90°C for 10 minutes and SDS-PAGE electrophoresis. The polyacrylamide gel was stained using InstantBlue® Coomassie protein stain (abcam). The protein bands with the expected sizes were excised from the gel and analysed by LC-MS performed by The Sainsbury Laboratory Proteomics facilities (Norwich, UK).

2.9 Cell death assay

Cell death assays in *N. benthamiana* to test hypersensitive response (HR) were carried out by transiently expressing the genes of interest as described in section 2.8.1. The HR phenotypes were scored 3 dpi using the previously published cell death phenotypic scale (Segretin et al., 2014) modified to a range from 0: no response, to 7: confluent cell death. Statistical analysis of the quantified HR phenotypes was performed with the besthr R library (MacLean, 2019)

2.10 Computational analyses

2.10.1 Phylogenetic analysis of grass NLRs

NLRs from diverse grass species (**Table A.I.7**) were identified by using InterProScan v5.36-75.0 with default parameters to annotate protein domains. The Pfam family identifier for the nucleotide binding domain (PF00931) was used to identify NLRs and to extract the individual domain from each protein using the Python script QKdomain_process.py (Bailey et al., 2018a). MAFFT (v7.481)-DASH was used to perform the structure-guided multiple sequence alignment using default parameters. The NB structures of *A. thaliana* ZAR1 (PDB 6J5T) and *Solanum lycopersicum* NRC1 (PDB 6S2P) were included in the structure-guided alignment. Variable sites represented in at least 40% of the aligned proteins and sequences that spanned at least 50% of the total alignment length were filtered using the QKphylogeny_alignment_analysis.py Python script (https://github.com/matthewmoscou/QKphylogeny). The phylogenetic tree was constructed using RAxML (v8.2.12) with the JTT amino acid substitution model, gamma model of rate heterogeneity and 1000 bootstraps. Sufficient bootstrapping was assessed with a convergence test using RAxML autoMRE after 250 bootstraps for the full NB and C17 clade phylogenies. The resulting phylogenetic trees were visualized using iTOL (Letunic and Bork, 2021) and *A. thaliana* ZAR1 was used as outgroup.

2.10.2 LRR domain annotation of Mla3

The boundaries of the LRR domain of Mla3 were established using the web server of InterProScan and the leucine-rich repeat domain superfamily IPR032675. Individual LRR repeats were annotated using the web server LRR predictor v1.0 (Martin et al., 2020a). Surface exposed residues, secondary structure, and protein disorder in the C-

terminus of Mla3 were predicted using the RaptorX Property Prediction tool (Wang et al., 2016).

2.10.3 Protein structure analyses

The structure of the C-terminus of Mla3 (from residue V868 to F958(*stop), $Mla3^{V868-*}$) in complex with Pwl2 was predicted using AlphaFold2-multimer (Jumper et al., 2021) from ColabFold v1.5.1 (unpaired mode). The signal peptide of Pwl2 was removed before modelling. The best ranked model with highest average pLDDT score was used for further analyses. ChimeraX was used for protein structure visualisation (Pettersen et al., 2021). The Matchmaker tool in ChimeraX was used for structure alignment with Pwl2 in complex with OsHIPP43-HMA provided by Dr. Rafał Zdrzałek from the Banfield lab at the John Innes Centre (Norwich, UK) (Zdrzalek, 2021).

2.10.4 *Mla* copy number variation

Illumina paired end whole genome sequencing data of barley accessions were trimmed using Trimmomatic (v0.39) using the following parameters: clipped reads based on TruSeq3 adapters with settings 2:30:10, trimming leading and trailing of reads with setting 5, sliding window trimming with settings 4:15, and requiring a minimum length of 36 bp after filtering for this parameters. *Mla* alleles from diverse barley accessions were identified based on *de novo* assembly of leaf transcriptomes using Trinity with Trimmomatic and default parameters. Transcripts of *Mla* alleles were scanned for *k*-mer coverage using the *sect* tool in *k*-mer analysis toolkit (v2.4.2) using trimmed reads as input and *k* of 27. Depth of sequencing and the *Bpm* gene at the *Mla* locus were used to determine single copy coverage levels. Coverage analysis and figure generation was performed using ggplot2 (v3.3.6) in R (v4.1.2).

Chapter 3: *Mla3* recognises the effector *PWL2* from the blast fungus *M. oryzae*

Results from this chapter are published on bioRxiv as part of the preprint manuscript by Brabham, H. J.[*] and Gómez De La Cruz, D.[*], et al. (Brabham et al., 2022). **Doi:** https://doi.org/10.1101/2022.10.21.512921

[*]Both authors contributed equally to the manuscript. My contribution corresponds to the results described in this chapter.

3.1 Introduction

The plant innate immune system heavily relies on intracellular immune receptors of the nucleotide binding leucine rich repeat (NLR) family, which recognise pathogen secreted effectors and trigger a robust immune response (Jones and Dangl, 2006). NLR genes are unevenly located within plant genomes and often exist as complex clusters that allow rapid expansion and diversification through recombination, duplication, and gene conversion events (Michelmore and Meyers, 1998; Barragan and Weigel, 2021). Multiple NLR recognition specificities can arise from recombination and swaps between paralogous genes within a cluster (Saur et al., 2021). One such example is the *Mildew locus a* (*Mla*) in barley. *Mla* is located in the short arm of chromosome 1H and is a cluster containing three families of CNLs named *Resistance gene homologues 1, 2* and 3 (*RGH1, RGH2* and *RGH3*) with nested regions of transposable elements (Wei et al., 2002). *Mla* NLR alleles of the *RGH1* family confer isolate-specific resistance against *Blumeria graminis* f. sp. *hordei* (*Bgh*), causal agent of barley powdery mildew (Jørgensen and Wolfe, 1994). This family of NLRs has undergone extensive functional diversification that gave rise to a large set of different recognition specificities (Seeholzer et al., 2010; Maekawa et al., 2018). There are over 30 *Mla* alleles within the *RGH1* family that are >90% identical at the protein level and yet recognise cognate sequence-unrelated effectors from *Bgh,* known as AVR_a genes (Seeholzer et al., 2010; Lu et al., 2016; Saur et al., 2019; Bauer et al., 2021). Most AVR_a effectors identified to date belong to the family of RALPH proteins with a catalytically inactive RNAse-like fold that comprise a lineage-specific effector family uniquely expanded in *Bgh* (Bauer et al., 2021; Seong and Krasileva, 2023). Direct recognition has been suggested for the *Mla1, Mla7, Mla10,* and *Mla13* alleles and their cognate AVR_{a1}, AVR_{a7}, AVR_{a10}, and AVR_{a13} effectors, respectively, suggesting that *Mla* alleles evolved to recognise a conserved structural fold of AVR_a *Bgh* effectors (Saur et al., 2019; Bauer et al., 2021).

Functional diversification in *Mla* is not only evidenced by the recognition of sequence unrelated effectors from *Bgh*. The *Mla* orthologues Sr33 in wheat and Sr50 in rye confer resistance against the wheat stem rust pathogen *Puccinia graminis* f. sp. *tritici* (*Pgt*) by recognising the effectors AvrSr33 and AvrSr50, respectively (Periyannan et al., 2013; Mago et al., 2015; Chen et al., 2017). *Bgh* and *Pgt* belong to highly divergent phyla, indicating that *Mla* NLRs evolved to recognise effectors with independent phylogenetic origin. In addition, *Mla* was also reported to underlie resistance against the wheat stripe rust pathogen *Puccinia striiformis* f. sp. *tritici* (*Pst*) in barley (Bettgenhaeuser et al., 2021), illustrating its ability to simultaneously confer resistance against multiple pathogens and contribute to host range dynamics, as *Pst* is a non-adapted pathogen in barley.

The locus conferring resistance to the blast fungus *M. oryzae* in barley, initially named *Rmo1* (*Resistance to Magnaporte oryzae 1*), was mapped to the *Mla* locus in the cultivar Baronesse (Inukai et al., 2006), which carries *Mla3* as the *RGH1* haplotype, and a set of paired NLRs in head-to-head orientation as the *RGH2* and *RGH3* haplotype. Interestingly, the *RGH2* allele in Baronesse, predicted to be the sensor NLR of the *RGH2-RGH3* pair, has a C-terminal Exo70F1 integrated domain (Brabham et al., 2018). Fine mapping established that *Rmo1* and the *Mla* locus are genetically linked in Baronesse. Genetic variation across barley accessions indicated that neither *RGH2* nor *RGH3* underlie *Rmo1,* as the barley accession Maritime carries identical *RGH2* and *RGH3* alleles as Baronesse, yet it is susceptible to *M. oryzae*. Barley transgenics expressing *Mla3* (*RGH1*) in the genetic background of Golden Promise, which is normally susceptible to blast, gained resistance against *M. oryzae,* thus confirming that *Mla3* is *Rmo1* (Brabham, 2019). This illustrates another example of multiple pathogen recognition by *Mla* and its remarkable functional diversification.

M. oryzae is a plant pathogenic fungus that is highly divergent from *Bgh* and causes blast disease on a wide range of grasses. However, individual isolates of *M. oryzae* are only pathogenic on a limited set of hosts (Hyon et al., 2012). Host-specific groups form phylogenetically related lineages that often have commonly gained and lost genes—most of which are effectors (Yoshida et al., 2016). Not surprisingly, host range dynamics in *M. oryzae* are usually ruled by recognition of effectors in a given host, frequently by NLRs. The majority of cultivated rice, for example, carries the resistance NLR pair *RGA4-RGA5* (*PiCO39*), which recognises the effector AVR1-CO39; hence, this effector is mostly absent in *M. oryzae* isolates from the rice-infecting lineage (Tosa et al., 2005; Cesari et al., 2013). This outlines that the presence of a particular effector can limit the ability of

a given isolate to infect certain grass species. Such is the case of the *PWL* (*Pathogenicity towards Weeping Lovegrass*) family of effectors—*PWL1, PWL2, PWL3* and *PWL4*—which are recognised and confer avirulence in weeping lovegrass (*E. curvula*) (Kang et al., 1995; Sweigard et al., 1995). Furthermore, the host jump of *M. oryzae* to wheat is attributed to the sequential loss of the effectors *PWT3* and *PWT4,* which are recognised by the corresponding wheat *R* genes *Rwt3* and *Rwt4* (Inoue et al., 2017)*,* encoding an NLR and a tandem protein kinase, respectively (Arora et al., 2023). It hypothesised that separation of these genes in widely deployed wheat cultivars served as a springboard for host adaptation of Lolium- and Avena-infecting isolates of *M. oryzae* through the stepwise loss of *PWT3* and *PWT4* (Inoue et al., 2017). Thus, NLRs significantly contribute to resistance against non-adapted pathogen isolates and host range dynamics.

In this chapter, I aimed to identify the gene underlying *AVR-Rmo1,* the *M. oryzae* effector recognised by *Mla3* (*Rmo1*) in the barley cultivar Baronesse. For this, I performed a forward genetics screen using the *M. oryzae* isolate KEN54-20, which is avirulent in Baronesse and therefore carries *AVR-Rmo1*. I generated KEN54-20 mutants that gained virulence in this barley accession, indicative of the loss of the avirulence function of *AVR-Rmo1*. High-throughput genome sequencing and *k-mer* analyses indicated that all virulent mutants had lost the effector *PWL2,* suggesting that it underlies *AVR-Rmo1*. *PWL2* is an effector known to condition pathogenicity towards weeping lovegrass (Sweigard et al., 1995). This unexpected result shows that, in addition to recognising AVR_{a3} from *Bgh, Mla3* also recognises the host specificity determinant *PWL2* from *M. oryzae.*

3.2 Results and discussion

3.2.1 *M. oryzae avr-Rmo1* mutants have a complete deletion of the effector *PWL2*

In order to identify *AVR-Rmo1*—the *M. oryzae* effector recognised by *Mla3*—Brabham (2019) performed UV mutagenesis on spores of the *M. oryzae* isolate KEN54-20 and screened for gain-of-virulence mutants on Baronesse, a KEN54-20 resistant barley cultivar that carries *Mla3*. Following a primary screen of spray inoculation on wild-type Baronesse (*Mla3*), a set of 72 putative mutants of KEN54-20 were identified (Brabham, 2019). I confirmed gain of virulence in twelve of these putative mutants using spot inoculation on detached leaves of Baronesse (*Mla3*), indicating *AVR-Rmo1* loss of function (*avr-Rmo1*) (**Figure 3.1A**). All tested isolates were virulent on the susceptible

cultivar Nigrate. To identify *AVR-Rmo1*, I sequenced the genome of *M. oryzae* wild-type KEN54-20 using long read (Oxford Nanopore Technologies) and short read (Illumina) sequencing technologies, and assembled the genome using the hybrid assembler MaSuRCA (Zimin et al., 2013). The final assembly comprised 39 contigs and had a size of 47.9 Mb. To identify shared mutations across all *avr-Rmo1* mutants that might explain the gain of virulence on Baronesse, I sequenced the genomes of the twelve confirmed mutant lines using whole genome Illumina sequencing, and compared them to the wild-type *M. oryzae* KEN54-20 genome. Using a window-based *k-mer* analysis, we screened for shared regions in the genome of all *avr-Rmo1* mutant lines that contained insertions, deletions, or SNPs. Strikingly, a region of 8 kb encompassing the known effector *PWL2* (Sweigard et al., 1995) was deleted across all mutants (**Figure 3.1B**). We were unable to define the exact boundaries of the deletions in each mutant mainly due to repetitive regions adjacent to *PWL2*. Manual inspection of aligned reads confirmed the complete deletion of *PWL2* in each *avr-Rmo1* mutant line. No additional shared mutations were identified across all isolates. This indicated that gain of virulence of the *M. oryzae avr-Rmo1* mutants in Baronesse (*Mla3*) was linked to the loss of the effector *PWL2* and suggested *PWL2* as a candidate for *AVR-Rmo1*.

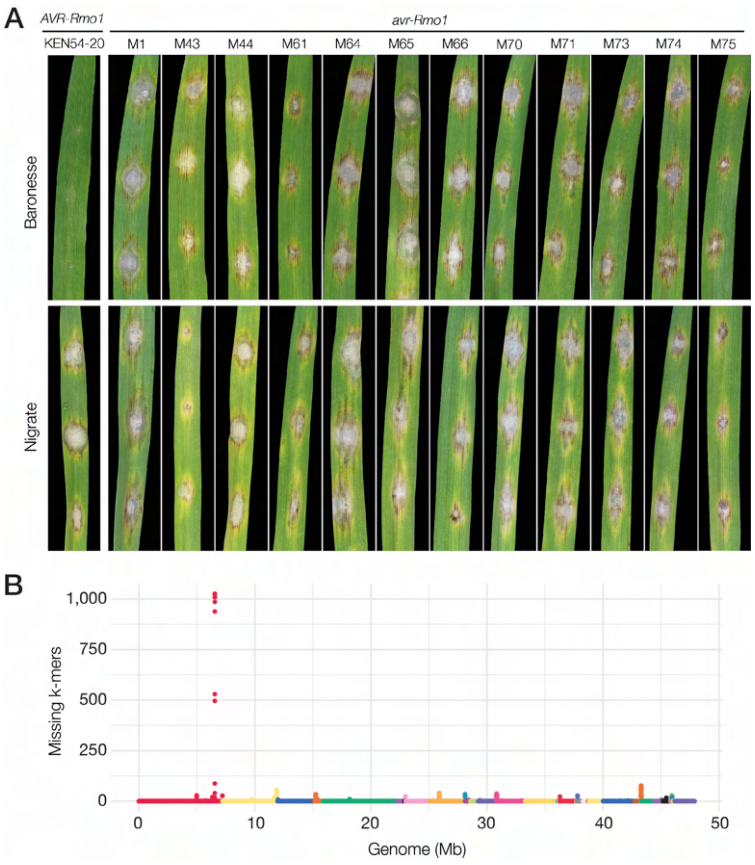

Figure 3.1 *M. oryzae avr-Rmo1* mutants are virulent on Baronesse and lost the effector *PWL2*.

(A) Baronesse (*Mla3*) leaves spot inoculated with *M. oryzae* KEN54-20 (*AVR-Rmo1*) and twelve independent *avr-Rmo1* mutants derived from UV mutagenesis. The barley cultivar Nigrate was used as susceptible control. Phenotypes are representative of three biological replicates with three technical replicates. **(B)** Genome-wide scan of regions with modified sequence relative to *M. oryzae* isolate KEN54-20. The number of shared missing *k*-mers among all mutants within a sliding window were determined using a window size of 10 kb and step size of 1 kb. Colour coding corresponds to individual contigs of the KEN54-20 genome. The sharp peak corresponds to the *PWL2* locus on scaffold 183 (red).

3.2.2 *AVR-Rmo1* is *PWL2*

Gain of virulence of the *M. oryzae avr-Rmo1* mutants on Baronesse (*Mla3*) could also be explained by different independent mutations in each line or by the loss of an additional gene neighbouring *PWL2* in the shared deletion. To investigate these hypotheses, and test whether *PWL2* is *AVR-Rmo1,* I transformed two independent *M. oryzae avr-Rmo1* mutant lines (M43 and M61) with the effector *PWL2* and performed infection assays on Baronesse and Mla3 transgenic plants. Transformed *avr-Rmo1* mutants contained ectopic integrations of *PWL2,* expressed under its native promoter, and followed by its native terminator (M43+*pPWL2:PWL2:tPWL2* and M61+ *pPWL2:PWL2:tPWL2*). I performed spot inoculation of detached leaves of Baronesse (*Mla3*) with wild-type KEN54-20, two *avr-Rmo1* mutant lines (M43 and M61) and two independently *PWL2*-transformed *avr-Rmo1* mutant lines (M43+*PWL2* and M61+*PWL2*). Both *avr-Rmo1* mutant lines of *M. oryzae* transformed with *PWL2* (M43+*PWL2* and M61+*PWL2*) as well as KEN54-20 were avirulent on Baronesse (*Mla3*), whereas the *avr-Rmo1* mutants were virulent. All tested isolates were virulent on the susceptible cultivar Nigrate (**Figure 3.2A**). To confirm that Baronesse was resistant to *M. oryzae* isolates that carry *PWL2* due to recognition by *Mla3* and not another resistance gene present in Baronesse, I performed detached leaf infection assays on transgenic *Mla3* Golden Promise barley plants, which is a KEN54-20 susceptible background in the absence of *Mla3* (**Figure 3.2B**). Similar to Baronesse, transgenic *Mla3* Golden Promise plants were resistant to *avr-Rmo1* mutants transformed with *PWL2* and wild-type KEN-54-20, but susceptible to *M. oryzae avr-Rmo1* mutants (**Figure 3.2B**). In all cases, *PWL2* was required and sufficient to complement *M. oryzae avr-Rmo1* mutants, indicating that *Mla3* specifically recognises *PWL2* and confirming that *PWL2* is *AVR-Rmo1*.

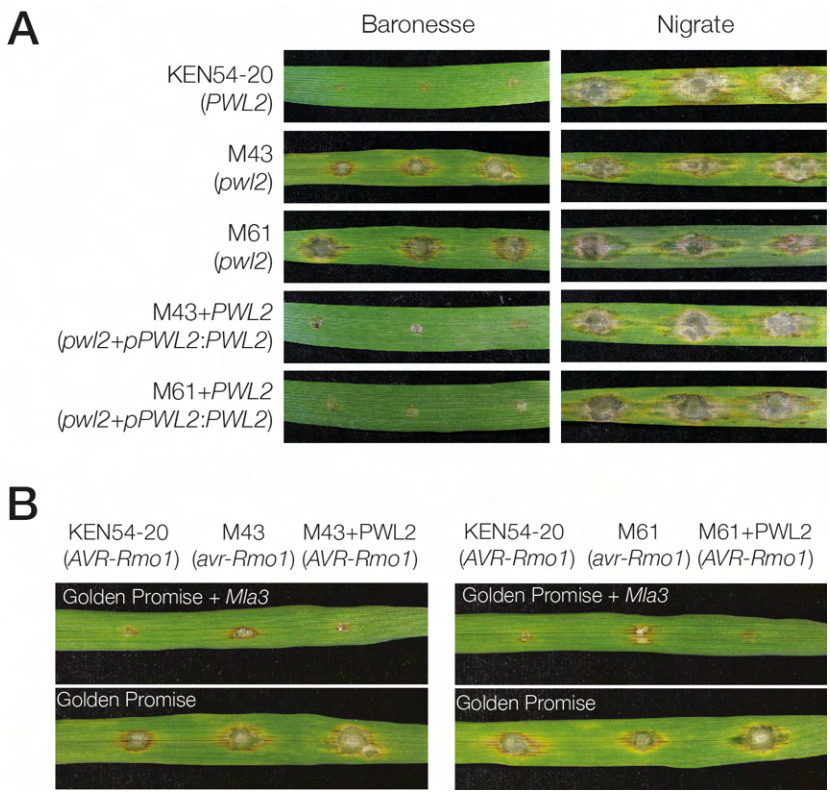

Figure 3.2 *AVR-Rmo1* is *PWL2*.

(A) *PWL2* complements *M. oryzae avr-Rmo1* mutants. Baronesse (*Mla3*) leaves spot inoculated with *M. oryzae* KEN54-20 (*AVR-Rmo1*) and *avr-Rmo1* mutants M43 and M61. *M. oryzae* isolate KEN54-20 is avirulent on Baronesse, whereas *avr-Rmo1* mutants M43 and M61 are virulent. Ectopic integration of *PWL2* driven by native promoter (*pPWL2:PWL2*) complements the phenotype of mutants M43 and M61. The barley cultivar Nigrate was used as susceptible control. **(B)** *Mla3* recognizes *PWL2* in transgenic Golden Promise + *Mla3*. Transgenic Golden Promise + *Mla3* (T_1-4 T_2) leaves spot inoculated with *M. oryzae* isolate KEN54-20 (*AVR-Rmo1*), *avr-Rmo1* mutants M43 and M61, and *avr-Rmo1* mutants M43 and M61 transformed with *PWL2* driven by its native promoter (*pPWL2:PWL2*). Wild-type Golden Promise was used as susceptible control. Phenotypes are representative of three biological replicates with three technical replicates.

Interestingly, *PWL2* is present as a single copy in the isolate KEN54-20, which significantly facilitated its identification as *AVR-Rmo1* through the forward genetics screen. Effectors of filamentous pathogens can have standing copy number variation across isolates (Qutob et al., 2009; Müller et al., 2019). The isolate Guy11, for example, which is commonly used as reference isolate of the rice-infecting lineage of *M. oryzae*, carries three copies of *PWL2* (Were, 2018). The UV-mutagenesis strategy to identify *AVR-Rmo1* would have been most likely unsuccessful with an isolate like Guy11 due to the relatively low odds of simultaneously mutating all copies of *PWL2*. In such case, a traditional map-based cloning approach involving crosses between a virulent and an avirulent isolate would have been a more suitable strategy, as previously reported for the

identification of other *AVR* genes in *M. oryzae* (Sweigard et al., 1995; Anh et al., 2018; Sugihara et al., 2023). Additionally, *PWL2* was completely lost in all *avr-Rmo1* mutants, suggesting the relative instability of this genomic region flanked by repetitive elements in the isolate KEN54-20. Such repetitive sequences most likely promoted errors during DNA repair, making the *PWL2*-neighbouring region prone to deletion. Altogether, these factors contributed to the rapid identification of *PWL2* as *AVR-Rmo1*.

3.2.3 Barley and weeping lovegrass evolved to recognise *PWL2*

PWL2 (*Pathogenicity Towards Weeping lovegrass 2*) is a known effector that contributes to host range dynamics in *M. oryzae*. It prevents *M. oryzae* isolates within the rice-infecting lineage from infecting weeping lovegrass (*Eragrostis curvula*) and is a major determinant of host-species specificity (Kang et al., 1995; Sweigard et al., 1995). To further confirm the identity of *AVR-Rmo1* as *PWL2,* I tested the ability of wild-type KEN54-20, the *avr-Rmo1* mutants and the *PWL2*-complemented *avr-Rmo1* mutans to infect weeping lovegrass, by performing spray inoculation on 10-day old seedlings. Similar to barley lines that carry *Mla3,* weeping lovegrass was resistant to *avr-Rmo1* mutants transformed with *PWL2* (M43+*PWL2* and M61+*PWL2*) and to KEN54-20, yet susceptible to two independent *avr-Rmo1* mutant lines—which lost *PWL2*—observed as restriction of plant growth and susceptible leaf lesions (**Figure 3.3A**). These results indicate that barley and weeping lovegrass evolved to recognise the effector *PWL2* from *M. oryzae*.

3.2.4 Specificity of *PWL2* recognition is conserved in barley and weeping lovegrass

The effector *PWL2* is highly prevalent across *M. oryzae* isolates (Chung et al., 2020; Latorre et al., 2020). In addition to the wild-type allele of *PWL2*—which is recognised in barley by *Mla3* and in weeping lovegrass— *pwl2-2* is an allele in which the aspartic acid in position 90 of the coding sequence is substituted by an asparagine (D90N). This single non-synonymous mutation results in the loss of recognition in weeping lovegrass, and is sufficient to confer virulence of *M. oryzae* isolates that carry *pwl2-2* on *E. curvula* (Sweigard et al., 1995). In order to test whether the D90N mutation in *pwl2-2* also abolishes recognition by *Mla3* in barley, I spot-inoculated detached leaves of Baronesse (*Mla3*) with a panel of diverse isolates of *M. oryzae* carrying different *PWL2* alleles. The *PWL2* allelic information of each isolate was obtained from RNA-seq data kindly provided by Dr. Motoki Shimizu. Out of a total of 17 isolates, five carrying wild-

type *PWL2* were avirulent on Baronesse (*Mla3*). The isolate Ina168, known to lack *PWL2* (i.e., *pwl2*), was not recognised by *Mla3* and caused virulent lesions on Baronesse. In agreement with previous reports on weeping lovegrass, the eight *M. oryzae* isolates that carry the *pwl2-2* allele (i.e., Pwl2 D90N) were not recognised by *Mla3* and were therefore virulent on Baronesse (**Figure 3.3B**). The isolates Naga69-150 and Ina85-182, known to carry both wild-type *PWL2* and *pwl2-2,* were avirulent on Baronesse due to recognition of the wild-type allele of the effector by *Mla3* (**Figure 3.3B**). Taken together, the phenotypes of the diverse isolates of *M. oryzae* in Baronesse indicate that specificity of *PWL2* recognition is maintained in barley and weeping lovegrass, as the D90N mutation in pwl2-2 is sufficient to evade recognition in both grass species.

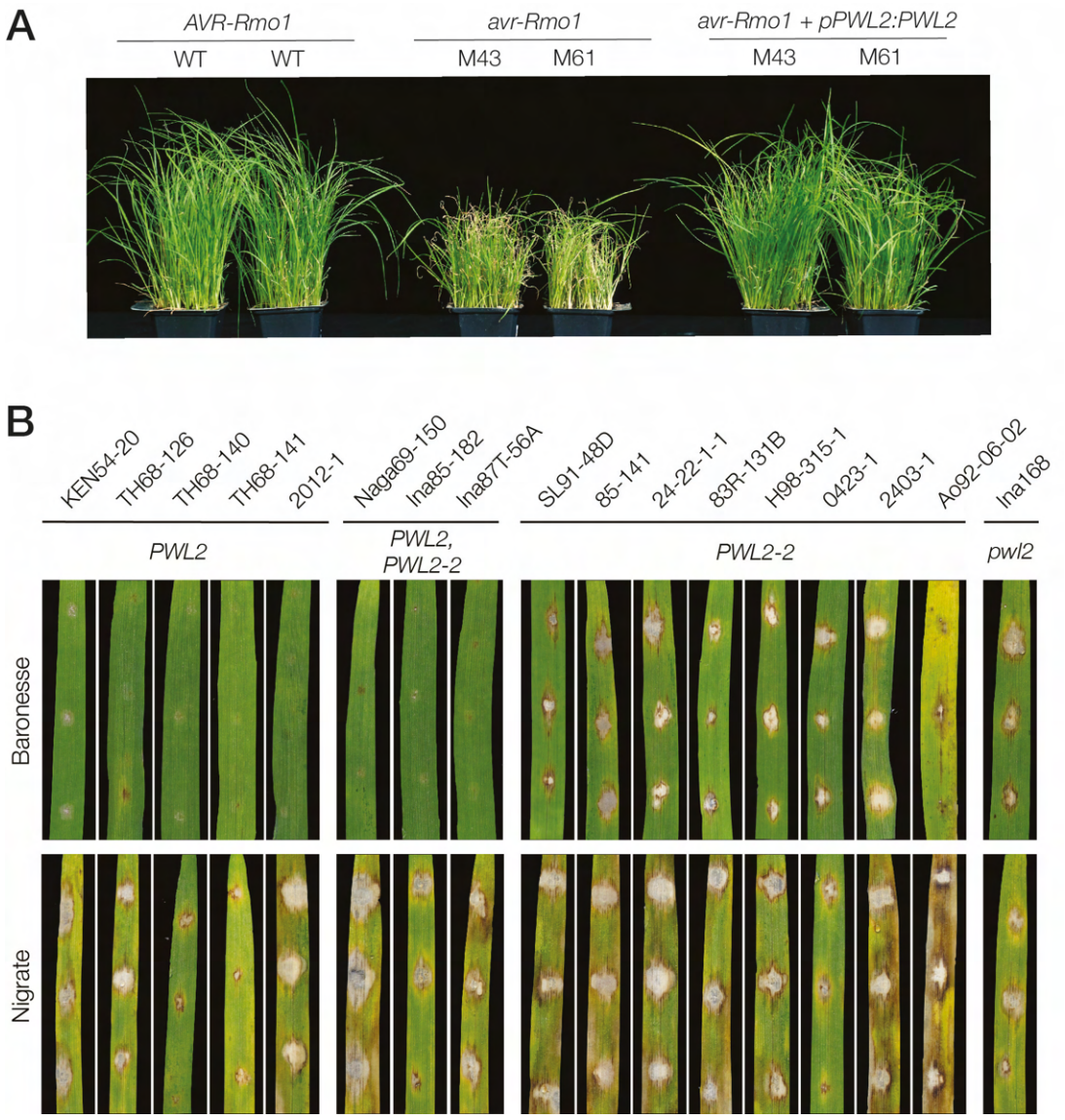

Figure 3.3 Barley and weeping lovegrass evolved to recognise *PWL2* with conserved recognition specificity.

(A) Weeping lovegrass spray inoculated with *M. oryzae* KEN54-20 (*AVR-Rmo1*), *avr-Rmo1* mutants M43 and M61, and *avr-Rmo1* mutants transformed with *PWL2* (M43+*PWL2* and M61+*PWL2*). **(B)** Baronesse (*Mla3*) spot inoculated with 17 different *M. oryzae* isolates representing *PWL2* natural variation. The isolates Naga69-150, Ina85-182 and Ina87T- 56A carry both *PWL2* and *pwl2-2*. The isolate Ina168 does not carry *PWL2*. The barley cultivar Nigrate was used as susceptible control. Phenotypes are representative of three biological replicates with three technical replicates.

Noteworthy, the isolate Ina87T-156A, initially reported to carry only the *pwl2-2* allele, was not virulent on Baronesse (**Figure 3.3B**). This could be explained by the presence of another effector being recognised by an *R* gene in this barley accession, or by the simultaneous presence of both wild-type *PWL2* and *pwl2-2*. I tested these hypotheses by mapping the locus conferring resistance to the isolate Ina87T-156A in Baronesse. For this, I performed spot inoculations with the isolate Ina87T-56A on the double haploid ORO mapping population (BCD74 x Baronesse, n=94. BCD47-susceptible parent, Baronesse-resistant parent) to map the locus conferring resistance. The resistant phenotype mapped to chromosome 1H (**Figure 3.4A**), and had strong linkage with a marker located in the *Mla* locus (**Figure 3.4B**), suggesting that resistance to the isolate Ina87T-56A could be conferred by *Mla3*. To test for the presence of additional *PWL2* alleles in the isolate Ina87T-56A, I sequenced the genome of this *M. oryzae* isolate using Oxford Nanopore Technologies. A tBLASTn search on the assembled Ina87T-56A genome using the protein sequence of wild-type Pwl2 as query identified three hits in two different contigs (**Figure 3.4C**). Two hits, located in opposite orientations in contig 7 and separated by approximately 30 kb, had the D90N substitution and therefore corresponded to two copies of the *pwl2-2* allele. The additional hit, located in contig 89, had 100% identity to wild-type *PWL2,* which is recognised by *Mla3* in Baronesse, explaining the avirulent phenotype of this isolate. Overall, this result is consistent with the conserved specificity of *PWL2* recognition in barley and weeping lovegrass.

It is possible that the D90N mutation in pwl2-2 affects protein stability and therefore favours escape of recognition in both grass species. Alternatively, the change of aspartic acid for asparagine might have an impact on intramolecular interactions that affect the overall protein structure and therefore its recognition. It can also have an effect at the intermolecular level, affecting the binding interface with Mla3 or the immune receptor in weeping lovegrass (in case of direct recognition), or with a guardee/decoy

protein (in case of indirect recognition). The latter case would be consistent with mutations of AVR effectors in solvent exposed regions at the binding interface with their corresponding NLRs that lead to escape of recognition (Białas et al., 2018; De la Concepcion et al., 2018; Ortiz et al., 2022).

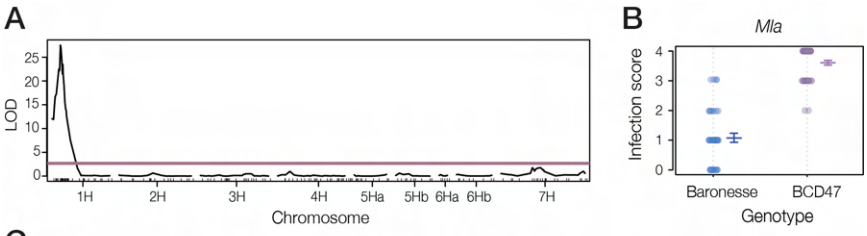

C

```
>contig_89
Length=391272

 Score = 257 bits (656),  Expect = 2e-78, Method: Compositional matrix adjust.
 Identities = 145/145 (100%), Positives = 145/145 (100%), Gaps = 0/145 (0%)
 Frame = +2
                    Signal Peptide
Query  1       MKCNNIILPFALVFFSTTVTAGGGWTNKQFYNDKGEREGSISIRKGSEGDFNYGPSYPGG  60
               MKCNNIILPFALVFFSTTVTAGGGWTNKQFYNDKGEREGSISIRKGSEGDFNYGPSYPGG
Sbjct  213635  MKCNNIILPFALVFFSTTVTAGGGWTNKQFYNDKGEREGSISIRKGSEGDFNYGPSYPGG  213814

Query  61      PDRMVRVHENNGNIRGMPPGYSLGPDHQEDKSDRQYYNRHGYHVGDGPAEygnhgggqwg  120
               PDRMVRVHENNGNIRGMPPGYSLGPDHQEDKSDRQYYNRHGYHVGDGPAEYGNHGGGQWG
Sbjct  213815  PDRMVRVHENNGNIRGMPPGYSLGPDHQEDKSDRQYYNRHGYHVGDGPAEYGNHGGGQWG  213994

Query  121     dgyygpppgEFTHEHREQREEGCNIM  145
               DGYYGPPGEFTHEHREQREEGCNIM
Sbjct  213995  DGYYGPPGEFTHEHREQREEGCNIM  214069

>contig_7
Length=6585452

 Score = 255 bits (651),  Expect = 8e-78, Method: Compositional matrix adjust.
 Identities = 144/145 (99%), Positives = 145/145 (100%), Gaps = 0/145 (0%)
 Frame = +2
                    Signal Peptide
Query  1       MKCNNIILPFALVFFSTTVTAGGGWTNKQFYNDKGEREGSISIRKGSEGDFNYGPSYPGG  60
               MKCNNIILPFALVFFSTTVTAGGGWTNKQFYNDKGEREGSISIRKGSEGDFNYGPSYPGG
Sbjct  562589  MKCNNIILPFALVFFSTTVTAGGGWTNKQFYNDKGEREGSISIRKGSEGDFNYGPSYPGG  562768

Query  61      PDRMVRVHENNGNIRGMPPGYSLGPDHQEDKSDRQYYNRHGYHVGDGPAEygnhgggqwg  120
               PDRMVRVHENNGNIRGMPPGYSLGPDHQE+KSDRQYYNRHGYHVGDGPAEYGNHGGGQWG
Sbjct  562769  PDRMVRVHENNGNIRGMPPGYSLGPDHQENKSDRQYYNRHGYHVGDGPAEYGNHGGGQWG  562948

Query  121     dgyygpppgEFTHEHREQREEGCNIM  145
               DGYYGPPGEFTHEHREQREEGCNIM
Sbjct  562949  DGYYGPPGEFTHEHREQREEGCNIM  563023


 Score = 255 bits (651),  Expect = 8e-78, Method: Compositional matrix adjust.
 Identities = 144/145 (99%), Positives = 145/145 (100%), Gaps = 0/145 (0%)
 Frame = -1
                    Signal Peptide
Query  1       MKCNNIILPFALVFFSTTVTAGGGWTNKQFYNDKGEREGSISIRKGSEGDFNYGPSYPGG  60
               MKCNNIILPFALVFFSTTVTAGGGWTNKQFYNDKGEREGSISIRKGSEGDFNYGPSYPGG
Sbjct  592172  MKCNNIILPFALVFFSTTVTAGGGWTNKQFYNDKGEREGSISIRKGSEGDFNYGPSYPGG  591993

Query  61      PDRMVRVHENNGNIRGMPPGYSLGPDHQEDKSDRQYYNRHGYHVGDGPAEygnhgggqwg  120
               PDRMVRVHENNGNIRGMPPGYSLGPDHQE+KSDRQYYNRHGYHVGDGPAEYGNHGGGQWG
Sbjct  591992  PDRMVRVHENNGNIRGMPPGYSLGPDHQENKSDRQYYNRHGYHVGDGPAEYGNHGGGQWG  591813

Query  121     dgyygpppgEFTHEHREQREEGCNIM  145
               DGYYGPPGEFTHEHREQREEGCNIM
Sbjct  591812  DGYYGPPGEFTHEHREQREEGCNIM  591738
```

Figure 3.4 The *M. oryzae* isolate Ina87T-156A carries *PWL2* and *pwl2-2*.

(A) LOD score plot mapping resistance to isolate Ina87T-156A to chromosome 1H in the ORO double haploid population (BCD47 x Baronesse, n=94) **(B)** Genotype vs. phenotype plot of the ORO double haploid population spot-inoculated with the *M. oryzae* isolate Ina87T-156A. The plot shows strong association of the K_Mla_RGH1_2920 marker at the *Mla* locus with resistance to *M. oryzae* isolate Ina87T-156A. Scores 0 and 1 = resistant and 2 to 4 = susceptible. **(C)** tBLASTn hits in the genome of isolate Ina87T-56A using the protein sequence of wild-type Pwl2 as query. Contigs in which hits were found are highlighted in blue. The frame of each hit is highlighted in green. Position D90 in protein alignments is highlighted in pink.

3.2.5 Weeping lovegrass lacks an *Mla* ortholog

The resistance gene that recognises *PWL2* in weeping lovegrass has not been identified so far. We constructed a maximum likelihood phylogenetic tree to determine if an *Mla* ortholog is present in *E. curvula* and related grass species. For this, we used the protein sequence of the nucleotide binding (NB) domain of NLRs from seven grass species representatives of the BOP clade (barley—*H. vulgare* (Mascher et al., 2021), rice—*Oryzae sativa* (Goff et al., 2002), and *Brachypodium distachyon* (Vogel et al., 2010)) and the PACMAD clade (weeping lovegrass—*E. curvula* (Carballo et al., 2019), maize—*Zea mays* (Schnable et al., 2009), *Setaria italica* (Bennetzen et al., 2012), and *Sorghum bicolor* (Paterson et al., 2009)). We superimposed the previous clade classification by Bailey et al. (2018), which placed the *RGH1* gene family—the gene family *Mla3* belongs to—in the C17 clade (Bailey et al., 2018b) (**Figure 3.5A**). The C17 clade contained 34 NLRs from *B. distachyon*, 36 NLRs from barley, 36 NLRs from rice, 30 NLRs from *S. bicolor*, 49 NLRs from *S. italica*, 25 NLRs from *Z. mays*, and 101 NLRs from weeping lovegrass. Several subclades within the C17 clade had well supported bootstrap and contained orthologous NLRs from the majority of the analysed grass species (**Figure 3.5B**). However, when looking at the *RGH1* subclade, only NLRs from barley and *B. distachyon* were found, suggesting that this gene family is absent in the PACMAD clade. A single NLR from weeping lovegrass, TVU02487, was found in the sub-tree that contains the *RGH1* sub-clade, but in a different clade outside and distinct from the *RGH1* sub-clade (**Figure 3.5C**). This result indicates that weeping lovegrass lacks an *Mla* ortholog and therefore, recognition of *PWL2* in this grass species is likely conferred by a resistance gene outside of the *RGH1* family.

These results suggest that independent loci in barley and weeping lovegrass convergently evolved to recognise *PWL2*. The mechanism of *PWL2* recognition has not been established in either grass species. However, if a model of indirect recognition is correct, perhaps *PWL2* has a common host target that is guarded by *Mla3* in barley and by the *R* gene of distinct origin in weeping lovegrass. Similar cases of convergent effector recognition by different plant species have been documented. The *P. syringae* effector AvrPphB, for example, cleaves the *A. thaliana* protein kinase PBS1 triggering recognition by the CNL RPS5 (Ade et al., 2007; DeYoung et al., 2012). AvrPphB is also recognised in soybean and barley via guarding of PBS1 orthologues. However, soybean lacks an RPS5 ortholog and *Pbr1* (AvrPphB Response 1), the barley NLR that recognises AvrPphB, is not orthologous to RPS5 (Jenner et al., 1991; Carter et al., 2018; Helm et al.,

2019). This indicates that independent NLRs convergently evolved to guard a conserved AvrPphB host target in distantly related plant species (Pottinger and Innes, 2020). If, however, Mla3 and the immune receptor in weeping lovegrass directly recognise Pwl2, it is likely that both *R* genes recognise similar binding interfaces of Pwl2, as specificity of recognition is maintained in these grass species. This would suggest that both immune receptors evolved to recognise a common structural feature of *PWL2*. Nonetheless, a mixed model in which one NLR evolved to directly recognise *PWL2,* whereas the other recognises modification of a *PWL2* host target is also plausible. Understanding the principles behind the mechanism of *PWL2* recognition by *Mla3* in barley might aid the identification of the *R* gene in weeping lovegrass conditioning the host range of rice-infecting isolates of *M. oryzae*.

3.3 Conclusions

3.3.1 Main conclusions

In this chapter I established that *AVR-rmo1*, the *M. oryzae* effector recognised by *Mla3,* is *PWL2*. A forward genetics screen using UV mutagenesis identified a group of *avr-Rmo1* mutants that gained virulence in the accession Baronesse (*Mla3*) and commonly lost *PWL2*. *PWL2*-complemented *avr-Rmo1* mutants became avirulent in Baronesse and in *Mla3* transgenic Golden Promise plants, confirming the identity of *PWL2* as *AVR-Rmo1*. *PWL2* is an effector known to condition pathogenicity of rice-infecting isolates of *M. oryzae* on weeping lovegrass (Sweigard et al., 1995). These results indicate that both barley and weeping lovegrass evolved to recognise the host-specificity determinant *PWL2*. I also established that the single amino acid substitution D90N in the Pwl2-2 allele is sufficient to escape recognition by *Mla3* in barley, as previously reported for weeping lovegrass. This suggests that specificity of *PWL2* recognition is maintained in both grass species. Even though the weeping lovegrass *R* gene recognising *PWL2* has not been identified, I showed that this grass species lacks an *Mla* ortholog, thus suggesting that recognition of *PWL2* convergently evolved from independent loci in these two distantly related monocot species. Overall, these results add evidence to the functional diversification of *Mla* and provide a platform to further understand the recognition of multiple pathogens by this NLR. Identifying the gene underlying AVR_{a3}—the *Bgh* effector recognised by *Mla3*—and understanding the molecular basis of AVR_{a3} and *PWL2* recognition will be crucial to shed light on the mechanisms driving recognition of multiple pathogens by *Mla*.

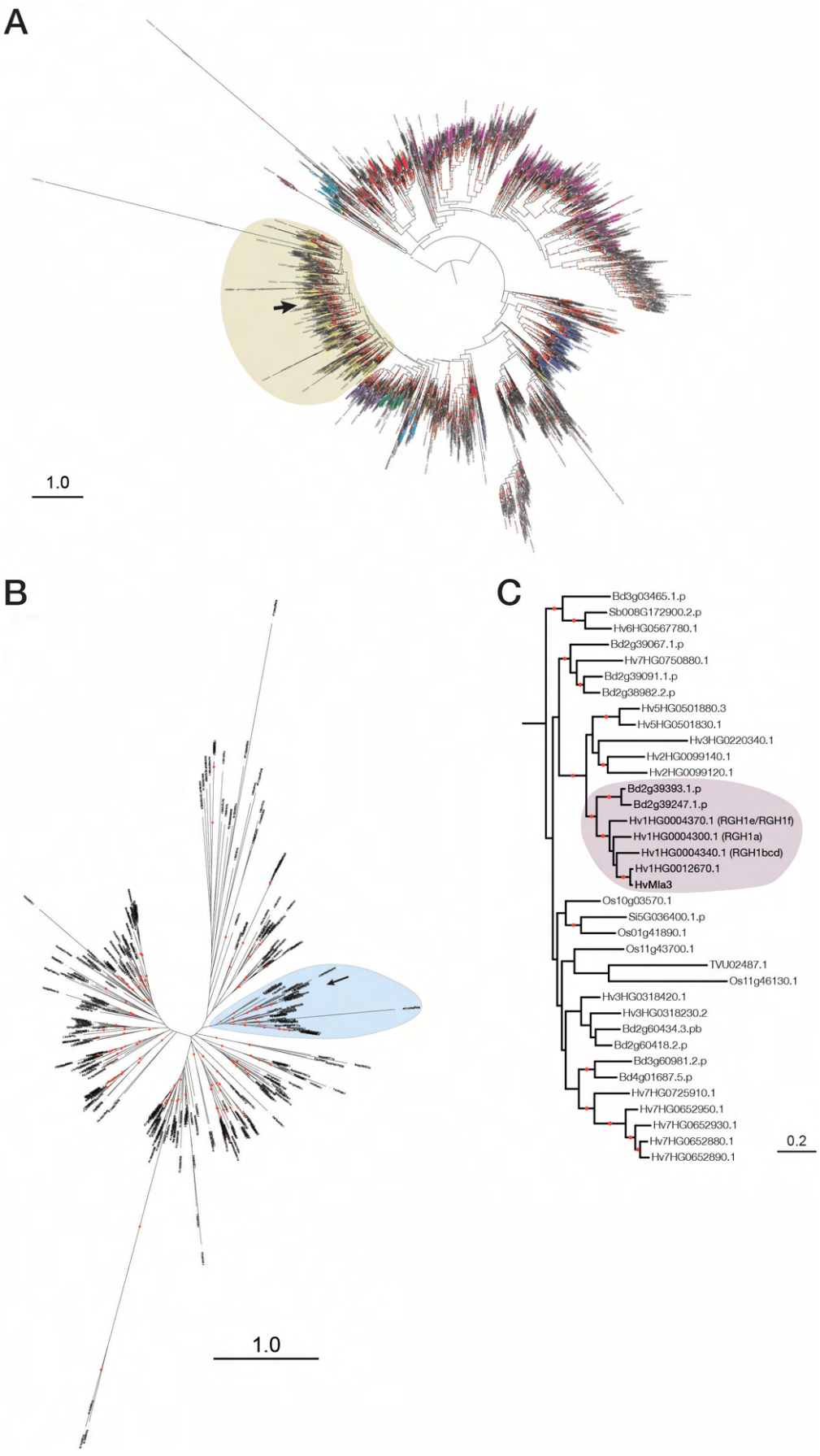
A
1.0
B
1.0
C
Bd3g03465.1.p
Sb008G172900.2.p
Hv6HG0567780.1
Bd2g39067.1.p
Hv7HG0750880.1
Bd2g39091.1.p
Bd2g38982.2.p
Hv5HG0501880.3
Hv5HG0501830.1
Hv3HG0220340.1
Hv2HG0099140.1
Hv2HG0099120.1
Bd2g39393.1.p
Bd2g39247.1.p
Hv1HG0004370.1 (RGH1e/RGH1f)
Hv1HG0004300.1 (RGH1a)
Hv1HG0004340.1 (RGH1bcd)
Hv1HG0012670.1
HvMla3
Os10g03570.1
Si5G036400.1.p
Os01g41890.1
Os11g43700.1
TVU02487.1
Os11g46130.1
Hv3HG0318420.1
Hv3HG0318230.2
Bd2g60434.3.pb
Bd2g60418.2.p
Bd3g60981.2.p
Bd4g01687.5.p
Hv7HG0725910.1
Hv7HG0652950.1
Hv7HG0652930.1
Hv7HG0652880.1
Hv7HG0652890.1
0.2

Figure 3.5 PACMAD grasses lack an ortholog of the *RGH1* (*Mla*) gene family.

(A) Structure-guided phylogenetic tree of NLR NB domain from several BOP and PACMAD grasses**.** Maximum likelihood phylogenetic tree based on structure-guided multiple sequence alignment of the nucleotide binding domain (Pfam: PF00931) of NLRs from barley, rice, *B. distachyon*, *S. bicolor*, *S. italica*, maize, and weeping lovegrass. Colour coding of clades is based on original classification by Bailey *et al.* (2018) with the C17 clade in yellow. The position of *Mla* is indicated by an arrow. **(B)** C17 clade from **A** displaying NLRs from barley, rice, *B. distachyon*, *S. bicolor*, *S. italica*, maize, and weeping lovegrass. Light blue indicates the subclade containing the RGH1 (Mla) protein family. The position of *Mla* is indicated by an arrow. The NB domain from *Arabidopsis thaliana* ZAR1 (PDB: 6J5T) was used as outgroup in **A** and **B**. **(C)** Sub-tree of the *RGH1* gene family and related NLRs highlighted in light blue in **B**. The sub-tree contains NLRs from all grass species except maize. (Hv: barley, Os: rice, Bd: *B. distachion,* Sb: *S. bicolor*, Si: *S. italica,* TVU: *E. curvula*). The *RGH1* subclade is highlighted in dark red. Bootstrap support with NLRs from both PACMAD and BOP grasses is observed within this sub-tree. Dots on branches indicate bootstrap support exceeding 80%.

3.3.2 Recognition of AVR_{a3} and Pwl2 by Mla3

Most *AVR_a* effectors from *Bgh* identified so far belong to the family of RALPH proteins and have an RNAse-like fold. A model of direct recognition has been proposed for the sequence unrelated *AVR_{a1}, AVR_{a6}*, *AVR_{a7}*, *AVR_{a10}* and *AVR_{a13}* effectors by their cognate *Mla* alleles in barley. Interaction of Mla-*AVR_a* corresponding pairs in yeast-two-hybrid assays and split luciferase experiments suggests the direct recognition of these sequence-unrelated structurally similar effectors by almost sequence identical *Mla* alleles (Saur et al., 2019; Bauer et al., 2021). The *Mla* orthologue Sr50 in rye also directly recognises the effector AvrSr50 from the wheat stem rust pathogen *Pgt* (Chen et al., 2017). This highlights the ability of NLRs with the same origin to recognise highly divergent pathogens, outlined by the fact that *Bgh* is an Ascomycete, whereas *Pgt* is a Basidiomycete. Interestingly, the crystal structure of the effector AvrSr50 revealed that it does not have an RNAse-like fold but rather has structural homology to cupin superfamily members and carbohydrate binding modules (Ortiz et al., 2022). This indicates that the *Mla* NLR family has evolved the functional capacity to directly recognise structurally similar effectors from *Bgh,* as well as sequence and structurally unrelated effectors like AvrSr50 from *Pgt*.

Mla has been reported to recognise multiple pathogens. The *Mla8* allele confers resistance against the non-adapted pathogen wheat stripe rust (*Pst*) (Bettgenhaeuser et al., 2021). However, the identity of *AVR_{a8}* from *Bgh* and the *Pst* effector recognised by *Mla8* remain unknown*,* as well as the identity of *AVR_{a3}* recognised by *Mla3*. Interestingly, the AlphaFold2 structure prediction of Pwl2 (Seong and Krasileva, 2023) and subsequent

structural similarity search on the Dali server suggest that Pwl2 has a similar fold to the AvrPiz-t and AVR-Pik *M. oryzae* effectors, which belong to the family of MAX effectors with a conserved fold of a six-stranded β-sandwich with two antiparallel β-sheets (de Guillen et al., 2015; Maqbool et al., 2015; De la Concepcion et al., 2018). This has been confirmed by the crystal structure of Pwl2 in complex with a host target (Zdrzalek, 2021). The MAX fold is structurally distinct from the RNAse-like fold present in most of the AVR_a *Bgh* effectors identified so far, and no *Bgh* effectors are predicted to cluster within the MAX effector family (Seong and Krasileva, 2023). This suggests that Mla3 most likely recognises two structurally distinct effectors from *M. oryzae* and *Bgh*.

Understanding the mechanism of recognition of structurally distinct effectors by *Mla* is one of the main questions that arises from these results. On the one hand, in agreement with the model of direct recognition of *Mla-*AVR_a cognate pairs, one possibility is that Mla3 directly binds to AVR_{a3} and Pwl2, which most likely have different overall structures. In this case, it remains to be established whether specificity of recognition of AVR_{a3} and Pwl2 is determined by the same or overlapping regions of Mla3, or if distinct binding interfaces in this NLR are required for recognition of each effector. Despite overall structural differences, AVR_{a3} and Pwl2 might share partial local conserved features that are recognised by Mla3. A second hypothesis corresponds to a model of indirect recognition in which these two effectors have commonly evolved to interact or modify the same host target guarded by Mla3. In any case, identification of *AVR*$_{a3}$ is necessary to elucidate the mechanism of recognition in parallel with that of *PWL2*. In the meantime, identifying the regions in Mla3 required for specificity of Pwl2 recognition and establishing whether Mla3 directly or indirectly recognises Pwl2 is crucial to understand the mechanisms driving multiple pathogen recognition in *Mla*.

Chapter 4: Specificity of Pwl2 recognition is determined by the C-terminal region of Mla3

4.1 Introduction

Nucleotide-binding leucine-rich repeat receptors (NLRs) encompass most of the resistance (*R*) genes in plants that confer intracellular recognition of pathogen-secreted effectors (Jones et al., 2016). Effector recognition by plant NLRs triggers a robust immune response, often associated with a form of programmed cell death termed hypersensitive response (HR) that halts pathogen invasion (Jones and Dangl, 2006). In general, NLRs have a conserved domain architecture that includes an N-terminal signalling domain, a central nucleotide binding NB-ARC domain, and a C-terminal leucine-rich repeat (LRR) domain (Bonardi et al., 2012; Kourelis et al., 2021). Based on the N-terminal domain, NLRs can be broadly classified into TNLs, which carry a Toll/interleukin-1 receptor (TIR) domain; CNLs, which have a coiled-coil (CC) N-terminal domain; or RNLs, which have an RPW8-type CC N-terminal domain (Shao et al., 2016; Duxbury et al., 2021). The expression of several truncated CNLs and TNLs carrying solely the N-terminal domain is often sufficient to trigger an immune response, highlighting the role of this region in signalling and cell death execution (Krasileva et al., 2010a; Collier et al., 2011; Maekawa et al., 2011; Bai et al., 2012; Cesari et al., 2016). The NB-ARC domain, on the other hand, has nucleotide binding and ATPase activities (Bonardi et al., 2012). The ADP bound state of the nucleotide binding pocket located in the NB-ARC domain is associated with the inactive state of NLRs (van Ooijen et al., 2008). Activation takes place when ADP is exchanged by ATP, hence promoting oligomerisation of the NB-ARC domain (Bonardi and Dangl, 2012) and formation of a wheel-like structure known as resistosome, which ultimately results in a cell death response (Wang et al., 2019a; Wang et al., 2019b; Ma et al., 2020; Martin et al., 2020b; Förderer et al., 2022b; Zhao et al., 2022). Lastly, the LRR domain is usually associated with effector recognition through direct binding or by sensing self-molecules modified by effectors (Qi and Innes, 2013). Effector recognition by the LRR region generally induces major structural changes that modify intramolecular interactions with the NB-ARC domain and promote ATP binding, thus leading to resistosome formation (Maruta et al., 2022). A subset of NLRs also have non-canonical integrated domains (IDs), which are generally host effector-targets that were integrated into the canonical NLR domain

architecture and mediate recognition, mostly through direct binding (Cesari et al., 2014; Kroj et al., 2016; Sarris et al., 2016; Marchal et al., 2022b).

NLRs that can act as single units that sense effectors and trigger an immune response without the aid of additional receptors are known as singleton NLRs. Some well-studied examples are the *A. thaliana ZAR1*, *Mla* in barley, *Sr35* in wheat, and *Sr50* in rye (Adachi et al., 2019a). Contrarily, all characterised NLRs with IDs act as sensors that detect effectors, but require another NLR—usually called helper—to initiate an immune response, thus functioning as pairs (Cesari et al., 2014; Cesari, 2018). Some examples are the RGA4/RGA5 and the Pik-1/Pik-2 pairs in rice, in which the sensors RGA5 and Pik-1 have an HMA ID that binds MAX effectors from *M. oryzae,* and RGA4 and Pik-2 act as helpers, respectively (Cesari et al., 2013; Césari et al., 2014; Białas et al., 2021). In addition, NLRs can also work as complex networks in which multiple sensors signal through one or more helper NLRs to trigger a hypersensitive response, and likewise, a single helper can assist more than one sensor (Wu et al., 2017). Such functional specialisation of NLRs implies asymmetrical evolutionary trajectories and origins (Wu et al., 2017; Prigozhin and Krasileva, 2021; Shimizu et al., 2022).

The clustered arrangement of NLRs in plant genomes promotes diversification through gene duplication and recombination events (Michelmore and Meyers, 1998). This allows for the emergence of different NLRs with novel functions, paralogous NLRs that extend the breadth of recognised pathogens, or NLR allelic variants with distinct recognition specificities of effectors (Prigozhin and Krasileva, 2021). Such is the case of the *Mla* locus in barley which comprises a complex cluster of three families of NLRs (*Resistance Gene Homologues 1, 2* and *3*) (Wei et al., 1999). The *Mla RGH1* family confers isolate specific resistance to the powdery mildew pathogen *Blumeria graminis* f. sp. *hordei* (*Bgh*) (Jørgensen and Wolfe, 1994), and exists as a series of over 30 alleles that recognise cognate AVR_a effectors from *Bgh* (Seeholzer et al., 2010). These alleles are >90% identical, yet they directly recognise sequence-unrelated effectors that are predicted to have a common RNAse-like fold (Lu et al., 2016; Saur et al., 2019; Bauer et al., 2021), highlighting remarkable functional diversification.

NLR specialisation and mode of effector recognition can be reflected in evolutionary signatures imprinted by distinct selective pressures throughout the different protein domains (Prigozhin and Krasileva, 2021). Indirect effector recognition requires monitoring of conserved effector activities on host proteins, and generally exerts purifying selection on NLR regions that sense effector targets. In contrast, regions that

directly bind effectors are most likely under diversifying selection as a means to maintain recognition of effectors that are rapidly evolving to avoid recognition (Prigozhin and Krasileva, 2021). This is illustrated, for example, by the high rate of non-synonymous mutations of the HMA ID in Pik-1 relative to its NB-ARC domain, or to the Pik-2 helper as a whole (Białas et al., 2018; Białas et al., 2021). In this case, the HMA domain of Pik-1 directly senses the effector AVR-Pik from *M. oryzae* to trigger an immune response (Maqbool et al., 2015). This diversifying selective pressure often results in the generation of expanded allelic series such as the *RPP13* locus in *A. thaliana* (Bittner-Eddy et al., 2000), the *L* locus in flax (Dodds et al., 2006), *Mla* in barley (Seeholzer et al., 2010) and *Pm3* in wheat (Srichumpa et al., 2005). Different Mla alleles directly bind to their corresponding AVR_a effectors (Saur et al., 2019). Not surprisingly, the LRR domain, thought to mediate recognition, contains most sites under positive selection (Seeholzer et al., 2010; Maekawa et al., 2018), indicating that determination of specificity lies within this region.

Functional diversification in *Mla* is not only reflected by the expanded allelic series that directly recognise non-allelic AVR_a effectors from *Bgh,* but also by the recognition of highly divergent pathogens. In addition to conferring resistance against *Bgh* isolates that carry corresponding AVR_a effectors, the *Mla8* allele confers resistance to the wheat stripe rust pathogen *Puccinia striiformis* f. sp. *tritici* (*Pst*) (Bettgenhaeuser et al., 2021), and the *Mla3* allele confers resistance against the blast fungus *M. oryzae* (Brabham, 2019). The genes underlying the cognate effectors AVR_{a8} and AVR_{a3} remain unknown; however it is hypothesised that they belong to the family of RALPH (RNAse-like protein expressed in haustoria) effectors with an RNAse-like fold, as the already identified AVR_{a1}, AVR_{a6}, AVR_{a7}, AVR_{a10}, AVR_{a13}, and AVR_{a22} (Bauer et al., 2021). In the previous chapter, I established that *Mla3* confers resistance against *M. oryzae* by recognising the known effector *PWL2*. Interestingly, Pwl2 belongs to the family of MAX effectors (Zdrzalek, 2021), and is structurally unrelated to the RNAse-like fold of AVR_a proteins. The secretome of *Bgh* does not contain any predicted MAX effectors (Seong and Krasileva, 2023), thus suggesting that *Mla3* recognises two structurally divergent effectors from different pathogens.

In this chapter, I aimed to establish the regions delimiting specificity of Pwl2 recognition by Mla3. For this, I took advantage of the natural variation amongst *Mla* alleles to find the closest allele to Mla3 that does not recognise Pwl2. I generated chimeric swaps between Mla3 and Mla23, which only differ by 19 amino acids at the C-terminus,

to delimit regions required for Pwl2 recognition. I established that swapping a single residue in the Mla23 and Mla34 alleles was sufficient to confer recognition of Pwl2. Mla3 is the only allele with a basic residue in this position, highlighting the role of this amino acid in specificity of Pwl2 recognition. It remains to be established whether similar, overlapping, or distinct regions of Mla3 determine specificity of recognition of the *Bgh* effector AVR_{a3}, and whether recognition of these two effectors is direct or indirect.

4.2 Results and discussion

4.2.1 Mla3 is functional in *Nicotiana benthamiana*

Previous studies have shown that transient expression of Mla10 alone, or the CC domain of Mla10 or other Mla orthologues (i.e. Sr33 and Sr35) is sufficient to trigger cell death in *N. benthamiana* (Maekawa et al., 2011; Bai et al., 2012; Cesari et al., 2016). In order to establish *N. benthamiana* as a suitable heterologous system to test hypotheses about Pwl2 recognition by Mla3, I tested whether Mla3 is functional and can trigger an immune response in this model dicot plant. To test whether full length Mla3 and/or its CC domain trigger an immune response in *N. benthamiana,* I overexpressed full length Mla3 or its CC domain in *N. benthamiana* using *Agrobacterium tumefaciens*-mediated transient leaf transformation. I did not observe HR when Mla3 was transiently expressed in *N. benthamiana,* in contrast to Mla10—which induced constitutive cell death even when expressed at a low levels—(**Figure 4.1A**). Noteworthy, expression of the Mla3-CC domain did result in cell death, in accordance with previous reports of phylogenetically related NLRs (**Figure 4.1A**) (Bai et al., 2012; Cesari et al., 2016). Several functional studies have found mutations that render NLRs autoactive. These autoactivating mutations are frequently found in the NB-ARC domain, at the conserved methionine-histidine-aspartate (MHD) motif (Bendahmane et al., 2002; van Ooijen et al., 2008), and are thought to change the conformation of the nucleotide binding pocket, thereby inducing preferential ATP binding and constitutive NLR activation (Bentham et al., 2017; Maruta et al., 2022). MHD mutations are therefore used as a proxy to test plant immune responses (Bai et al., 2012). To test the capacity of Mla3 to function in *N. benthamiana*, I generated single amino acid substitutions in the full-length context of Mla3 that were previously reported to enhance the autoactivity of Mla10. Three independent point mutations in the MHD motif of Mla3 (which is valine-histidine-aspartate, VHD, in Mla proteins), namely H501G, H501Q and D502V, resulted in constitutive cell death activity (**Figure 4.1A**). The F99E substitution in the CC domain of Mla10 previously resulted in

a potentiated autoinducing cell death activity (Bai et al., 2012). However, this substitution did not render Mla3 autoactive (**Figure 4.1A**). Expression of all constructs was confirmed by western blot (**Figure 4.1C**), demonstrating that absence of cell death was not due to lack of protein accumulation. Mla3 and Mla3^{F99E} protein levels were considerably higher than the autoactive mutants (Mla3^{H501G}, Mla3^{H501Q} and Mla3^{D502V}) likely due to the cell death phenotype induced by the latter. Taken together, the constitutive cell death of the Mla3-CC domain and the Mla3 MHD mutants indicate that this NLR is functional in *N. benthamiana,* a dicot heterologous system. This result validates the use of this model plant as suitable for further characterisation of Pwl2 recognition by Mla3.

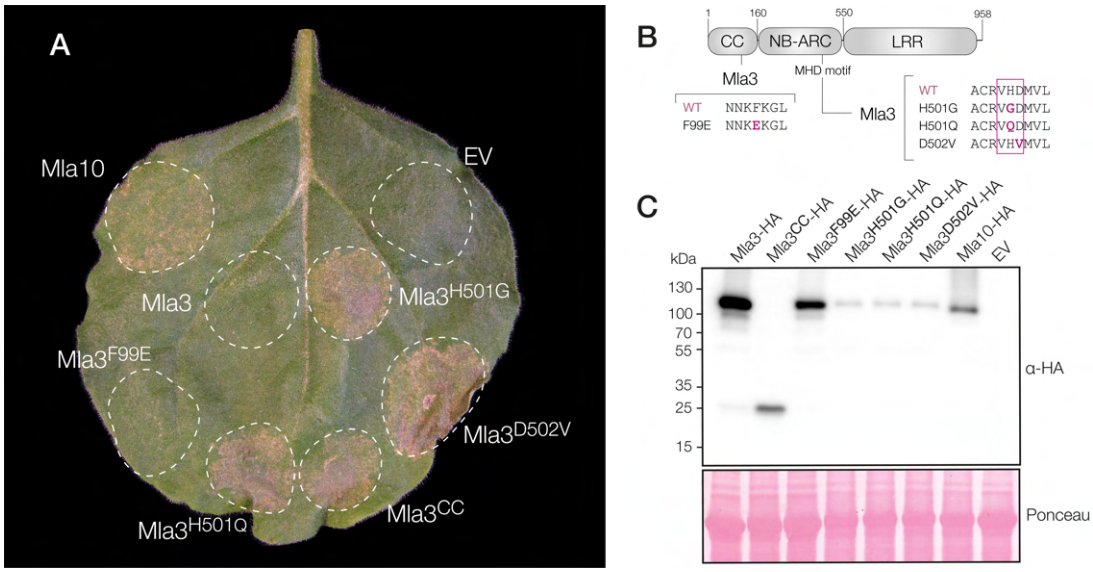

Figure 4.1 Mla3 is functional in *N. benthamiana*.

Cell death-inducing activity of full-length Mla3, Mla3-CC domain, and single amino acid Mla3 mutants in the CC domain (F99E) and the VHD motif (H501Q, H501G and D502V), using transient expression in *N. benthamiana*. Mla10 was used as positive control of autoactivity and empty vector (EV) was used as negative control. All constructs were expressed at an OD_{600} = 0.25, except Mla10 which was expressed at an OD_{600} = 0.1. **(A)** Representative photo of a *N. benthamiana* leaf expressing the indicated constructs. All proteins were expressed under the strong Mas Ω promoter and C-terminally fused to a 6xHA epitope tag. Photos were taken 3 dpi. The experiment was independently repeated three times with 8-10 technical replicates. **(B)** Schematic representation of Mla3 and the mutated sites. Substituted residues are shown in dark pink in the sequence alignment. The VHD motif is marked by a rectangle. **(C)** Anti-HA immunoblots of Mla3-6xHA (115.6 kDa), Mla3^{CC}-6xHA (25.7 kDa), Mla3^{F99E}-6xHA (115.6 kDa), Mla3^{H501G}-6xHA (115.6 kDa), Mla3^{H501Q}-6xHA (115.6 kDa), Mla3^{D502V}-6xHA (115.6 kDa) and Mla10-6xHA (114.6 kDa) expressed in *N. benthamiana*. Total protein extracts were prepared from leaves harvested 3 days after agroinfiltration. Protein loading was checked with Ponceau S solution (Sigma).

4.2.2 Mla3 recognises Pwl2 in *N. benthamiana*

Recent reports have shown that Mla1, Mla6, Mla7, Mla10, Mla13 and Mla22 trigger cell death in *N. benthamiana* when co-expressed with their corresponding *Bgh* effectors AVR_{a1}, AVR_{a6}, AVR_{a7}, AVR_{a10}, AVR_{a13} and AVR_{a22} (Saur et al., 2019; Bauer et al., 2021). In addition, co-expression of the rye Mla orthologue Sr50 and its cognate effector AvrSr50 from wheat stem rust also leads to cell death in *N. benthamiana* and tobacco leaves (Chen et al., 2017). To assess Pwl2 recognition by Mla3 in *N. benthamiana,* I performed transient Mla3-Pwl2 co-expression assays using *A. tumefaciens* to test for hypersensitive response. Co-expression of Mla3 and Pwl2 resulted in strong cell death, which is a hallmark of effector recognition (**Figure 4.2A**). When co-expressed with an empty vector, Pwl2 did not induce HR, indicating that cell death is specifically triggered by Mla3 activation. Co-expression of Mla3 with AVR-PikD, another *M. oryzae* effector which belongs to the family of MAX effectors, did not result in cell death, highlighting that Mla3 is specifically recognising Pwl2.

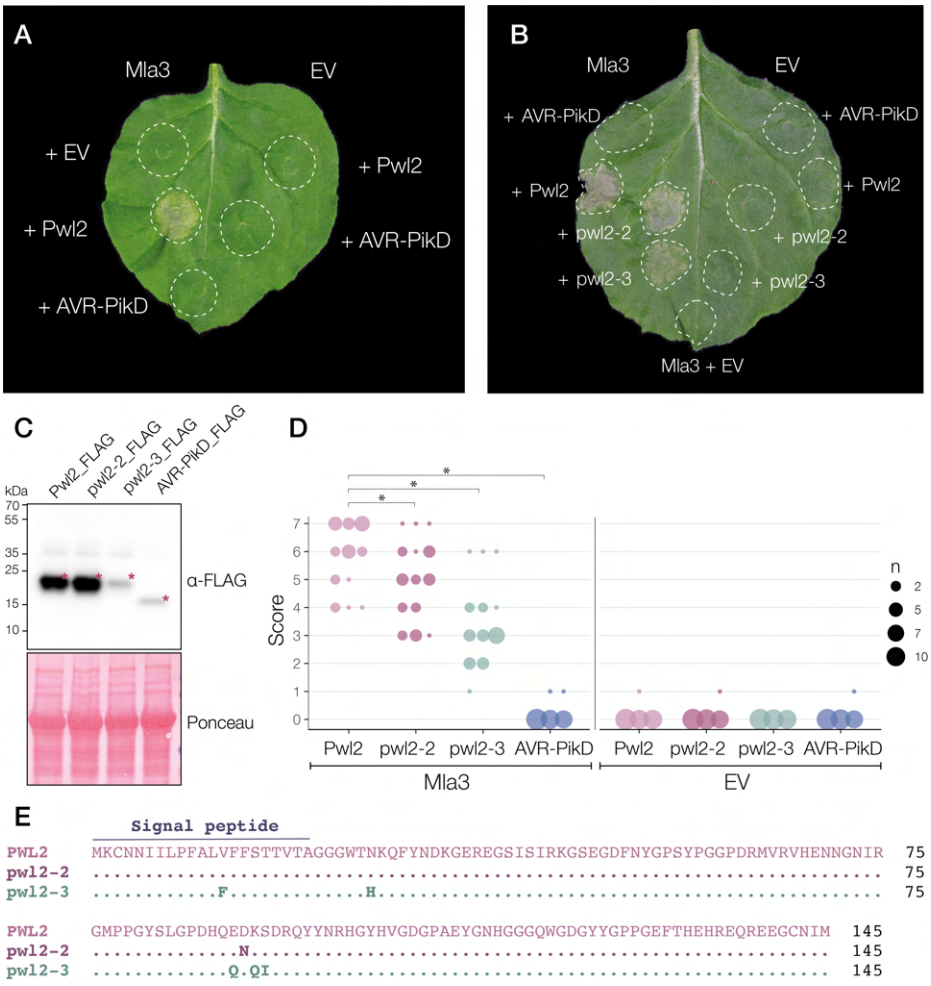

Figure 4.2 Mla3 recognises all Pwl2 alleles in *N. benthamiana.*

Mla3 triggers cell death upon co-expression with wild-type Pwl2, pwl2-2 and pwl2-3. The *M. oryzae* effector AVR-PikD and empty vector (EV) were used as negative controls. **(A and B)** Representative photo of a *N. benthamiana* leaf expressing the indicated constructs. Mla3 was expressed under the constitutive Mas Ω promoter and C-terminally fused to a 6xHA epitope tag. All Pwl2 alleles and AVR-PikD were expressed under the constitutive 35S Ω promoter, without signal peptide and C-terminally fused to a 3xFLAG tag. Photos were taken 3 dpi. **(C)** Anti-FLAG immunoblots of Pwl2-3xFLAG (17.3 kDa), pwl2-2-3xFLAG (17.3 kDa), pwl2-3-3xFLAG (17.3 kDa) and AVR-PikD-3xFLAG (14 kDa) expressed in *N. benthamiana.* Total protein extracts were prepared from leaves harvested 3 days after agroinfiltration. Protein loading was checked with Ponceau S solution (Sigma). **(D)** HR phenotypes from **B** were scored at three days post-agroinfiltration. The results are presented as a dot plot, where the size of a dot is proportional to the number of technical replicates with the same score within the same biological replicate. The experiments were independently repeated three times with 8-10 technical replicates; the three data point columns of each tested condition correspond to results from different biological replicates. Significant differences between conditions were calculated based on bootstrapping rank statistics and are indicated with asterisk (*). The details of the statistical analysis are shown in **Figure A.II.1. (E)** Protein sequence alignment of Pwl2 alleles.

Expression of Mla3 and Pwl2 was sufficient to trigger a hypersensitive response, indicating that no additional components were necessary to elicit effector recognition. This suggests the function of Mla3 as a singleton NLR, as previously reported for Mla10 (Bai et al., 2012; Adachi et al., 2019a). Mla3 can sense Pwl2 and elicit an immune response as a single functional unit. Even though it has not been characterised at the structural level like ZAR1 or Sr35—two well studied singleton NLRs (Wang et al., 2019a; Wang et al., 2019b; Förderer et al., 2022b; Zhao et al., 2022)—Mla3 presumably does not rely on other NLRs to function. In addition, Pwl2 elicited a hypersensitive response when co-expressed with Mla3 in *N. benthamiana,* suggesting either that this NLR directly binds to Pwl2 to trigger an immune response, or that the potential guardee or decoy required for indirect recognition of Pwl2 is highly conserved across phylogenetically distant plant species to natively mediate recognition by Mla3 in barley—a monocot species—and in *N. benthamiana*—a dicot plant. A model of direct recognition would fit previous reports of different Mla alleles that directly bind their corresponding AVR_a effectors from *Bgh* (Saur et al., 2019). However, Mla3 recognises two different effectors—Pwl2 and AVR_{a3}—and direct recognition of unrelated effectors from distinct pathogens by a single NLR has not yet been reported.

Pwl2 is highly prevalent across *M. oryzae* isolates (Latorre et al., 2020) and polymorphisms in Pwl2 alleles determine the outcome of infection in particular hosts. A single amino acid substitution (D90N) present in the pwl2-2 allele is sufficient to overcome recognition by Mla3 in barley and by a yet unknown *R* gene in weeping

lovegrass (Sweigard et al., 1995) (see section 3.2.4), therefore isolates that carry this allele are able to successfully infect such host plants. In addition, *M. oryzae* isolates that infect wheat carry another Pwl2 allele—pwl2-3—which has five amino acid polymorphisms compared to wild-type Pwl2 (V13F, N27H, E89Q, K91Q, S92I) (**Figure 4.2E**), and escapes resistance mediated by Mla3. Therefore, wheat blast isolates that carry pwl2-3 are virulent on barley. I performed transient co-expression assays to test whether recognition of the Pwl2 alleles in barley (or lack thereof) was recapitulated in *N. benthamiana*. Interestingly, both pwl2-2 and pw2-3 triggered cell death when co-expressed with Mla3, showing that Mla3 has the potential to recognise all alleles when transiently overexpressed in *N. benthamiana*. None of the Pwl2 alleles triggered HR when co-expressed with an empty vector. The cell death response triggered by recognition of wild-type Pwl2 was significantly stronger compared to recognition of pwl2-2 across biological replicates (**Figure 4.2B and D**). More evidently, the cell death phenotype triggered by recognition of pwl2-3 is weaker than that of Pwl2 and pwl2-2 (**Figure 4.2B and D**). This observation may be explained by lower protein levels of pwl2-3 compared to other alleles (**Figure 4.2C**), likely due to lower expression efficiency or higher protein turnover that can impact the strength of recognition. Overall, this indicates that recognition of wild-type Pwl2 by Mla3 is stronger than pwl2-2 and pwl2-3. Considering that this is a heterologous overexpression system, the threshold required to trigger an immune response upon recognition of the Pwl2 alleles by Mla3 might be considerably lower in *N. benthamiana* than in native conditions in barley, explaining the differences in outcomes in each plant species. Most likely, the strength of recognition of pwl2-2 and pwl2-3 by Mla3 is not sufficient to confer robust resistance in barley against *M. oryzae* isolates carrying these alleles.

Wild-type Pwl2 only differs from pwl2-2 and pwl2-3 by one and five amino acids, respectively (**Figure 4.2E**). Interestingly, three of the polymorphisms in pwl2-3 (E89Q, K91Q and S92I) are in the same region containing the D90N mutation in pwl2-2, which is sufficient to evade recognition in barley and weeping lovegrass. This suggests that this region plays an important role in effector recognition. It is possible that these polymorphisms affect protein stability; nonetheless, accumulation levels of pwl2-2 were comparable to Pwl2. Since all Pwl2 alleles triggered HR upon recognition by Mla3 in *N. benthamiana*, is unlikely that the polymorphisms in pwl2-2 and pwl2-3 affect a potential catalytic activity, considering a model of indirect recognition. I therefore hypothesise that these mutations likely impact binding of Pwl2 to Mla3, or to a potential guardee or decoy

protein. Elucidating the mechanism of Pwl2 recognition by Mla3 would allow NLR engineering strategies to enhance recognition of all Pwl2 alleles to translate into effective disease resistance.

4.2.3 The barley accession S13—which carries *Mla23*—recognises *PWL2*

Previous work showed that among a series of near-isogenic barley lines with different *Mla* alleles in the Siri genetic background, the accession S13—which carries *Mla23*—is resistant to *M. oryzae* KEN54-20, unlike its susceptible parent Siri (Brabham, 2019). *Mla23* is the most closely related allele to *Mla3,* with 98.6% protein sequence identity and variation limited to the C-terminus of the NLR. To test whether the barley accession S13 also recognises Pwl2, I performed spot inoculations on a panel of barley accessions using wild-type KEN54-20, an isolate lacking *PWL2* derived from UV mutagenesis (*pwl2*) (M61, section 3.2.1), and a *PWL2*-complimented *pwl2* mutant (M61+*PWL2*). The near isogenic line S02, which carries an *Mla* locus identical to Baronesse (*Mla3*), is resistant to *M. oryzae* isolates that carry *PWL2,* but susceptible to the *pwl2* mutant, just like Baronesse. Interestingly, the accession S13 had the same infection phenotypes as S02 and Baronesse, indicating that *PWL2* is also recognised in this accession (**Figure 4.3**). In this case, resistance to *M. oryzae* is mediated by the *Mla* locus, as S13 is a near-isogenic line that only differs genetically at this locus from its parent Siri, which is susceptible to *M. oryzae* in all cases. Manual inspection of available RNA-seq data from leaf tissue confirmed expression of *Mla23* (*RGH1*) but not of *RGH2* and *RGH3* in S13. These results, and the close phylogenetic relationship between *Mla3* and *Mla23,* suggest that *Mla23* could potentially recognise *PWL2* and thus confer resistance to *M. oryzae* in S13.

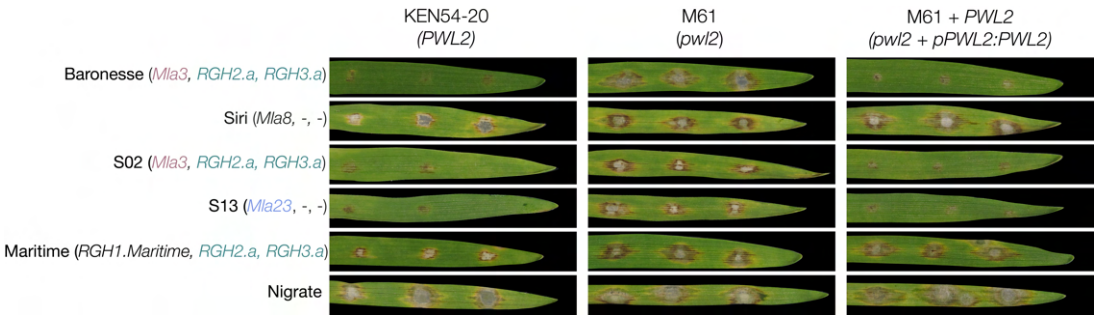

Figure 4.3 The Siri near isogenic line S13 recognises *PWL2*.

Spot infection assays with *M. oryzae* isolate KEN54-20 (*PWL2*), *pwl2* mutant M61, and M61 complemented with *PWL2* (*pwl2* + *pPWL2:PWL2*) on a panel of barley accessions comprised of Baronesse, Siri, the near isogenic lines S02 and S13, Maritime and Nigrate. Allelic variants of NLR genes in the *Mla* locus are indicated in parenthesis.

Figure 4.3 The Siri near isogenic line S13 recognises *PWL2* (continued)

Siri, Maritime, and Nigrate were used as susceptible controls. Infected leaves were imaged 7 dpi. Phenotypes are representative of three biological replicates with three technical replicates.

4.2.4 Close relatives of Mla3 do not recognise Pwl2 in *N. benthamiana*

Based on the *M. oryzae* infection phenotypes on the barley accession S13, I hypothesised that *Mla23* and other phylogenetically close relatives of *Mla3* might recognise *PWL2*. The closest *Mla3* related alleles are *Mla23, Mla34, Mla35* and *Mla39* (**Figure 4.4A**), which share 98.6%, 96.7%, 97.7% and 96.6% protein identity with Mla3, respectively. I performed transient expression assays in *N. benthamiana* to test whether these Mla alleles trigger a hypersensitive response upon co-expression with the Pwl2 alleles. None of the Mla3 close relatives recognised Pwl2, as no cell death was observed in any case apart from co-expression with Mla3 (**Figure 4.4B to F**). Expression of Mla34 resulted in cell death in combination with all the Pwl2 alleles, as well as with AVR-PikD or empty vector, showing the autoimmune phenotype of this allele under the tested conditions in *N. benthamiana* (**Figure 4.4E**). Protein levels of all tested Mla alleles were comparable, except for Mla35 which had lower protein accumulation (**Figure 4.4G**).

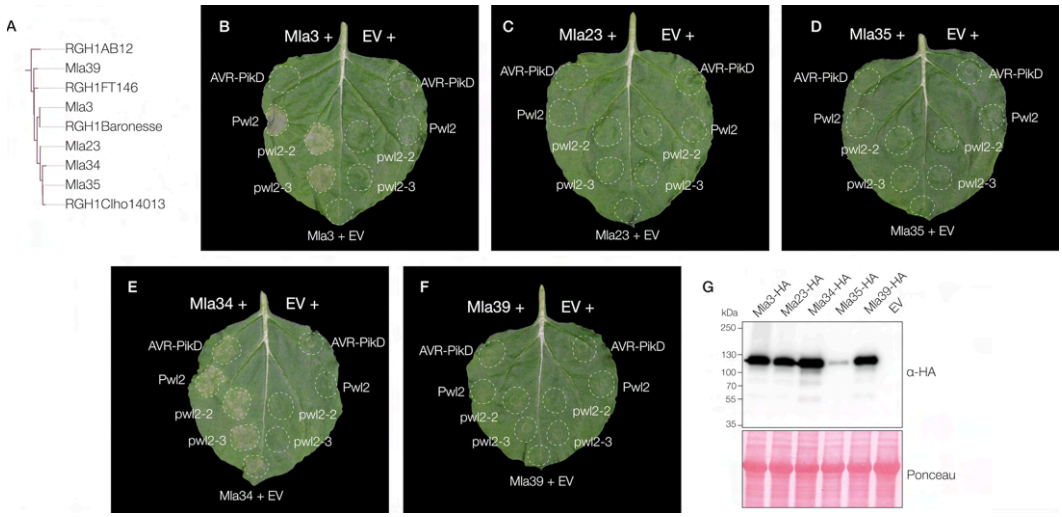

Figure 4.4 Mla3 close relatives do not recognise Pwl2 in *N. benthamiana.*

Only Mla3, but not its phylogenetically close relatives, trigger cell death upon co-expression with Pwl2. The *M. oryzae* effector AVR-PikD and empty vector (EV) were used as negative controls. **(A)** Phylogenetic tree showing the sub-clade of the RGH1 alleles closely related to *Mla3*. **(B to F)** Representative photo of a *N. benthamiana* leaf expressing the indicated constructs. Expression of Mla34 **(E)** resulted in autoactivity. All Mla alleles were expressed under the constitutive Mas Ω promoter and C-terminally fused to a 6xHA epitope tag.

Figure 4.4 Mla3 close relatives do not recognise Pwl2 in *N. benthamiana* (continued).

All Pwl2 alleles and AVR-PikD were expressed under the constitutive 35S Ω promoter, without signal peptide and C-terminally fused to a 3xFLAG tag. Photos were taken 3 dpi. The experiment was independently repeated three times with 8-10 technical replicates. **(G)** Anti-HA immunoblots of Mla3-6xHA (115.6 kDa), Mla23-6xHA (114.6 kDa), Mla34-6xHA (114.6 kDa), Mla35-6xHA (114.6 kDa) and Mla39-6xHA (115.6 kDa) expressed in *N. benthamiana*. Total protein extracts were prepared from leaves harvested 3 days after agroinfiltration. Protein loading was checked with Ponceau S solution (Sigma).

The lack of Pwl2 recognition by Mla23 in *N. benthamiana* (**Figure 4.4C**) contrasted with the resistant phenotype against KEN54-20 of the barley accession S13 (**Figure 4.3**). Previous reports have shown the presence of more than one *RGH1* allele in the *Mla* locus of different barley accessions, highlighting the complexity of the locus (Seeholzer et al., 2010; Brabham, 2019). To test whether another *RGH1* allele in addition to *Mla23* is also present in S13, we looked for *Mla3* unique reads in the available leaf RNA-seq data from this barley accession. Surprisingly, we detected *Mla3* specific sequence reads in addition to reads mapping to *Mla23*, indicating that *Mla3* is present in this barley line. Thus, recognition of *PWL2* and therefore resistance to KEN54-20 in S13 is—most likely—conferred by *Mla3* rather than *Mla23*. Altogether, these results show that Mla3, but none of its close relatives can recognise *PWL2*.

4.2.5 The Mla3 residue K926 is critical for Pwl2 recognition

4.2.5.1 A polymorphic eight-amino acid region at the C-terminus of Mla3 is crucial for specificity of Pwl2 recognition

Mla3 and Mla23 are almost identical (98.6% protein identity), but only Mla3 recognises Pwl2. Therefore, the few differences between these two alleles at the C-terminus are crucial for specificity of Pwl2 recognition. To determine whether a specific region or residues determine Pwl2 recognition by Mla3, I evaluated the 19 amino acid differences between Mla3 and Mla23 at the C-terminus (**Figure 4.5A**) by splitting the region comprising all polymorphic sites into three sub-regions: Swap1 from position 926 to 933, Swap2 from position 935 to 951, and the C-terminal extension of Mla3, comprising the last 7 amino acids (952 to 958) which are absent in Mla23 (**Figure 4.5A**). The boundaries of the subdivisions were chosen to equally distribute the number of amino acid differences between each sub-region. I generated reciprocal chimeras between Mla3 and Mla23 for each of these sub-regions and used them in transient expression

assays to test their ability to recognise Pwl2 in *N. benthamiana*. The only Mla3 chimera that completely lost the ability to trigger an immune response upon co-expression with Pwl2 was the one carrying the Swap1 region from Mla23. Conversely, the Mla23 chimera carrying the Swap1 region from Mla3 was the only one that gained the ability to trigger HR upon Pwl2 recognition (**Figure 4.5B and C**). The Mla3 version without the C-terminal extension was still able to cause cell death, although slightly weaker than wild-type Mla3, and adding the C-terminal extension from Mla3 to Mla23 was not sufficient to confer Pwl2 recognition (**Figure 4.5B and C**). This indicates that the last seven amino acids in Mla3 are neither strictly required nor sufficient to confer Pwl2 recognition. Indeed, other Mla alleles such as Mla39 share this region with Mla3, yet they do not recognise Pwl2 (**Figure 4.4F and 4.7**). These residues, however, might contribute to enhance the strength of recognition. No relative change of Pwl2 recognition was observed for the Swap2 chimeras (**Figure 4.5B and C**), indicating that polymorphic residues in this region do not play a critical role in recognising the effector, or the properties of the swapped amino acids were not different enough to impact recognition. In all cases, absence of cell death was not due to lack of protein expression, as all Mla3 and Mla23 chimeras were expressed in planta (**Figure 4.5D**). Overall, these results highlight the importance of the residues within the Swap1 region for specificity of Pwl2 recognition.

Several studies have shown that specificity of recognition is encoded in the LRR region of singleton NLRs and most NLRs that directly bind to their cognate effectors to trigger an immune response (Srichumpa et al., 2005; Seeholzer et al., 2010; Ravensdale et al., 2012; Steinbrenner et al., 2015). Swapping the whole LRR domain between Mla10 and Mla22 conferred exchanged specificity of AVR_{a10} and AVR_{a22} recognition (Bauer et al., 2021). Moreover, exchanging the LRR domain of Mla10 and Mla13 for the LRR domain of Sr35 resulted in gain of recognition of AvrSr35 (Förderer et al., 2022b). Swaps between Mla1 and Mla6 established that the region comprising the third LRR repeat to the very C-terminus of Mla1 is required for AVR_{a1} recognition, whereas only the region from the ninth LRR repeat is required to maintain specificity of AVR_{a6} recognition by Mla6 (Shen et al., 2003). This demonstrates that different LRR regions determine recognition specificity of AVR_a effectors by their corresponding Mla alleles. In agreement with previous reports, specificity of Pwl2 recognition is also determined by the C-terminus of Mla3, although in this case, by a much narrower region compared to Mla1 and Mla6. Nonetheless, I used two highly similar alleles to generate the swaps, which

might disregard contributions of the LRR domain outside of the polymorphic C-terminal region between Mla3 and Mla23 for recognition specificity. Region swaps with more distant Mla alleles might aid in the identification of additional residues or regions that are important for specificity of Pwl2 recognition. In addition, it remains to be established whether recognition specificity of Pwl2 and AVR_{a3} is determined by the same, overlapping, or distinct regions in the LRR domain and C-terminus of Mla3.

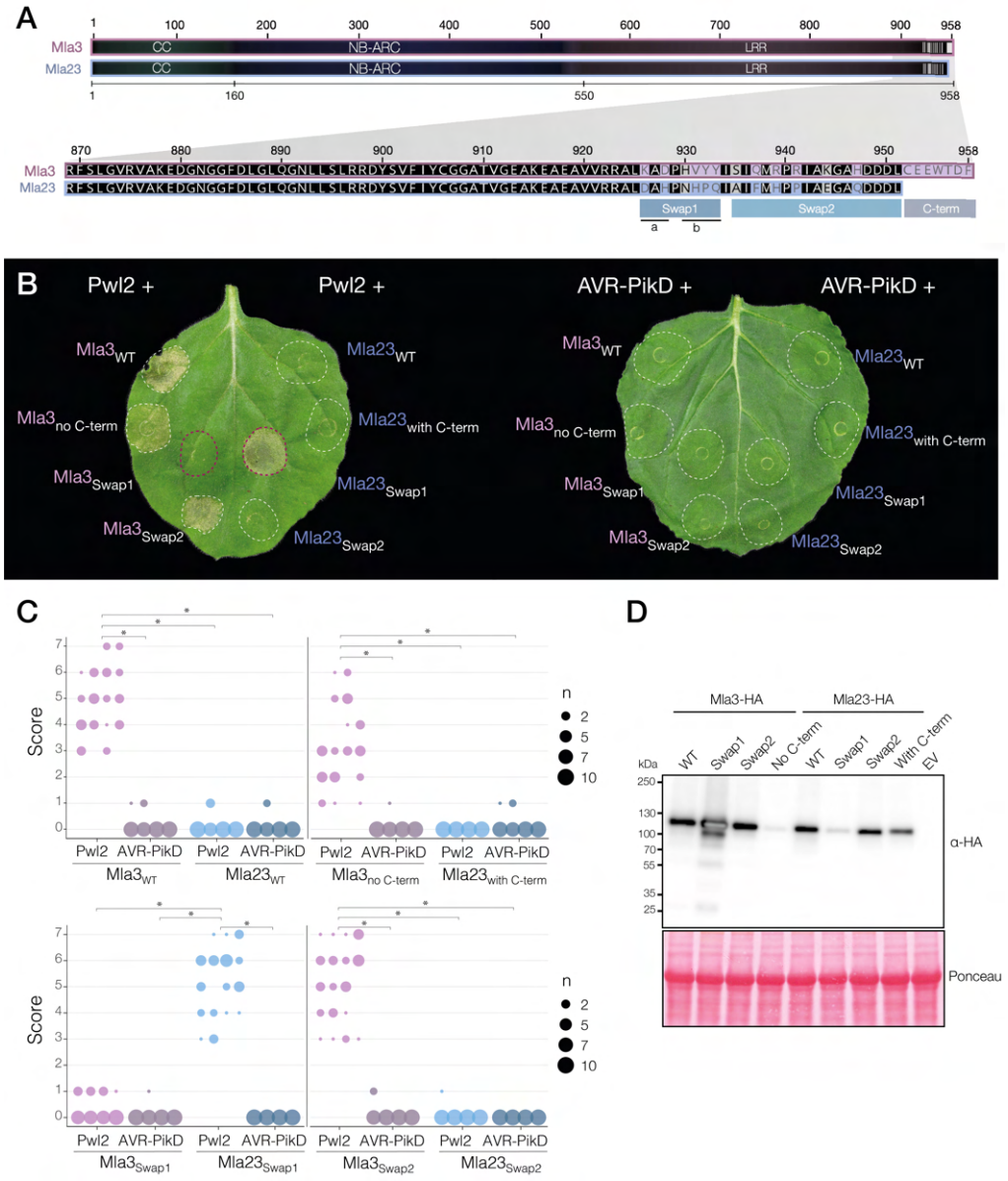

Figure 4.5 A region containing six polymorphic residues in Mla3 is important for Pwl2 recognition.

A chimeric swap of six polymorphisms between Mla3 and Mla23 inverted specificity of Pwl2 recognition between the two Mla alleles. **(A)** Schematic protein alignment of Mla3 and Mla23. Domain boundaries are marked below the alignment. Black indicates conservation and white bars highlight amino acid differences at the end of the LRR domain.

Figure 4.5 A region containing six polymorphic redisues in Mla3 is important for Pwl2 recognition (continued).

The last 90 residues of the alignment are magnified to highlight the differences between Mla3 and Mla23. The regions delimiting the chimeras between Mla3 and Mla23 are shown in boxes (i.e., Swap1, Swap2, and C-term). **(B)** Representative photos of *N. benthamiana* leaves expressing the indicated chimeric constructs according to the swaps indicated in **A**. The *M. oryzae* effector AVR-PikD was used as negative control. Red dashed circles highlight an exchanged HR response between the Mla3 and Mla23 chimeric variants. All Mla variants were expressed under the constitutive Mas Ω promoter and C-terminally fused to a 6xHA epitope tag. Pwl2 and AVR-PikD were expressed under the constitutive 35S Ω promoter, without signal peptide and C-terminally fused to a 3xFLAG tag. Photos were taken 3 dpi. **(C)** HR phenotypes from **B** were scored at three days post-agroinfiltration. The results are presented as a dot plot, where a size of a dot is proportional to the number of technical replicates with the same score within the same biological replicate. The experiments were independently repeated four times with 8-10 technical replicates; the three data point columns of each tested condition correspond to results from different biological replicates. Significant differences between conditions were calculated based on bootstrapping rank statistics and are indicated with asterisk (*). The details of the statistical analysis are shown in **Figure A.II.2**. **(D)** Anti-HA immunoblots of the Mla-6xHA chimeric constructs used in **B** expressed in *N. benthamiana*. Total protein extracts were prepared from leaves harvested 3 days after agroinfiltration. Protein loading was checked with Ponceau S solution (Sigma).

4.2.5.2 A single amino acid substitution confers Pwl2 recognition by Mla23

With the aim of establishing whether the Swap1 region of Mla3 was required as a whole, or if specific amino acids within this region were sufficient to confer Pwl2 recognition, I further split Swap1 into Swap1a (926-928) and Swap1b (930-933) (Figure 4.5A). I generated reciprocal chimeras and reciprocal single amino acid substitutions for each polymorphic site within these regions in Mla3 and Mla23 and tested them in HR assays in *N. benthamiana*. I found that Mla23 gained Pwl2 recognition when carrying the Swap1a region from Mla3, and vice versa for the reciprocal Mla3 chimera (**Figure 4.6A to C**). Surprisingly, I observed the same phenotypes for the single amino acid mutants Mla23^{D926K} and Mla3^{K926D} (**Figure 4.6A to C**), indicating that lysine 926 in the Swap1a region is both sufficient and required for Pwl2 recognition. The HR response of Mla3^{D928H} and Mla23^{H928D}—which have a single mutation also located in Swap1a—did not differ from that of wild-type Mla3 and Mla23 (**Figure 4.6A to C**), suggesting that these residues (D/H928) do not contribute significantly to Pwl2 recognition. The Mla3 chimera containing the Swap1b region from Mla23 weakly recognised Pwl2; however, the corresponding Mla23 chimera did not gain Pwl2 recognition (**Figure 4.6A to C**). In addition, the single amino acid swaps in the Swap1b region did not abolish the ability of Mla3 to trigger HR upon co-expression of Pwl2 (see Mla3^{H930N}, Mla3^{V931H}, Mla3^{Y932P} and

Mla3^{Y933Q} in **Figure 4.6A and C**), nor were they sufficient to confer effector recognition by Mla23 (see Mla23^{N930H}, Mla23^{H931V}, Mla23^{P932Y} and Mla23^{Q933Y} in **Figure 4.6B and C**). This suggests that the residues within this region collectively contribute to effector recognition, yet they are not sufficient to confer it. All chimeric and mutant versions of Mla3 and Mla23 were expressed, indicating that lack of cell death was not due to impaired protein accumulation (**Figure 4.6D**). Altogether, the evidence highlights a crucial role of residue K926 in conferring specificity of Pwl2 recognition by Mla3.

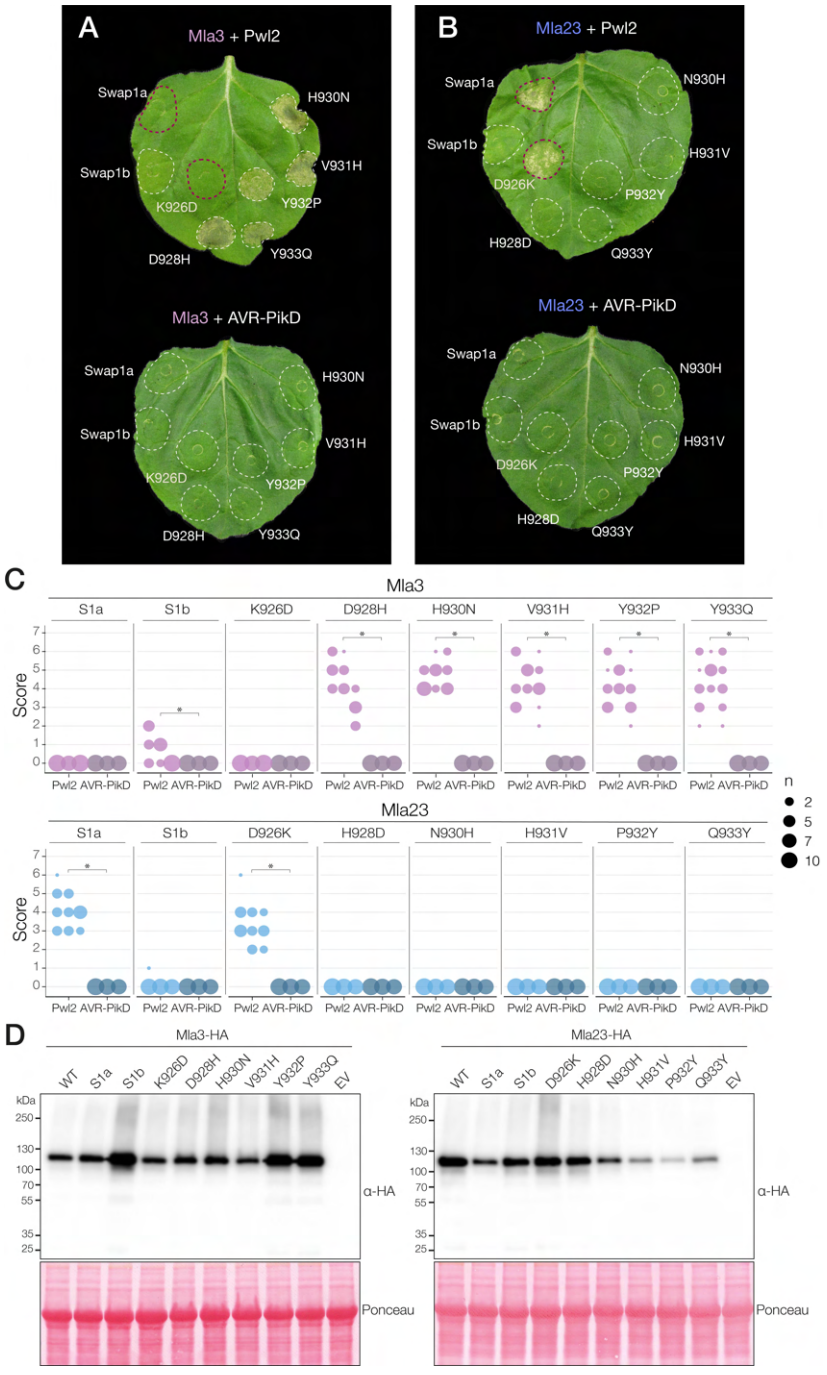

Figure 4.6 The D926K substitution in Mla23 is sufficient to confer Pwl2 recognition.

The chimeric Swap1a between Mla3 and Mla23 inverted specificity of Pwl2 recognition between the two Mla alleles, as well as the reciprocal residue substitution at position 926 **(A-B)** Representative photos of *N. benthamiana* leaves expressing the indicated chimeric constructs and reciprocal single amino acid substitutions in Mla3 **(A)** and Mla23 **(B)**. The *M. oryzae* effector AVR-PikD was used as negative control. Red dashed circles highlight an exchanged HR response between the Mla3 and Mla23 constructs. All Mla variants were expressed under the strong Mas Ω promoter and C-terminally fused to a 6xHA epitope tag. Pwl2 and AVR-PikD were expressed under the constitutive 35S Ω promoter, without signal peptide and C-terminally fused to a 3xFLAG tag. Photos were taken three dpi. **(C)** HR phenotypes from A and B were scored at three days post-agroinfiltration. The results are presented as a dot plot, where a size of a dot is proportional to the number of technical replicates with the same score within the same biological replicate. The experiments were independently repeated three times with 8-10 technical replicates; the three data point columns of each tested condition correspond to results from different biological replicates. Significant differences between conditions were calculated based on bootstrapping rank statistics and are indicated with asterisk (*). The details of the statistical analysis are shown in **Figure A.II.3**. **(D)** Anti-HA immunoblots of the Mla-6xHA (~115 kDa) chimeric constructs used in **A** and **B** expressed in *N. benthamiana*. Total protein extracts were prepared from leaves harvested 3 days after agroinfiltration. Protein loading was checked with Ponceau S solution (Sigma).

Despite their sequence similarity, not all Mla alleles require the co-chaperone protein RAR1 (Required for Mla12 resistance 1) to function, which positively controls protein levels of RAR1-dependent alleles (Bieri et al., 2004). Remarkably, a single amino acid substitution (glycine-to-aspartic acid) in the LRR region of Mla6 and Mla13 abrogated their RAR1 dependence (Halterman and Wise, 2004). Although the predicted position of this mutation is outside of the solvent-exposed β-sheet of the sixth LRR and is therefore distinct from residues that are hypothesised to determine recognition specificity (Shen et al., 2003; Halterman and Wise, 2004), this result illustrates that single LRR residues can determine inter- or intramolecular interactions that define the outcome of resistance. In this case, I not only established that the single residue K926 in the C-terminus of Mla3 is crucial for Pwl2 recognition but is also sufficient to confer recognition by Mla23. Thus, I hypothesise that K926 is located at the Mla3-Pwl2 binding interface, or at the interface with a protein targeted by Pwl2 that potentially mediates recognition. Interestingly, K926 is not predicted to be part of a β-sheet in a defined LRR, but rather exposed in an α-helix at the very C-terminus of Mla3. This suggests that regions outside of the concave inner surface of the LRR domain of Mla3 are crucially involved in Pwl2 recognition.

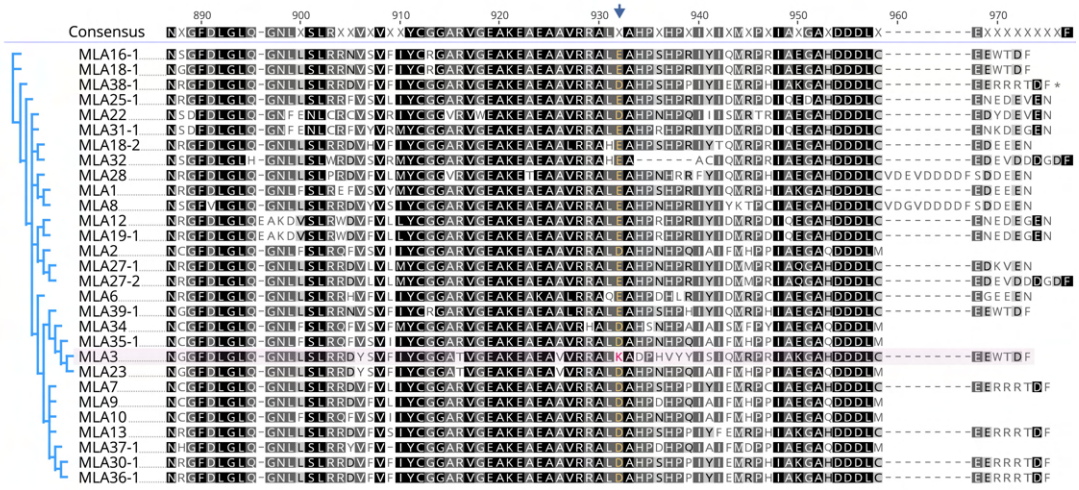

Figure 4.7 Protein alignment of the C-terminal region of different Mla alleles.

Colour coding of residues is based on similarity. Mla3 is highlighted in light pink. K926 in Mla3 is coloured in pink as the only positively charged residue in that position amongst Mla alleles, which have either D or E coloured in yellow.

4.2.5.3 A lysine (K) residue in position 926 enables Pwl2 recognition by Mla34 but not Mla35 or Mla39

The presence of either glutamic acid (E) or aspartic acid (D)—both negatively charged residues—at position 926 is conserved among most Mla alleles. Mla3 is the only Mla allele with a positively charged lysine in this position (**Figure 4.7**). I tested whether introducing K926 to other phylogenetically close Mla3 relatives was sufficient to confer Pwl2 recognition, as in the case of Mla23. For this I introduced the D926K mutation in Mla34 and Mla35, and E926K in Mla39, and tested their ability to trigger HR upon co-expression with Pwl2 in *N. benthamiana*. In the case of Mla34, the D926K substitution abolished autoactivity as Mla34^{D926K} did not trigger cell death in combination with an empty vector and, moreover, it conferred specific Pwl2 recognition (**Figure 4.8B**). It is possible that this substitution of opposite properties (acidic to basic) changed intramolecular interactions that stabilised Mla34 in an inactive state in the absence of an effector. Nonetheless, introducing a lysine in Mla35 or Mla39 (Mla35^{D926K} and Mla39^{E926K}) did not lead to cell death response when co-expressed with Pwl2 (**Figure 4.8C and D**). All proteins accumulated well in planta (**Figure 4.8E**). These results indicate that even though K926 plays a critical role in Pwl2 recognition by Mla3, it is likely that other conserved residues in Mla3, Mla23 and Mla34 that are polymorphic in Mla35 and Mla39 also play a role in Pwl2 recognition.

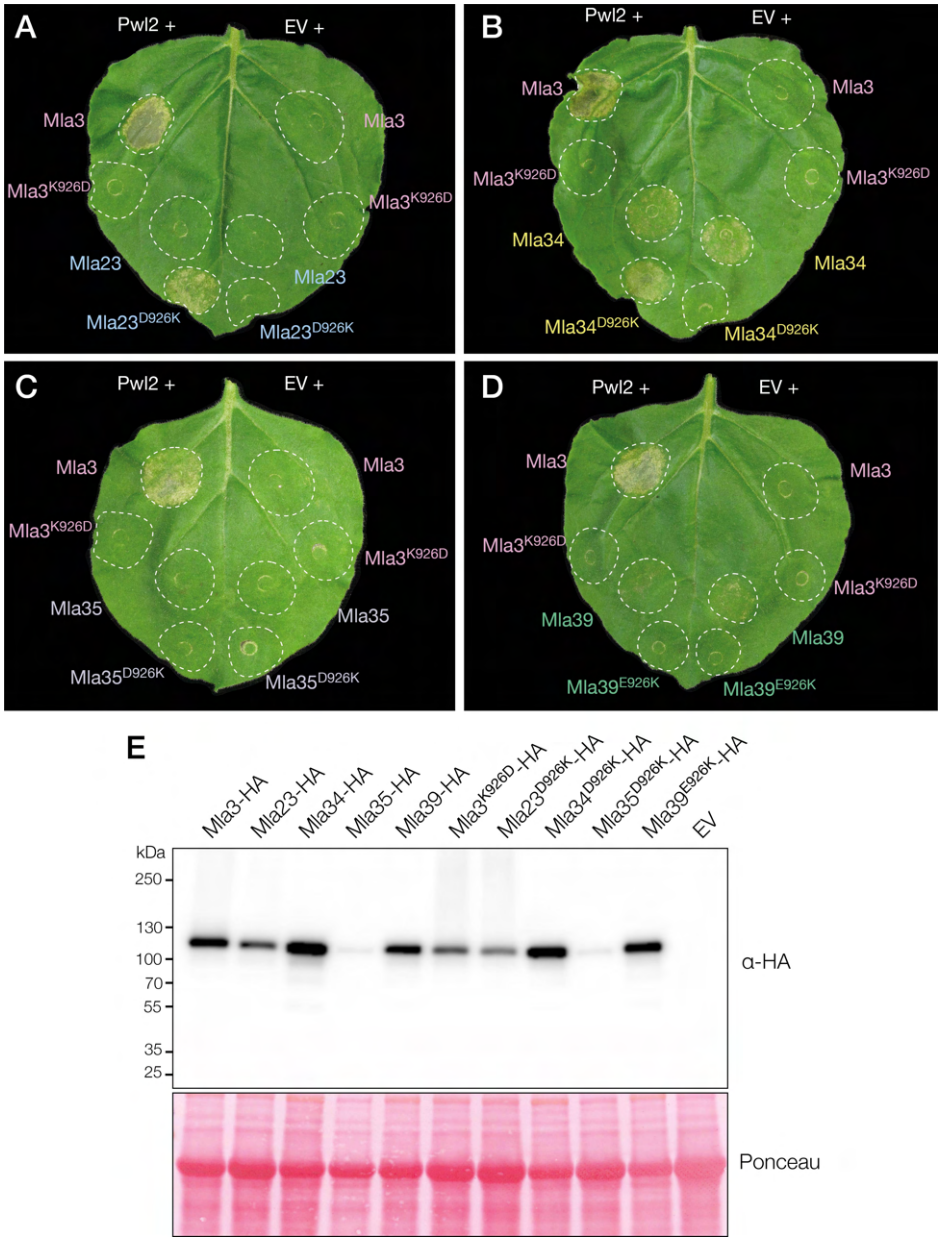

Figure 4.8 The D926K substitution confers Pwl2 recognition by Mla34 but not by Mla35 or Mla39 in *N. benthamiana*.

Only Mla34, but not Mla35 or Mla39 gained the ability to trigger cell death upon Pwl2 recognition with the D926K mutation. This substitution also abolished Mla34 autoactivity. Co-infiltration with empty vector (EV) was used as negative control. **(A to D)** Representative photo of a *N. benthamiana* leaf expressing the indicated constructs. All Mla alleles were expressed under the strong Mas Ω promoter and C-terminally fused to a 6xHA epitope tag. Pwl2 was expressed under the constitutive 35S Ω promoter, without signal peptide and C-terminally fused to a 3xFLAG tag. Photos were taken 3 dpi. The experiment was independently repeated two times with 8-10 technical replicates. **(E)** Anti-HA immunoblots of the Mla-6xHA (~115 kDa) variants used in **A to D** expressed in *N. benthamiana*. Total protein extracts were prepared from leaves harvested 3 days after agroinfiltration. Protein loading was checked with Ponceau S solution (Sigma).

4.2.5.4 A positively charged amino acid is required in position 926 to confer Pwl2 recognition by Mla3

Since Mla3 is the only allele with a positively charged residue in position 926 (K in contrast to D or E) (**Figure 4.7**), I hypothesised that either a basic residue is required for Pwl2 recognition, or that the negative charge in the side chain of glutamic acid (E) or aspartic acid (D) interferes with recognition of this effector. If the latter case is true, replacement of K926 for different amino acids other than D or E would not significantly impact Pwl2 recognition. To test this, I generated Mla3 variants with all possible amino acid substitutions instead of lysine in position 926 and tested their ability to trigger cell death when co-expressed with Pwl2. Only wild-type Mla3 and Mla3^{K926R} elicited HR upon Pwl2 recognition. The response of Mla3^{K926R} to Pwl2 was slightly weaker compared to wild-type Mla3 across all replicates (**Figure 4.9A**). Mla3^{K926H} did not recognise Pwl2 despite the basic nature of histidine, likely due to marked structural differences compared to lysine and arginine. All Mla3 variants were expressed in *N. benthamiana,* indicating that lack of HR was not due to impaired protein accumulation (**Figure 4.9B**). Overall, these results indicate that a positively charged side chain is required in position 926 to confer recognition of Pwl2. If this position is truly solvent exposed in the surface of the C-terminus of Mla3, it might play a crucial role in the binding interface with Pwl2 (in the case of a direct model of effector recognition) or with the protein mediating its recognition (in the case of a model of indirect recognition by Mla3).

In the study of RAR1 dependence by Mla alleles, only a glycine-to-aspartate mutation in the sixth LRR alleviated the requirement for RAR1 in Mla6 and Mla13-mediated resistance. Substitution for the structurally similar but uncharged residue asparagine did not abrogate RAR1 dependence (Halterman and Wise, 2004), indicating the crucial role of a negatively charged side chain in this position for RAR1 independence, possibly by altering intra or intermolecular interactions. This charge-specific requirement is similar to the residue K926 in Mla3, as only the basic amino acids lysine and arginine in this position conferred Pwl2 recognition. I hypothesise that the positive charge of K and R in position 926 in Mla3 plays a role in charge complementarity to recognise Pwl2 either directly or indirectly. As established by the Cryo-EM resistosome structure of Sr35, recognition of AvrSr35 is based on both shape and charge complementarity (Förderer et al., 2022b; Zhao et al., 2022). It is therefore likely that Pwl2 or its host target mediating recognition have a negative charge in the region that matches the corresponding positive surface of Mla3 provided by K926.

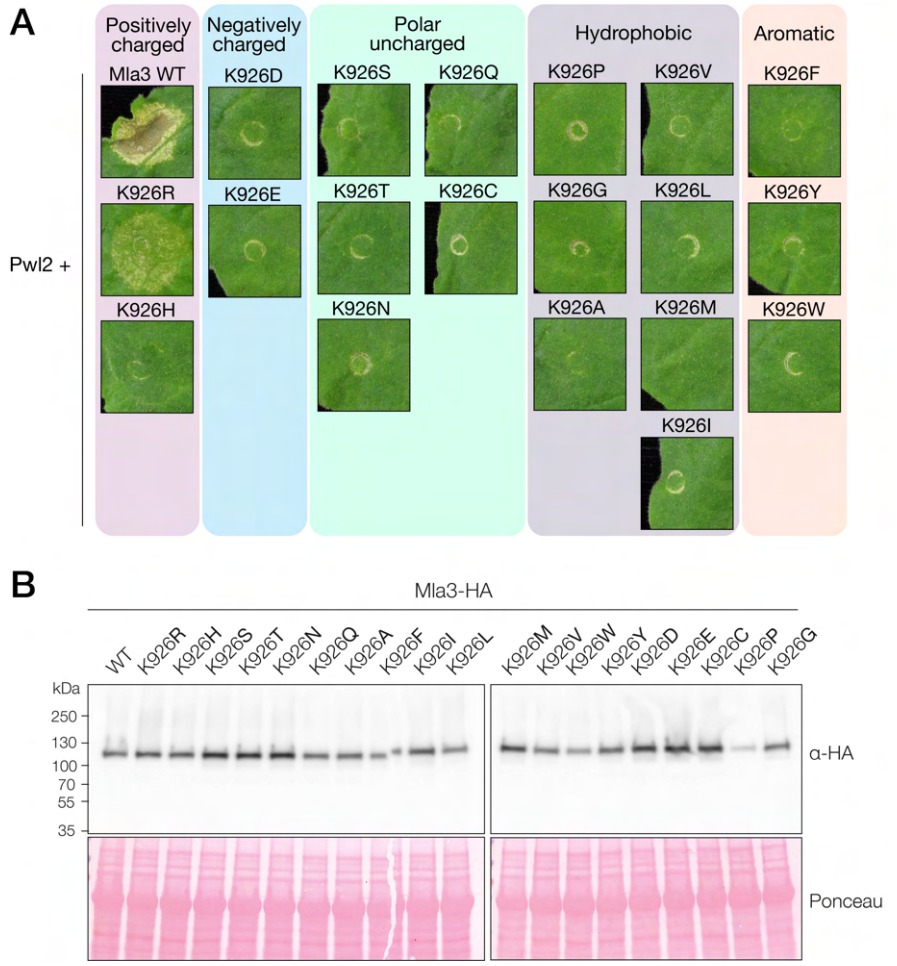

Figure 4.9 The K926R substitution maintains recognition of Pwl2 by Mla3.

Out of all the 19 possible amino acid substitutions to replace K926, arginine (R) was the only residue that maintained Pwl2 recognition by Mla3. **(A)** Representative *N. benthamiana* leaf panels showing HR response after co-expressing Pwl2 and the indicated Mla3 K926 substitutions. All Mla3 variants were expressed under the strong Mas Ω promoter and C-terminally fused to a 6xHA epitope tag. Pwl2 was expressed under the 35S Ω promoter, without signal peptide and C-terminally fused to a 3xFLAG tag. Photos were taken 3 dpi. The experiment was independently repeated two times with 6-8 technical replicates. **(B)** Anti-HA immunoblots of the Mla3-6xHA (~115 kDa) variants used in **A** expressed in *N. benthamiana.* Total protein extracts were prepared from leaves harvested 3 days after agroinfiltration. Protein loading was checked with Ponceau S solution (Sigma).

4.3 Conclusions

4.3.1 Main conclusions

In this chapter, I established that Mla3 is functional in *N. benthamiana* as Mla3 MHD mutants induce constitutive cell death when transiently overexpressed. I showed that Mla3 triggers a hypersensitive response when co-expressed with Pwl2, indicating that either Mla3 directly binds and recognises Pwl2, or a protein guarded by Mla3 to mediate

Pwl2 recognition is conserved in barley and *N. benthamiana*. Intriguingly, Mla3 also recognises the pwl2-2 and pwl2-3 alleles in *N. benthamiana,* although the cell death response elicited by these alleles is weaker compared to recognition of wild-type Pwl2. This contrasts the susceptibility phenotype of the barley accession Baronesse (*Mla3*) to *M. oryzae* isolates that carry *pwl2-2* or *pwl2-3*. The strength of recognition of these alleles might not be sufficient to confer functional resistance in barley. Furthermore, I showed that none of the Mla3 related alleles recognise Pwl2, despite high sequence identity (>96%). There are only 19 polymorphisms between Mla3 and Mla23, all located within the last 30 C-terminal residues. By performing chimeric swaps between Mla3 and Mla23, I established that a region of eight amino acids is crucial for specificity of Pwl2 recognition. More specifically, I showed that the D926K substitution within this region was required and sufficient to confer Pwl2 recognition by Mla23 and Mla34. Mla3 is the only allele with a lysine (K) in position 926, while all the other alleles carry a negatively charged residue (D or E). I therefore replaced K926 in Mla3 by all possible amino acids and found that only lysine and arginine—both positively charged—confer Pwl2 recognition. Even though other polymorphic residues between Mla3 and Mla23 were required for full recognition of Pwl2 by Mla3, they were not sufficient to confer recognition when introduced to Mla23. This indicates that while amino acids different from K926 collectively play a role in recognition of Pwl2, they are not required nor sufficient in isolation to confer effector recognition. This is a novel report delimiting specificity of recognition of an Mla allele to the high resolution of a single residue that is sufficient to confer Pwl2 recognition when introduced into two alleles that normally do not recognise this effector.

4.3.2 Signatures of direct effector recognition in allelic series

The LRR region of NLRs is known to determine recognition specificity, especially in singleton NLRs that directly recognise cognate effectors (Srichumpa et al., 2005; Seeholzer et al., 2010; Ravensdale et al., 2012; Steinbrenner et al., 2015). Several functional studies have established the important role of specific residues in this region for effector recognition. Mutation of LRR residues in ROQ1 and RPP1 that make direct contact with XopQ and ATR1, respectively, abolished effector binding and thus resulted in loss of immune response (Ma et al., 2020; Martin et al., 2020b). By mapping the binding interface of Sr35 with AvrSr35 onto the LRR domain of TaSH1—an Sr35 homologue in wheat—only eight amino acid substitutions were required to gain AvrSr35 recognition

by TaSH1(Förderer et al., 2022b). In addition, only 12 amino acid swaps in the LRR region of the Mla ortholog Sr33 were sufficient to confer recognition of AvrSr50. These amino acids were predicted to be located in the Sr50 binding interface with AvrSr50 based on their high variability amongst other homolog NLRs, as indicative of their role in recognition specificity (Tamborski et al., 2022).

Here, I took advantage of natural variation in Mla alleles to establish regions in Mla3 that are important for recognition of Pwl2 at a very high resolution. Variation in the C-terminus, towards the end of what has been traditionally reported as the LRR domain of Mla immune receptors, allowed delimiting an eight amino acid region crucial for Pwl2 recognition, and subsequent identification of a single residue (K926) strictly required to detect Pwl2 and trigger an immune response. Seeholzer et al. (2010) reported that solvent-exposed residues in the LRR region of Mla alleles are under diversifying selection (Seeholzer et al., 2010; Maekawa et al., 2018), similar to other NLR allelic series such as *RPP13* in *A. thaliana* (Steinbrenner et al., 2015), *L* in flax (Ravensdale et al., 2012) and *Pm3* in wheat (Srichumpa et al., 2005). These NLRs are known or hypothesised to directly bind to their corresponding effectors. It has been proposed that direct recognition of effectors by NLRs underlies a strong selective pressure governing effector-NLR co-evolution, resulting in remarkable diversifying selection on both parts (Saur et al., 2021).

Direct effector binding requires NLRs to rapidly adapt to maintain recognition of effectors that are under pressure to mutate surface residues to avoid being detected. This results in extensive NLR diversification and expansion of pathogen effectors as allelic variants or sequence-unrelated but structurally similar families. One such example is the RNAse-like protein repertoire of AVR_a effectors from *Bgh,* which are directly recognised by the extensive *Mla* allelic series (Saur et al., 2021). The study of the LRR region of homologous and allelic NLRs allowed for the identification of hypervariable positions in LRR units that highly correlate with surface-exposed regions. These positions likely determine recognition specificity and underlie effector binding sites (Prigozhin and Krasileva, 2021). Most of these variable residues in the Mla family are located in the second half of the LRR domain, towards the C-terminus of the NLR, suggesting the important role of this region in effector binding (Tamborski et al., 2022). Most polymorphic sites in Mla3 including the residue K926 reside within this C-terminus, suggesting that a model of direct recognition might also apply for Pwl2. Opposite to NLRs that directly bind effectors, NLRs like ZAR1 that indirectly recognise cognate

effectors do not display such levels of variability in the LRR region, likely due to purifying selection acting to maintain sensing of a conserved effector activity on a host protein (Prigozhin and Krasileva, 2021).

Identification of AVR_{a3} from *Bgh* would allow establishing whether the same principles of specificity of recognition by Mla3 also apply for this effector. It would be interesting to establish whether similar or overlapping regions of Mla3 are important for AVR_{a3} and Pwl2 recognition, or if the regions conferring specificity of recognition are different altogether. One way or the other, a model of direct recognition of two likely structurally distinct effectors by Mla3 remains puzzling.

Chapter 5: The C-terminus of Mla3 directly recognises Pwl2 by mimicking the binding interface of a host target

5.1 Introduction

Intracellular immune receptors of the nucleotide-binding leucine rich repeat (NLRs) class are key components of the plant innate immune system to sense pathogens and trigger disease resistance (Jones and Dangl, 2006). They detect the presence or activity of pathogen-secreted effectors in a highly specific manner to activate defences and halt infection (Dodds and Rathjen, 2010). The domain architecture of NLRs is broadly conserved (Jones et al., 2016) and comprises a central nucleotide-binding NB-ARC domain, a C-terminal leucine rich repeat (LRR) region, and a variable N-terminal signalling domain—which can either be of a coiled coil (CC), Toll/interleukin 1 receptor (TIR) or CC-RPW8 type (Shao et al., 2016; Duxbury et al., 2021). Some NLRs also carry non-canonical integrated domains (IDs) that are derived from effector host targets and act as baits to detect effectors when integrated within the NLR domain architecture (Cesari et al., 2014; Kroj et al., 2016).

NLRs recognise pathogens in different ways: they can either directly bind and recognise cognate effectors or they can interact with host proteins that are targeted or modified by effectors, mediating indirect recognition (Cesari, 2018). Host proteins targeted by effectors and sensed by NLRs can be classified as either guardees or decoys, depending on their function in the host plant (Dodds and Rathjen, 2010). If the host target has a role in immunity or is targeted by an effector as part of its virulence function, it is termed a guardee. If the function of the protein mediating recognition is solely to mimic an effector target and serve as an effector trap, it is a decoy (van der Hoorn and Kamoun, 2008). Indirect recognition usually involves enzymatic activity of effectors on guardees or decoys, which is subsequently sensed by NLRs (Dodds and Rathjen, 2010). An additional mechanism combines direct recognition with the decoy model and involves NLRs with IDs. In this case, the integrated domain acts as a decoy to directly bind an effector and trigger an immune response (Cesari et al., 2014).

The LRR domain of NLRs usually plays a critical role in both direct and indirect effector recognition. For instance, indirect recognition of the *P. syringae* effector AvrPphB

by the *Arabidopsis* CNL RPS5 requires cleavage of the host protein kinase PBS1 by AvrPphB (Ade et al., 2007). Recognition of PBS1 cleavage requires the entire LRR domain of RPS5 to effectively trigger an immune response (Qi et al., 2012). Similarly, the *Arabidopsis* CNL ZAR1 forms a pre-activation complex with the pseudo-kinase RKS1 to detect uridylation of the protein PBL2 by the *Xanthomonas* effector AvrAC, and ZAR1 interaction with RKS1 is mediated primarily by the LRR domain (Baudin et al., 2017; Wang et al., 2019a; Wang et al., 2019b). The wheat CNL Sr35 directly recognises AvrSr35 through the C-terminal region of the LRR (Förderer et al., 2022b; Zhao et al., 2022). Direct recognition has also been reported for the TNLs ROQ1 and RPP1, which physically interact with their cognate effectors XopQ and ATR1, respectively, through the LRR region and a post-LRR domain known as C-JID, commonly found in TNLs (Ma et al., 2020; Martin et al., 2020b). The C-JID domain resembles the complementary-determining regions of antibodies, as loops that emerge from a β-sandwich structure make specific contact with the corresponding effectors (Martin et al., 2020b). In general, multiple mechanistic and structural studies have confirmed the crucial role of the LRR domain and post LRR regions in effector recognition (Ravensdale et al., 2012; Maruta et al., 2022).

NLRs were thought to follow a gene-for-gene model in which one *R* gene recognises a single corresponding pathogen effector (Flor, 1971). However, growing evidence has revealed multiple exceptions to this model. Some NLRs that sense effectors, such as NLRs with IDs, require an additional helper NLR to function (Cesari et al., 2013; Huh et al., 2017a; Wu et al., 2017; Zdrzałek et al., 2020), meaning that more than one NLR is required to recognise a single effector and trigger resistance. Moreover, a few NLRs have the ability to recognise multiple pathogens. One example is the paired NLRs RPS4 and RRS1 that recognise the structurally distinct effectors PopP2 and AvrRps4 from the bacterial pathogens *R. solanacearum* and *P. syringae*, respectively, as well as an unknown effector from the fungus *C. higginisianum* (Deslandes et al., 2003; Narusaka et al., 2009). RRS1 is a sensor NLR with a WRKY domain integrated after the LRR region, and RPS4 acts as a helper NLR that is thought to relay the immune signal after effector recognition by RRS1 (Sarris et al., 2015). Both Pop2 and AvrRps4 bind to similar regions of the RRS1 WRKY domain, triggering an immune response (Zhang et al., 2017; Mukhi et al., 2021). Thus, the ID of RRS1 serves as bait to recognise distinct effectors from different pathogens. ZAR1 confers resistance to *P. syringae* by recognising the effectors HopZ1a and HopF2a, and to *X. campestris* by recognising AvrAC (Lewis et al., 2010;

Wang et al., 2015; Seto et al., 2017). These effectors are indirectly recognised through host receptor-like cytoplasmic kinases and effector enzymatic activity on them, such as uridylation of PBL2 by AvrAC (Lewis et al., 2013; Wang et al., 2015; Wang et al., 2019a). In general, the few studied cases of multiple pathogen recognition require an NLR-ID targeted by different effectors (Sarris et al., 2015), indirect recognition via common effector targets (Baudin et al., 2017; Wang et al., 2019a), or recognition of homologous effectors from distinct pathogens (Schultink et al., 2017; Thomas et al., 2020).

Mla is a CNL from barley that confers isolate-specific resistance against *Blumeria graminis* f. sp. *hordei* (*Bgh*), the causal agent of barley powdery mildew (Jørgensen and Wolfe, 1994). It comprises an expanded allelic series in which over 30 almost identical Mla variants recognise sequence unrelated cognate AVR_a effectors from *Bgh* (Seeholzer et al., 2010). AVR_a effectors identified so far are predicted to share an RNAse-like fold (Bauer et al., 2021), and direct interaction has been shown for four Mla-AVR_a corresponding pairs (Saur et al., 2019), suggesting that Mla recognises a conserved fold amongst sequence-divergent effectors. Mla has undergone functional diversification, as its rye orthologue Sr50 directly recognises the effector AvrSr50 from the rust pathogen *Puccinia graminis* f. sp. *tritici* (*Pgt*) (Mago et al., 2015; Chen et al., 2017; Ortiz et al., 2022), which is structurally distinct from *Bgh* AVR_a effectors. In addition, the Mla3 allele confers resistance against *Bgh* isolates that carry the cognate effector AVR_{a3}, and against the blast fungus *M. oryzae* by recognising the effector Pwl2. Pwl2 belongs to the family of MAX effectors (Guo et al., 2018b; Zdrzalek, 2021), which have a shared structural fold that is distinct from the RNAse-like fold of AVR_a effectors. This indicates that Mla3 recognises structurally distinct effectors from two phylogenetically distant pathogens.

In this chapter, I set out to establish the mechanism of Pwl2 recognition by Mla3. I hypothesised that, in line with a model of direct recognition of AVR_a *Bgh* effectors by their matching Mla alleles (Saur et al., 2019), Mla3 directly recognises Pwl2 from *M. oryzae*. I show that Mla3 associates with Pwl2 in planta, and that association occurs through the LRR domain and C-terminal region of Mla3. I also show that the last 85 amino acids of Mla3 are sufficient to bind Pwl2 in planta, in yeast and in *E. coli,* strongly suggesting direct effector recognition. The predicted structure of the C-terminus of Mla3 in complex with Pwl2 resembles the structure of Pwl2 bound to OsHIPP43, an HMA-containing effector target protein in rice (Zdrzalek, 2021). This indicates that Mla3 directly recognises Pwl2 by mimicking the binding interface of a Pwl2 host target. The gene underlying AVR_{a3} from *Bgh* remains unknown. However, a scenario in which Mla3 directly recognises

AVR_{a3}—similar to other Mla-AVR_a pairs—would be the first report of a single NLR without an integrated domain that confers resistance to multiple pathogens by directly recognising structurally distinct effectors.

5.2 Results and Discussion

5.2.1 Full length Mla3 and Pwl2 do not associate in yeast

Recent work from Saur et al. (2019) demonstrated that different Mla alleles, namely Mla7, Mla10 and Mla13 associate with their cognate mildew effectors AVR_{a7}, AVR_{a10} and AVR_{a13}, respectively, in yeast-two-hybrid and split luciferase assays (Saur et al., 2019), suggesting direct effector recognition. In addition, the Mla orthologue Sr50 in rye associates with the effector AvrSr50 from *Pgt* in yeast-two-hybrid assays (Chen et al., 2017). Based on this, I hypothesised that Mla3 directly recognises Pwl2 to confer resistance against *M. oryzae* and I performed a yeast-two-hybrid assay to test it. Structural studies of Pwl2 have shown that it belongs to the group of MAX effectors and that the PWL effector family binds to OsHIPP43, an HMA-containing protein in rice (Zdrzalek, 2021). Therefore, I used OsHIPP43 as positive control for the assay. Indeed, when co-transformed with OsHIPP43 fused to the Gal4-DNA binding domain (BD) and either of the Pwl2 alleles fused to the Gal4-activation domain (AD), yeasts grew on selective media lacking L/W/H/A, indicating protein association. Contrarily, when yeasts were co-transformed with Gal4BD-Mla3 and Gal4AD-Pwl2, Gal4AD-pwl2-2 or Gal4AD-pwl2-3, I did not observe growth on selective media (**Figure 5.1**). This result can potentially be explained by the lack of binding, or by limitations of the assay such as lack of proper folding of these proteins (of Mla3, in particular), or by the absence of a homologous protein in yeast that mediates complex formation between Mla3 and Pwl2. I intended to use Mla10 and AVR_{a10} as controls for direct NLR-effector binding. Nonetheless, when Mla10 was fused to the Gal4BD and AVR_{a10} was fused to the Gal4AD, I did not observe any yeast growth on the selective media lacking L/W/H/A, indicating that Mla10 and AVR_{a10} did not interact under the conditions tested and contrasting with a previous report (Saur et al., 2019) (**Figure 5.1**). Noteworthy, Saur et al. (2019) used the LexA–B42 system rather than the Gal4 system in the yeast-two-hybrid experiments to show direct interaction. These two systems might differ in the sensitivity or stringency to detect interactions, explaining the differences in results for the interaction between Mla10 and AVR_{a10}. Overall, these results suggest either that the yeast-

two-hybrid system used is not optimal to test effector association with Mla alleles under the conditions that I tested, or that Mla3 does not interact with Pwl2.

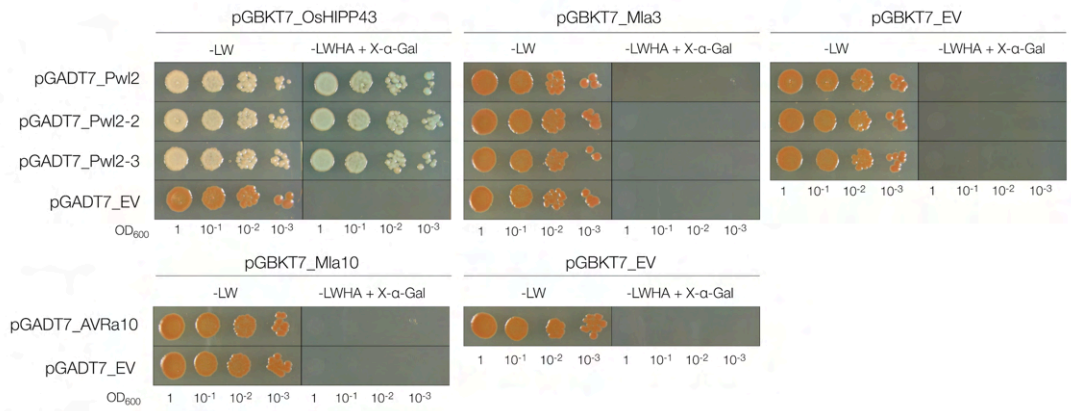

Figure 5.1 Full length Mla3 does not associate with Pwl2 in yeast.

Yeast-two-hybrid assay to test association between Mla3 and the Pwl2 alleles. Yeast cells were co-transformed with the indicated constructs. The plasmids pGBKT7 and pGADT7 contain the Gal4 binding domain and the Gal4 activating domain, respectively, fused to the indicated gene. OsHIPP43 was used as positive control for interaction with the Pwl2 alleles. Yeast growth on SD–LW media indicates co-transformation with both indicated plasmids. Yeast growth on SD–LWHA + X-α-gal media indicates protein association. Photos were taken after 4 days of growth at 28℃. The experiment was repeated three times with similar results.

5.2.2 Mla3 associates with Pwl2 *in planta*

5.2.2.1 The Mla3 MADA-like mutant Mla3^{L11E} has reduced ability to trigger cell death

Transient co-expression of Mla3 and Pwl2 in *N. benthamiana* triggers a quick and strong cell death response as a result of effector recognition (**Figure 4.2B and D**). Such a strong response is disadvantageous for biochemical assays *in planta* as cell death leads to protein degradation. Previous reports have shown that mutations in the MADA motif in the N-terminal α1-helix of some CNLs abolish the induction of cell death activity upon activation, without compromising effector recognition and subsequent NLR oligomerisation (Adachi et al., 2019b; Ahn et al., 2022; Contreras et al., 2022). I generated a MADA-like mutation within the α1-helix in the CC domain of Mla3 and tested its ability to induce cell death upon co-expression with Pwl2 in *N. benthamiana*. For this, I substituted the leucine at position 11 by glutamic acid in Mla3 (Mla3^{L11E}) and transiently co-expressed it with wild-type Pwl2, pwl2-2 or pwl2-3. Even though Mla3^{L11E} recognition of Pwl2 and Pwl2-2 still lead to cell death, the HR response was significantly weaker in comparison to the response by wild-type Mla3 (**Figure 5.2A and C**). Mla3^{L11E} did not

respond to pwl2-3, in comparison to wild-type Mla3, which triggered a moderate response upon recognition of this allele. The *M. oryzae* effector AVR-PikD was used as negative control of effector recognition (**Figure 5.2A and C**). Expression levels of Mla3^{L11E} were comparable to wild-type Mla3, indicating that the reduced cell death phenotype triggered by Mla3 ^{L11E} was not due to lack of protein stability or insufficient protein accumulation (**Figure5.2B**). Altogether this indicates that the L11E substitution in the α1-helix of Mla3 does not interfere with the ability of Mla3 to recognise Pwl2, but rather hinders its ability to cause cell death, facilitating subsequent biochemical assays *in planta.*

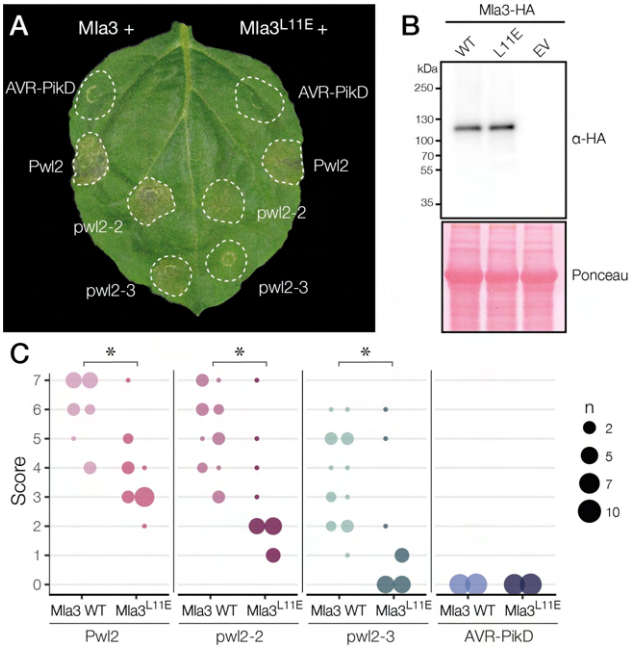

Figure 5.2 The MADA-like mutant Mla3^{L11E} has hindered ability to trigger cell death upon recognition of Pwl2 in *N. benthamiana*

The mutation L11E compromises the ability of Mla3 to trigger cell death upon co-expression with wild-type Pwl2, pwl2-2 and pwl2-3, compared to wild-type Mla3. The *M. oryzae* effector AVR-PikD was used as negative controls. **(A)** Representative photo of a *N. benthamiana* leaf expressing the indicated constructs. Mla3 and Mla3^{L11E} were expressed under the strong Mas Ω promoter and C-terminally fused to a 6xHA epitope tag. All Pwl2 alleles and AVR-PikD were expressed under the 35S Ω promoter, without signal peptide and C-terminally fused to a 3xFLAG tag. Photos were taken 3 dpi. **(B)** Anti-HA immunoblot of Mla3-6xHA and Mla3^{L11E}-6xHA (115.6 kDa) expressed in *N. benthamiana.* Total protein extracts were prepared from leaves harvested 3 days after agroinfiltration. Protein loading was checked with Ponceau S solution (Sigma). **(C)** HR phenotypes from **A** were scored at three days post-agroinfiltration. The results are presented as a dot plot, where a size of a dot is proportional to the number of technical replicates with the same score within the same biological replicate. The experiments were independently repeated two times with 8-10 technical replicates; the two data point columns of each tested condition correspond to results from different biological replicates. Significant differences between conditions were calculated based on bootstrapping rank statistics and are indicated with asterisk (*). The details of the statistical analysis are shown in **Figure A.III.1.**

5.2.2.2 Full length Mla3 co-immunoprecipitates with Pwl2 in *N. benthamiana* protein extracts

In order to test whether Mla3 and Pwl2 associate in a physiologically relevant context, I performed co-immunoprecipitation (co-IP) assays in *N. benthamiana*. For this, I transiently co-expressed Pwl2, pwl2-2 or pwl2-3—all C-terminally fused to a 3xFLAG epitope tag—with Mla3^{L11E}_6xHA in *N. benthamiana* leaves. I used the MADA-like mutant Mla3^{L11E} with reduced ability to cause HR to avoid protein degradation due to cell death, and the Mla23 allele and the *M. oryzae* effector AVR-PikD as negative controls. I performed leaf protein extraction, immunoprecipitation with an α-HA affinity matrix, and western blot analyses. The co-IP assay showed that Mla3^{L11E} strongly associates with Pwl2, and, to a lower extent, with pwl2-2. pwl2-3 and AVR-PikD did not co-IP with Mla3^{L11E} (**Figure 5.3**). These results corroborate the HR phenotypes of Mla3^{L11E} recognition of the Pwl2 alleles in *N. benthamiana* (**Figure 5.2A and C**), indicating that the strength of immune response correlates with the strength of association between Mla3 and Pwl2. None of the effectors tested co-immunoprecipitated with Mla23, in agreement with lack of recognition. This indicates that recognition of Pwl2 occurs upon association with Mla3, yet it does not rule out the possibility that there is an unknown plant protein mediating complex formation to facilitate effector recognition.

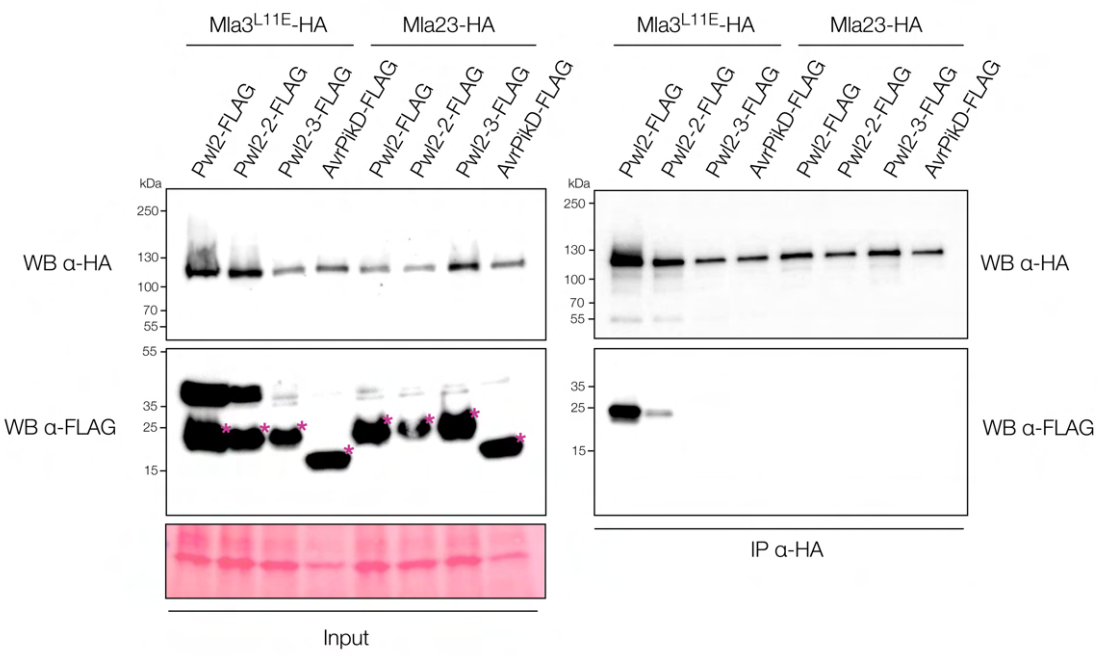

Figure 5.3 Mla3^{L11E} associates with Pwl2 *in planta.*

Co-immunoprecipitation assay upon co-expressing Mla3^{L11E}-6xHA or Mla23-6xHA (~115 kDa) with Pwl2-3xFLAG, Pwl2-2-3xFLAG or Pwl2-3-3xFLAG (17.3 kDa) in *N. benthamaiana*. AVR-PikD-3xFLAG (14 kDa) and Mla23-6xHA were used as negative controls. Total protein extracts were prepared from leaves harvested 3 days after agroinfiltration. Immunoprecipitation (IP) was performed with anti-HA agarose beads. Total proteins (Input) and pulled-down fractions (IP) were detected with the appropriate antibodies. Asterisks show the expected protein band for each treatment, to differentiate from non-specific bands. Protein loading was checked with Ponceau S solution (Sigma). The experiment was independently repeated three times. WB: Western Blot.

5.2.2.3 Mla23^{D926K} associates with Pwl2 in *N. benthamiana*

The single amino acid mutation D926K in Mla23 was sufficient to confer recognition of Pwl2 by this Mla allele (**Figure 4.6B and C**), and the reciprocal substitution in Mla3 abolished it (**Figure 4.6A and C**). To test whether gain of Pwl2 recognition by Mla23^{D926K} correlates with gain of association, I performed co-IP experiments by transiently co-expressing Mla3, Mla23 or the variants Mla3^{K926D} and Mla23^{D926K}—all C-terminally tagged with 6xHA—with Pwl2-3xFLAG in *N. benthamiana* leaves. I used the effector AVR-PikD as negative control. I pulled down the Mla-6xHA tagged variants by using an α-HA affinity matrix. The western blot indicated that Mla23^{D926K} gained association with Pwl2, although not as strong as wild type Mla3 (**Figure 5.4**). This correlates with the intensity of HR response triggered by Mla23^{D926K} upon co-expression with Pwl2 in comparison to Mla3 (**Figure 4.6 A-C**). Interestingly, Mla3^{K926D} retained faint Pwl2 association (**Figure 5.4**), despite the lack of a visible immune response. Overall, this indicates that the cell death response triggered by Mla3 or Mla23^{D926K}, and Pwl2 correlates with strength of association according to co-IP results. It is worth mentioning that while co-IP experiments are qualitative rather than quantitative, qualitative correlations can be hypothesised based on band intensity on western blots. Strict quantitative conclusions about strength of binding would require protein–protein interaction assays *in vitro*.

5.2.2.4 The LRR domain of Mla3 is required and sufficient for association with Pwl2 *in planta*

Next, I set out to determine which domains of Mla3 are required for association with Pwl2. For this, I generated truncations containing each individual domain of Mla3 (CC^{L11E}-x6HA, NB-ARC-x6HA and LRR-6xHA), as well as combinations of domains (CC^{L11E}-NB-ARC-6xHA and NB-ARC-LRR-6xHA) (**Figure 5.5A**), and tested their ability to associate with Pwl2-3xFLAG in co-IP assays, using full length Mla3^{L11E} as

positive control. The domain boundaries of the truncations were based on previous studies of Mla proteins (Shen et al., 2003; Halterman and Wise, 2004; Seeholzer et al., 2010). I performed the co-IP using an α-FLAG affinity matrix to pull down Pwl2 instead of an α-HA affinity matrix, to avoid pulling Mla3 truncations of different sizes. The co-IP assay showed that the NB-ARC-LRR truncate and the LRR domain alone pulled down with Pwl2 (**Figure 5.5B**). This indicates that the LRR domain of Mla3 is required and sufficient to associate with Pwl2, in agreement with previous reports of NLR-effector association (Ravensdale et al., 2012; Ma et al., 2020; Martin et al., 2020b; Förderer et al., 2022b; Zhao et al., 2022).

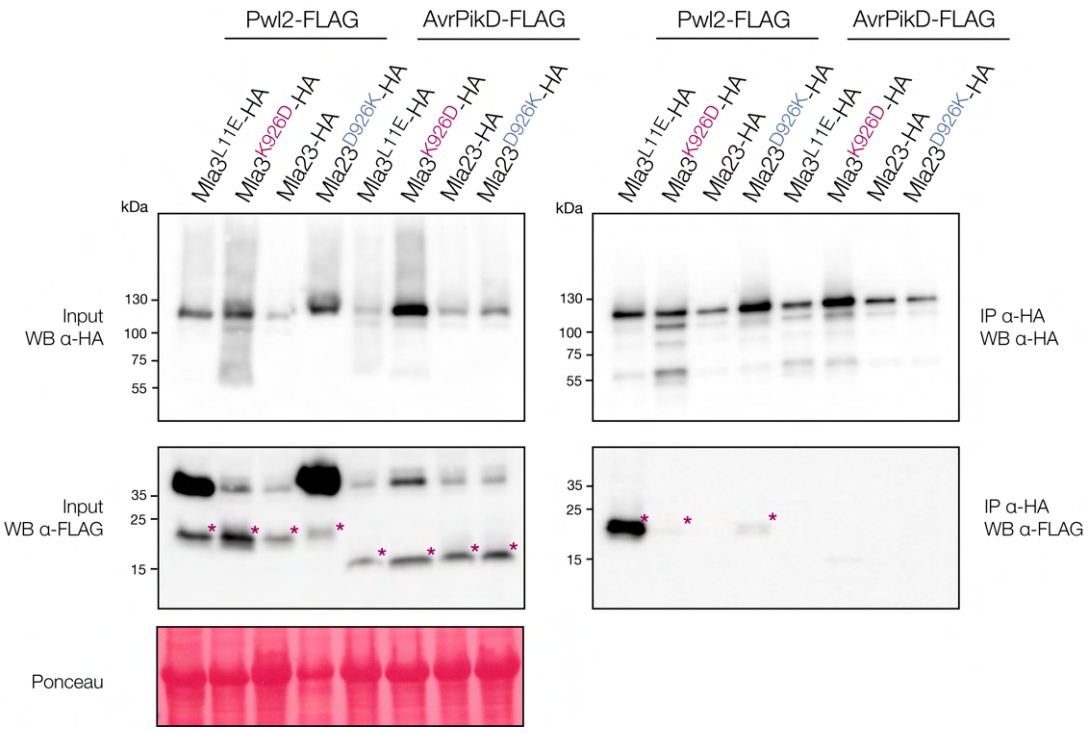

Figure 5.4 Mla23^{D926K} gained association with Pwl2 in *N. benthamiana*.

Co-immunoprecipitation assay done by co-expressing Mla3^{L11E}-6xHA, Mla3^{K926D}-6xHA, Mla23-6xHA or Mla23^{D926K}-6xHA (~115 kDa) with Pwl2-3xFLAG (17.3 kDa) and AVR-PikD-3xFLAG (14 kDa) in *N. benthamiana*. AVR-PikD-3xFLAG was used as negative control. Total protein extracts were prepared from leaves harvested 3 days after agroinfiltration. Immunoprecipitation (IP) was performed with anti-HA agarose beads. Total protein (Input) and pulled-down fractions (IP) were detected with the appropriate antibodies. Asterisks show the expected protein band for each treatment, to differentiate from non-specific bands. Protein loading was checked with Ponceau S solution (Sigma). The experiment was independently repeated three times. WB: Western Blot.

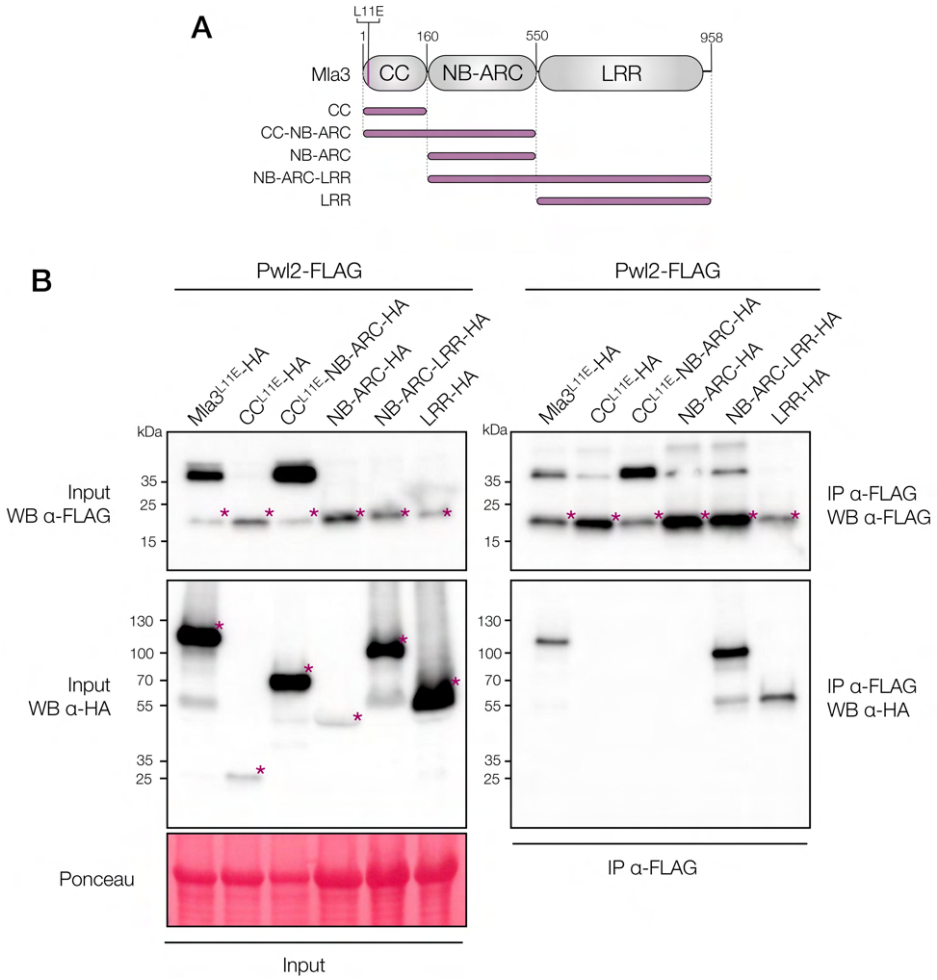

Figure 5.5 The LRR domain of Mla3 associates with Pwl2 in *N. benthamiana*

(**A**) Schematic diagram of the domain architecture of Mla3 and the boundaries used to delimit the truncations for the constructs used in the co-immunoprecipitation assay shown in (**B**). (**B**) Western blots (WB) of the co-immunoprecipitation assay done by co-expressing Mla3^{L11E}-6xHA (115.6 kDa), CC^{L11E}-6xHA (25.7 kDa), CC^{L11E}-NB-ARC-6xHA (70 kDa), NB-ARC-6xHA (52 kDa), NB-ARC-LRR-6xHA (97.5 kDa) or LRR-6xHA (53.2 kDa) with Pwl2-3xFLAG (17.3 kDa) in *N. benthamiana*. Total protein extracts were prepared from leaves harvested 3 days after agroinfiltration. Immunoprecipitation (IP) was performed with anti-FLAG agarose beads. Total protein (Input) and pulled-down fractions (IP) were detected with the appropriate antibodies. Asterisks show the expected protein band for each treatment, to differentiate from non-specific bands. Protein loading was checked with Ponceau S solution (Sigma). The experiment was independently repeated three times.

5.2.3 The C-terminus of Mla3 directly interacts with Pwl2

5.2.3.1 The last 85 amino acids of Mla3 are sufficient to associate with Pwl2 *in planta*

Growing evidence supports the key role of the LRR domain and the C-terminus in NLR recognition specificity and NLR-effector association. In the case of the TNLs

ROQ1 and RPP1, which directly recognise XopQ and ATR1, respectively, association with the corresponding effector occurs through the end of the LRR domain and the post-LRR C-JID domain. This region forms a horseshoe-shaped scaffold that binds to the effector, triggering subsequent NLR oligomerisation (Ma et al., 2020; Martin et al., 2020b). I performed a domain architecture search with InterProScan to establish the correct boundaries of the LRR domain of Mla3. The leucine-rich repeat domain superfamily (IPR032675) matches Mla3 from position 530 to 835. No known domains are found beyond this position. I also predicted the positions of the leucine rich repeats in Mla3 using the web server LRRpredictor v1.0 (Martin et al., 2020a) and found that the last predicted leucine rich repeat is located from residue 864 to 871. Next, I used RaptorX Property Prediction tool (Wang et al., 2016) to look for disordered regions beyond the last predicted leucine rich repeat, and found that from position V874 to G891, Mla3 is predicted to be highly disordered and solvent exposed. Noteworthy, the polymorphisms in Mla3 that are critical for specificity of Pwl2 recognition compared to Mla23 are beyond what is predicted as canonical LRR (i.e., K926 is after the last predicted leucine rich repeat) (section 4.2.5).

This evidence prompted me to test whether Mla3 uses its post-LRR C-terminus as bait for Pwl2, similar to the C-JID domain in ROQ1 and RPP1 (Ma et al., 2020; Martin et al., 2020b). For this, I cloned the last 85 amino acids of Mla3 starting from residue V874 (Mla_V874), and the last 48 residues starting from V911 (Mla_V911) (**Figure 5.6A**)—both C-terminally tagged with 6xHA—and tested whether these fragments associate with Pwl2-3xFLAG in co-IP experiments. I used full length LRR-6xHA (from section 5.2.2.4) as positive control for association, and AVR-PikD-3xFLAG as negative control. Western blots after α-HA immunoprecipitation showed that, even though the Mla3_V874 fragment was not as strongly expressed as Mla3_LRR, it was sufficient to associate with Pwl2 (**Figure 5.6B**). In contrast, the Mla3_V911 truncation did not express well or was not stable in *N. benthamiana*, and therefore association with Pwl2 could not be assessed. Overall, these results show that the C-terminus of Mla3 comprising the last 85 residues are sufficient to associate with Pwl2. Noteworthy, this region contains all polymorphisms between Mla3 and Mla23—which does not associate with Pwl2 (**Figure 5.3**). I therefore hypothesise that the last 85 amino acids of Mla3 are not only sufficient but also required for effector association.

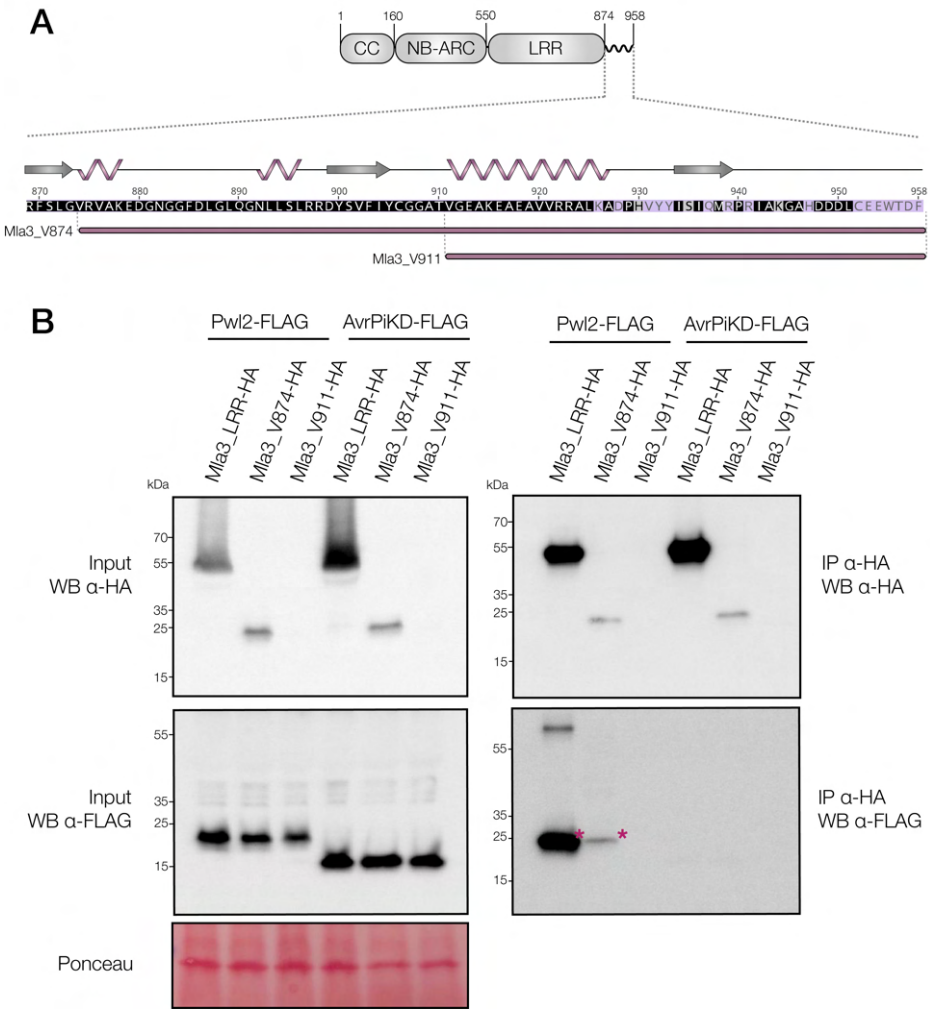

Figure 5.6 The last 85 residues of Mla3 are sufficient to associate with Pwl2 in *N. benthamiana.*

(**A**) The last 85 amino acids of Mla3 are not predicted to be part of the LRR domain. The sequence of the highlighted region is shown with the predicted secondary structure on top. Residues with black background are conserved in Mla23, and residues with pink background are polymorphic in Mla23. The boundaries delimiting the constructs used in **B** are shown. (**B**) Western blots (WB) of the co-immunoprecipitation assay upon co-expressing Mla3-LRR-6xHA (53.2 kDa) (from figure 5.5A), Mla3_V874-6xHA (17 kDa) or Mla3_V911-6xHA (13 kDa), with Pwl2-3xFLAG (17.3 kDa) or AVR-PikD-3xFLAG (14 kDa) in *N. benthamiana*. Total protein extracts were prepared from leaves harvested 3 days after agroinfiltration. Immunoprecipitation (IP) was performed with anti-HA agarose beads. Total protein (Input) and pulled-down fractions (IP) were detected with the appropriate antibodies. Asterisks show the expected protein band for each treatment, to differentiate from non-specific bands. Protein loading was checked with Ponceau S solution (Sigma). The experiment was independently repeated two times.

5.2.3.2 Pwl2 associates with the C-terminus of Mla3 in yeast

Association of Pwl2 with the LRR domain of Mla3 and with the fragment Mla3_V874 in co-IP experiments prompted me to test whether interaction of Pwl2 with

Mla3 truncations can be detected in yeast-two-hybrid assays. I generated constructs of each of the individual domains of Mla3 (CC, NB-ARC and LRR) or combinations of adjacent domains (CC-NB-ARC and NB-ARC-LRR), as well as the C-terminal region Mla3_V874 fused to Gal4BD, and tested association with Pwl2 fused to Gal4AD. I used the rice HMA-containing protein OsHIPP43 as positive control for interaction with Pwl2. I did not observed growth on selective media without L/W/H/A when yeasts were co-transformed with full length domains or combination of domains of Mla3 and AD-Pwl2, suggesting lack of association in yeast (**Figure 5.7**). Absence of association between Pwl2 and LRR-containing fragments, which contrasts with the results observed *in planta*, might be explained by inadequate folding of Mla3 fragments in yeast. Nonetheless, I did observe growth when yeasts were co-transformed with BD-Mla3_V874 and AD-Pwl2 (**Figure 5.7**), indicating association and agreeing with the co-IP results in *N. benthamiana*. This suggests either that recognition of Pwl2 by Mla3 is truly direct, or that a protein mediating recognition of Pwl2 is sufficiently conserved in yeast, *N. benthamiana* and barley. Host-pathogen coevolution is an intricate process driven by adaptation and selective pressures on all parts involved. It is therefore unlikely that a protein would be targeted by an effector from a plant pathogen in a system that has not coevolved with such pathogen, and is divergent from plants. Therefore, the evidence suggests that Mla3 directly recognises Pwl2.

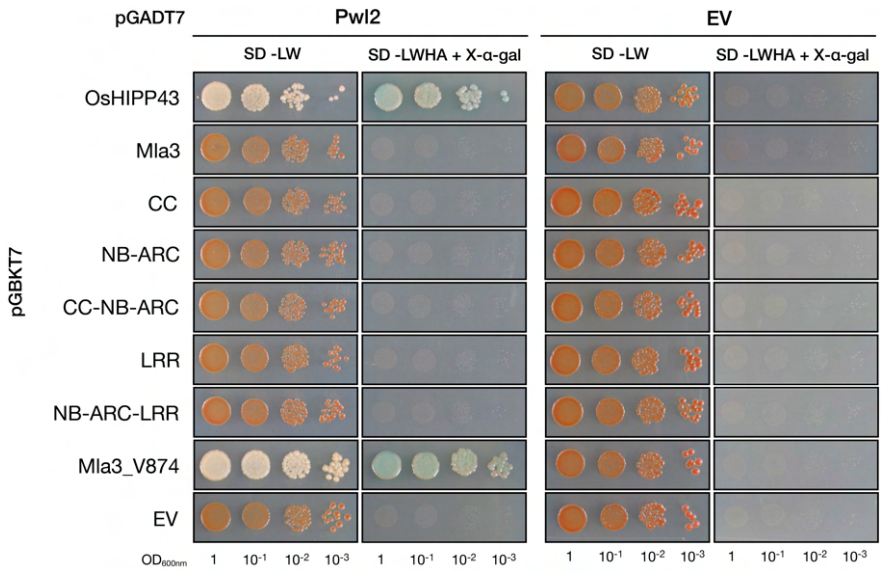

Figure 5.7 The last 85 residues of Mla3 are sufficient to associate with Pwl2 in yeast.

Yeast-two-hybrid assay to test association between Mla3 domains or Mla3 truncations (CC, CC-NB-ARC, NB-ARC, NB-ARC-LRR, LRR and Mla3_V874) and Pwl2.

Figure 5.7 The last 85 residues of Mla3 are sufficient to associate with Pwl2 in yeast (continued)

Yeast cells were co-transformed with the indicated constructs. The plasmids pGBKT7 and pGADT7 contain the Gal4 binding domain and the Gal4 activating domain, respectively, fused to the indicated gene. OsHIPP43 was used as positive control for interaction with Pwl2. Yeast growth on SD–LW media indicates co-transformation with both indicated plasmids. Yeast growth on SD–LWHA + X-α-gal media indicates protein association. Photos were taken after 4 days of growth at 28°C. The experiment was repeated two times with similar results.

5.2.3.3 Pwl2 associates with the C-terminus of Mla3 in *E. coli* protein extracts

In order to test direct recognition of Pwl2 by Mla3 by an orthogonal method, I aimed to co-purify Pwl2 in complex with Mla3_V874 from *E. coli*. For this, I co-transformed *E. coli* with plasmids for recombinant expression of Pwl2 fused to an N-terminal 6x-Histidine affinity tag and Mla3_V874 as an untagged protein. I purified 6xHis-Pwl2 from *E. coli* protein extracts using nickel affinity chromatography (IMAC) and subsequent size exclusion chromatography (SEC). Because Mla3_V874 did not have an affinity tag, it could only be purified through this method if it formed a complex with Pwl2 (**Figure 5.8A**). Protein bands corresponding to the expected sizes of 6xHis-Pwl2 (15.5 kDa) and Mla3_V874 (10.5 kDa) were visible at every step of the purification process on a Coomassie Blue-stained SDS-PAGE gel (**Figure 5.8B**). There was a clear enrichment of bands of the expected sizes of 6xHis-Pwl2 and Mla3_V874 after the IMAC purification step compared to the soluble fraction of the cell lysate (**Figure 5.8B** lane 3). This sample was subsequently used as input for SEC. Eluted fractions under the highest peak of absorbance where pooled and analysed; unfortunately, resolution during SEC was not successful as bands of sizes significantly higher than 6xHis-Pwl2 and Mla3_V874 were present on the stained gel. In addition to the expected bands, a band of intermediate size between 6xHis-Pwl2 and Mla3_V874 was visible, likely corresponding to untagged Pwl2 (13 kDa), possibly due to spontaneous tag cleavage (**Figure 5.8B** lane 4). To corroborate this, I removed the 6xHis tag from Pwl2 by treating the sample with 3C-protease, followed by another round of IMAC and SEC. As a result, two bands of the expected sizes of Pwl2 and Mla3_V874 were visible on the Coomassie Blue-stained gel (**Figure 5.8B** lane 5). The size of the band corresponding to untagged Pwl2 matched the size of the previous intermediate band in between 6xHis-Pwl2 and Mla3_V874. The protein identity of the bands on the gel with the expected sizes of Pwl2 and Mla3_V874 was confirmed by mass spectrometry. Peptides with the expected spectra for both Pwl2 and Mla3_V874 were identified in each sample from the different purification stages

(IMAC, SEC, and tag cleavage followed by IMAC and SEC) (**Figure 5.8C**). Overall, these results indicate that Mla3_V874 co-purified with Pwl2, confirming direct interaction. The purification process had an overall low yield that did not allow to further characterise the Pwl2-Mla3_V874 complex, e.g. through crystallisation trials to solve the structure. Nonetheless, it provided sufficient evidence to confirm direct recognition of Pwl2 by Mla3.

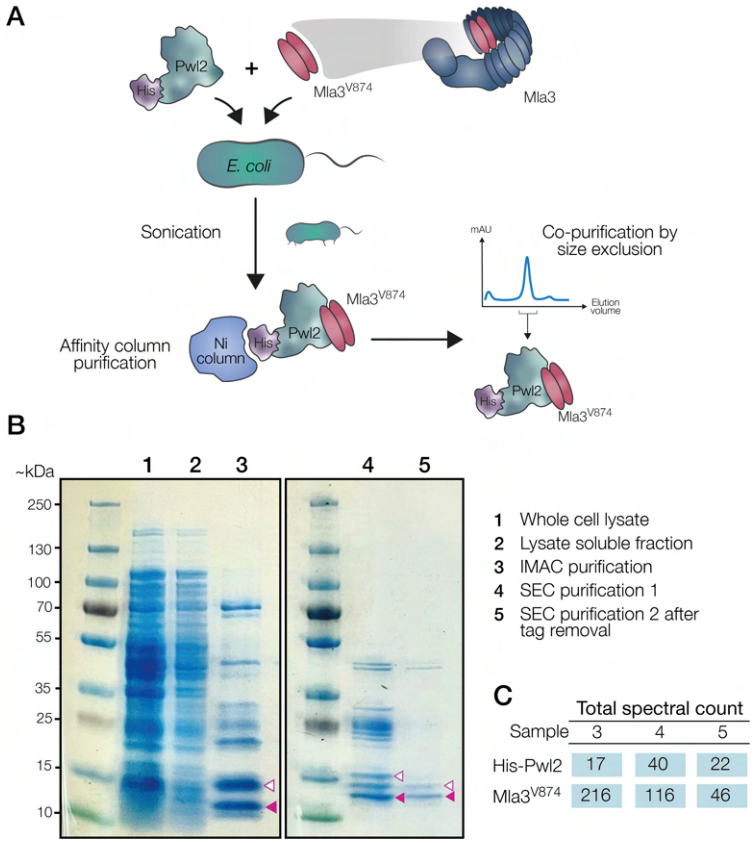

Figure 5.8 The last 85 residues of Mla3 co-purify with Pwl2 in *E. coli* protein extracts.

(A) Diagram of the method used to co-purify Pwl2 with the C-terminus of Mla3 (Mla^{V874}) from *E. coli*. Pwl2 was N-terminally fused to a 6xHis tag, whereas Mla^{V874} was untagged. Briefly, constructs containing the coding sequence of each protein were co-transformed in *E. coli*. Cell culture supernatant was sonicated and the soluble faction of the lysate was used for protein purification through IMAC (immobilized affinity chromatography) using a nickel column, followed by SEC (size exclusion chromatography). **(B)** Coomassie Blue-stained SDS-PAGE gel with protein samples after sonication (1), separation of the soluble fraction (2), IMAC purification (3), SEC purification (4), and SEC purification after treating the sample with 3C protease to remove the 6xHis tag from Pwl2 (5). Bold pink arrows indicate a band matching the expected size of Mla^{V874} (10.5 kDa), and white arrows indicate a band matching the expected size of 6xHis-Pwl2 (15.5 kDa) in lanes 3 and 4, and Pwl2 (13 kDa) in lane 5. **(C)** Total spectrum count of peptides corresponding to Pwl2^{V874} and Mla3 from mass spectrometry analysis of gel bands highlighted in **B**.

5.2.4 The C-terminus of Mla3 mimics the binding interface of a Pwl2 plant target

5.2.4.1 Expression of OsHIPP43 impairs recognition of Pwl2 by Mla3 in *N. benthamiana*

Pwl2 belongs to the family of MAX effectors, which comprises several *M. oryzae* sequence-unrelated effectors that share a similar fold (de Guillen et al., 2015). MAX effectors are known to interact with HMA containing proteins in plants, which are putative virulence targets and act as baits to trigger an immune response when present as integrated domains within NLRs (Ortiz et al., 2017; De la Concepcion et al., 2018; Guo et al., 2018b; Oikawa et al., 2020; Maidment et al., 2021). Pwl2 interacts with the HMA-containing rice protein OsHIPP43, and the structure of the complex has been solved (Zdrzalek, 2021). I set out to determine whether binding of Pwl2 with OsHIPP43 inhibits or impairs Pwl2 recognition by Mla3 in *N. benthamiana*. For this, I tested the HR response triggered by Mla3 and Pwl2 in the presence of OsHIPP43 with gradual increments in the expression levels of the latter. I used the protein thioredoxin h5 from *Arabidopsis thaliana* (AtTRXh5) as negative control, as it is unrelated, yet has a similar size to OsHIPP43 and is targeted by pathogens (Lorang et al., 2012). Simultaneous expression of OsHIPP43 with Pwl2 and Mla3 resulted in attenuated cell death response in comparison to co-expression of AtTRXh5, Pwl2 and Mla3 (**Figure5.9A and B**). This difference was more evident when OsHIPP43 was expressed at higher levels. Recognition of Pwl2 by Mla3 remained unaffected by gradual increments in the expression of AtTRXh5, whereas the intensity of HR sharply decreased when OsHIPP43 had highest expression (**Figure5.9A and B**). Western blots showed that accumulation of Mla3 and Pwl2 in leaf spots agroinfiltrated with AtTRXh5 was visibly lower than in leaf spots agroinfiltrated with OsHIPP43 (**Figure5.9C**), likely due to the stronger cell death response in the former. Noteworthy, OsHIPP43 has a homologue in barley (HORVU.MOREX.r3.3HG0267040.1) with 95% protein identity in the HMA domain (**Figure5.9D**). I performed these and further experiments with OsHIPP43 rather than the barley homologue, as the interaction between Pwl2 and the HMA in OsHIPP43 has been well characterised. Altogether, these results suggest that interaction of Pwl2 with OsHIPP43 impairs Pwl2 recognition by Mla3.

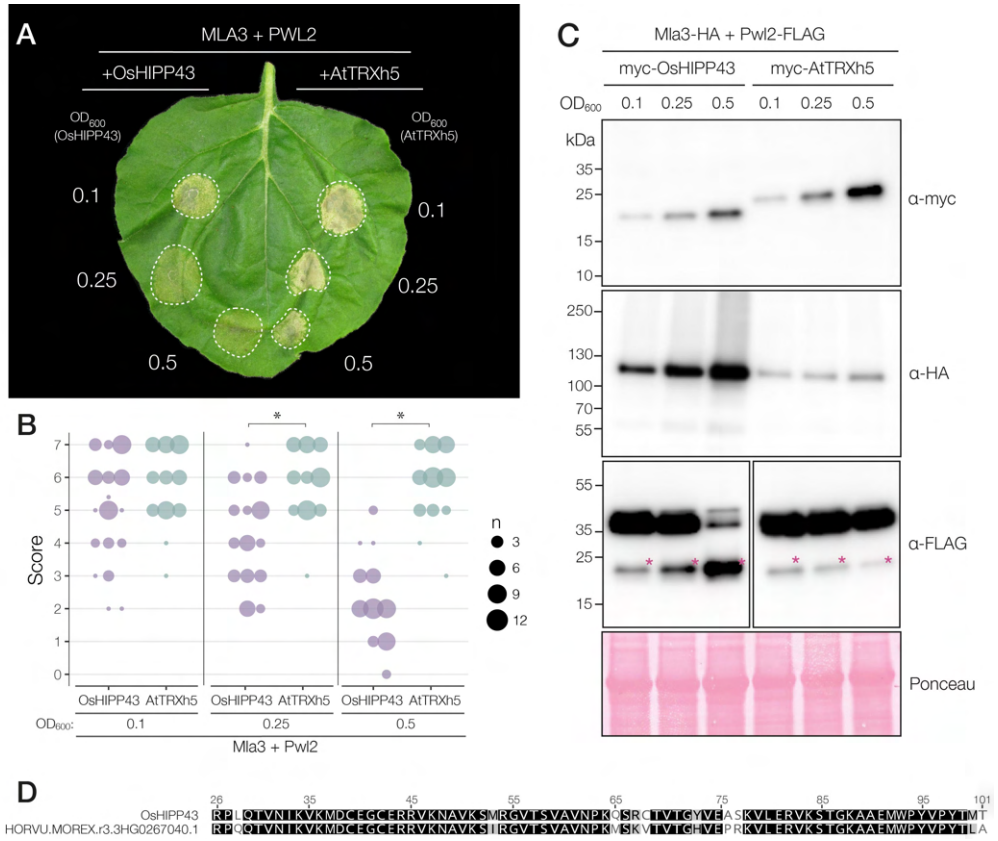

Figure 5.9 Interaction of Pwl2 with OsHIPP43 impairs recognition by Mla3 in *N. benthamiana*.

Gradual increase in the expression of OsHIPP43 weakens recognition of Pwl2 by Mla3. The *A. thaliana* protein AtTRXh5 was used as negative control. **(A)** Representative photo of a *N. benthamiana* expressing the indicated constructs. The marked OD_{600} values denote the concentration of the *A. tumefaciens* suspensions used for infiltration carrying either OsHIPP43 or AtTRXh5. Mla3 was expressed under the strong Mas Ω promoter and C-terminally fused to a 6xHA epitope tag. Pwl2 was expressed under the 35S Ω promoter, without signal peptide and C-terminally fused to a 3xFLAG tag. OsHIPP43 and AtTRXh5 were expressed under the 35S Ω promoter and N-terminally fused to a 4xmyc tag. Photos were taken 3 dpi. **(B)** HR phenotypes from **A** were scored at three days post-agroinfiltration. The results are presented as a dot plot, where a size of a dot is proportional to the number of technical samples with the same score within the same biological replicate. The experiments were independently repeated three times with 8-10 technical replicates; the three data point columns of each tested condition correspond to results from different biological replicates. Significant differences between conditions were calculated based on bootstrapping rank statistics and are indicated with asterisk (*). The details of the statistical analysis are shown in **Figure A.III.2.** **(C)** Western blots to confirm protein expression in **A** using the appropriate antibodies. Mla3-6xHA (115.6 kDa), Pwl2-3xFLAG (17.3 kDa), 4xmyc-OsHIPP43 (16 kDa) and 4xmyc-TRXh5 (18 kDa). Total protein extracts were prepared from leaves harvested 3 days after agroinfiltration. Protein loading was checked with Ponceau S solution (Sigma). **(D)** Protein sequence alignment of the HMA domain in OsHIPP43 and the HMA domain of the closest homologue in barley, HORV.MOREX.r3.3HG0267040.1. The alignment is coloured based on amino acid similarity.

5.2.4.2 The predicted structure of Pwl2 in complex with the C-terminus of Mla3 resembles the structure of Pwl2 bound to OsHIPP43

5.2.4.2.1 Structure prediction of Pwl2 in complex with the C-terminus of Mla3

The impaired recognition of Pwl2 by Mla3 in the presence of OsHIPP43 prompted me to hypothesise that OsHIPP43 and Mla3 compete to interact with Pwl2. To address this, I used AlphaFold2 to predict the structure of Pwl2 in complex with the C-terminus of Mla3 (from residue V868 to include a predicted β-strand preceding V874. I will refer to this fragment as $Mla3^{V868-*}$). The best ranked model had a pLDDT score of 71.7 and a pTM score of 0.703. The multiple sequence alignment that AlphaFold2 used as input for the structure prediction had significantly deeper sequence coverage for $Mla3^{V868-*}$ than Pwl2 (**Figure 5.10A**). However, the coverage of the last ~20 amino acids of $Mla3^{V868-*}$ decreased sharply in comparison to the rest of the sequence (**Figure 5.10A**). The top ranked model of the complex had a relatively low per-residue confidence estimate between positions 10-25 and in the last 10 residues of $Mla3^{V868-*}$, and in the C-terminus of Pwl2 (pLDDT<60). Outside these regions, the model confidence is relatively high (pLDDT >80) (**Figure5.10B**). A low per-residue pLDDT score means that the model predicts these regions as highly disordered or as regions that only become structured as part of a complex in physiological conditions. These regions with low pLDDT score also had a high predicted aligned error (**Figure5.10C**), suggesting that the position of these residues relative to any other region within the complex is mostly uncertain. Taking this into account and to avoid adding confounding error, I decided to remove the last 30 amino acids of Pwl2 for further structural analyses, which are predicted to be highly disordered and have low prediction confidence. In fact, the structure of Pwl2 in complex with OsHIPP43 showed that these residues are indeed disordered (Zdrzalek, 2021).

5.2.4.2.2 Structure comparison of Pwl2 in complex with $Mla3^{V868-*}$ and OsHIPP43

Next, I compared the prediction model of $Mla3^{V868-*}$ in complex with Pwl2, to the experimentally solved structure of Pwl2 bound to the HMA domain of OsHIPP43 provided by Dr. Rafal Zdrzalek. Remarkably, both complexes share striking structural similarities. The structure prediction of Pwl2 is almost identical to the actual structure of the effector in complex with OsHIPP43. In both complexes, $Mla3^{V868-*}$ and OsHIPP43 interact with Pwl2 in similar positions (**Figure 5.11A-C**) and both proteins share overall

structural features (**Figure 5.11D**) despite the lack of sequence similarity between Mla3^{V868-*} and OsHIPP43 (**Figure 5.11E**), and the absence of a known domain at the C-terminus of Mla3. The HMA domain of OsHIPP43 is formed by four antiparallel β-strands and two α-helices, and the C-terminus of Mla3 comprises three parallel β-strands and one α-helix (**Figure 5.11D**). Even though the order and orientation of the β-strands in both structures is different (**Figure 5.11D**), the α1-helices in both of them are aligned and placed in the same position to interact with Pwl2, allowing the β-sheets to be placed in similar disposition (**Figure 5.11C**).

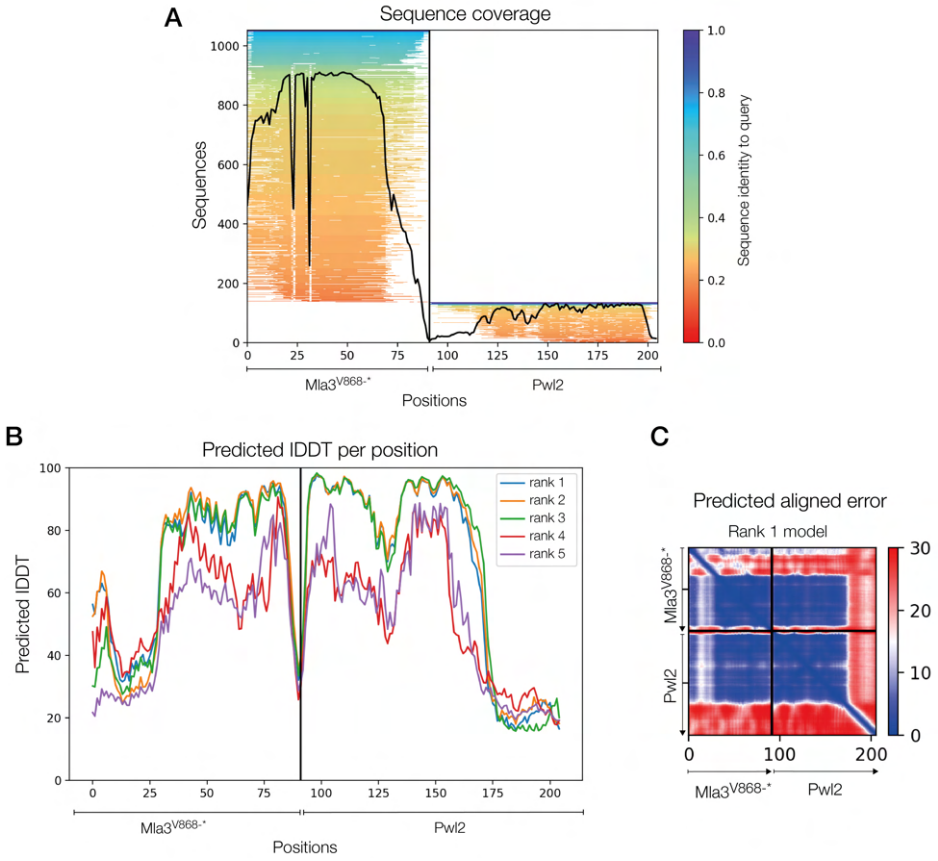

Figure 5.10 Metrics of the predicted structural model of Mla3^{V868-*} in complex with Pwl2.

(A) Sequence coverage in the multiple sequence alignment (MSA) that was used as input for the network analysis by Alphafold2. Sequence identity of each sequence in the MSA to Mla3^{V868-*} and Pwl2 is color-coded according to the scale shown on the right. **(B)** Predicted LDDT (local Distance Difference Test) score per residue of the top five models predicted by Alphafold2 and ranked according to highest pLDDT score, as a confidence estimate per residue of the model. **(C)** Predicted aligned error of the top ranked model predicted by Alphafold2 indicating the expected position error of a given residue in x if the actual structure was aligned with the predicted structure on a given residue y. The predicted error is color-coded according to the scale shown on the right.

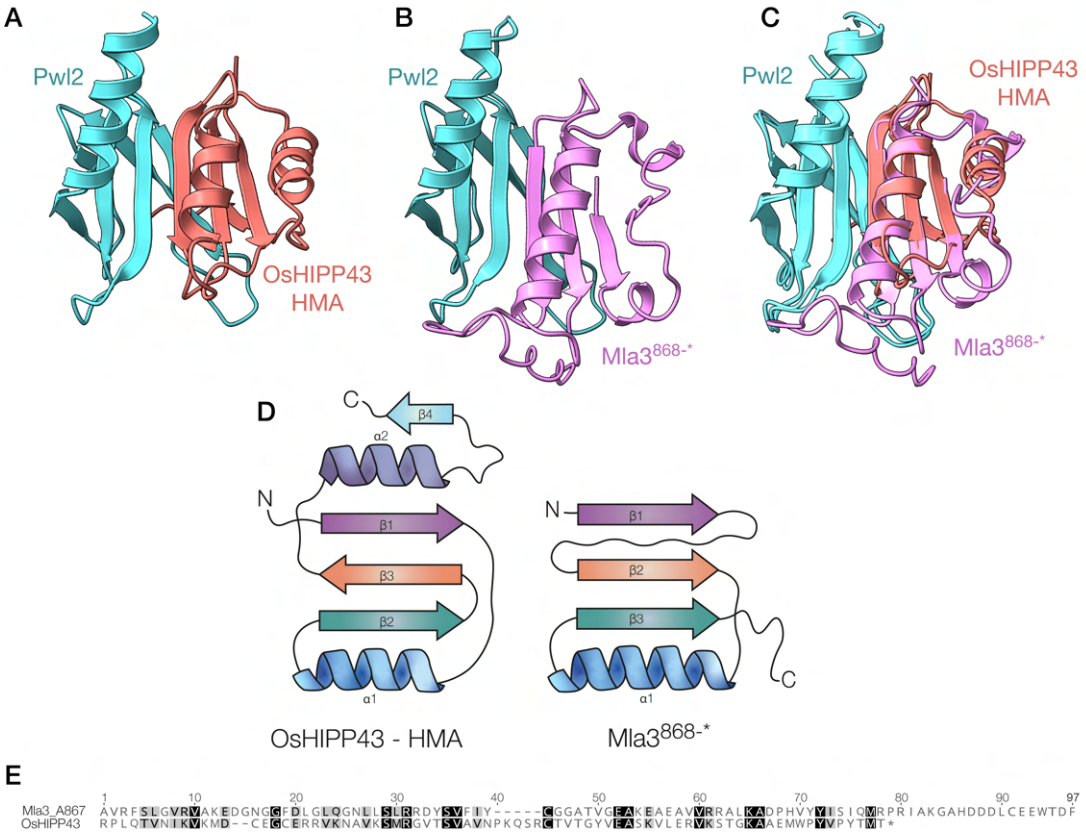

Figure 5.11 The predicted structure of Pwl2 in complex with the C-terminus of Mla3 has structural similarity with Pwl2 bound to OsHIPP43.

(A) Structure of Pwl2 in complex with the HMA domain of OsHIPP43 solved by Dr. Rafal Zdrzalek. **(B)** Alphafold2 structure prediction of Pwl2 interacting with Mla3^{V868-*} (the C-terminus of Mla3, from residue V868 to stop (*)). **(C)** Structure alignment of **A** and **B. (D)** Diagram of the secondary structure of the HMA of OsHIPP43 and Mla3^{V868-*}. **(E)** Protein sequence alignment of the C-terminus of Mla3 (last 97 residues of Mla3; the alignment starts at position 967 of Mla3 up to the final residue 958) and the HMA domain of OsHIPP43 (from original residue 26 to 101). Amino acids are shaded based on similarity. The overall sequence similarity between the two proteins is 35% and 17% sequence identity.

With the aim of comparing the residues in Pwl2 that are making contact with OsHIPP43 and Mla3^{V868-*}, I predicted the binding interface of Mla3^{V868-*} and Pwl2 using the web server PDBePISA v1.52 (https://www.ebi.ac.uk/msd-srv/prot_int/cgi-bin/piserver). The binding interface of Pwl2 with OsHIPP43 significantly overlaps with the binding interface with Mla3^{V868-*} (**Figure 5.12**), explaining the impaired recognition of Pwl2 by Mla3 in presence of OsHIPP43. Both Mla3 and OsHIPP43 compete to bind overlapping residues in Pwl2. In addition, similar regions in OsHIPP43 and Mla3^{V868-*} are in contact with Pwl2, as both these proteins bind to Pwl2 mostly through the α1-helix and the subsequent β-strand in each protein (β2 in OsHIPP43 and β3 in Mla3^{V868-*}) (**Figure 5.12 and Figure 5.11D**).

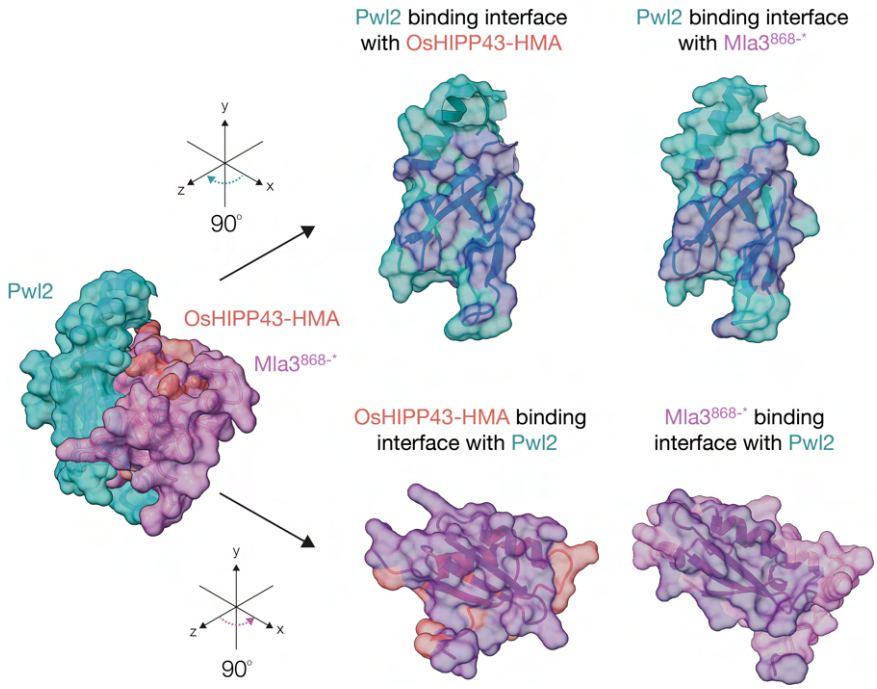

Figure 5.12 Comparison of the binding interface of Pwl2 with OsHIPP43 and Pwl2 with Mla3^{V868-*}.

The surface of the predicted structure of Pwl2 in complex with Mla3^{V868-*} is superimposed with the surface of the Pwl2–OsHIPP43 complex (left). The upper panel shows the surface of Pwl2 residues that are in contact with OsHIPP43 (left) or Mla3^{V868-*} (right) highlighted in dark blue. The structure of both complexes was rotated 90^{o} in clockwise direction on the y axis, and the structures of OsHIPP43 and Mla3^{V868-*} (which would be on top) were removed for clarity. The lower panel shows the surface of the residues in OsHIPP43 and Mla3^{V868-*} that are interacting with Pwl2 highlighted in purple. The structure of both complexes was rotated 90^{o} in anti-clockwise direction on the y axis, and the structure of Pwl2 (which would be on top) was removed for clarity.

Interaction of Pwl2 with OsHIPP43 and Mla3^{V868-*} is based on both shape and charge complementarity. Pwl2 has an overall negative surface charge in the binding interface, whereas both OsHIPP43 and Mla3^{V868-*} mostly have a positive charge on the side facing Pwl2 (**Figure 5.13**). I predicted the structure of the C-terminus of different Mla alleles (Mla23, Mla10, Mla13, Mla7 and Mla6) and compared them to Mla3, with the aim of looking for structural features in Mla3 that might explain its unique ability to recognise Pwl2. The C-terminal region of all analysed Mla alleles share an almost identical structure (**Figure5.14A**). However, most of their electrostatic surface is largely negative in contrast to Mla3, which is predominantly positively charged and complements the negative surface of Pwl2. This result highlights the requirement of a positive surface for interaction with Pwl2, which is unique in Mla3 and sets it apparat from other alleles.

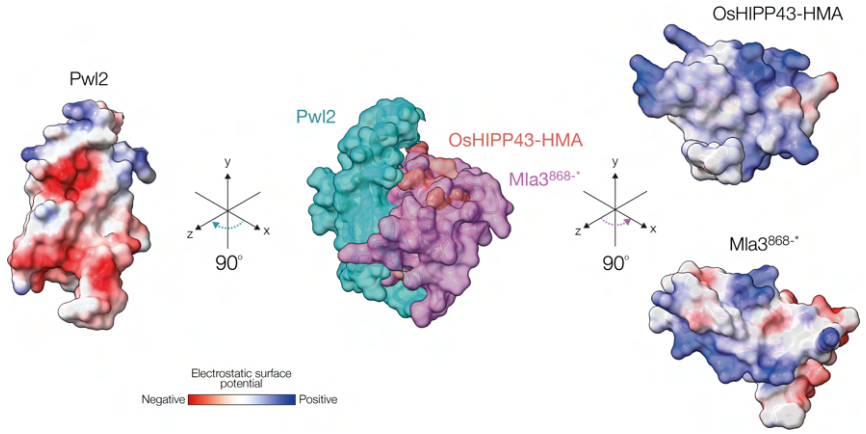

Figure 5.13 Electrostatic surfaces at the binding interface of Pwl2 in complex with OsHIPP43 and Mla3^{V868-*}.

The surface of the predicted structure of Pwl2 in complex with Mla3^{V868-*} and the surface of the Pwl2–OsHIPP43 complex are superimposed (middle). The left panel shows the electrostatic surface of Pwl2 at the binding interface with OsHIPP43 and Mla3^{V868-*}. The structure was rotated 90° in clockwise direction on the y axis, and the structures of OsHIPP43 and Mla3^{V868-*} (which would be on top) were removed for clarity. The right panel shows the electrostatic surfaces of OsHIPP43 (top) and Mla3^{V868-*} (bottom) at the binding interface with Pwl2. The structure of both complexes was rotated 90° in anti-clockwise direction on the y axis, and the structure of Pwl2 (which would be on top) was removed for clarity.

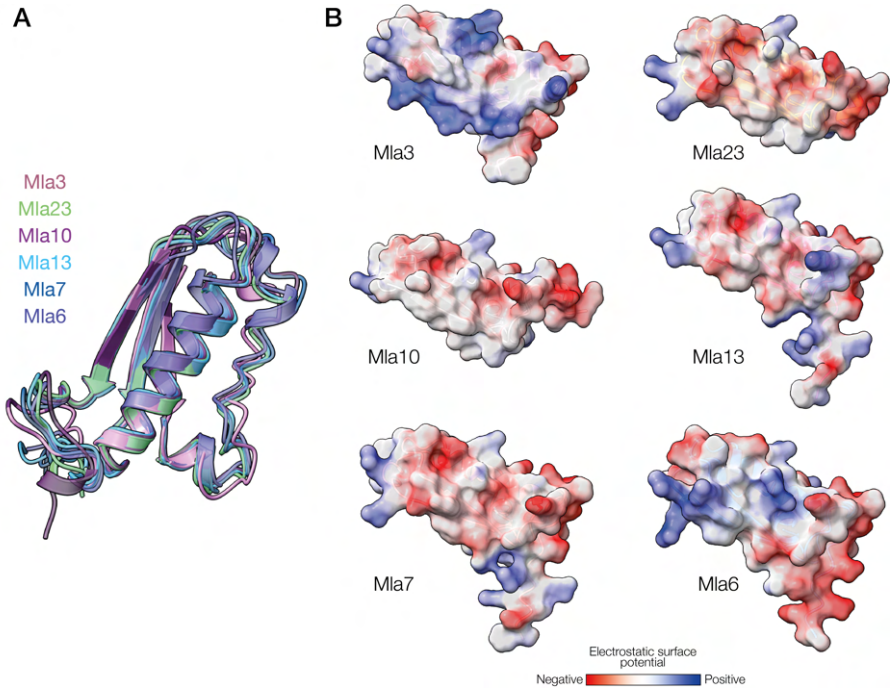

Figure 5.14 Comparison of the structure prediction of the C-terminus of different Mla alleles vs. Mla3.

(A) Super imposition of the Alphafold2 structure prediction of the C-terminus (V868-*) of Mla3, Mla23, Mla10, Mla13, Mla7 and Mla6. **(B)** Electrostatic surface of the C-terminus (V868-*) of Mla3, Mla23, Mla10, Mla13, Mla7 and Mla6 at the predicted binding interface between Pwl2 and Mla3.

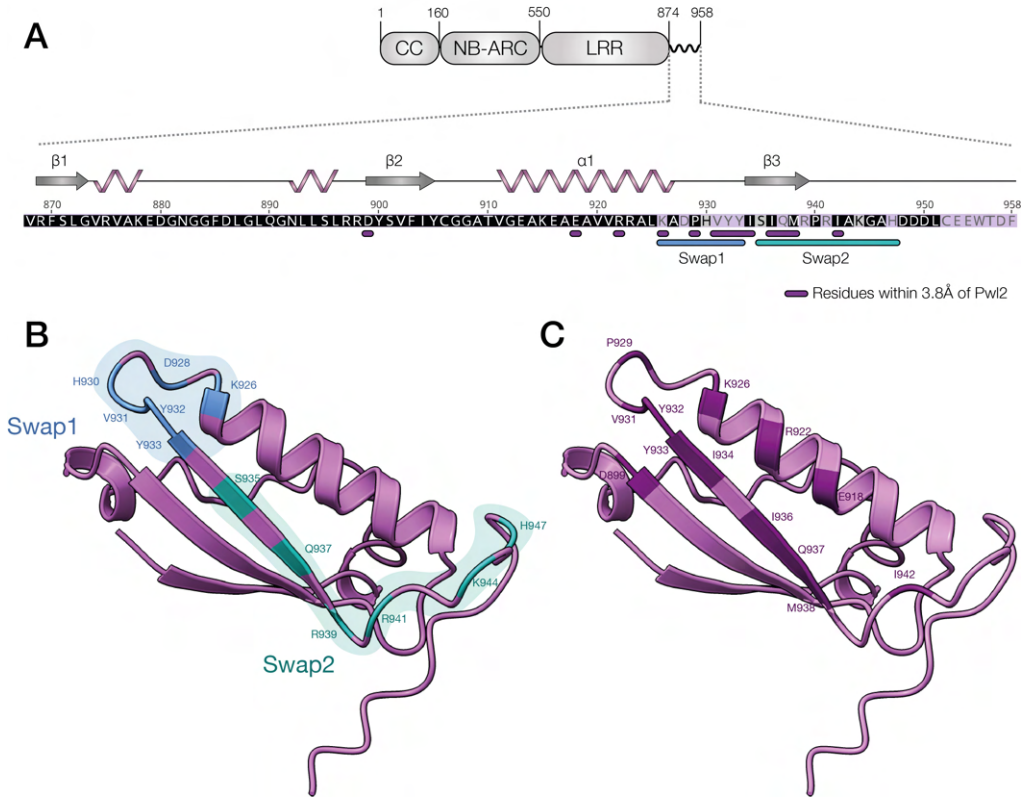

Figure 5.15 Comparison of residues in Mla3^{V868-*} interacting with Pwl2, and the Swap regions used for studies of recognition specificity.

(A) Sequence of the C-terminus of Mla3 and its predicted secondary structure. Residues highlighted in pink and grey are polymorphic in Mla23 (pink: no similarity in Mla23, grey: similarity in Mla23). The first two short α-helices are not numbered as the confidence score of the model in these regions is low. Residues predicted to interact with Pwl2 are underlined in purple; these are within 3.8Å of Pwl2. Residues within the Swap1 and Swap2 regions used to make chimeric constructs with Mla23 for specificity studies are underlined in blue and green, respectively. **(B)** Predicted structure of Mla3^{V868-*} with polymorphic residues compared to Mla23 within the Swap1 and Swap2 regions highlighted in blue and green, respectively. **(C)** Predicted structure of Mla3^{V868-*} with the residues predicted to interact with Pwl2 highlighted in purple.

5.2.4.2.3 Validation of the predicted model of Pwl2 in complex with Mla3^{V868-*}

In order to validate the prediction model of Pwl2 in complex with the C-terminal region of Mla3, I analysed the binding interface between the two proteins in context with results from the studies of specificity of Pwl2 recognition (Chapter 4). The predicted binding interface in Mla3^{V868-*} is mostly located between the α1-helix and the subsequent β3-strand, which coincides with the region containing most residues that are polymorphic in Mla23—in particular those located in the Swap1 and Swap2 subregions defined in section 4.2.5.1(**Figure 5.15A**). The chimeric construct in which Mla3 contained the Swap1 region of Mla23 completely lost the ability to recognise Pwl2, and conversely,

when Mla23 contained the Swap1 region of Mla3, it gained recognition of the effector. I did not observe such exchange of recognition specificity for the Swap2 chimeric constructs (section 4.2.5.1) (**Figure 4.5B and C**). Four out of five residues that are in contact with Pwl2 within the Swap1 region are polymorphic in Mla23 (K926, V931, Y932 and Y933) (**Figure 5.15**), and are predicted to interact with Pwl2 through hydrogen bonds. Consequently, the reciprocal change of this region between Mla3 and Mla23 resulted in exchanged recognition of Pwl2. On the other hand, amongst the four amino acids within the Swap2 region that are predicted to interact with Pwl2, Q937 is the only residue that is polymorphic in Mla23 (**Figure 5.15**) and is predicted to form a single hydrogen bond. Hence, swapping this amino acid possibly had insignificant impact on the Swap2 chimeric constructs, which did not result in exchanged Pwl2 recognition. Overall, the biological data from previous mutagenesis experiments in Mla3 and Mla23 supports the predicted structure of Pwl2 in complex with the C-terminus of Mla3.

I established that the residue K926 is crucial for Pwl2 recognition by Mla3 (section 4.2.5.2). Interestingly, both Mla3^{V868-*} and OsHIPP43 share a lysine that is in contact with Pwl2 and is located in the same position at the end of the α1-helix (K926 in Mla3 and K51 in OsHIPP43) (**Figure 5.16A**). In both cases, this residue interacts with Pwl2 through multiple hydrogen bonds (**Figure 5.16B**). Moreover, the K926R substitution in Mla3 was the only mutation that maintained recognition of Pwl2, indicating that a positively charged amino acid with similar structure is required to recognise Pwl2 (section 4.2.5.4). The residue K926 is predicted to interact with a negatively charged pocket on the surface of Pwl2, similar to residue K51 of OsHIPP43 (**Figure 5.17**). Along with K926, the residue R922 of Mla3 $^{V868-*}$ located in the previous turn of the α1-helix also interacts with the same negative pocket in Pwl2 and matches the residue K47 of OsHIPP43. This further demonstrates that charge complementarity plays a critical role in binding of Mla3 and OsHIPP43 to Pwl2, as two conserved positively charged residues (R922 and K926 in Mla3, and K47 and K51 in OsHIPP43) fit inside a negatively charged pocket in the binding interface of Pwl2 (**Figure 5.17**). In addition, both Mla3^{V868-*} and OsHIPP43 have a glutamic acid interacting with Pwl2 in similar positions (E918 in Mla3 $^{V868-*}$ and E43 in OsHIPP43). Thus, there is overall conservation of the residues in the α-helix of Mla3^{V868-*} and OsHIPP43 that are in contact with Pwl2 (E918-R922-K926 in Mla3, and E43-K47-K51 in OsHIPP43) (**Figure 5.17**). Furthermore, the amino acids V931, I934 and I936 of Mla3 match the residues V56, V59 and V61 of OsHIPP43, indicating similarity of residues that are interacting with Pwl2 in

the loop and β-strand that follow the α1-helix of Mla3^{V868-*} and OsHIPP43 (**Figure 5.17**). Valine and isoleucine have similar structures and hydrophobic side chains, suggesting that these three residues in OsHIPP43 (V56-V59-V61) and Mla3 (V931-I934-I936) form a conserved hydrophobic patch that interacts with Pwl2. Overall, the striking similarities between the two structures suggest that the C-terminus of Mla3 mimics the binding interface of OsHIPP43 to interact with Pwl2.

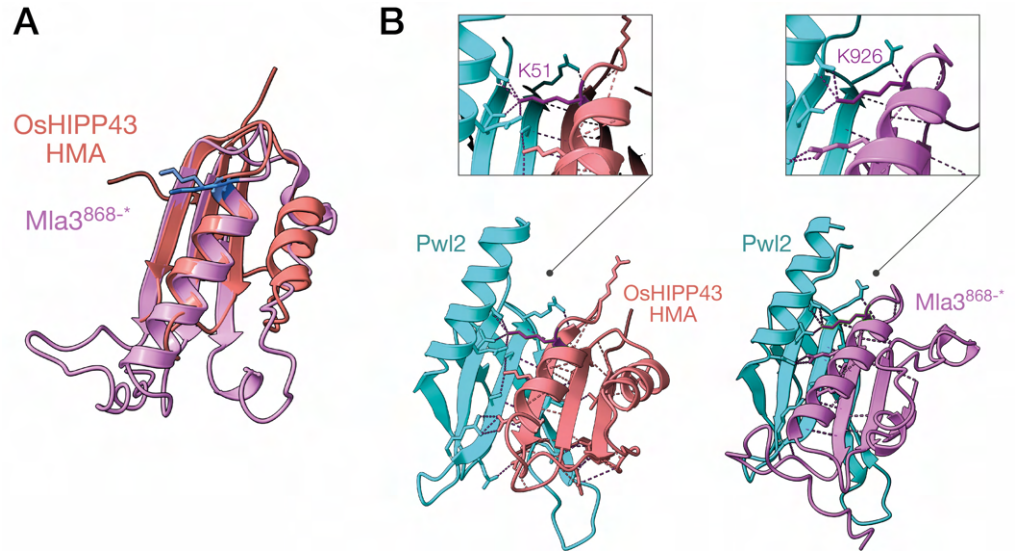

Figure 5.16 OsHIPP43 has a lysine in the same position of K926 in Mla3.

The residue K926 in Mla3 is critical for Pwl2 binding and recognition. **(A)** Superimposed structures of the HMA domain of OsHIPP43 and Mla3^{V868-*}. The residue K926 of Mla3 and K51 of OsHIPP43 are located in the same position, highlighted in blue. **(B)** Structure of Pwl2 in complex with OsHIPP43 (left) and Mla3^{V868-*} (right). Residues forming hydrogen bonds at the binding interface are shown as sticks. Hydrogen bonds at the binding interface are shown as dashed lines. Upper squares contain a magnified view of the residues K51 in OsHIPP43 and K926 in Mla3^{V868-*}, and the hydrogen bonds they form with Pwl2. Both K51 and K926 are highlighted in purple.

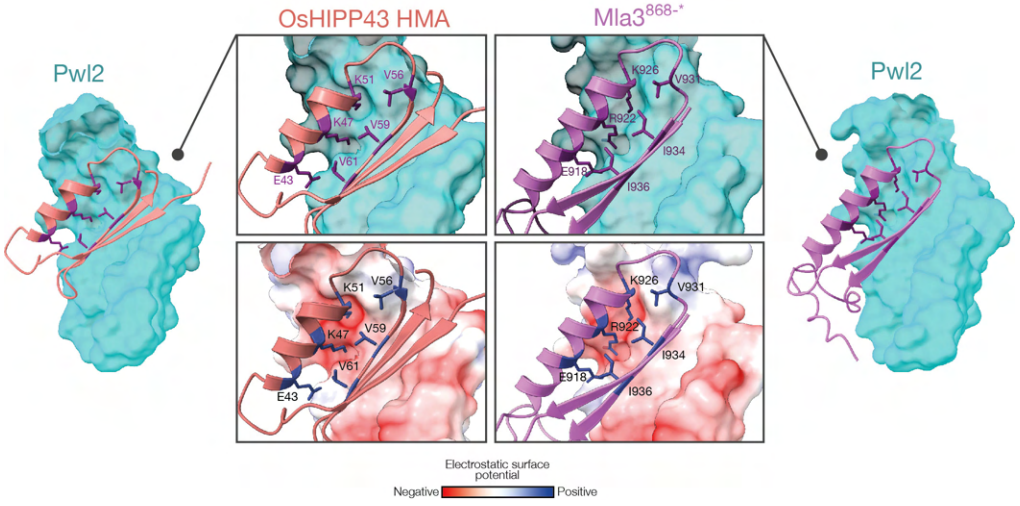

Figure 5.17 Conservation of residues of Mla3^{V868-*} and OsHIPP43 at the binding interface with Pwl2.

Structure of Pwl2 in complex with OsHIPP43-HMA (left) or Mla3^{V868-*} (right). The β1 strand of Mla3^{V868-*} was removed to better appreciate the binding interface. The middle panels magnify the binding interface of each complex. Conserved or similar residues at the binding interface are shown as sticks. Bottom panels display the electrostatic surface of Pwl2 at the binding interface in each complex.

5.2.4.2.4 The D90N substitution of pwl2-2 is not located in the Mla3 binding interface

The single amino acid substitution D90N in the pwl2-2 allele abolishes effector recognition in barley and weeping lovegrass (section 3.2.4) (Sweigard et al., 1995), and compromised the strength of recognition (section 4.2.2) and association with Mla3 in *N. benthamiana* (section 5.2.2.2). However, according to the predicted structure of Pwl2 in complex with Mla3^{V868-*}, the residue D90 in Pwl2 is not located at the binding interface. Nonetheless, prediction of intramolecular hydrogen bonds showed that D90 interacts with a Pwl2 amino acid that makes direct contact with K926 in Mla3 (**Figure 5.18**). This suggests that the D90N mutation might affect intramolecular dynamics that impact the binding interface and ultimately affect the strength of effector recognition by Mla3. Interestingly, this mutation does not affect binding of pwl2-2 to OsHIPP43. The binding interface of Pwl2 with OsHIPP43 has more intermolecular contacts than the predicted interaction with Mla3^{V868-*} (**Figure 5.16B**). This complex binding interface is likely more robust to changes induced by mutations that escape recognition, such as the D90N substitution in pwl2-2. Indeed, mutagenesis experiments failed to disrupt the interaction between OsHIPP43 and Pwl2 (Zdrzalek, 2021). Alternatively, this mutation may also affect binding with additional points of contact in the LRR domain of Mla3. This is a perfect example in which selective pressure on Pwl2 to escape recognition has given way to mutations that successfully avoid detection without affecting target binding.

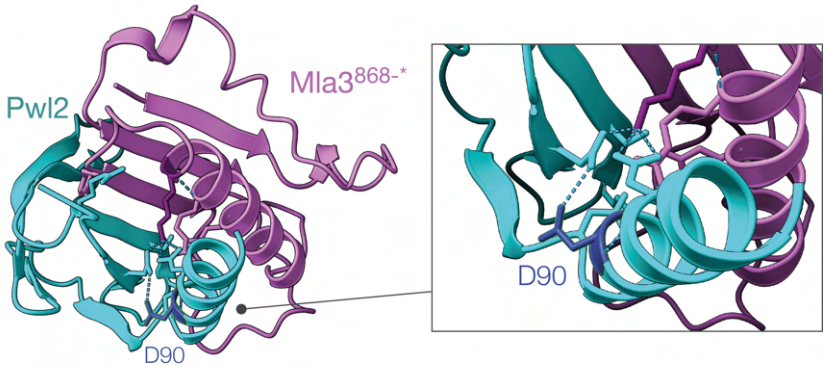

Figure 5.18 The residue D90 in Pwl2 is not located at the binding interface with Mla3.

The D90N substitution in the pwl2-2 allele impairs Pwl2 recognition by Mla3, yet this residue is not located at the binding interface. Predicted structure of Pwl2 in complex with Mla^{V868-*}. Residue D90 in Pwl2 is highlighted in dark blue and shown as sticks. Residue K926 in Mla3 is highlighted in purple and shown as sticks. Residues making hydrogen bonds with D90 in Pwl2 and K926 in Mla3 are also shown as sticks. Hydrogen bonds are shown as dashed lines. The square contains a magnified view of residue D90 in Pwl2 and the hydrogen bonds with nearby residues.

5.3 Conclusions

5.3.1 Main conclusions

In this chapter I aimed to establish the mechanism of Pwl2 recognition by Mla3. I showed that Mla3 associates with Pwl2 *in planta*, and that the LRR domain is required and sufficient for association. Based on sequence analysis, I redefined the boundaries of the LRR domain of Mla3 and found that the last 85 amino acids are not predicted to be part of the canonical LRR region. This C-terminus comprises all polymorphic sites in Mla23—which does not recognise Pwl2—and is sufficient to associate with Pwl2 *in planta*. I showed interaction between the C-terminus of Mla3 and Pwl2 in yeast and *E. coli,* indicating that Mla3 directly recognises this effector. Furthermore, I established that co-expression of Mla3, Pwl2 and OsHIPP43—a Pwl2 target in rice—impaired effector recognition in *N. benthamiana*. To address whether this was due to competition of Mla3 and OsHIPP43 for overlapping binding interfaces with Pwl2, I predicted the structure of the C-terminus of Mla3 in complex with Pwl2 and compared it to the solved structure of the Pwl2–OsHIPP43 complex. Surprisingly, the predicted binding interface of Pwl2 with the C-terminus of Mla3 overlaps almost completely with the OsHIPP43 binding interface. Despite the lack of sequence similarity between OsHIPP43 and the last 85 amino acids of Mla3, there is remarkable structural resemblance between the two proteins. Moreover, there is striking similarity and conservation of residues at the binding

interface with Pwl2 on both proteins. Pwl2 has an overall negatively charged binding interface, and both Mla3 and OsHIPP43 are positively charged at the Pwl2-interacting sites. These surface areas of positive charge in Mla3 are not conserved amongst other Mla alleles, which are predicted to have a predominantly negative surface, explaining the unique ability of Mla3 to recognise Pwl2. Mutagenesis experiments that established the determinants of specificity of Pwl2 recognition by Mla3 (chapter 4) support the structure prediction of Pwl2 in complex with the C-terminus of Mla3. Overall, these results indicate that the C-terminus of Mla3 mimics the binding interface of OsHIPP43 to directly bind to Pwl2 and elicit an immune response. Whether AVR_{a3} from *Bgh* also targets an HMA-containing protein in barley and whether the C-terminus of Mla3 directly binds to AVR_{a3} through a similar binding interface remain open questions until the gene underlying this effector is identified.

5.3.2 Direct recognition of structurally distinct effectors by Mla3

Documented cases of multiple pathogen recognition by NLRs are rare, and all instances studied to date involve sensing of conserved effector activities on shared host targets that act as guardees/decoys, or on NLR-IDs (Lewis et al., 2013; Sarris et al., 2015; Wang et al., 2015; Zhang et al., 2017; Mukhi et al., 2021). ROQ1 directly recognises the effectors HopQ1, XopQ and RipB from *P. syringae, Xanthomonas* spp., and *Ralstonia* spp, respectively (Schultink et al., 2017; Thomas et al., 2020), but all three effectors are homologous and likely have nearly identical structures. Here, I demonstrated that Mla3 directly recognises the effector Pwl2 from *M. oryzae* by mimicking the binding interface of the HMA-containing Pwl2 host target OsHIPP43. Mla3 also recognises the effector AVR_{a3} from *Bgh,* which is hypothesised to be structurally distinct to Pwl2. All AVR_a effectors identified so far belong to the group of RALPH proteins with a common RNAse-like fold (Bauer et al., 2021), and the family of MAX effectors seems to be absent from the secretome of *Bgh* (Seong and Krasileva, 2023).

Regardless of whether Mla3 recognises AVR_{a3} directly or indirectly, this is the first report of an NLR that works as a single unit to confer resistance against multiple pathogens by directly binding to one of the structurally distinct recognised effectors. It remains unknown whether the same region of Mla3 is required to recognise both Pwl2 and AVR_{a3}, and so far, no AVR_a effectors have been reported to target HMA-containing proteins. Intramolecular interactions between the LRR and other NLR domains are tightly regulated, and mutations affecting such contacts often results in constitutive NLR

activation (Slootweg et al., 2013; Maruta et al., 2022). Therefore, it seems unlikely that a singleton NLR evolved two distinct interfaces to directly bind structurally distinct effectors without resulting in disrupted intramolecular arrangements and impaired function. I hypothesise that, in spite of being structurally distinct, Pwl2 and AVR_{a3} might share local structural features that convergently interact with the C-terminus of Mla3. In this case, the C-terminal region of Mla3 acts as a pseudo-ID that mimics an effector target. As such, it represents a mixed model in between singleton NLRs, which autonomously sense effectors and trigger an immune response—mostly in a one-to-one fashion—and specialised sensor NLRs with IDs that lost the ability to activate immune signalling and require helper NLRs, but can have the versatility of recognising multiple effectors/pathogens.

Chapter 6: *Mla3* copy number variation and allelic diversity

6.1 Introduction

Intracellular NLR receptors are major components of the plant immune system (Jones and Dangl, 2006). They activate immune signalling upon specific recognition of pathogen-secreted molecules—known as effectors—and trigger defence responses that halt infection (Dodds and Rathjen, 2010). The number of genes encoding NLRs greatly varies across plant genomes often due to lineage specific expansions and contractions of NLR families (Baggs et al., 2017; Baggs et al., 2020). For example, NLRs of the TIR type (aka TNLs, with an N-terminal Toll/interleukin-1 receptor domain) are absent in monocots (Tarr and Alexander, 2009; Gao et al., 2018), whereas NLRs of the CC type (aka CNLs, with a coiled-coil N-terminal domain) are greatly expanded in Solanaceae species (Seo et al., 2016). NLRs are frequently arranged in genomic clusters as a result of gene conversion events, unequal crossing over and/or tandem duplications (Meyers et al., 1998; Michelmore and Meyers, 1998; Meyers et al., 2003; Kuang et al., 2004). This clustered organisation provides a versatile platform to generate new functional diversity and copy number variation (CNV) within and across species (Barragan and Weigel, 2021).

A remarkable example of NLR genomic clusters is the cluster in soybean containing *Rps11,* a giant NLR (27.7 kb) that confers broad-spectrum resistance against the oomycete pathogen *Phytophthora sojae* (Ping et al., 2016; Wang et al., 2021). This cluster contains several large NLR genes of single origin that were derived from different rounds of tandem duplication events. The large size of NLRs within this cluster is attributed to unequal recombination events that led to promoter fusions and expanded chimeric LRR domains (Wang et al., 2021). These inter- and intragenic recombination events, particularly in the LRR domain, can generate mutations that alter recognition specificity or result in broad spectrum resistance (Michelmore and Meyers, 1998), as in the case of *Rps11*. Furthermore, this NLR cluster displays outstanding structural and CNV across soybean accessions, ranging from five to 23 gene copies within the cluster (Wang et al., 2021). Unequal crossing over events have resulted in gene deletions and duplications that illustrate the complex and highly dynamic nature of NLR clusters.

The *Mla* (*Mildew locus a*) locus in barley contains three different NLR families (*RGH1, RGH2,* and *RGH3*) and exhibits significant structural and CNV across

accessions (Wei et al., 1999; Wei et al., 2002). In the reference cultivar Morex, the locus contains a tandem duplication of 39.7 kb and three gene-rich regions in which NLRs have been shuffled by nested complexes of transposable elements and rounds of inversion and duplication that have expanded the locus (Wei et al., 1999; Wei et al., 2002; Mascher et al., 2021). Members of the *RGH1 Mla* family confer isolate-specific resistance against barley powdery mildew (*Blumeria graminis* f. sp. *hordei, Bgh*) and exist as an expanded series of over 30 characterised alleles with distinct *Bgh* recognition specificities (Jørgensen and Wolfe, 1994; Seeholzer et al., 2010; Maekawa et al., 2018). CNV has been reported for different *RGH1 Mla* alleles (Bettgenhaeuser et al., 2021). The *Mla8* allele, for example, exists as a single-copy gene in tested barley accessions that harbour this allele. In contrast, barley haplotypes that carry *Mla7* display higher order copy number variation, with an estimate of minimum three copies in the haploid genome (Bettgenhaeuser et al., 2021). However, the implications of *Mla* CNV on the phenotypic outcome of *Bgh* resistance has not yet been assessed.

CNV is prevalent across plant genomes, and regions implicated in CNV have been postulated to often contain genes involved in response to biotic and abiotic stress (Springer et al., 2009; Yu et al., 2011; Zheng et al., 2011; McHale et al., 2012; Saxena et al., 2014). In soybean, the *Rhg1* locus has been deployed for resistance against the soybean cyst nematode (SCN) *Heterodera glycines* (Kim et al., 2011). Interestingly, this locus does not contain NLRs but rather four unrelated genes, three of which encode a predicted amino acid transporter, an α-SNAP protein, and a protein with a WI12 (wound-inducible protein 12) region, and all three are required for resistance (Cook et al., 2012). The *Rhg1* haplotype present in SCN-resistant cultivated soybean can harbour three to ten tandem copies of the 31 kb segment carrying the three genes required for resistance, whereas susceptible varieties have only a single copy of the region (Cook et al., 2012; Cook et al., 2014). *Rhg1* copy number diversification likely occurred through unequal crossing over events (Lee et al., 2015). Expression analyses established that SCN resistance mediated by *Rhg1* is conferred by increased expression of the three unrelated genes within the 31 kb segment, derived from CNV in the resistant varieties (Cook et al., 2012; Cook et al., 2014). SCN resistance correlates with the number of *Rhg1* copies, which in turn correlates with *Rhg1* mRNA and protein abundance (Cook et al., 2014; Huang et al., 2021). The in-depth study of *Rhg1* has revealed an additional layer of complexity in disease resistance mechanisms, in which expression polymorphisms derived from CNV determine the outcome of pathogen infection.

Different Mla alleles have been classified as either fast- or slow-acting, depending on the *Bgh* arrested infection stage (Boyd et al., 1995; Caldo et al., 2006). The fast-acting alleles *Mla1, Mla6,* and *Mla13* halt fungal growth before or during haustorium formation, which manifests as cell death of a single infected cell; whereas the slow-acting alleles *Mla7, Mla12* and *Mla3* terminate fungal growth after formation of haustoria and secondary hyphae, involving cell death of the attacked epidermal cell and surrounding mesophyll cells (Boyd et al., 1995; Caldo et al., 2006). Interestingly, the slow *Mla12*-dependent resistance shifts to a rapid response when *Mla12* is overexpressed (Shen et al., 2003), suggesting that response dynamics do not depend on the infection stage at which *Bgh* expresses the corresponding effector recognised by *Mla12,* but rather by *Mla12* transcript (and likely protein) abundance. *Mla7* and *Mla3* are known to exist as multiple copies in the barley accessions that exhibit resistance against *Bgh* isolates carrying cognate effectors (Brabham, 2019; Bettgenhaeuser et al., 2021). However, it has not yet been established whether CNV of these *Mla* alleles is correlated with transcript levels, and whether increased copy number shifts the timing of response and enhances disease resistance due to higher expression levels, such in the case of *Rhg1* in soybean (Cook et al., 2012; Cook et al., 2014).

In this chapter, I set out to examine *Mla3* diversity and CNV across barley accessions, and their correlation with resistance against *M. oryzae* through recognition of *PWL2,* and against a *Bgh* isolate that carries AVR_{a3}. I identified barley accessions carrying *Mla3*-related alleles with limited polymorphisms that are able to recognise *PWL2* from *M. oryzae,* but differ in copy number and expression levels. Even though the *Mla3*-related alleles in these accessions have the ability to recognise *PWL2*, not all are resistant to blast. I discuss the implications of these results in the evolution of *Mla3* towards functional resistance in barley against the highly divergent fungal pathogens *Bgh* and *M. oryzae.*

6.2 Results and discussion

6.2.1 Mla3 functions in a dosage-dependent manner

6.2.1.1 An *Mla3* variant that recognises Pwl2 in *N. benthamiana* does not confer *M. oryzae* resistance in barley

Brabham (2019) previously showed that multiple copies of *Mla3* are required for functional resistance against *M. oryzae* in barley (Brabham, 2019). RenSeq data, chromosome flow sorting, long-range linkage and *k*-mer coverage analysis on

chromosome 1H established that the barley accession Baronesse carries three identical copies of *Mla3,* and one of *Mla3*Δ*6,* an additional *Mla3* copy with an in-frame six-nucleotide deletion. Only barley transgenics carrying two or more copies of *Mla3,* but not *Mla3*Δ*6,* gained resistance to *M. oryzae*, suggesting that the six base pair deletion impaired effective *PWL2* recognition (Brabham, 2019). The six-nucleotide deletion translates into a non-synonymous substitution and additional deletion of two residues. Interestingly, this deletion resides within the LRR domain of Mla3 (**Figure 6.1A**) and is upstream of the C-terminal region which I found to be critical for interaction with Pwl2 (section 5.2.3). I tested the ability of Mla3Δ6 to trigger cell death in *N. benthamiana* when co-expressed with Pwl2 to assess whether this Mla3 variant is functionally capable of recognising Pwl2. If the six-nucleotide deletion does not abolish Pwl2 recognition, it is possible that Mla3Δ6 did not confer resistance to *M. oryzae* in barley transgenics due to insufficient copy number and low expression levels. Interestingly, Mla3Δ6 triggered HR upon co-expression with all Pwl2 alleles, similar to wild-type Mla3 (**Figure 6.1B**). Both Mla3 and Mla3Δ6 were over-expressed under the strong Mas Ω promoter. This indicates that, when over-expressed in *N. benthamiana*, Mla3Δ6 can recognise Pwl2 and activate an immune response. I thus propose that lack of resistance against *M. oryzae* in barley transgenics carrying *Mla3*Δ*6* can be attributed to insufficient expression (or protein accumulation) levels that do not meet the required threshold to trigger an immune response, rather than lack of Pwl2 recognition.

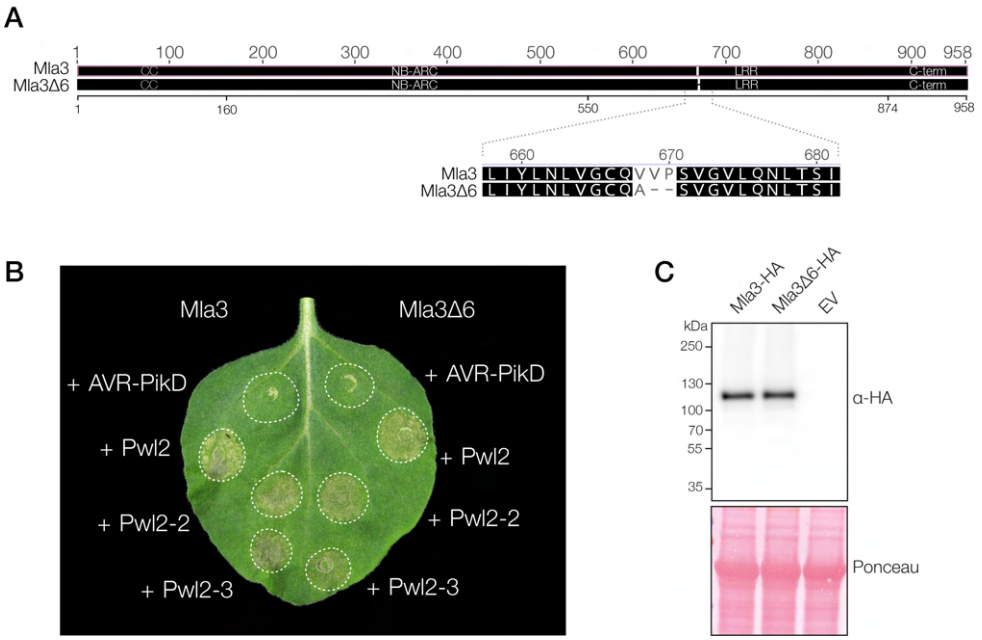

Figure 6.1 The MlaΔ6 variant recognises Pwl2 in *N. benthamiana*.

MlaΔ6 differs from Mla3 by one amino acid polymorphism and a two-residue deletion. It does not function in barley transgenics, yet it is able to recognise all Pwl2 alleles in *N. benthamiana*. (**A**) Pairwise protein alignment of Mla3 and Mla3Δ6. Residues are coloured based on similarity. Black: identical residues. White: No similarity. Highlighted differences between the two proteins are magnified. (**B**) Representative photo of a leaf of *N. benthamiana* expressing the indicated constructs. Mla3 and Mla3Δ6 were expressed under the strong Mas Ω promoter and C-terminally fused to a 6xHA tag. All Pwl2 alleles and AVR-PikD were expressed under the 35S Ω promoter, without signal peptide and C-terminally fused to a 3xFLAG tag. Photos were taken 3 dpi. AVR-PikD was used as negative control. The experiment was independently repeated two times with 8-10 technical replicates. (**C**) Anti-HA immunoblot of Mla3-6xHA and Mla3Δ6-6xHA (~115.5 kDa) expressed in *N. benthamiana*. Total protein extracts were prepared from leaves harvested 3 days after agroinfiltration. Protein loading was checked with Ponceau S solution (Sigma).

6.2.1.2 The barley accession HOR21599 has a single copy *Mla3*-related allele and is susceptible to *M. oryzae*

Amongst the genome assemblies of 20 barley varieties from the barley pan-genome project (Jayakodi et al., 2020), our group identified the barley accession HOR21599, which carries a single copy of an Mla3 variant that differs only from wild-type Mla3 by two amino acids in the LRR region (S671P and L710F) (**Figure 6.2A**). To test whether this *Mla3* proto allele confers resistance against *M. oryzae,* I performed spot infection assays in HOR21599, using barley accessions that carry *Mla3* as resistant controls (i.e. Baronesse and the Siri near isogenic lines S02 and S13). The accession HOR21599 is susceptible to the *M. oryzae* isolate KEN54-20, indicating that HOR21599 does not recognise *M. oryzae* under native conditions. In this experiment, however, I also included the *M. oryzae pwl2* mutant M61 and M61+*PWL2* as controls to initially test specific *PWL2* recognition. Surprisingly, HOR21599 is resistant against the isolate M61+*PWL2,* even though it is susceptible to wild-type KEN54-20 and M61 (*pwl2*) (**Figure 6.2B**). *PWL2* was ectopically transformed in the isolate M61+*PWL2*, meaning that multiple integrations of the effector occurred in the genome, likely increasing its expression levels (N.B. actual expression levels of *PWL2* in the isolate M61+*PWL2* during infection remain to be confirmed through RNA sequencing in a virulent interaction). Taking this into account, I hypothesised that the *Mla* allele in HOR21599, which is almost identical to *Mla3* but is only present as single copy, is able to recognise *PWL2* when overexpressed in *N. benthamiana,* as in the case of *Mla3Δ6*. To test this, I transiently expressed *Mla-HOR21599* under the strong Mas Ω promoter and Pwl2 under the constitutive 35S promoter, using AVR-PikD as negative control. Interestingly,

Mla-HOR21599 triggered an HR response upon co-expression of Pwl2, indicating that it is molecularly able to recognise the effector under the tested conditions.

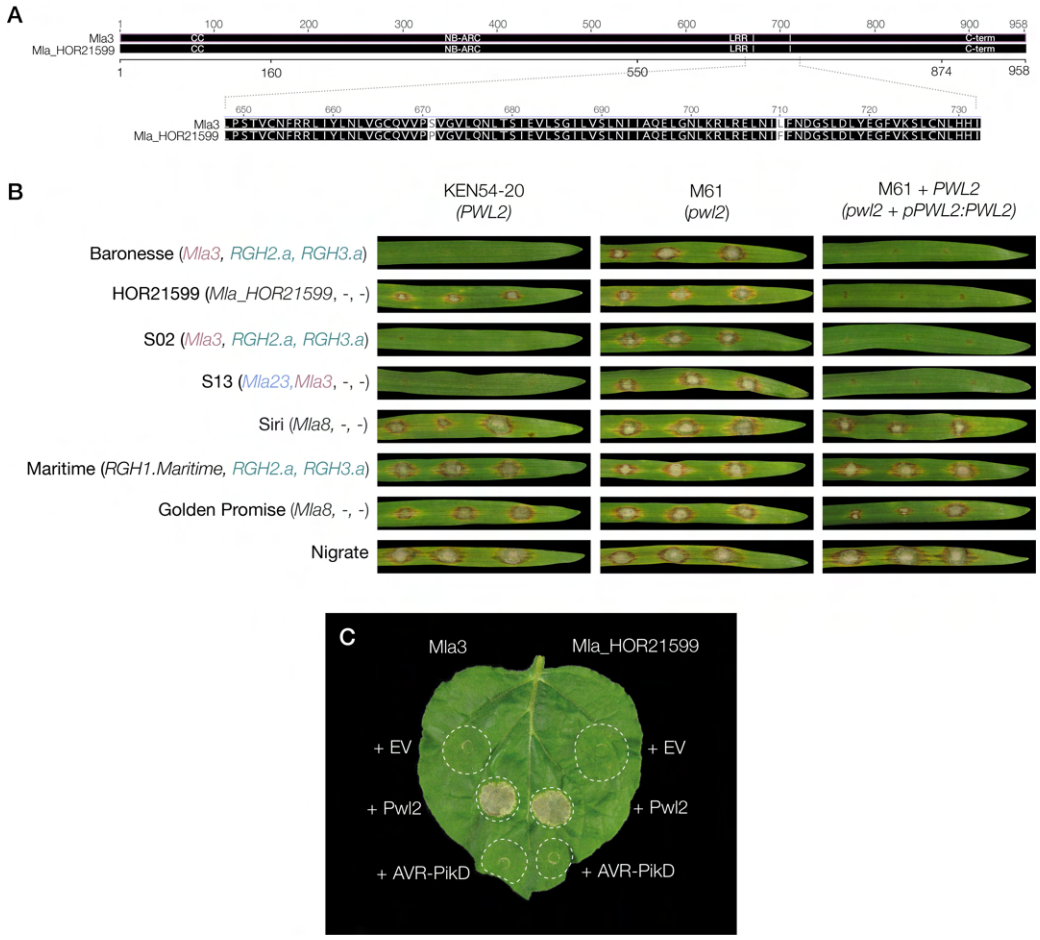

Figure 6.2 The barley accession HOR21599 has an Mla3-related allele.

The Mla allele of HOR21599 is 99.8% identical to Mla3 at the protein level. HOR21599 is susceptible to *M. oryzae,* yet it recognises Pwl2 when the effector is artificially transformed into *M. oryzae* and when it is overexpressed in *N. benthamiana.* (**A**) Pairwise protein alignment of Mla3 and Mla-HOR21599. Residues are coloured based on similarity. Black: identical residues. White: No similarity. Highlighted differences between the two proteins are magnified. (**B**) Spot infection assays with *M. oryzae* isolate KEN54-20 (*PWL2*), *pwl2* mutant M61, and *PWL2*-complemented mutant M61+*PWL2* (*pwl2* + *pPWL2:PWL2:tPWL2*) on a panel of barley accessions made by Baronesse, HOR21599, the Siri near isogenic lines S02 and S13, Siri, Maritime, Golden Promise and Nigrate. The *Mla* locus of each accession is described in parenthesis. Siri, Maritime, Golden Promise and Nigrate were used as susceptible controls. Infected leaves were imaged 7 dpi. Phenotypes are representative of three biological replicates with three technical replicates each. (**C**) Representative photo of a leaf of *N. benthamiana* agroinfiltrated with the indicated constructs. Mla3 and Mla-HOR21599 where expressed under the strong Mas Ω promoter and C-terminally fused to a 6xHA tag. Pwl2 and AVR-PikD were expressed under the 35S Ω promoter, without signal peptide and C-terminally fused to a 3xFLAG tag. Photos were taken 3 dpi. AVR-PikD and empty vector (EV) were used as negative controls. The experiment was independently repeated three times with 8-10 technical replicates.

Given that the accession HOR21599 was resistant to *M. oryzae* when *PWL2* was complemented in the M61 mutant, and that Mla-HOR21599 recognised Pwl2 when both were transiently overexpressed, this suggests that resistance against *M. oryzae* derived from recognition of *PWL2* by *Mla3* variants works in a dosage dependent manner. A certain threshold of expression is required in barley for functional disease resistance, which can be achieved through high levels of the NLR or the effector, either one derived from the presence of multiple copies. In agreement with this, available RNA-seq data revealed that *Mla-HOR21599* is expressed as 17.52 transcripts per million (tpm) in HOR21599, whereas *Mla3* is expressed as 120.5 tpm in Baronesse—almost seven times more. These results outline that copy number variation plays a role in *Mla3* function and evolution. Different stages of the evolutionary trajectory of *Mla3* copy numbers can be observed in barley natural variation. The two extremes are the accession HOR21599, which has a single copy of an *Mla3* proto-allele and is naturally susceptible to *M. oryzae*, and Baronesse, which has three copies of *Mla3* and one of *Mla3Δ6* and is completely resistant against the blast fungus. This also illustrates that the evolutionary arms race between barley and *M. oryzae* exerts pressure on *Mla3* and *PWL2* not only at the protein sequence level (i.e. on the amino acids residing in the binding interface), but also at the level of copy number and protein dosage to finely tune their expression.

6.2.2 Recognition of *PWL2* by *Mla3*-related alleles in wild barley accessions

6.2.2.1 The wild barley accessions WBDC221 and WBDC233 are resistant to *M. oryzae* and carry an *Mla3*-related allele that recognises *PWL2*

Based on the previous results, I was interested in assessing *PWL2* recognition and *Mla3* natural variation across barley accessions. For this purpose, I screened the wild barley diversity collection (WBDC), which is a panel of 316 different wild barley accessions (*H. vulgare* L. ssp. *spontaneum*), for resistance against blast by carrying out spot-inoculations with *M. oryzae*. More specifically, I screened for differential responses to *PWL2* vs. *pwl2 M. oryzae* isolates. I used the wild-type *M. oryzae* isolate KEN54-20 and the *pwl2* mutants M43 and M61 and included Baronesse and Nigrate as resistant and susceptible controls, respectively. Amongst the 316 different WBDC accessions tested, the majority showed low infection scores (**Figure 6.3**), highlighting the significant potential of this wild barley collection as a genetic resource to identify sources of resistance. In this case, however, I was interested in looking for accessions that differentially responded to wild-type KEN54-20 and the *pwl2* mutants M43 and M61,

suggesting *PWL2* recognition. Two accessions, WBDC221 and WBDC233, had identical disease response to Baronesse and were resistant to KEN54-20 but susceptible to M43 and M61 (**Figure 6.3**). Such a differential response to isolates with and without *PWL2* can imply two different scenarios: it is possible that the two WBDC accessions carry *Mla* alleles similar to *Mla3* that meet an expression level sufficient to function and effectively recognise *PWL2,* or that recognition of *PWL2* is conferred by an unrelated *Mla* allele or an unrelated resistance gene altogether.

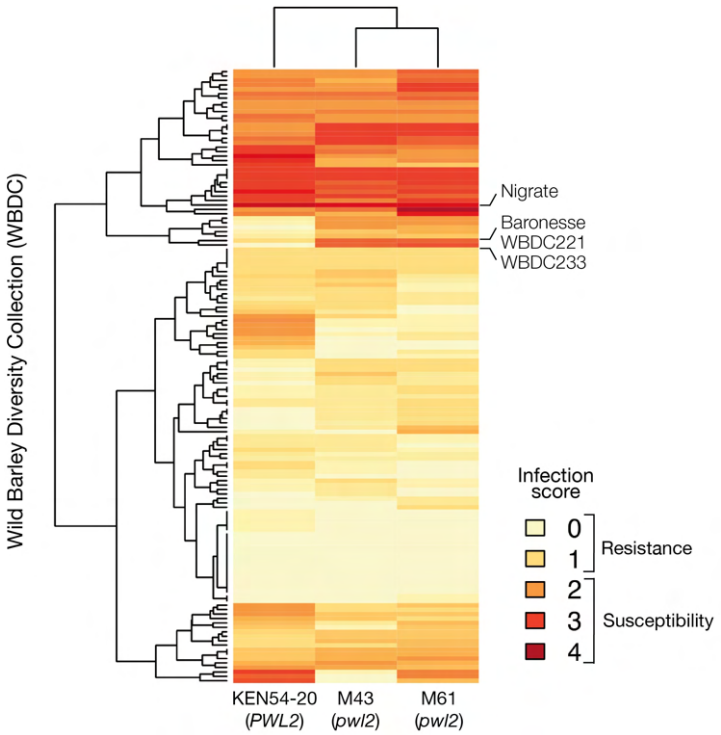

Figure 6.3 Resistance against *M. oryzae* of two wild barley accession is dependent on the presence of *PWL2*.

Heat map of the phenotypic response to *M. oryzae* spot inoculation on 316 barley accessions from the wild barley diversity collection (WBDC). The colour gradient from light yellow to dark red corresponds to infection scores, where 0-1 correspond to resistant phenotypes and 2-4 to susceptibility. Baronesse (*Mla3*) was used as control for *PWL2* recognition, and Nigrate was used as susceptible control. Each column corresponds to the response against the indicated *M. oryzae* isolate used for spot inoculations: wild-type KEN54-20 (*PWL2*) and two independent *pwl2* mutants, M43 and M61. The phenotype is an average of the infection score of a given genotype derived from three technical replicates. The highlighted accessions WBDC221 and WBDC233 had a similar phenotype to Baronesse (*Mla3*).

To address the first hypothesis, I looked at available genomic sequencing data from WBDC221 and WBDC233 and found that these accessions carry each an Mla allele that is 98.5% and 99% identical to Mla3 at the protein level, respectively (**Figure 6.5**). The LRR region of the Mla alleles in the two WBDC accessions differs by seven amino

acids from Mla3 (one of which is S671P, also present in Mla-HOR21599), and two and six additional differences are located throughout the CC and NB-ARC domains of Mla-WBDC233 and Mla-WBDC221, respectively (**Figure 6.4**). Compared to Mla3, both Mla-WBDC221/233 alleles carry the G37R substitution in the CC domain, and the D177G substitution near the P-loop motif in the NB domain. Additionally, Mla-WBDC221 has the R212K mutation within the P-loop motif, as well as the H461P, E462G, and N466T polymorphisms in the WHD region of the NB-ARC domain (**Figure 6.4**). Noteworthy, the 85 C-terminal residues critical for interaction with Pwl2 are identical to Mla3.

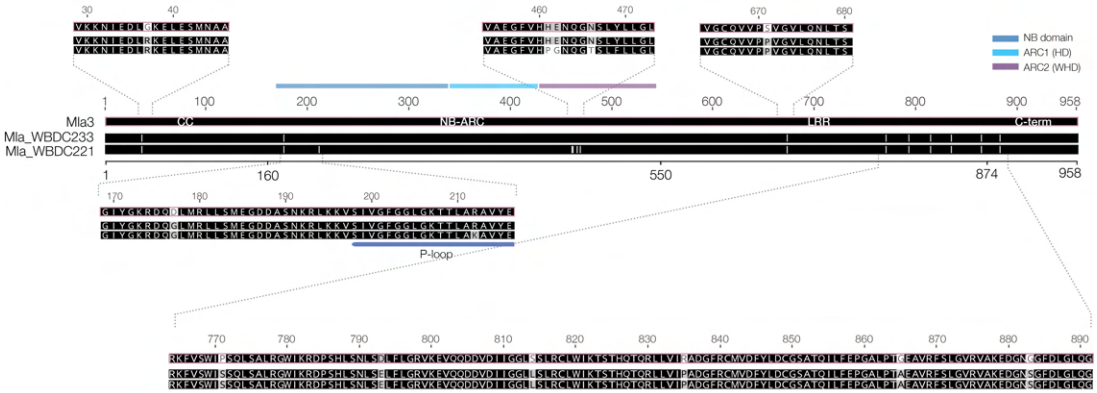

Figure 6.4 Protein alignment of Mla3 and the Mla alleles of the accessions WBDC221 and WBDC233.

Mla_WBDC221 and Mla_WBDC233 are 98.5% and 99% identical to Mla3 at the protein level. Residues are coloured based on similarity. Black: identical residues. Grey: similar residues. White: No similarity. Highlighted differences between the three proteins are magnified.

I then confirmed the results of the primary *M. oryzae* infection screen in the whole WBDC panel by doing leaf spot inoculations focusing specifically on WBDC221 and WBDC233, and using an expanded set of barley accessions as controls (i.e., including Baronesse, and the Siri near isogenic lines S02 and S13, all of which carry wild-type *Mla3*). In this experiment, I also included the *PWL2*-complemented mutant M61+*PWL2* to further validate *PWL2* recognition in these accessions. In agreement with the primary screen, both WBDC221 and WBDC233 are resistant to *M. oryzae* isolates that carry *PWL2* (KEN54-20 and M61+*PWL2*), but susceptible to the *pwl2* mutant M61 (**Figure 6.5A**). I used the accessions Golden Promise, Siri and Nigrate as susceptible controls. Altogether, the evidence strongly suggests *Mla* as the resistance gene conferring *PWL2* recognition in these wild barley accessions.

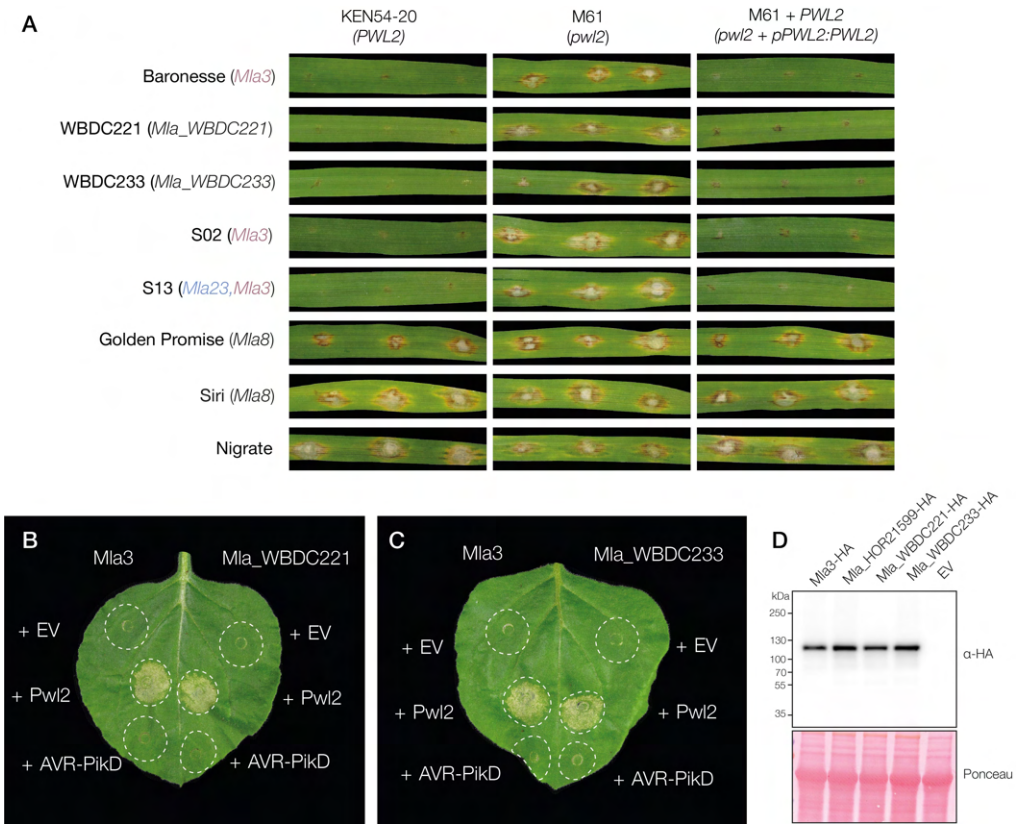

Figure 6.5 Mla-WBDC221 and Mla-WBDC233 recognise Pwl2.

The barley accessions WDBC221 and WBDC233 are resistant to *M. oryzae* isolates that carry *PWL2*. (**A**) Spot infection assays with *M. oryzae* isolate KEN54-20 (*PWL2*), *pwl2* mutant M61, and *PWL2*-complemented mutant M61+*PWL2* (*pwl2* + *pPWL2:PWL2:tPWL2*) on a panel of barley accessions made by Baronesse, WBDC221, WBDC233, the Siri near isogenic lines S02 and S13, Siri, Golden Promise and Nigrate. The *Mla* locus of each accession is described in parenthesis. Siri, Golden Promise and Nigrate were used as susceptible controls. Infected leaves were imaged 7 dpi. Phenotypes are representative of three biological replicates with three technical replicates. (**B-C**) Representative photo of a leaf of *N. benthamiana* agroinfiltrated with the indicated constructs. Mla3, Mla-WBDC221 and Mla-WBDC233 were expressed under the strong Mas Ω promoter and C-terminally fused to a 6xHA tag. Pwl2 and AVR-PikD were expressed under the 35S Ω promoter, without signal peptide and C-terminally fused to a 3xFLAG tag. Photos were taken 3 dpi. AVR-PikD and empty vector (EV) were used as negative controls. The experiment was independently repeated three times with 8-10 technical replicates. (**D**) Anti-HA immunoblot of Mla3-6xHA, Mla-HOR21599-6xHA, Mla-WBDC221-6xHA and Mla-WBDC233-6xHA (~115.5 kDa) expressed in *N. benthamiana*. Total protein extracts were prepared from leaves harvested 3 days after agroinfiltration. Protein loading was checked with Ponceau S solution (Sigma).

Given the sequence similarity of the Mla alleles in WBDC221 and WBDC233 to Mla3, I tested whether these alleles recognise Pwl2 in *N. benthamiana*. For this, I cloned *Mla-WBDC221* and *Mla-WBDC233* for transient expression and co-expressed each of them with Pwl2. Both alleles triggered cell death upon recognition of Pwl2 with similar HR intensity as Mla3 (**Figure 6.5B and C**). This indicates that the amino acid differences

in Mla-WBDC221 and Mla-WBDC233 compared to Mla3 do not impair Pwl2 recognition. Not surprisingly, these differences are outside the C-terminal region that I found to be critical for binding with Pwl2. Altogether, these results suggest that the *Mla* allele in the accessions WBDC221 and WBDC233 confers resistance to *M. oryzae* by recognising *PWL2*. The mapping populations derived from crosses between WBDC221 or WBDC233 and the susceptible parents Nigrate or Manchuria are under current development to ultimately confirm *Mla* as the locus conferring resistance.

6.2.2.2 *Mla-WBDC221* and *Mla-WBDC233* are functional as single copy genes

So far, the evidence suggests that *Mla3* is required as multiple copies and functions in a dosage-dependent manner to confer effective resistance against *M. oryzae* in barley. Therefore, I was interested in establishing the copy number of the *Mla* alleles in WBDC221 and WBDC233 and their expression levels. A *k*-mer analysis using available genomic sequencing data revealed that the accessions WBDC221 and WBDC233 carry one and three copies, respectively, based on the frequency of *k*-mer multiplicity (**Figure 6.6**). When manually comparing genomic data with RNA-seq data, we established that only one of the three *Mla* copies in WBDC233 is expressed. Interestingly, *Mla-WBDC221* and *Mla-WBDC233* are expressed as 22.08 and 25.53 tpm, in contrast to 120.5 tpm of *Mla3* in Baronesse, which is approximately five times more. This underlines an interesting case in which a single copy of either of these *Mla3*-related alleles is sufficient to confer functional resistance against *M. oryzae* by recognising *PWL2*, in contrast to *Mla-HOR21599, Mla3*Δ*6* and even wild-type *Mla3,* which require both high copy number and high expression to be functional.

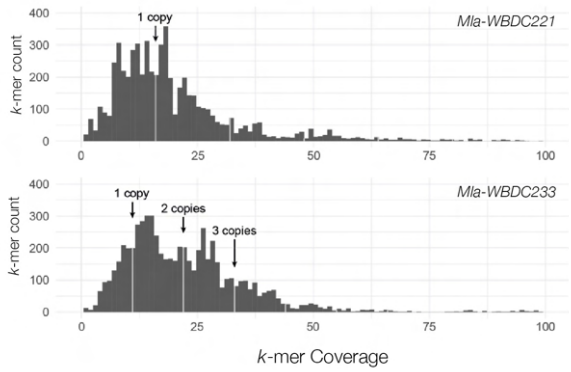

Figure 6.6 *Mla-WBDC221* and *Mla-WBDC233* are present as single and three copies, respectively.

Frequency of *k*-mer coverage of the *Mla* alleles of WBDC221 and WBDC233. Depth of genome sequencing and the *Bpm* gene at the *Mla* locus of each accession were used as reference to determine single copy levels.

Amino acid differences in Mla-WBDC221 and Mla-WBDC233 in comparison to wild-type Mla3 might explain why these two alleles have overcome the requirement for elevated expression levels to function. I propose that such polymorphisms either increase protein stability of these NLR variants or lower the threshold for effector recognition and immune activation by increasing binding affinity to Pwl2, reducing autoinhibition, or promoting NLR oligomerisation upon activation. Protein accumulation in *N. benthamiana* does not seem to differ between Mla3 and related alleles (**Figure6.5D**), hence not supporting the protein stability hypothesis. Nonetheless, transient expression assays in *N. benthamiana* were performed under artificial overexpression conditions in this dicot system, which might differ significantly from native conditions in barley. Ultimately, these models can be tested through quantitative comparative proteomics to establish if expression levels correlate with protein levels (e.g., whether elevated expression levels of *Mla3* due to multiple copy number in Baronesse translate into high protein levels); through in vitro protein binding assays with purified full-length Mla3, Mla3-related alleles and Pwl2; or through optimising the conditions of transient expression in *N. benthamiana* to detect subtle differences in the HR response of wild-type alleles or autoactive mutants. Either way, these strategies can be technically challenging and require rigorous optimisation. Therefore, I propose them as a subject for future studies.

6.2.3 WBDC233 is fully resistant to *Bgh* carrying AVR_{a3}, unlike HOR21599 or WBDC221

I was interested in establishing the impact of copy number and polymorphisms of *Mla3*-related alleles in recognition of AVR_{a3} and hence, in functional resistance against *Bgh*. For this, I performed barley powdery mildew infections in HOR21599, WBDC221 and WBDC233—three barley accessions that have single copy *Mla3* variants—with the *Bgh* isolate BM20/1/11, which is avirulent in Baronesse and therefore carries AVR_{a3}. I used the Siri near isogenic lines S02 and S13, as well as Baronesse, as resistant controls, and Siri, Golden Promise and Manchuria as susceptible controls. Amongst the three barley accessions of interest, only WBDC233 was fully resistant to *Bgh,* similar to Baronesse and S02. The accession S13 showed a necrotic reaction, which also indicates resistance, as fungal growth was completely restricted. The accession WBDC221 showed leaf chlorotic lesions and some fungal sporulation, although to a lower extent than HOR21599, which was as susceptible as Siri, Golden Promise and Manchuria (**Figure 6.7**). Resistance to *Bgh* in WBDC233 could be conferred by recognition of AVR_{a3} by

Mla-WBDC233 or by recognition of an additional effector by a different resistance gene. The mapping population derived from the cross between WBDC233 and Manchuria is under current development to establish the locus or loci associated with resistance. Unfortunately, since the gene underlying AVR_{a3} has not been identified yet, functional studies of AVR_{a3} with these *Mla3* variants in *N. benthamiana* is not possible.

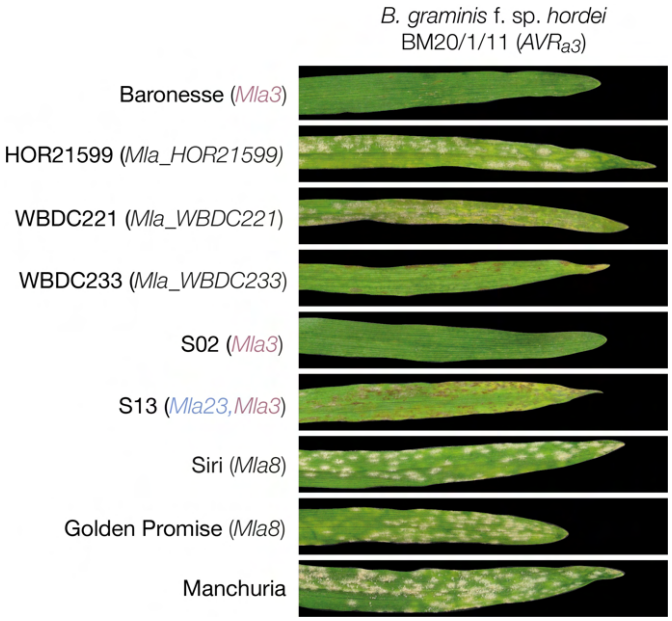

Figure 6.7 WBDC233 is fully resistant to *Bgh* carrying AVR_{a3}.

Barley accessions Baronesse, HOR21599, WBDC221, WBDC233, Siri near isogenic lines S02 and S13, Siri, Golden Promise and Manchuria inoculated with *Bgh* isolate BM20/1/11 carrying AVR_{a3}. Baronesse, S02 and S13 were used as resistant controls. Siri, Golden Promise and Manchuria were used as susceptible controls. Infected leaves were imaged 7 dpi. Phenotypes are representative of two biological replicates with eight technical replicates.

Given that *Mla-WBDC221* and *Mla-WBDC233* have similar expression levels, and assuming a scenario in which Mla-WBDC233 is functional against AVR_{a3}, polymorphisms in Mla-WBDC221 will be crucial to understand recognition of this effector. There are only four differences between the two alleles, all located in the NB-ARC domain, suggesting that likely they do not play a role in specificity of AVR_{a3} recognition. Therefore, these polymorphisms might have an effect on protein stability or intramolecular interactions that render Mla-WBDC233 "trigger-happy" compared to Mla-WBDC221 (Segretin et al., 2014), explaining the partially susceptible phenotype against *Bgh* in the latter. Based on the few differences between Mla3 and Mla-HOR21599 (i.e., S671P and L710F, and S671P is also present in Mla-WBDC233), I hypothesise that,

as discussed earlier in this chapter, functional resistance against *Bgh* requires a threshold of expression levels to be met that *Mla-HOR21599* does not reach due to insufficient copy number. Alternatively, recognition of AVR_{a3} and Pwl2 might occur through distinct Mla3 binding interfaces and the L710F polymorphism in Mla-HOR21599 abrogates AVR_{a3} but not Pwl2 recognition.

6.3 Conclusions

6.3.1 Main conclusions

In this chapter, I aimed to assess *Mla3* natural variation in terms of copy number and allelic diversity. The blast resistant cultivar Baronesse carries three wild-type copies of *Mla3,* which is expressed as 120.5 tpm. I identified two Mla3 variants, Mla3Δ6 and Mla-HOR21599, that are molecularly able to recognise Pwl2, yet they are not functional in barley. Golden Promise transgenic plants transformed with *Mla3Δ6* did not gain resistance against *M. oryzae*, likely due to insufficient expression. Similarly, the barley accession HOR21599 carries a single copy of the *Mla3* proto-allele Mla-HO21599, which is expressed only as 17.52 tpm, and is susceptible to blast. These two alleles triggered HR upon recognition of Pwl2 in *N. benthamiana*, indicating that they are functional and that specificity of Pwl2 recognition is not impaired. Interestingly, HOR21599 was resistant against the isolate M61+*PWL2*, which has multiple integrations of *PWL2* and likely elevated *PWL2* expression levels. Thus, the evidence indicates that effective blast resistance in barley conferred by *Mla3* recognition of *PWL2* requires high expression levels driven by multiple copies of either the NLR or the effector.

Furthermore, I found two wild barley accessions, WBDC221 and WBDC233, that are resistant to *M. oryzae* and have differential response to *pwl2* mutants, indicating recognition of *PWL2*. Each of these accessions have a single functional copy of an *Mla* variant (*Mla-WBDC221* or *Mla-WBDC233,* respectively) that is >98.5% identical to Mla3 at the protein level, and both are expressed five time less than *Mla3* in Baronesse. Both Mla-WBDC221 and Mla-WBDC233 recognised Pwl2 in *N. benthamiana.* This indicates that polymorphisms in these alleles balance out the high copy number and expression requirement for effective resistance in barley. Finally, when comparing HOR21599, WBDC221 and WBDC233, only WBDC233 was as resistant as Baronesse against *Bgh* carrying AVR_{a3}, suggesting that both, copy number and gain of function mutations play a role in recognition of Pwl2 and AVR_{a3}.

6.3.2 *Mla3* evolution towards functional resistance against *M. oryzae* and *Bgh*

NLR genetic variation encompasses not only sequence polymorphisms, but also CNV, as illustrated by *Mla*. CNV has been shown to influence gene expression in both metazoan and plants (Stranger et al., 2007), and to have significant impact on diverse traits (Perry et al., 2007; Pearce et al., 2011; Wingen et al., 2012). One good example is the *Rhg1* locus in soybean. Pathogen resistance conferred by *Rhg1* and *Mla3* depends on expression levels, which in turn are determined by CNV in resistant cultivars (Cook et al., 2012; Cook et al., 2014). However, as illustrated by *Mla3,* variation at the protein sequence level can alter the dosage required and the efficiency of effector recognition. Different studies have reported mutations that increase the sensitivity and reduce the activation threshold of NLRs, making them "trigger-happy", which results in an enhanced hypersensitive response (Harris et al., 2013; Stirnweis et al., 2013; Segretin et al., 2014; Giannakopoulou et al., 2015). Generally, these mutations are located in the NB-ARC domain, likely altering intramolecular interactions and/or ATP binding. This modulation of nucleotide binding or hydrolysis could potentially lead to enhanced oligomerisation dynamics (Harris et al., 2013; Stirnweis et al., 2013). Nonetheless, alteration of these intramolecular interactions can also happen due to mutations in the LRR region that result in reduced autoinhibition (Moffett et al., 2002). A better biochemical understanding of NLR activation mechanisms will aid in determining how specific amino acid polymorphisms contribute to immune receptor activation dynamics.

Based on the evidence presented in this chapter, I propose a mixed evolutionary model for *Mla3* function based on positive dosage, in which effective resistance is not only determined by molecular recognition and specificity, but also by dosage controlled by copy number. Different number of copies can be found in nature and often lead to distinct resistance phenotypes: HOR21599 has a single *Mla3* proto-allele and is susceptible to *M. oryzae* and *Bgh,* while Baronesse has four *Mla3* copies and is resistant to both fungal pathogens. An alternative evolutionary trajectory may lead to overcoming the high expression barrier for functional resistance by creating more efficient NLR variants with gain of function mutations that confer resistance while being expressed at single copy levels. Such would be the case of WBDC233 and WBDC221. Some of the mutations in these alleles might impact effector binding affinity, and/or intramolecular interactions that change activation and oligomerisation dynamics, rendering them more "trigger-

happy" (Segretin et al., 2014) upon recognition of both Pwl2 and AVR_{a3} (like in the case of WBDC233) or Pwl2 only (like in WBDC221). It remains to be determined if other *Mla* alleles, or even other NLRs that directly recognise their cognate pathogen effectors follow similar evolutionary trajectories. *Mla7* is also present and required as multiple copies to confer resistance against *Bgh* and wheat stripe rust (Bettgenhaeuser et al., 2021). Allele mining of *Mla7*-related alleles on a diversity panel such as the WBDC accessions would prove helpful to test this hypothesis.

6.4 Contributions to research

I would like to thank Lauriane Cattaldo for her significant contribution to the large screen for *M. oryzae* resistance in the panel of WBDC accessions.

Chapter 7: General discussion

Despite significant progress in the study of plant NLR biology, the evolutionary forces that have shaped NLR diversity and function remain a subject of intense investigation. Due to their high-specificity, NLRs are often studied in isolation with single pathogens or effectors. However, complex pathogen and microbial communities, rather than single units, exert selective pressures that influence the NLR landscape in plants. While an understudied area, investigating the recognition of multiple pathogens by NLRs provides a valuable experimental system to understand the forces driving the coevolution of NLRs and effectors across several pathogens, and bridge the gap between mechanistic and evolutionary research on complex plant–microbe interactions.

In this thesis, I explored the functional diversification of *Mla* in barley by delving into the recognition of two distantly related pathogens—*Bgh* and *M. oryzae*—by the *Mla3* allele. I focused on understanding *Mla3*-mediated resistance against blast and characterising the principles ruling recognition and specificity. In chapter 3, I established that *Mla3* recognises *PWL2,* a *M. oryzae* effector known to limit host specificity towards weeping lovegrass. I showed that *Mla3* in barley and an unrelated, still unknown NLR in weeping lovegrass convergently evolved to recognise *PWL2* with conserved specificity. In chapter 4, I shed light upon the regions in *Mla3* determining *PWL2* specificity of recognition. I leveraged *Mla* natural variation to generate chimeric versions of Mla3 using an Mla3-related allele that does not recognise Pwl2. I defined an eight amino acid window in the C-terminus of Mla3 that is required for Pwl2 recognition and established that a single positively charged residue within the region is crucial for recognition of this effector. In chapter 5, I used protein-protein interaction assays to understand the mechanism of Pwl2 recognition. I established that Pwl2 directly binds to the C-terminus of Mla3, which is distinct and subsequent to the LRR domain, and contains the polymorphisms that define specificity of recognition. I showed that presence of the Pwl2 host target OsHIPP43 impacts recognition by Mla3, as both plant proteins compete to bind the same interface in Pwl2. Structure prediction of Pwl2 in complex with the C-terminus of Mla3 suggests that this NLR mimics the binding interface of OsHIPP43 to recognise Pwl2, shedding light on the possible evolutionary processes that shaped effector recognition. Lastly, in chapter 6, I assessed Mla3 copy number variation and allelic diversity across barley accessions to understand the principles defining functional

Mla3-mediated resistance against *Bgh* and *M. oryzae* in barley. I found that *Mla3* functions in a dosage-dependent manner, and based on natural diversity, I hypothesised that certain polymorphisms abolish the requirement of high expression without abrogating effector recognition, possibly by reducing the sensitivity threshold to trigger an immune response.

7.1 *Mla* allelic functional diversification

The study of *Mla* has provided a valuable framework for NLR research, contributing to our understanding of fundamental concepts in CNL function and evolution. The *Mla* expanded allelic series illustrates the remarkable functional diversification of this NLR: different alleles recognise sequence-unrelated effectors (Lu et al., 2016; Saur et al., 2019; Bauer et al., 2021) and divergent pathogens (Periyannan et al., 2013; Mago et al., 2015; Chen et al., 2017; Brabham, 2019; Bettgenhaeuser et al., 2021), have variable requirements and response timings (Boyd et al., 1995; Shen et al., 2003; Bieri et al., 2004; Caldo et al., 2006), and even opposite phenotypes as a result of conserved mutations (Crean et al., 2023). For example, mutations in the α1-helix of the CC domain have been shown to impair CNL immune signalling whilst maintaining resistosome integrity triggered by effector recognition (Wang et al., 2019a; Contreras et al., 2022). Based on the definition of the MADA-like motif in Mla10 (Adachi et al., 2019b), I generated the $Mla3^{L11E}$ MADA-like mutant which exhibited impaired cell death activity upon Pwl2 recognition. Interestingly, alanine mutations in this region unexpectedly rendered the Mla13 allele constitutively active, triggering effector-independent cell death (Crean et al., 2023). In addition, the mutation F99E in the CC domain induced an autoimmune phenotype in Mla10 and Mla13 (Bai et al., 2012; Crean et al., 2023), but not in Mla3. Some alleles such as Mla10 and Mla34 are autoactive when transiently expressed in *N. benthamiana*, in contrast to Mla3 or Mla23. The requirement for the co-chaperone RAR1 also varies among alleles, and RAR1-independency was derived from divergent evolutionary origins (Shen et al., 2003; Bieri et al., 2004; Halterman and Wise, 2004). Moreover, overlapping but distinct regions in Mla1 and Mla6 are required to maintain recognition of the corresponding AVR_{a1} and AVR_{a6} *Bgh* effectors (Shen et al., 2003), suggesting incomplete conservation of the binding interface to recognise cognate AVR_a effectors amongst Mla alleles.

Throughout this thesis, I have emphasised that the rye Mla ortholog Sr50 confers resistance against the highly divergent pathogen wheat stem rust (*Pgt*) through direct recognition of the effector AvrSr50 (Mago et al., 2015; Chen et al., 2017), which is

structurally unrelated to the RNAse-like fold present in the AVR_a effectors identified so far (Bauer et al., 2021; Ortiz et al., 2022). Furthermore, as the main subject of this thesis, I have emphasised the recognition of multiple divergent pathogens by certain Mla alleles, such as Mla3 and Mla8 (Brabham, 2019; Bettgenhaeuser et al., 2021). I have shown that Mla3 directly binds to the MAX effector Pwl2 from *M. oryzae,* which has a distinct structural conformation to known AVR_a *Bgh* effectors (Zdrzalek, 2021). Overall, different lines of evidence highlight the remarkable functional diversification across *Mla* alleles, which have a single origin and are >90% protein identical, yet function in diverse ways and confer resistance against multiple pathogens by recognising sequence-unrelated and structurally distinct effectors. The different *Mla* alleles appear to have followed distinct evolutionary trajectories that allowed such diversification. How a narrow range of amino acid polymorphisms amongst alleles has led to such versatility in effector recognition and function remains to be determined. While it is likely that *Mla* diversification has been driven by strong selection pressures imposed by direct recognition of pathogen effectors (Saur et al., 2021), the precise mechanisms that have shaped *Mla* evolution are still unknown.

7.2 The role of *Mla* in host range dynamics

Two reports have shed light on the role of *Mla* in host range dynamics. Bettgenhaeuser et al. (2021) established that the *Mla8* allele confers resistance to the non-adapted pathogen wheat stripe rust (*Pst*) in barley (Bettgenhaeuser et al., 2021), and I found that *Mla3* recognises the host-species specificity determinant *PWL2* from *M. oryzae*. Understanding the implications of multiple pathogen recognition in host range dynamics is crucial to maintain barriers to non-adapted pathogens in breeding programmes. A devastating example of the consequences of overlooking these implications was the introgression of the *Pc2* locus into commercial oat varieties to provide resistance against oat crown rust caused by *Puccinia coronata* (Welsh et al., 1954). *Pc2*-associated resistance was quickly found to be coupled with susceptibility to Victoria blight conferred by the *Vb* locus (Meehan and Murphy, 1946). Victoria blight is caused by the necrotrophic pathogen *Bipolaris victoriae*, and requires the *Vb* locus in oat to mediate sensitivity to victorin, a host selective toxin secreted by the fungus (Lorang et al., 2007). *Pc2* and *Vb* are in complete genetic coupling, suggesting that the two loci are potentially the same gene conferring resistance to one disease, but susceptibility to another (Wolpert

and Lorang, 2016). Interestingly, sensitivity to victorin in barley has been mapped to the *Mla* locus in the accession Baronesse (Lorang et al., 2010; Brabham, 2019).

PWL2 is widely present across *M. oryzae* isolates from the rice-infecting lineage, making the deployment of *Mla3* in rice as an *R* gene against blast an attractive strategy to limit the devastating losses caused by this pathogen. However, it is crucial to determine whether the *RGH1* allele in the *Mla* locus of Baronesse (i.e *Mla3*) underlies sensitivity to victorin in order to avoid a similar outcome to the introgression of *Pc2* in oat. In *A. thaliana,* the CNL LOV1 confers victorin sensitivity by guarding AtTRXh5, a thioredoxin targeted by victorin (Sweat and Wolpert, 2007; Lorang et al., 2012). An outstanding scenario in which *Mla3* confers victorin sensitivity in addition to resistance against *Bgh* and *M. oryzae* would raise a new wealth of questions around the true versatility of *Mla*. So far, the evidence suggests that Mla3 directly recognises AVR_{a3} and Pwl2, and the requirement of a thioredoxin for sensitivity to victorin in barley has not been determined yet. Thus, incorporating recognition of victorin into the model would add complexity to the understanding of this NLR. While the ability to recognize multiple pathogens may be advantageous, it may also come at a cost of being exploited by necrotrophic pathogens that benefit from triggering cell death, such as *B. victoriae*. Overall, understanding the implications of multiple pathogen recognition and host-range dynamics of *Mla* is crucial to harness such versatility and deploy integral strategies that maintain barriers to non-adapted and/or opportunistic necrotrophic pathogens.

7.3 Direct effector recognition and positive selection in NLRs

Most of the sites that are under positive selection in Mla alleles are located on the surface of the concave side of the LRR domain (Seeholzer et al., 2010; Tamborski et al., 2022). This pattern is not only common for Mla alleles present in cultivated barley, but also for wild barley and barley landraces from which cultivated barley has been derived (Maekawa et al., 2018). These observations suggest that selection pressure to maintain recognition of *Bgh* has existed for an extended evolutionary time span, leading to the extensive diversification of *Mla* alleles even prior to the domestication of barley (Maekawa et al., 2018). Diversifying selection on both NLRs and their cognate recognised effectors is one of the hallmarks of direct effector recognition (Saur et al., 2021). This implies that effectors are under pressure to evade recognition while maintaining their function, and host NLRs are positively selected to evolve new recognition specificities that maintain recognition of evolving effectors (Ellis et al., 2007; Chen et al., 2022). Other

plant NLRs such as *L* in flax, *Pm3* in wheat, and *RPP1* and *RPP13* in *A. thaliana,* which are predicted or known to directly recognise corresponding effectors, have highly polymorphic sites in the LRR and C-terminal regions that determine specificity of recognition and effector binding, similar to *Mla* (Bittner-Eddy et al., 2000; Srichumpa et al., 2005; Ravensdale et al., 2012; Prigozhin and Krasileva, 2021).

The mode of effector recognition by NLRs can be predicted based on sequence diversity (Prigozhin and Krasileva, 2021). Shannon entropy analyses measure the amino acid variability at a given position in a protein sequence alignment. High entropy values correlate with polymorphic positions that are surface exposed and can predict fast evolving protein–protein contact sites (Magliery and Regan, 2005; Prigozhin and Krasileva, 2021). Most of the polymorphisms and high entropy values in NLR families with elevated diversity—such as Mla—cluster on the surface of the LRR domain, and predict regions that determine specificity of recognition and effector binding (Prigozhin and Krasileva, 2021). Not surprisingly, NLRs that directly bind their corresponding effectors have high entropy values, whereas NLRs that indirectly recognise effectors have reduced variability on account of purifying selection pressure that maintains recognition of the activity of effectors on conserved targets (Prigozhin and Krasileva, 2021).

In chapters 4 and 5, I showed that Mla3 directly binds Pwl2 through the C-terminal region, which contains polymorphisms that determine specificity of recognition. Indeed, residues with highest Shannon entropy and variability across Mla alleles are located in the concave surface of the LRR region (Tamborski et al., 2022), and are concentrated in the last LRR repeats and the C-terminus that follows the LRR domain (**Figure 7.1A**). The predicted binding interface of Mla3 with Pwl2 partially overlaps with the region of lowest amino acid conservation amongst alleles (**Figure 7.1A**). This suggests that this particular region is involved not only in direct recognition of Pwl2 by Mla3, but also of different AVR_a effectors by other Mla alleles. Similarly, the contact sites between the C-JID domain of ROQ1 and RPP1, and their corresponding effectors XopQ and ATR1 display low conservation (Ma et al., 2020; Martin et al., 2020b). Noteworthy, the α-helix in Mla3 that contains the residue K926 crucial for Pwl2 recognition is highly conserved across Mla alleles (**Figure 7.1B**), which share a negative amino acid (D/E) in position 926. Pwl2 recognition exclusively requires a positively charged residue in this location, which confers Mla3 a unique positive electrostatic surface that sets it apart from other Mla alleles. If AVR_{a3} directly binds the same or an overlapping interface in Mla3, this invariable α-helix and the uniqueness of the residue K926 would suggest that this

region in Mla3 is a novel atypical binding interface amongst Mla alleles that is potentially serving to recognise multiple effectors.

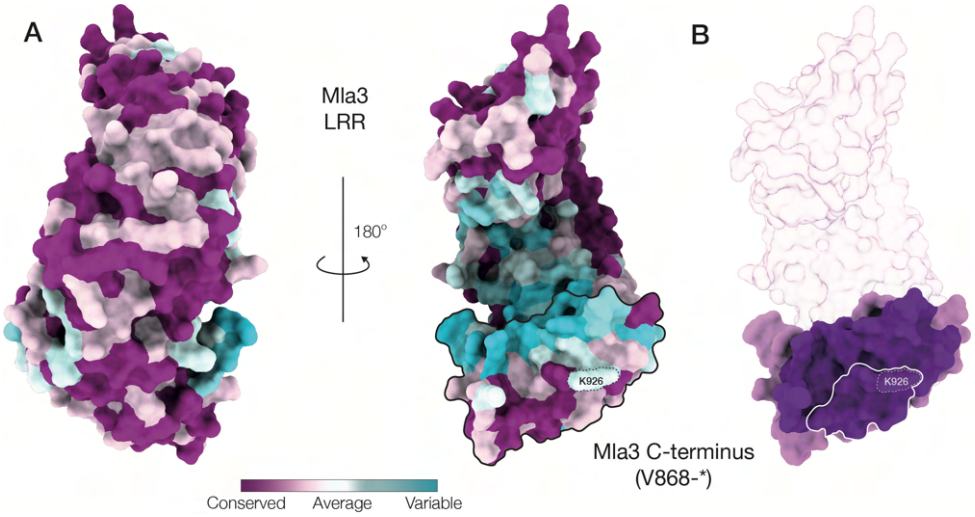

Figure 7.1 Residue conservation in the LRR domain and C-terminus of Mla3.

(A) Structure prediction of the LRR domain and C-terminus of Mla3 with the protein surface coloured according to residue conservation amongst Mla alleles. The C-terminus that is sufficient to bind Pwl2 is delimited in black, and the position of the residue K926 is marked by a dashed line. **(B)** Structure prediction of the C-terminus of Mla3 that binds Pwl2. The binding interface with Pwl2 is coloured in purple. The α-helix containing the residue K926 is delimited by a white line. K926 is marked by a dashed line.

7.4 What mechanisms led to direct recognition of unrelated effectors by Mla3?

Plant NLRs tightly coevolve with pathogen effectors and recognise them in a highly specific manner (Białas et al., 2018). For this reason, evolution of direct recognition of structurally distinct effectors seems to be more of an outstanding exception than a rule, and in fact, such a case had not been documented in nature. Instead, NLRs with integrated domains or guardee proteins targeted by pathogens are more robust strategies to sense unrelated effectors that convergently evolved to interact with shared host proteins (Narusaka et al., 2009; Wang et al., 2015; Baudin et al., 2017), making Mla3 recognition of Pwl2 and AVR_{a3} a rather unique case. Even though the gene underlying AVR_{a3} is still unknown, we can predict that it is structurally unrelated to Pwl2 based on the absence of MAX effectors in *Bgh* (Seong and Krasileva, 2023). Moreover, the direct recognition of different AVR_a effectors by corresponding Mla alleles (Saur et al., 2019) suggests that Mla3 and AVR_{a3} might not be an exception. Thus, the question

of how a singleton NLR evolved to recognise multiple unrelated effectors through direct binding is both intriguing and puzzling.

Pwl2 belongs to the family of sequence-unrelated MAX effectors (de Guillen et al., 2015), the same way that AVR_{a3} likely belongs to the family of RALPHs that have an RNAse-like fold (Bauer et al., 2021). Most effectors from filamentous pathogens belong to sequence-unrelated but structurally similar families that have a conserved core but variable surface residues that adapt according to evolutionary selection pressures (Derbyshire and Raffaele, 2023; Seong and Krasileva, 2023). Exposed variable regions in effectors accumulate mutations that build up surface frustration due to the inability of residues to achieve minimum energy (Ferreiro et al., 2018; Derbyshire and Raffaele, 2023). Residues residing in frustrated surfaces are often involved in binding interfaces that release frustration upon interaction with partners (Ferreiro et al., 2018). Thus, the high variability in frustrated effector surfaces allows for shuffling binding interfaces (Derbyshire and Raffaele, 2023).

The effector AvrSr35 from the wheat stem rust pathogen *Pgt* forms homodimers that dissociate upon recognition by Sr35 (Zhao et al., 2022). Interestingly, the AvrSr35 dimerization interface completely overlaps with the Sr35 binding interface, as residues involved in AvrSr35 dimerization are directly recognised by the LRR repeats 10, 11 and 13 of Sr35 (Zhao et al., 2022). Similar to Mla3 and Pwl2, this is another case in which a singleton CNL evolved to directly recognise an interface that the effector utilises to interact with itself (as in AvrSr35) or with a host target (as in Pwl2 with OsHIPP43). I hypothesise that these effector interfaces are frustrated regions that only become thermodynamically stable upon binding with interacting partners. Thus, since is it energetically favourable, Mla3 and Sr35 evolved to efficiently "trap" their corresponding effectors by recognising these specific interfaces. In doing so, the C-terminus of Mla3 mimics the binding interface of OsHIPP43 with Pwl2. As members of expanded effector families that diversified through variable surface exposed regions (Derbyshire and Raffaele, 2023), Pwl2 and AVR_{a3} may have convergently evolved similar frustrated surfaces to interact with host targets. This would not require both effectors to have overall similar structures, but only overlapping frustrated regions that possibly interact with a common host target. Therefore, by recognising the frustrated region of Pwl2 through its C-terminus, Mla3 also recognises the homologous interface of AVR_{a3} **(Figure 7.2)**. Targeting of HMA-containing plant proteins by RALPH effectors has yet to be determined to support this hypothesis. Nonetheless, if this mechanism is solely guided

by processes that are energetically favourable, cases of direct recognition of multiple unrelated effectors would be more common. I hypothesise that the pressure to keep NLRs inactive in the absence of steric clash due to effector binding strongly constrains the evolution of surfaces that can accommodate several structurally distinct effectors. A more common solution to this problem is the integration of effector targets within sensor NLRs, which lost the ability to execute immune signalling and require a helper NLR to do so (Cesari et al., 2014; Cesari, 2018).

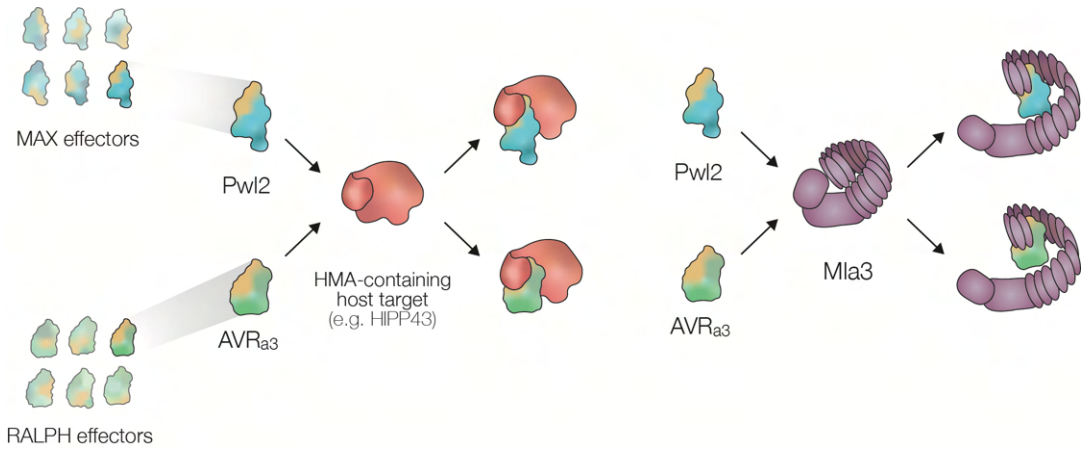

Figure 7.2 Model of evolution of direct recognition of Pwl2 and AVR_{a3} by Mla3.

MAX effectors in *M. oryzae* and RALPH effectors in *Bgh* are expanded families of sequence unrelated structurally similar proteins. These effector families have diversified by repatterning frustrated surface residues that allows switching potential binding interfaces (Derbyshire and Raffaele, 2023); binding interfaces are shaded in yellow on the surface of effectors. Pwl2 and AVR_{a3} may have convergently evolved a conserved binding interface through shared residue frustration, enabling interaction with a common host target (in this case, HIPP43, an HMA-containing host protein). Due to the thermodynamic advantage of interacting through these residues, i.e. reaching a state of minimum energy, Mla3 evolved to bind both effectors by mimicking the binding interface of the common target.

7.5 Harnessing the versatility of the Mla3 C-terminus

By mimicking the binding interface of OsHIPP43, the C-terminus of Mla3 acts somewhat as a pseudo-integrated domain that allows recognition of multiple effectors. This observation highlights the remarkable versatility of Mla3, as it is a singleton NLR that autonomously senses unrelated effectors and triggers an immune response without the requirement of a helper NLR. Thus, Mla3 represents a unique mode-of-action in-between singleton NLRs that directly recognise single effectors (Chen et al., 2017; Förderer et al., 2022b; Zhao et al., 2022), and paired NLRs in which the sensor NLR-ID specialises in sensing one or more effectors through its ID, and the helper NLR executes

immune signalling (Cesari et al., 2014) (**Figure 7.3**). This concept makes Mla3 a desirable system for NLR engineering towards expanded disease resistance, as it would involve a single NLR, rather than a pair. If the C-terminus of Mla3 is truly mimicking an HMA-containing protein, it could be engineered to extend recognition of other MAX effectors, such as AVR1-CO39, which binds the HMA domain of RGA5 through a similar interface of that between Pwl2 and OsHIPP43 (Guo et al., 2018b; Cesari et al., 2022). Depending on intramolecular interactions between the C-terminus of Mla3 and other NLR domains, and its role in keeping Mla3 in an inactive state, this region could potentially be edited to mimic different effector targets or engineered for made-to-order pathogen recognition (Förderer et al., 2022a; Marchal et al., 2022a). It is still unknown whether Mla alleles other than Mla3 and Mla8 recognise multiple effectors, and if the C-terminus is commonly involved in recognition. Understanding how the Mla allelic series recognises cognate effectors would allow harnessing this functionally diverse NLR as a toolkit to engineer new sources of disease resistance.

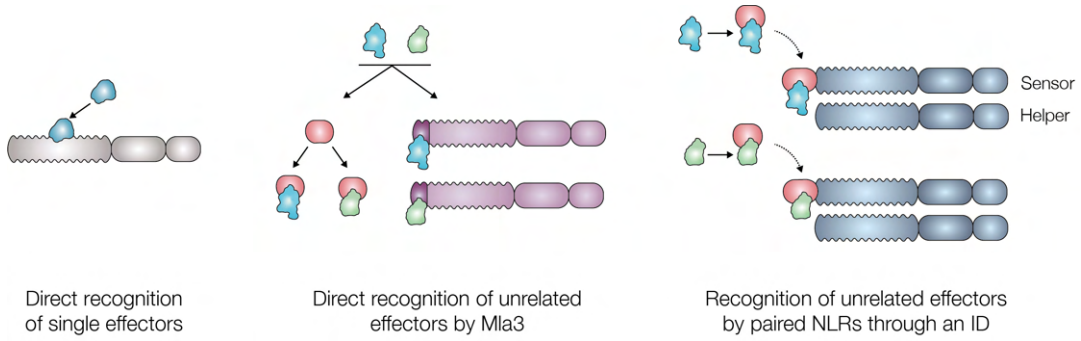

Figure 7.3 Effector recognition through direct binding.

Left model: singleton NLRs can directly recognise effectors through the LRR domain, generally in a one-to-one manner (i.e., one NLR recognises one effector). Middle model: Mla3 (in pink) directly recognises structurally unrelated effectors through its C-terminus by mimicking the binding interface of a shared effector target (in orange). As singleton NLR, Mla3 does not require a helper NLR to trigger immunity upon effector binding. Right model: A shared host target of unrelated effectors was integrated within a sensor NLR that requires a helper NLR to act as a pair and elicit an immune response upon effector interaction with the integrated domain (ID).

7.6 Lessons from the dosage requirement for Mla3 function

7.6.1 It may all be about kinetics

In chapter 6, I showed that Mla3 is required as multiple copies to reach a threshold of expression level to confer effective resistance against *M. oryzae* and *Bgh*. Although not an NLR, a similar example is *Rhg1* in soybean, a locus comprising three

genes that confer resistance against the soybean cyst nematode when present as more than three tandem copies, which correlates with elevated expression levels (Cook et al., 2012; Cook et al., 2014). *Mla3* has been classified as a "slow-acting" allele, as it allows *Bgh* to grow secondary hyphae on cells around the primary haustoria-infected cell (Boyd et al., 1995; Caldo et al., 2006). Overexpression of *Mla12*, another slow-acting allele, significantly increased the speed of the immune response against *Bgh,* suggesting that the amount of this allele is rate-limiting for disease resistance (Shen et al., 2003). *Mla3* might function through similar dynamics.

The binding affinity between Pwl2 and OsHIPP43 is remarkably strong, with a K_D in the upper nanomolar range (Zdrzalek, 2021). Intriguingly, the D90N mutation in pwl2-2 has no impact on the strength of binding with OsHIPP43 (Zdrzalek, 2021), but it does affect its interaction with Mla3. While this Pwl2 allele weakly associates and triggers HR with Mla3 in *N. benthamiana*, its recognition is not robust enough to elicit an immune response in barley. Moreover, the presence of OsHIPP43 impaired Mla3 recognition of Pwl2, as both proteins compete for the same binding interface. Collectively, the evidence indicates that Pwl2 interacts with OsHIPP43 with much greater affinity than with Mla3. Thus, to achieve the threshold required to trigger a robust immune response in barley, I hypothesise that Mla3 must be available in high amounts to alter the kinetics of OsHIPP43–Pwl2 binding and overcome the competition for interaction with Pwl2. It remains to be addressed whether other Mla alleles also mimic targets to trap effectors, and whether the delayed immune response of alleles such as Mla12 is likewise due to lower binding affinity with effectors compared to their host targets.

7.6.2 Trigger-happy mutations that sensitise NLRs

Interestingly, the blast-resistant wild barley accessions WBDC233 and WBDC221 have *Mla* alleles that are almost identical to *Mla3* but are expressed as a single copy. In contrast, the cultivar HOR21599 has a proto-Mla3 allele also present as a single copy but is susceptible to *M. oryzae*. When overexpressed in *N. benthamiana* along with Pwl2*,* the Mla alleles from these three barley accessions triggered HR in similar levels to Mla3*,* indicating that they can all recognise the effector. Mla-HOR21599 differs from Mla3 by only two amino acids in the LRR region, whereas Mla-WBDC233 and Mla-WBDC221 have a few more differences spread over the CC, NB-ARC and LRR domains. I proposed that these polymorphisms may increase affinity or stabilise binding to Pwl2, or result in

a "trigger-happy" state of Mla-WBDC223 and Mla-WBDC221 that lowers the activation threshold compared to Mla3. This means that even at low concentrations that are not sufficient to outcompete binding of Pwl2 with OsHIPP43, the Mla alleles from the wild barley accessions get activated when bound to low free amounts of Pwl2. I did not observe significant differences in the intensity of HR upon Pwl2 recognition by Mla3 versus Mla-WBDC233 or Mla-WBDC221. However, subtle differences may only be noticeable under lower expression levels, or even only under native conditions in barley. Testing the ability of the accessions WBDC221 and WBDC233 to confer resistance against *M. oryzae* isolates carrying either pwl2-2 or pwl2-3 could address this model. In theory, Mla3 can also recognise these Pwl2 alleles as they elicit cell death upon co-expression in *N. benthamiana,* but weaker than wild-type Pwl2. Perhaps Mla-WBDC221 and Mla-WBDC233 are sensitive enough to trigger an immune response despite the low binding affinity with pwl2-2 and pwl2-3 thanks to the polymorphisms that induce the "trigger-happy" state.

7.6.3 Unlocking hidden NLRs

Even though the accession HOR21599 is susceptible to a wild-type *M. oryzae* isolate carrying Pwl2, it is resistant to a *pwl2* mutant complemented with the effector. This complemented mutant likely has multiple ectopic integrations of *PWL2* that result in elevated expression levels and compensate for the low amounts of Mla-HOR21599, thus resulting in NLR activation. The observation that disease resistance goes in hand with fine-tuning of both NLR and effector expression levels suggests that the NLR repertoire and potential sources of resistance in nature might be richer than it seems. Many NLRs with low expression levels like Mla-HOR21599 might go unnoticed through resistance screens that use pathogen isolates with basal levels of effector expression. However, leveraging isolates with effector copy number variation or artificial effector overexpression can unlock hidden NLRs that would otherwise remain ignored. Even though such NLRs may have been defeated in the coevolutionary arms race with pathogens due to expression polymorphisms of their cognate effectors (Gilroy et al., 2011; Pais et al., 2018), boosting their expression through gene editing is a useful and appealing strategy to resurrect them.

7.6.4 Opposing pressures that result in effector copy number variation

PWL2 exhibits standing copy number variation across different *M. oryzae* isolates (Were, 2018), but it is unclear whether a high *PWL2* copy number provides any virulence advantage in susceptible plant genetic backgrounds. It would be interesting to test whether the barley accession HOR21599 is resistant to wild-type isolates carrying an increased number of *PWL2* copies, such as the isolate KE002, which has five identical copies (Were, 2018). It is possible that isolates with low *PWL2* copy numbers, such as KEN54-20, have evolved in response to selection pressure to avoid recognition by accessions expressing low levels of *Mla3*-like alleles. In parallel, testing if KE002 has any advantage compared to KEN54-20 when infecting susceptible barley accessions like Golden Promise would illustrate how opposing selective pressures have maintained standing effector copy number variation in pathogen populations. While having multiple effector copies can facilitate efficient host manipulation, it may also increase the risk of recognition by NLRs that require reaching a certain binding threshold to trigger resistance. Thus, losing some but not all effector copies may represent a trade-off that allows the pathogen to avoid recognition by such NLRs whilst maintaining the effector virulence function.

7.7 The revolution of protein structure prediction

Advances in computational protein structure prediction have had a significant impact on the field of plant-microbe interactions. While X-ray crystallography and Cryo-EM can provide detailed structural information on single proteins and protein complexes, these techniques have several limiting factors: they are time-consuming and expensive, and require extensive optimisation and specialised expertise. Recent developments in protein structure prediction have revolutionised the field by enabling researchers to generate 3D models of proteins with high confidence, opening possibilities and triggering insightful questions. While computational models cannot fully replace experimental structural data, they can serve as a robust platform to formulate and test hypotheses to address questions that would have been otherwise challenging or even unthinkable; see for example the studies done by Derbyshire and Raffaele (2023), and Seong and Krasileva (2023).

In chapter 5, I used AlphaFold2 to predict the structure of the C-terminus of Mla3 in complex with Pwl2 and found that it mimics the binding interface of the Pwl2-host target OsHIPP43. This intriguing observation prompted numerous hypotheses that

could shed light on the molecular and evolutionary mechanisms underlying the recognition of unrelated effectors by Mla3. I previously hypothesised that AVR_{a3} may have convergently evolved to target an HMA-containing host protein through a similar interface as Pwl2. To explore this idea, we can leverage advanced protein–protein interaction models and computational tools to find *Bgh* effectors that may target HMA-containing proteins, listing them as potential AVR_{a3} candidates. In parallel, we can also perform a focused structural search in the *Bgh* secretome by limiting the range of search to the Pwl2 binding interface, rather than the entire protein. Pwl2 folds into a six-stranded β-sandwich with antiparallel β-sheets characteristic of MAX effectors; however, it also has an unusual α-helix that interacts with OsHIPP43 and Mla3 and sets it apart from members of this group. Although in a different configuration, RALPH effectors also have an α-helix followed by two antiparallel β-sheets that may resemble to some extent the binding interface of Pwl2 (**Figure 7.4**). Thorough structural comparison analyses will be helpful to shortlist and functionally validate AVR_{a3} candidates.

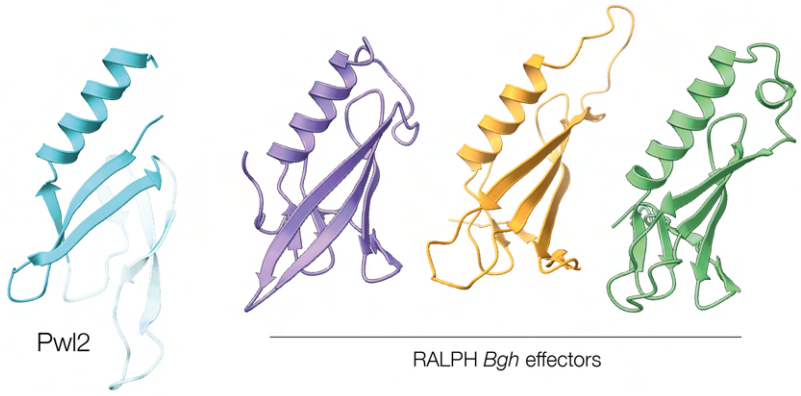

Figure 7.4 Structure comparison of Pwl2, a MAX effector from *M. oryzae*, and RALPH effectors from *Bgh*.

Left: Structure of Pwl2 experimentally determined by X-ray crystallography (Zdrzalek, 2021). The region that contains the main predicted interface with Mla3 is highlighted in bold blue. The rest of the protein is faded with transparency. Right: Structure prediction of three randomly chosen *Bgh* effectors (Blugr2_5222 in purple, Blugr2_544 in yellow and Blugr2_3 in green) that cluster within the RALPH effector family according to Seong and Krasileva, 2023.

The NLR conferring Pwl2 recognition in weeping lovegrass remains yet to be identified. In chapter 1, I established that barley and weeping lovegrass recognise Pwl2 with conserved specificity, suggesting a similar mechanism of recognition. Based on this hypothesis, predicting the structure of the C-terminus of weeping lovegrass NLRs and identifying those with shared features with Mla3, such as a positively charged electrostatic interface, a basic amino acid located at the same position as the residue K926, and

conserved Pwl2-interacting amino acids in the last β-sheet, may lead to the identification of the weeping lovegrass *R* gene underlying host-specificity of rice-infecting isolates of *M. oryzae*. These are exciting times in which discovery of avirulence effectors and plant NLRs driven by structure prediction techniques may already be at hand.

7.8 Concluding remarks and future questions

The research underlying this thesis aimed to shed light on the molecular mechanism behind multiple pathogen recognition by Mla3, a member of the functionally diversified *Mla* allelic series. Far from closing a full story, the findings from this work provide insights that trigger further questions about the multifaceted evolutionary arms race between *Mla* in barley, and complex communities of plant pathogenic fungi. First and foremost, the most intriguing subject is the identity of AVR_{a3}: does it have an RNAse-like fold? Does it share a particular structural feature with the Pwl2 interface recognised by Mla3? Does Mla3 recognise both Pwl2 and AVR_{a3} through the same binding interface? Does AVR_{a3} interact with OsHIPP43? Do RALPH effectors target HMA-containing proteins? Is there an evolutionary relationship between RALPH and MAX effectors?

Additional questions also emerge regarding the versatility of Mla3: Does Mla3 confer victorin sensitivity in barley? If so, how would this fit into the current proposed model of multiple pathogen recognition by this NLR? Is recognition of multiple unrelated effectors prevalent across Mla alleles? Is the Pwl2 recognition interface in the C-terminus of Mla3 an innovation of this allele? Do other Mla alleles or NLRs also mimic the interface of effector targets to directly recognise avirulence genes? Can the C-terminus of Mla3 be edited to enhance binding of Pwl2 and outcompete OsHIPP43? Can it be engineered to expand recognition of other MAX effectors? Would engineering of the C-terminus of Mla3 be constrained by its potential role in intramolecular regulation of other NLR domains in an inactive state? Can we engineer the C-terminus of Mla3 or replace it with known effector targets to achieve made-to-order pathogen recognition?

Regarding recognition of Pwl2 in weeping lovegrass: Can we identify the unknown NLR recognising this effector through structural similarity searches using the C-terminus of Mla3? Does this NLR directly recognise Pwl2? Does it mimic the binding interface of a Pwl2 target? Does it recognise multiple pathogens? Does it confer victorin sensitivity? What mechanisms drove convergent evolution of this NLR in weeping lovegrass and Mla3 in barley towards recognition of Pwl2?

Finally, do other NLR allelic series also exhibit such functional diversification as Mla? What type of selection pressure drove diversification of Sr33 and Sr50, both Mla orthologues, towards recognition of unrelated effectors from wheat stem rust (*Pgt*), rather than maintaining recognition of powdery mildew in wheat? Is there a conserved evolutionary mechanism driving allelic diversity between *Mla* in barley and *Pm3* in wheat? More broadly, why is direct recognition the predominant form of effector detection in filamentous pathogens? What is the role of complex communities of plant pathogens and diverse effector families in the evolution of multiple pathogen recognition? Can we learn from Mla3 to engineer multiple pathogen recognition? Answering these fundamental questions will help advance our understanding of plant–pathogen coevolution and contribute to bridge the gap between mechanistic and evolutionary research towards a more integral view of plant and microbial systems.

Appendix I

Supplementary information for Chapter 2: Materials and Methods

Table A.I.1 List of barley accessions used in this study.

Accession	Source
Baronesse	Oregon State University
Nigrate	USDA-GRIN
Golden Promise	John Innes Centre
Maritime	Wolfgang Spielmeyer
Manchuria	USDA-GRIN
Siri	John Innes Centre
S02	John Innes Centre
S13	John Innes Centre
HOR21599	IPK Leibniz Institute
WBDC221	USDA-GRIN
WBDC233	USDA-GRIN

Table A.I.2 List of *Magnaporthe oryzae* isolates used in this study.

Isolate	Genotype description	*PWL2 allele*	Source
KEN54-20	Wild type (*AVR-Rmo1*)	*PWL2*	Terauchi group, IBRC, Japan
M1	*avr-Rmo1* (derived from KEN54-20)	*pwl2*	This study
M43	*avr-Rmo1* (derived from KEN54-20)	*pwl2*	This study
M44	*avr-Rmo1* (derived from KEN54-20)	*pwl2*	This study
M61	*avr-Rmo1* (derived from KEN54-20)	*pwl2*	This study
M64	*avr-Rmo1* (derived from KEN54-20)	*pwl2*	This study
M65	*avr-Rmo1* (derived from KEN54-20)	*pwl2*	This study
M66	*avr-Rmo1* (derived from KEN54-20)	*pwl2*	This study
M70	*avr-Rmo1* (derived from KEN54-20)	*pwl2*	This study
M71	*avr-Rmo1* (derived from KEN54-20)	*pwl2*	This study
M73	*avr-Rmo1* (derived from KEN54-20)	*pwl2*	This study
M74	*avr-Rmo1* (derived from KEN54-20)	*pwl2*	This study
M75	*avr-Rmo1* (derived from KEN54-20)	*pwl2*	This study
M43+PWL2	M43 complemented with *PWL2* (*pPWL2:PWL2:tPWL2*)	*pwl2+PWL2*	This study
M61+PWL2	M61 complemented with *PWL2* (*pPWL2:PWL2:tPWL2*)	*pwl2+PWL2*	This study
TH68-126	Wild type	*PWL2*	Terauchi group, IBRC, Japan
TH68-140	Wild type	*PWL2*	Terauchi group, IBRC, Japan
TH68-141	Wild type	*PWL2*	Terauchi group, IBRC, Japan
2012-1	Wild type	*PWL2*	Terauchi group, IBRC, Japan
Naga69-150	Wild type	*PWL2, pwl2-2*	Terauchi group, IBRC, Japan
Ina85-182	Wild type	*PWL2, pwl2-2*	Terauchi group, IBRC, Japan
Ina87T-56A	Wild type	*PWL2, pwl2-2*	Terauchi group, IBRC, Japan
SL91-48D	Wild type	*pwl2-2*	Terauchi group, IBRC, Japan
85-141	Wild type	*pwl2-2*	Terauchi group, IBRC, Japan
24-22-1-1	Wild type	*pwl2-2*	Terauchi group, IBRC, Japan
83R-131B	Wild type	pwl2-2	Terauchi group, IBRC, Japan
H98-315-1	Wild type	pwl2-2	Terauchi group, IBRC, Japan

Table A.I.2 List of *Magnaporthe oryzae* isolates used in this study (continued).

Isolate	Genotype description	*PWL2 allele*	Source
0423-1	Wild type	*pwl2-2*	Terauchi group, IBRC, Japan
2403-1	Wild type	*pwl2-2*	Terauchi group, IBRC, Japan
Ao92-06-02	Wild type	*pwl2-2*	Terauchi group, IBRC, Japan
Ina168	Wild type	*pwl2*	Terauchi group, IBRC, Japan

Table A.I.3 Level 0 constructs generated or used in this study.

Backbone plasmid	Gene	Source
pICH41308	Mla3	This study
pICSL01005	Mla3	This study
pICSL01005	Mla3_CC	This study
pICSL01005	Mla3_CC-NBARC	This study
pICSL01005	Mla3_NBARC	This study
pICSL01005	Mla3_NBARC-LRR	This study
pICSL01005	Mla3_LRR	This study
pICSL01005	Mla_V874	This study
pTwist_Kan_High_Copy	Mla23	This study
pTwist_Kan_High_Copy	Mla34	This study
pTwist_Kan_High_Copy	Mla35	This study
pTwist_Kan_High_Copy	Mla39	This study
pUC57_Kan	Mla10	Kamoun lab (TSL)
pICSL01005	$Mla3^{F99E}$	This study
pICSL01005	$Mla3^{H501Q}$	This study
pICSL01005	$Mla3^{H501G}$	This study
pICSL01005	$Mla3^{D502V}$	This study
pICSL01005	$Mla3^{L11E}$	This study
pICSL01005	$Mla3^{no\ C\text{-}term}$	This study
pICSL01005	$Mla3^{Swap1}$	This study
pICSL01005	$Mla3^{Swap2}$	This study
pICSL01005	$Mla23^{with\ C\text{-}term}$	This study
pICSL01005	$Mla23^{Swap1}$	This study
pICSL01005	$Mla23^{Swap2}$	This study
pICSL01005	Mla3Δ6	This study
pICSL01005	Mla3-HOR21599	This study
pTwist_Kan_High_Copy	Mla-WBDC221	This study
pTwist_Kan_High_Copy	Mla-WBDC233	This study
pTwist_Kan_High_Copy	Pwl2	This study
pICSL01005	pwl2-2	This study
pICSL01005	pwl2-3	This study
pICSL01005	AVR-PikD	This study
pTwist_Kan_High_Copy	AVR_{a10}	This study
pICSL01005	AtTRXh5	This study
pICH41308	OsHIPP43	Kamoun lab (TSL)

Table A.I.4 List of level 1 constructs generated in this study for transient expression in *N. benthamiana*

Backbone plasmid	Promoter	Gene	Tag	Terminator
pICH47732	pICH85281 (Mas + Ω)	Mla10	pICSL50009 (6xHA C-term tag)	pICSL60008 (AtHSP18 terminator)
pICH47732	pICH85281 (Mas + Ω)	Mla3 (wild type, mutants, and chimeras)	pICSL50009 (6xHA C-term tag)	pICSL60008 (AtHSP18 terminator)
pICH47732	pICH85281 (Mas + Ω)	Mla3_CC	pICSL50009 (6xHA C-term tag)	pICSL60008 (AtHSP18 terminator)
pICH47732	pICH85281 (Mas + Ω)	$Mla3^{L11E}$_CC	pICSL50009 (6xHA C-term tag)	pICSL60008 (AtHSP18 terminator)
pICH47732	pICH85281 (Mas + Ω)	Mla3_CC-NBARC	pICSL50009 (6xHA C-term tag)	pICSL60008 (AtHSP18 terminator)
pICH47732	pICH85281 (Mas + Ω)	Mla3_NBARC	pICSL50009 (6xHA C-term tag)	pICSL60008 (AtHSP18 terminator)
pICH47732	pICH85281 (Mas + Ω)	Mla3_NBARC-LRR	pICSL50009 (6xHA C-term tag)	pICSL60008 (AtHSP18 terminator)
pICH47732	pICH85281 (Mas + Ω)	Mla3_LRR	pICSL50009 (6xHA C-term tag)	pICSL60008 (AtHSP18 terminator)
pICH47732	pICH85281 (Mas + Ω)	Mla_V874	pICSL50009 (6xHA C-term tag)	pICSL60008 (AtHSP18 terminator)
pICH47732	pICH85281 (Mas + Ω)	Mla_V911	pICSL50009 (6xHA C-term tag)	pICSL60008 (AtHSP18 terminator)
pICH47732	pICH85281 (Mas + Ω)	Mla23 (wild type, mutants, and chimeras)	pICSL50009 (6xHA C-term tag)	pICSL60008 (AtHSP18 terminator)
pICH47732	pICH85281 (Mas + Ω)	Mla34 (wild type and mutant)	pICSL50009 (6xHA C-term tag)	pICSL60008 (AtHSP18 terminator)
pICH47732	pICH85281 (Mas + Ω)	Mla35 (wild type and mutant)	pICSL50009 (6xHA C-term tag)	pICSL60008 (AtHSP18 terminator)
pICH47732	pICH85281 (Mas + Ω)	Mla39 (wild type and mutant)	pICSL50009 (6xHA C-term tag)	pICSL60008 (AtHSP18 terminator)
pICH47732	pICH85281 (Mas + Ω)	Mla3Δ6	pICSL50009 (6xHA C-term tag)	pICSL60008 (AtHSP18 terminator)
pICH47732	pICH85281 (Mas + Ω)	Mla-HOR21599	pICSL50009 (6xHA C-term tag)	pICSL60008 (AtHSP18 terminator)
pICH47732	pICH85281 (Mas + Ω)	Mla-WBDC233	pICSL50009 (6xHA C-term tag)	pICSL60008 (AtHSP18 terminator)
pICH47732	pICH85281 (Mas + Ω)	Mla-WBDC221	pICSL50009 (6xHA C-term tag)	pICSL60008 (AtHSP18 terminator)
pICH47732	pICH51266 (Long 35S + Ω)	Pwl2	pICSL50007 (3xFLAG C-term tag)	pICH41414 (35S terminator)
pICH47732	pICH51266 (Long 35S + Ω)	pwl2-2	pICSL50007 (3xFLAG C-term tag)	pICH41414 (35S terminator)
pICH47732	pICH51266 (Long 35S + Ω)	pwl2-3	pICSL50007 (3xFLAG C-term tag)	pICH41414 (35S terminator)
pICH47732	pICH51266 (Long 35S + Ω)	AVR-PikD	pICSL50007 (3xFLAG C-term tag)	pICH41414 (35S terminator)
pICH47732	pICSL13001 (Long 35s CaMV)	OsHIPP43	pICSL30009 (4xMyc N-term tag)	pICH41414 (35S terminator)
pICH47732	pICSL13001 (Long 35s CaMV)	AtTRXh5	pICSL30009 (4xMyc N-term tag)	pICH41414 (35S terminator)

Table A.I.5 List of level 1 constructs generated for or used in yeast-two-hybrid assays.

Backbone plasmid	Gene	Source
pGBKT7	Mla3	This study
pGBKT7	Mla3_CC	This study
pGBKT7	Mla3_CC-NBARC	This study
pGBKT7	Mla3_NBARC	This study
pGBKT7	Mla3_NBARC-LRR	This study
pGBKT7	Mla3_LRR	This study
pGBKT7	Mla_V874	This study
pGBKT7	Mla10	This study
pGBKT7	OsHIPP43	Talbot lab (TSL)
pGADT7	Pwl2	This study
pGADT7	pwl2-2	This study
pGADT7	pwl2-3	This study
pGADT7	AVR-PikD	This study
pGADT7	AVR_{a10}	This study

Table A.I.6 List of level 1 constructs generated in this study for recombinant protein production

Backbone plasmid	N-term affinity tag	Gene	Source
pOPIN_F6_Kan	-	Mla3_V874	This study
pOPIN_F5_Carb	pICSL30019 (6xHis 3C cleavable)	Pwl2	This study

Table A.I.7 List of plant genomes used in NLR phylogenetic analyses.

Family	Tribe	Species	Acronym	Source	References
Poaceae	Andropogoneae	*Zea mays*	Zm	Zea mays RefGen_V4; https://www.maizegdb.org	Schnable et al. (2009)
Poaceae	Andropogoneae	*Sorghum bicolor*	Sb	Sorghum bicolor v3.1.1 DOE-JGI, http://phytozome.jgi.doe.gov/	Paterson et al. (2009)
Poaceae	Chloridoideae	*Eragrostis curvula*	Ec	NCBI, GCA_007726485.1	Carballo et al. (2019)
Poaceae	Paniceae	*Setaria italica*	Si	Setaria italica v2.2 DOE-JGI, http://phytozome.jgi.doe.gov/	Bennetzen et al. (2012)
Poaceae	Oryzoideae	*Oryza sativa*	Os	Rice RGAP V7; http://rice.uga.edu/	Goff et al. (2002)
Poaceae	Brachypodieae	*Brachypodium distachyon*	Bd	Brachypodium distachyon v3.1 DOE-JGI, http://phytozome.jgi.doe.gov/	IBI (2010); Gordon et al. (2017)
Poaceae	Triticeae	*Hordeum vulgare*	Hv	Morex V3; http://doi.org/10.5447/ipk/2021/3	Mascher et al. (2021)

Appendix II

Supplementary information for Chapter 4: Specificity of Pwl2 recognition is determined by the C-terminal region of Mla3.

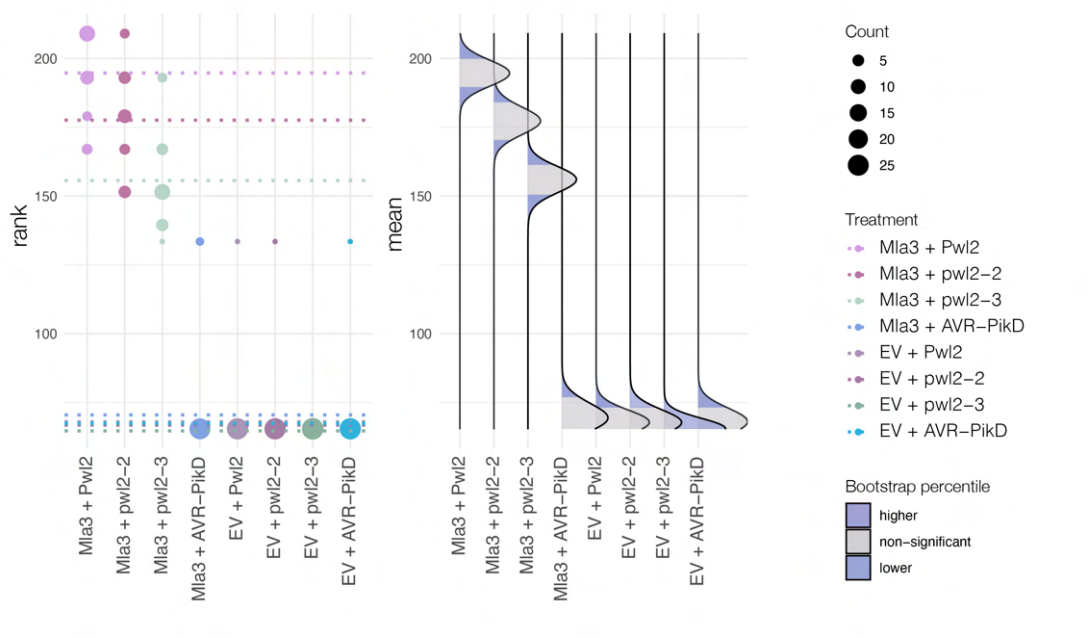

Figure A.II.1 Statistical analysis of the cell death response of Mla3 upon recognition of Pwl2 alleles

Statistical analysis of the hypersensitive response shown in **Figure 4.2** performed with the estimation method from the besthr R library (MacLean, 2019). The left panel shows the ranked data (dots) and the corresponding mean (dashed line) of each treatment. The size of each dot is proportional to the number of observations with that specific ranking value. The right panel shows the distribution of 1000 bootstrap sample rank means, with the areas in blue highlighting the 0.025 and 0.975 percentiles of the distribution. The grey area indicates the 95% confidence interval of the ranked mean. The difference of HR response is considered statistically significant if the confidence interval of the ranked mean of a given treatment falls outside of the confidence interval of another condition (i.e., within or beyond the blue percentile of the mean distribution of another condition).

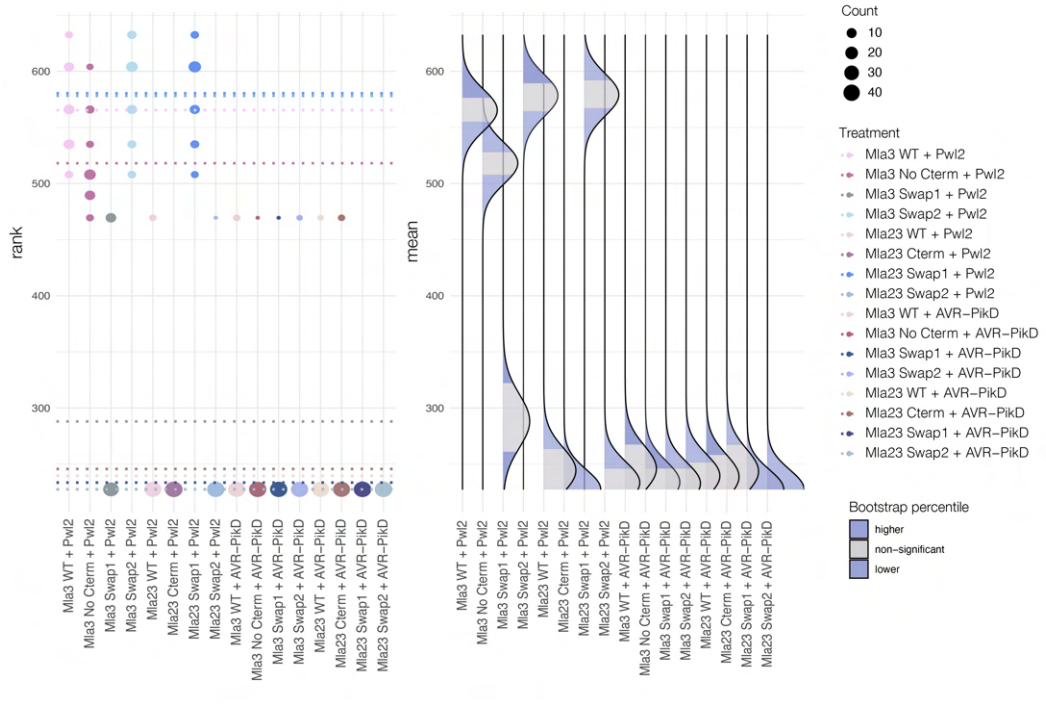

Figure A.II.2 Statistical analysis of the cell death response of Mla3 and Mla23 chimeras

Statistical analysis of the hypersensitive response shown in **Figure 4.5** performed with the estimation method from the besthr R library (MacLean, 2019). The left panel shows the ranked data (dots) and the corresponding mean (dashed line) of each treatment. The size of each dot is proportional to the number of observations with that specific ranking value. The right panel shows the distribution of 1000 bootstrap sample rank means, with the areas in blue highlighting the 0.025 and 0.975 percentiles of the distribution. The grey area indicates the 95% confidence interval of the ranked mean. The difference of HR response is considered statistically significant if the confidence interval of the ranked mean of a given treatment falls outside of the confidence interval of another condition (i.e., within or beyond the blue percentile of the mean distribution of another condition).

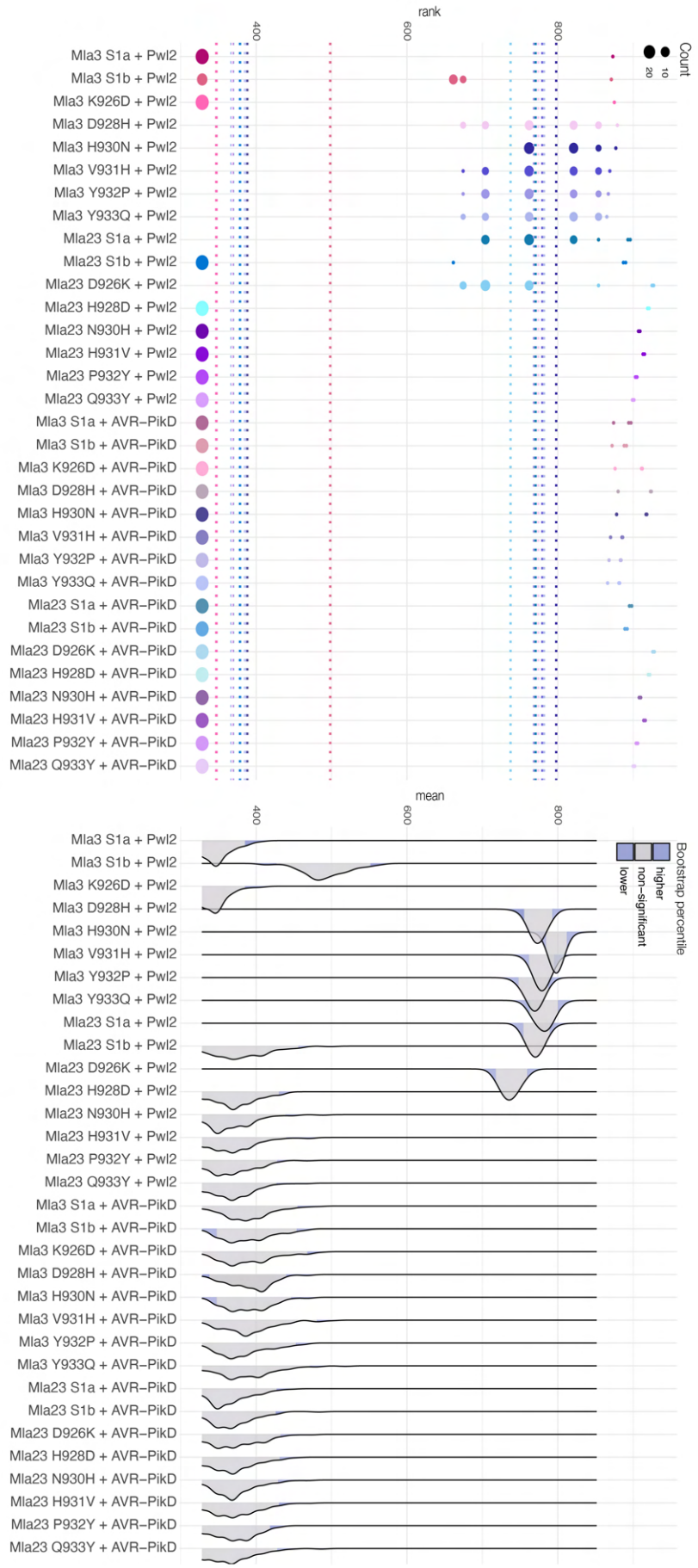
rank
400
600
800
Count
10
20
Mla3 S1a + Pwl2
Mla3 S1b + Pwl2
Mla3 K926D + Pwl2
Mla3 D928H + Pwl2
Mla3 H930N + Pwl2
Mla3 V931H + Pwl2
Mla3 Y932P + Pwl2
Mla3 Y933Q + Pwl2
Mla23 S1a + Pwl2
Mla23 S1b + Pwl2
Mla23 D926K + Pwl2
Mla23 H928D + Pwl2
Mla23 N930H + Pwl2
Mla23 H931V + Pwl2
Mla23 P932Y + Pwl2
Mla23 Q933Y + Pwl2
Mla3 S1a + AVR−PikD
Mla3 S1b + AVR−PikD
Mla3 K926D + AVR−PikD
Mla3 D928H + AVR−PikD
Mla3 H930N + AVR−PikD
Mla3 V931H + AVR−PikD
Mla3 Y932P + AVR−PikD
Mla3 Y933Q + AVR−PikD
Mla23 S1a + AVR−PikD
Mla23 S1b + AVR−PikD
Mla23 D926K + AVR−PikD
Mla23 H928D + AVR−PikD
Mla23 N930H + AVR−PikD
Mla23 H931V + AVR−PikD
Mla23 P932Y + AVR−PikD
Mla23 Q933Y + AVR−PikD
mean
400
600
800
Bootstrap percentile
higher
non−significant
lower
Mla3 S1a + Pwl2
Mla3 S1b + Pwl2
Mla3 K926D + Pwl2
Mla3 D928H + Pwl2
Mla3 H930N + Pwl2
Mla3 V931H + Pwl2
Mla3 Y932P + Pwl2
Mla3 Y933Q + Pwl2
Mla23 S1a + Pwl2
Mla23 S1b + Pwl2
Mla23 D926K + Pwl2
Mla23 H928D + Pwl2
Mla23 N930H + Pwl2
Mla23 H931V + Pwl2
Mla23 P932Y + Pwl2
Mla23 Q933Y + Pwl2
Mla3 S1a + AVR−PikD
Mla3 S1b + AVR−PikD
Mla3 K926D + AVR−PikD
Mla3 D928H + AVR−PikD
Mla3 H930N + AVR−PikD
Mla3 V931H + AVR−PikD
Mla3 Y932P + AVR−PikD
Mla3 Y933Q + AVR−PikD
Mla23 S1a + AVR−PikD
Mla23 S1b + AVR−PikD
Mla23 D926K + AVR−PikD
Mla23 H928D + AVR−PikD
Mla23 N930H + AVR−PikD
Mla23 H931V + AVR−PikD
Mla23 P932Y + AVR−PikD
Mla23 Q933Y + AVR−PikD

Figure A.II.3 Statistical analysis of the cell death response of Mla3 and Mla23 reciprocal Swap1 mutants.

Statistical analysis of the hypersensitive response shown in **Figure 4.6** performed with the estimation method from the besthr R library (MacLean, 2019). The upper panel shows the ranked data (dots) and the corresponding mean (dashed line) of each treatment. The size of each dot is proportional to the number of observations with that specific ranking value. The lower panel shows the distribution of 1000 bootstrap sample rank means, with the areas in blue highlighting the 0.025 and 0.975 percentiles of the distribution. The grey area indicates the 95% confidence interval of the ranked mean. The difference of HR response is considered statistically significant if the confidence interval of the ranked mean of a given treatment falls outside of the confidence interval of another condition (i.e., within or beyond the blue percentile of the mean distribution of another condition).

Appendix III

Supplementary information for Chapter 5: The C-terminus of Mla3 directly recognises Pwl2 by mimicking the binding interface of a host target.

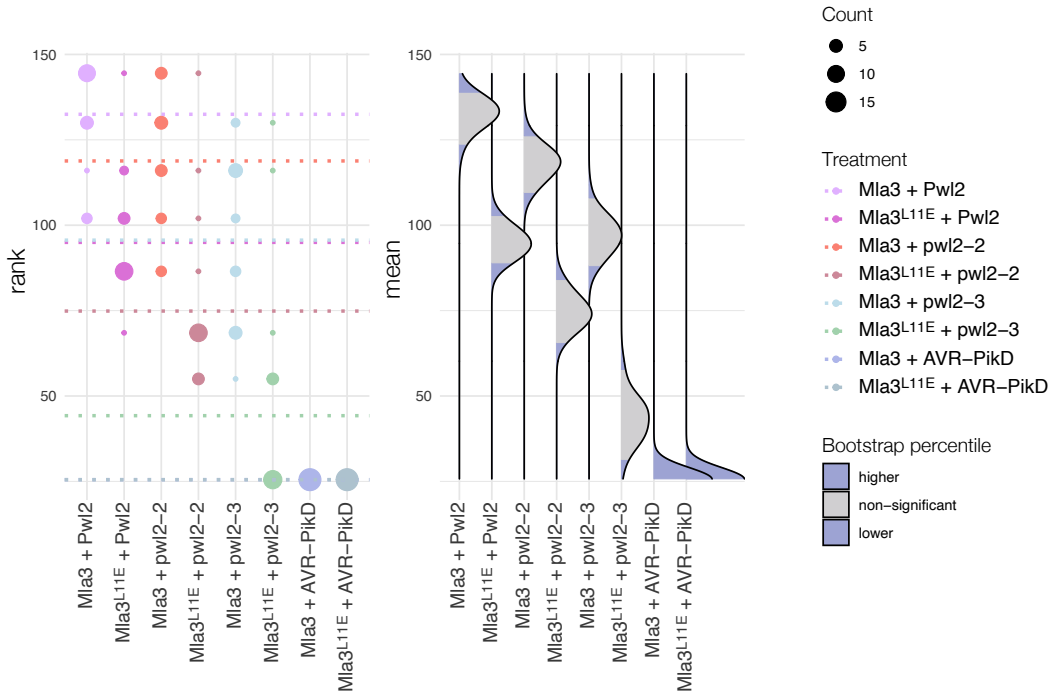

Figure A.III.1 Statistical analysis of the cell death response of Mla3^{L11E} upon recognition of Pwl2.

Statistical analysis of the hypersensitive response shown in **Figure 5.2** performed with the estimation method from the besthr R library (MacLean, 2019). The upper panel shows the ranked data (dots) and the corresponding mean (dashed line) of each treatment. The size of each dot is proportional to the number of observations with that specific ranking value. The lower panel shows the distribution of 1000 bootstrap sample rank means, with the areas in blue highlighting the 0.025 and 0.975 percentiles of the distribution. The grey area indicates the 95% confidence interval of the ranked mean. The difference of HR response is considered statistically significant if the confidence interval of the ranked mean of a given treatment falls outside of the confidence interval of another condition (i.e., within or beyond the blue percentile of the mean distribution of another condition).

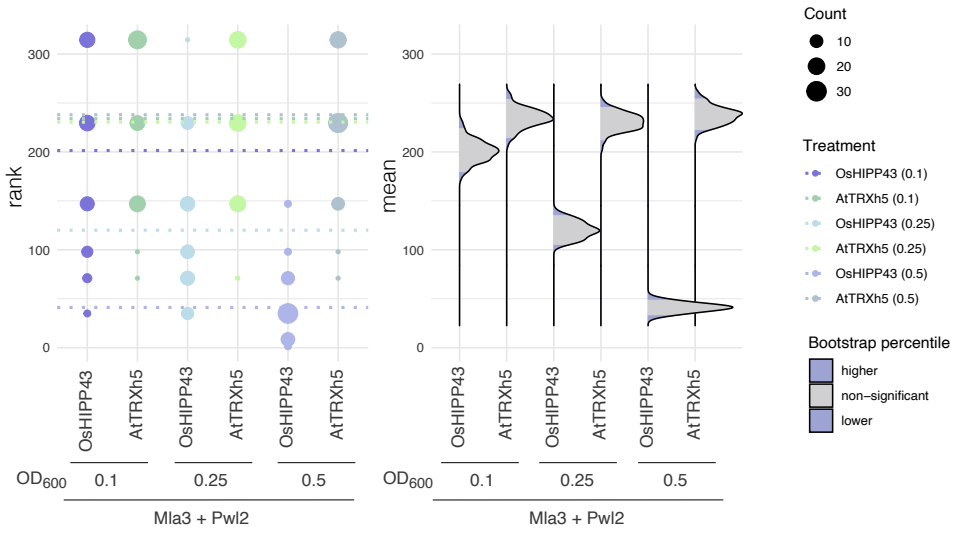

Figure A.III.2 I Statistical analysis of the cell death response of Mla3 upon recognition of Pwl2 in the presence of OsHIPP43 or AtTRXh5.

Statistical analysis of the hypersensitive response shown in **Figure 5.9** performed with the estimation method from the besthr R library (MacLean, 2019). The left panel shows the ranked data (dots) and the corresponding mean (dashed line) of each treatment. The size of each dot is proportional to the number of observations with that specific ranking value. The right panel shows the distribution of 1000 bootstrap sample rank means, with the areas in blue highlighting the 0.025 and 0.975 percentiles of the distribution. The grey area indicates the 95% confidence interval of the ranked mean. The difference of HR response is considered statistically significant if the confidence interval of the ranked mean of a given treatment falls outside of the confidence interval of another condition (i.e., within or beyond the blue percentile of the mean distribution of another condition).

References

Adachi, H., Derevnina, L., and Kamoun, S. (2019a). NLR singletons, pairs, and networks: evolution, assembly, and regulation of the intracellular immunoreceptor circuitry of plants. Curr. Opin. Plant Biol. 50, 121-131.

Adachi, H., Contreras, M., Harant, A., Wu, C.-h., Derevnina, L., Sakai, T., Duggan, C., Moratto, E., Bozkurt, T.O., Maqbool, A., Win, J., and Kamoun, S. (2019b). An N-terminal motif in NLR immune receptors is functionally conserved across distantly related plant species. eLife 8, e49956.

Ade, J., DeYoung, B.J., Golstein, C., and Innes, R.W. (2007). Indirect activation of a plant nucleotide binding site–leucine-rich repeat protein by a bacterial protease. Proceedings of the National Academy of Sciences 104, 2531-2536.

Aghnoum, R., Bvindi, C., Menet, G., D'hoop, B., Maciel, J.L.N., and Niks, R.E. (2019). Host/nonhost status and genetics of resistance in barley against three pathotypes of Magnaporthe blast fungi. Euphytica 215, 116.

Ahn, H.-K., Lin, X., Olave-Achury, A.C., Derevnina, L., Contreras, M.P., Kourelis, J., Kamoun, S., and Jones, J.D.G. (2022). Effector-dependent activation and oligomerization of NRC helper NLRs by Rpi-amr3 and Rpi-amr1. bioRxiv, 2022.2004.2025.489359.

Andolfo, G., Di Donato, A., Chiaiese, P., De Natale, A., Pollio, A., Jones, J.D.G., Frusciante, L., and Ercolano, M.R. (2019). Alien Domains Shaped the Modular Structure of Plant NLR Proteins. Genome Biology and Evolution 11, 3466-3477.

Anh, V.L., Inoue, Y., Asuke, S., Vy, T.T.P., Anh, N.T., Wang, S., Chuma, I., and Tosa, Y. (2018). Rmg8 and Rmg7, wheat genes for resistance to the wheat blast fungus, recognize the same avirulence gene AVR-Rmg8. Mol. Plant Pathol. 19, 1252-1256.

Arora, S., Steed, A., Goddard, R., Gaurav, K., O'Hara, T., Schoen, A., Rawat, N., Elkot, A.F., Korolev, A.V., Chinoy, C., Nicholson, M.H., Asuke, S., Antoniou-Kourounioti, R., Steuernagel, B., Yu, G., Awal, R., Forner-Martínez, M., Wingen, L., Baggs, E., Clarke, J., Saunders, D.G.O., Krasileva, K.V., Tosa, Y., Jones, J.D.G., Tiwari, V.K., Wulff, B.B.H., and Nicholson, P. (2023). A wheat kinase and immune receptor form host-specificity barriers against the blast fungus. Nature Plants.

Axtell, M.J., and Staskawicz, B.J. (2003). Initiation of RPS2-specified disease resistance in Arabidopsis is coupled to the AvrRpt2-directed elimination of RIN4. Cell 112, 369-377.

Baggs, E., Dagdas, G., and Krasileva, K.V. (2017). NLR diversity, helpers and integrated domains: making sense of the NLR IDentity. Curr. Opin. Plant Biol. 38, 59-67.

Baggs, E.L., Monroe, J.G., Thanki, A.S., O'Grady, R., Schudoma, C., Haerty, W., and Krasileva, K.V. (2020). Convergent Loss of an EDS1/PAD4 Signaling Pathway in

Several Plant Lineages Reveals Coevolved Components of Plant Immunity and Drought Response[OPEN]. The Plant Cell 32, 2158-2177.

Bai, S., Liu, J., Chang, C., Zhang, L., Maekawa, T., Wang, Q., Xiao, W., Liu, Y., Chai, J., Takken, F.L.W., Schulze-Lefert, P., and Shen, Q.-H. (2012). Structure-Function Analysis of Barley NLR Immune Receptor MLA10 Reveals Its Cell Compartment Specific Activity in Cell Death and Disease Resistance. PLoS Path. 8, e1002752.

Bailey, P.C., Schudoma, C., Jackson, W., Baggs, E., Dagdas, G., Haerty, W., Moscou, M., and Krasileva, K.V. (2018a). Dominant integration locus drives continuous diversification of plant immune receptors with exogenous domain fusions. Genome biology 19, 1-18.

Bailey, P.C., Schudoma, C., Jackson, W., Baggs, E., Dagdas, G., Haerty, W., Moscou, M., and Krasileva, K.V. (2018b). Dominant integration locus drives continuous diversification of plant immune receptors with exogenous domain fusions. Genome Biology 19, 23.

Barragan, A.C., and Weigel, D. (2021). Plant NLR diversity: the known unknowns of pan-NLRomes. The Plant Cell 33, 814-831.

Baudin, M., Hassan, J.A., Schreiber, K.J., and Lewis, J.D. (2017). Analysis of the ZAR1 Immune Complex Reveals Determinants for Immunity and Molecular Interactions. Plant Physiol. 174, 2038.

Bauer, S., Yu, D., Lawson, A.W., Saur, I.M.L., Frantzeskakis, L., Kracher, B., Logemann, E., Chai, J., Maekawa, T., and Schulze-Lefert, P. (2021). The leucine-rich repeats in allelic barley MLA immune receptors define specificity towards sequence-unrelated powdery mildew avirulence effectors with a predicted common RNase-like fold. PLoS Path. 17, e1009223.

Bendahmane, A., Farnham, G., Moffett, P., and Baulcombe, D.C. (2002). Constitutive gain-of-function mutants in a nucleotide binding site–leucine rich repeat protein encoded at the Rx locus of potato. The Plant Journal 32, 195-204.

Bennetzen, J.L., Schmutz, J., Wang, H., Percifield, R., Hawkins, J., Pontaroli, A.C., Estep, M., Feng, L., Vaughn, J.N., Grimwood, J., Jenkins, J., Barry, K., Lindquist, E., Hellsten, U., Deshpande, S., Wang, X., Wu, X., Mitros, T., Triplett, J., Yang, X., Ye, C.-Y., Mauro-Herrera, M., Wang, L., Li, P., Sharma, M., Sharma, R., Ronald, P.C., Panaud, O., Kellogg, E.A., Brutnell, T.P., Doust, A.N., Tuskan, G.A., Rokhsar, D., and Devos, K.M. (2012). Reference genome sequence of the model plant Setaria. Nat. Biotechnol. 30, 555-561.

Bentham, A., Burdett, H., Anderson, P.A., Williams, S.J., and Kobe, B. (2017). Animal NLRs provide structural insights into plant NLR function. Ann. Bot. 119, 698-702.

Bentham, A.R., Zdrzałek, R., De la Concepcion, J.C., and Banfield, M.J. (2018). Uncoiling CNLs: Structure/Function Approaches to Understanding CC Domain Function in Plant NLRs. Plant and Cell Physiology 59, 2398-2408.

Berhin, A., Nawrath, C., and Hachez, C. (2022). Subtle interplay between trichome development and cuticle formation in plants. New Phytol. 233, 2036-2046.

Bettgenhaeuser, J., Hernández-Pinzón, I., Dawson, A.M., Gardiner, M., Green, P., Taylor, J., Smoker, M., Ferguson, J.N., Emmrich, P., Hubbard, A., Bayles, R., Waugh, R., Steffenson, B.J., Wulff, B.B.H., Dreiseitl, A., Ward, E.R., and Moscou, M.J. (2021). The barley immune receptor Mla recognizes multiple pathogens and contributes to host range dynamics. Nature Communications 12, 6915.

Bhullar, N.K., Zhang, Z., Wicker, T., and Keller, B. (2010). Wheat gene bank accessions as a source of new alleles of the powdery mildew resistance gene Pm3: a large scale allele mining project. BMC Plant Biol. 10, 88.

Bhullar, N.K., Street, K., Mackay, M., Yahiaoui, N., and Keller, B. (2009). Unlocking wheat genetic resources for the molecular identification of previously undescribed functional alleles at the Pm3 resistance locus. Proceedings of the National Academy of Sciences 106, 9519-9524.

Bi, G., Su, M., Li, N., Liang, Y., Dang, S., Xu, J., Hu, M., Wang, J., Zou, M., Deng, Y., Li, Q., Huang, S., Li, J., Chai, J., He, K., Chen, Y.-h., and Zhou, J.-M. (2021). The ZAR1 resistosome is a calcium-permeable channel triggering plant immune signaling. Cell 184, 3528-3541.e3512.

Białas, A., Langner, T., Harant, A., Contreras, M.P., Stevenson, C.E.M., Lawson, D.M., Sklenar, J., Kellner, R., Moscou, M.J., Terauchi, R., Banfield, M.J., and Kamoun, S. (2021). Two NLR immune receptors acquired high-affinity binding to a fungal effector through convergent evolution of their integrated domain. eLife 10, e66961.

Białas, A., Zess, E.K., De la Concepcion, J.C., Franceschetti, M., Pennington, H.G., Yoshida, K., Upson, J.L., Chanclud, E., Wu, C.-H., Langner, T., Maqbool, A., Varden, F.A., Derevnina, L., Belhaj, K., Fujisaki, K., Saitoh, H., Terauchi, R., Banfield, M.J., and Kamoun, S. (2018). Lessons in Effector and NLR Biology of Plant-Microbe Systems. Molecular Plant-Microbe Interactions® 31, 34-45.

Bieri, S., Mauch, S., Shen, Q.-H., Peart, J., Devoto, A., Casais, C., Ceron, F., Schulze, S., Steinbiß, H.-H., Shirasu, K., and Schulze-Lefert, P. (2004). RAR1 Positively Controls Steady State Levels of Barley MLA Resistance Proteins and Enables Sufficient MLA6 Accumulation for Effective Resistance. The Plant Cell 16, 3480-3495.

Birch, P.R.J., Boevink, P.C., Gilroy, E.M., Hein, I., Pritchard, L., and Whisson, S.C. (2008). Oomycete RXLR effectors: delivery, functional redundancy and durable disease resistance. Curr. Opin. Plant Biol. 11, 373-379.

Bittner-Eddy, P.D., Crute, I.R., Holub, E.B., and Beynon, J.L. (2000). RPP13 is a simple locus in Arabidopsis thaliana for alleles that specify downy mildew resistance to different avirulence determinants in Peronospora parasitica. The Plant Journal 21, 177-188.

Boller, T., and Felix, G. (2009). A Renaissance of Elicitors: Perception of Microbe-Associated Molecular Patterns and Danger Signals by Pattern-Recognition Receptors. Annu. Rev. Plant Biol. 60, 379-406.

Bonardi, V., and Dangl, J. (2012). How complex are intracellular immune receptor signaling complexes? Frontiers in Plant Science 3.

Bonardi, V., Cherkis, K., Nishimura, M.T., and Dangl, J.L. (2012). A new eye on NLR proteins: focused on clarity or diffused by complexity? Curr. Opin. Immunol. 24, 41-50.

Bonardi, V., Tang, S., Stallmann, A., Roberts, M., Cherkis, K., and Dangl, J.L. (2011). Expanded functions for a family of plant intracellular immune receptors beyond specific recognition of pathogen effectors. Proceedings of the National Academy of Sciences 108, 16463-16468.

Bourras, S., McNally, K.E., Ben-David, R., Parlange, F., Roffler, S., Praz, C.R., Oberhaensli, S., Menardo, F., Stirnweis, D., Frenkel, Z., Schaefer, L.K., Flückiger, S., Treier, G., Herren, G., Korol, A.B., Wicker, T., and Keller, B. (2015). Multiple Avirulence Loci and Allele-Specific Effector Recognition Control the Pm3 Race-Specific Resistance of Wheat to Powdery Mildew. The Plant Cell 27, 2991-3012.

Bourras, S., Kunz, L., Xue, M., Praz, C.R., Müller, M.C., Kälin, C., Schläfli, M., Ackermann, P., Flückiger, S., Parlange, F., Menardo, F., Schaefer, L.K., Ben-David, R., Roffler, S., Oberhaensli, S., Widrig, V., Lindner, S., Isaksson, J., Wicker, T., Yu, D., and Keller, B. (2019). The AvrPm3-Pm3 effector-NLR interactions control both race-specific resistance and host-specificity of cereal mildews on wheat. Nature Communications 10, 2292.

Boyd, L.A., Smith, P.H., Foster, E.M., and Brown, J.K.M. (1995). The effects of allelic variation at the Mla resistance locus in barley on the early development of Erysiphe graminis f.sp. hordei and host responses. The Plant Journal 7, 959-968.

Brabham, H. (2019). Multiple pathogen recognition at the Mla locus in barley ([Great Britain]: University of East Anglia).

Brabham, H.J., Hernández-Pinzón, I., Holden, S., Lorang, J., and Moscou, M.J. (2018). An ancient integration in a plant NLR is maintained as a trans-species polymorphism. bioRxiv, 239541.

Brabham, H.J., Gómez De La Cruz, D., Were, V., Shimizu, M., Saitoh, H., Hernández-Pinzón, I., Green, P., Lorang, J., Fujisaki, K., Sato, K., Molnár, I., Šimková, H., Doležel, J., Russell, J., Taylor, J., Smoker, M., Gupta, Y.K., Wolpert, T., Talbot, N.J., Terauchi, R., and Moscou, M.J. (2022). Barley MLA3 recognizes the host-specificity determinant PWL2 from rice blast (M. oryzae). bioRxiv, 2022.2010.2021.512921.

Brunner, S., Hurni, S., Streckeisen, P., Mayr, G., Albrecht, M., Yahiaoui, N., and Keller, B. (2010). Intragenic allele pyramiding combines different specificities of wheat Pm3 resistance alleles. The Plant Journal 64, 433-445.

Burdett, H., Bentham, A.R., Williams, S.J., Dodds, P.N., Anderson, P.A., Banfield, M.J., and Kobe, B. (2019). The Plant "Resistosome": Structural Insights into Immune Signaling. Cell Host & Microbe 26, 193-201.

Caldo, R.A., Nettleton, D., Peng, J., and Wise, R.P. (2006). Stage-Specific Suppression of Basal Defense Discriminates Barley Plants Containing Fast- and Delayed-Acting Mla Powdery Mildew Resistance Alleles. Molecular Plant-Microbe Interactions® 19, 939-947.

Carballo, J., Santos, B.A.C.M., Zappacosta, D., Garbus, I., Selva, J.P., Gallo, C.A., Díaz, A., Albertini, E., Caccamo, M., and Echenique, V. (2019). A high-quality genome of Eragrostis curvula grass provides insights into Poaceae evolution and supports new strategies to enhance forage quality. Scientific Reports 9, 10250.

Carter, M.E., Helm, M., Chapman, A.V.E., Wan, E., Restrepo Sierra, A.M., Innes, R.W., Bogdanove, A.J., and Wise, R.P. (2018). Convergent Evolution of Effector Protease Recognition by Arabidopsis and Barley. Molecular Plant-Microbe Interactions® 32, 550-565.

Casey, L.W., Lavrencic, P., Bentham, A.R., Cesari, S., Ericsson, D.J., Croll, T., Turk, D., Anderson, P.A., Mark, A.E., Dodds, P.N., Mobli, M., Kobe, B., and Williams, S.J. (2016). The CC domain structure from the wheat stem rust resistance protein Sr33 challenges paradigms for dimerization in plant NLR proteins. Proceedings of the National Academy of Sciences 113, 12856-12861.

Castel, B., Ngou, P.-M., Cevik, V., Redkar, A., Kim, D.-S., Yang, Y., Ding, P., and Jones, J.D.G. (2019). Diverse NLR immune receptors activate defence via the RPW8-NLR NRG1. New Phytol. 222, 966-980.

Catanzariti, A.-M., Dodds, P.N., Ve, T., Kobe, B., Ellis, J.G., and Staskawicz, B.J. (2010). The AvrM effector from flax rust has a structured C-terminal domain and interacts directly with the M resistance protein. Mol Plant Microbe Interact 23, 49-57.

Cesari, S. (2018). Multiple strategies for pathogen perception by plant immune receptors. New Phytol. 219, 17-24.

Cesari, S., Bernoux, M., Moncuquet, P., Kroj, T., and Dodds, P. (2014). A novel conserved mechanism for plant NLR protein pairs: the 'integrated decoy' hypothesis. Frontiers in Plant Science 5.

Cesari, S., Moore, J., Chen, C., Webb, D., Periyannan, S., Mago, R., Bernoux, M., Lagudah, E.S., and Dodds, P.N. (2016). Cytosolic activation of cell death and stem rust resistance by cereal MLA-family CC–NLR proteins. Proceedings of the National Academy of Sciences 113, 10204-10209.

Cesari, S., Xi, Y., Declerck, N., Chalvon, V., Mammri, L., Pugnière, M., Henriquet, C., de Guillen, K., Chochois, V., Padilla, A., and Kroj, T. (2022). New recognition specificity in a plant immune receptor by molecular engineering of its integrated domain. Nature Communications 13, 1524.

Cesari, S., Thilliez, G., Ribot, C., Chalvon, V., Michel, C., Jauneau, A., Rivas, S., Alaux, L., Kanzaki, H., Okuyama, Y., Morel, J.-B., Fournier, E., Tharreau, D., Terauchi, R., and Kroj, T. (2013). The Rice Resistance Protein Pair RGA4/RGA5 Recognizes the Magnaporthe oryzae Effectors AVR-Pia and AVR1-CO39 by Direct Binding The Plant Cell 25, 1463-1481.

Césari, S., Kanzaki, H., Fujiwara, T., Bernoux, M., Chalvon, V., Kawano, Y., Shimamoto, K., Dodds, P., Terauchi, R., and Kroj, T. (2014). The NB-LRR proteins RGA4 and RGA5 interact functionally and physically to confer disease resistance. The EMBO Journal 33, 1941-1959.

Chen, J., Zhang, X., Rathjen, John P., and Dodds, P.N. (2022). Direct recognition of pathogen effectors by plant NLR immune receptors and downstream signalling. Essays in Biochemistry 66, 471-483.

Chen, J., Upadhyaya, N.M., Ortiz, D., Sperschneider, J., Li, F., Bouton, C., Breen, S., Dong, C., Xu, B., Zhang, X., Mago, R., Newell, K., Xia, X., Bernoux, M., Taylor, J.M., Steffenson, B., Jin, Y., Zhang, P., Kanyuka, K., Figueroa, M., Ellis, J.G., Park, R.F., and Dodds, P.N. (2017). Loss of AvrSr50 by somatic exchange in stem rust leads to virulence for Sr50 resistance in wheat. Science 358, 1607-1610.

Chia, K.-S., Kourelis, J., Vickers, M., Sakai, T., Kamoun, S., and Carella, P. (2022). The N-terminal executioner domains of NLR immune receptors are functionally conserved across major plant lineages. bioRxiv, 2022.2010.2019.512840.

Chuma, I., Zhan, S.W., Asano, S., Nga, N.T., Vy, T.T., Shirai, M., Ibaragi, K., and Tosa, Y. (2010). PWT1, an avirulence gene of Magnaporthe oryzae tightly linked to the rDNA Locus, is recognized by two staple crops, common wheat and barley. Phytopathology 100, 436-443.

Chung, H., Goh, J., Han, S.-S., Roh, J.-H., Kim, Y., Heu, S., Shim, H.-K., Jeong, D.G., Kang, I.J., and Yang, J.-W. (2020). Comparative Pathogenicity and Host Ranges of Magnaporthe oryzae and Related Species. Plant Pathol J 36, 305-313.

Collier, S.M., Hamel, L.-P., and Moffett, P. (2011). Cell Death Mediated by the N-Terminal Domains of a Unique and Highly Conserved Class of NB-LRR Protein. Molecular Plant-Microbe Interactions® 24, 918-931.

Contreras, M.P., Pai, H., Tumtas, Y., Duggan, C., Yuen, E.L.H., Cruces, A.V., Kourelis, J., Ahn, H.-K., Lee, K.-T., Wu, C.-H., Bozkurt, T.O., Derevnina, L., and Kamoun, S. (2022). Sensor NLR immune proteins activate oligomerization of their NRC helpers in response to plant pathogens. The EMBO Journal n/a, e111519.

Contreras, M.P., Pai, H., Selvaraj, M., Toghani, A., Lawson, D.M., Tumtas, Y., Duggan, C., Yuen, E.L.H., Stevenson, C.E.M., Harant, A., Maqbool, A., Wu, C.-H., Bozkurt, T.O., Kamoun, S., and Derevnina, L. (2023). Resurrection of plant disease resistance proteins via helper NLR bioengineering. bioRxiv, 2022.2012.2011.519957.

Cook, D.E., Bayless, A.M., Wang, K., Guo, X., Song, Q., Jiang, J., and Bent, A.F. (2014). Distinct Copy Number, Coding Sequence, and Locus Methylation Patterns Underlie Rhg1-Mediated Soybean Resistance to Soybean Cyst Nematode Plant Physiol. 165, 630-647.

Cook, D.E., Lee, T.G., Guo, X., Melito, S., Wang, K., Bayless, A.M., Wang, J., Hughes, T.J., Willis, D.K., Clemente, T.E., Diers, B.W., Jiang, J., Hudson, M.E., and Bent, A.F. (2012). Copy Number Variation of Multiple Genes at Rhg1 Mediates Nematode Resistance in Soybean. Science 338, 1206-1209.

Couto, D., and Zipfel, C. (2016). Regulation of pattern recognition receptor signalling in plants. Nature Reviews Immunology 16, 537.

Crean, E.E., Bilstein-Schloemer, M., Maekawa, T., Schulze-Lefert, P., and Saur, I.M.L. (2023). A dominant-negative avirulence effector of the barley powdery mildew fungus provides mechanistic insight to barley MLA immune receptor activation. bioRxiv, 2023.2001.2011.523539.

Cruz-Mireles, N., Eseola, A.B., Osés-Ruiz, M., Ryder, L.S., and Talbot, N.J. (2021). From appressorium to transpressorium—Defining the morphogenetic basis of host cell invasion by the rice blast fungus. PLoS Path. 17, e1009779.

Cui, H., Tsuda, K., and Parker, J.E. (2015). Effector-Triggered Immunity: From Pathogen Perception to Robust Defense. Annu. Rev. Plant Biol. 66, 487-511.

Dangl, J.L., and McDowell, J.M. (2006). Two modes of pathogen recognition by plants. Proceedings of the National Academy of Sciences 103, 8575-8576.

de Guillen, K., Ortiz-Vallejo, D., Gracy, J., Fournier, E., Kroj, T., and Padilla, A. (2015). Structure Analysis Uncovers a Highly Diverse but Structurally Conserved Effector Family in Phytopathogenic Fungi. PLoS Path. 11, e1005228.

De la Concepcion, J.C., Franceschetti, M., Maqbool, A., Saitoh, H., Terauchi, R., Kamoun, S., and Banfield, M.J. (2018). Polymorphic residues in rice NLRs expand binding and response to effectors of the blast pathogen. Nature Plants 4, 576-585.

De la Concepcion, J.C., Fujisaki, K., Bentham, A.R., Cruz Mireles, N., Sanchez de Medina Hernandez, V., Shimizu, M., Lawson, D.M., Kamoun, S., Terauchi, R., and Banfield, M.J. (2022). A blast fungus zinc-finger fold effector binds to a hydrophobic pocket in host Exo70 proteins to modulate immune recognition in rice. Proceedings of the National Academy of Sciences 119, e2210559119.

DeFalco, T.A., and Zipfel, C. (2021). Molecular mechanisms of early plant pattern-triggered immune signaling. Mol. Cell 81, 3449-3467.

Derbyshire, M.C., and Raffaele, S. (2023). Surface frustration re-patterning underlies the structural landscape and evolvability of fungal orphan candidate effectors. bioRxiv, 2023.2001.2006.522876.

Derevnina, L., Contreras, M.P., Adachi, H., Upson, J., Vergara Cruces, A., Xie, R., Skłenar, J., Menke, F.L.H., Mugford, S.T., MacLean, D., Ma, W., Hogenhout, S.A., Goverse, A., Maqbool, A., Wu, C.-H., and Kamoun, S. (2021). Plant pathogens convergently evolved to counteract redundant nodes of an NLR immune receptor network. PLoS Biol. 19, e3001136.

Deslandes, L., Olivier, J., Peeters, N., Feng, D.X., Khounlotham, M., Boucher, C., Somssich, I., Genin, S., and Marco, Y. (2003). Physical interaction between RRS1-R, a protein conferring resistance to bacterial wilt, and PopP2, a type III effector targeted to the plant nucleus. Proceedings of the National Academy of Sciences 100, 8024-8029.

DeYoung, B.J., Qi, D., Kim, S.-H., Burke, T.P., and Innes, R.W. (2012). Activation of a plant nucleotide binding-leucine rich repeat disease resistance protein by a modified self protein. Cell. Microbiol. 14, 1071-1084.

Dodds, P.N., and Rathjen, J.P. (2010). Plant immunity: towards an integrated view of plant–pathogen interactions. Nature Reviews Genetics 11, 539-548.

Dodds, P.N., Lawrence, G.J., and Ellis, J.G. (2001). Six amino acid changes confined to the leucine-rich repeat beta-strand/beta-turn motif determine the difference between the P and P2 rust resistance specificities in flax. Plant Cell 13, 163-178.

Dodds, P.N., Lawrence, G.J., Catanzariti, A.-M., Teh, T., Wang, C.-I.A., Ayliffe, M.A., Kobe, B., and Ellis, J.G. (2006). Direct protein interaction underlies gene-for-gene specificity and coevolution of the flax resistance genes and flax rust avirulence genes. Proceedings of the National Academy of Sciences 103, 8888-8893.

Dong, S., and Ma, W. (2021). How to win a tug-of-war: the adaptive evolution of Phytophthora effectors. Curr. Opin. Plant Biol. 62, 102027.

Dongus, J.A., and Parker, J.E. (2021). EDS1 signalling: At the nexus of intracellular and surface receptor immunity. Curr. Opin. Plant Biol. 62, 102039.

Duxbury, Z., Wu, C.-h., and Ding, P. (2021). A Comparative Overview of the Intracellular Guardians of Plants and Animals: NLRs in Innate Immunity and Beyond. Annu. Rev. Plant Biol. 72, 155-184.

Duxbury, Z., Ma, Y., Furzer, O.J., Huh, S.U., Cevik, V., Jones, J.D.G., and Sarris, P.F. (2016). Pathogen perception by NLRs in plants and animals: Parallel worlds. Bioessays 38, 769-781.

Duxbury, Z., Wang, S., MacKenzie, C.I., Tenthorey, J.L., Zhang, X., Huh, S.U., Hu, L., Hill, L., Ngou, P.M., Ding, P., Chen, J., Ma, Y., Guo, H., Castel, B., Moschou, P.N., Bernoux, M., Dodds, P.N., Vance, R.E., and Jones, J.D.G. (2020). Induced proximity of a TIR signaling domain on a plant-mammalian NLR chimera activates defense in plants. Proceedings of the National Academy of Sciences 117, 18832-18839.

Dyck, P.L. (1987). The association of a gene for leaf rust resistance with the chromosome 7D suppressor of stem rust resistance in common wheat. Genome 29, 467-469.

Dyck, P.L., and Samborski, D.J. (1979). Adult-plant leaf rust resistance in PI 250413, an introduction of common wheat. Canadian Journal of Plant Science 59, 329-332.

El Kasmi, F., Chung, E.-H., Anderson, R.G., Li, J., Wan, L., Eitas, T.K., Gao, Z., and Dangl, J.L. (2017). Signaling from the plasma-membrane localized plant immune receptor RPM1 requires self-association of the full-length protein. Proceedings of the National Academy of Sciences 114, E7385-E7394.

Ellis, J.G., Dodds, P.N., and Lawrence, G.J. (2007). Flax Rust Resistance Gene Specificity is Based on Direct Resistance-Avirulence Protein Interactions. Annu. Rev. Phytopathol. 45, 289-306.

Ellis, J.G., Lawrence, G.J., Luck, J.E., and Dodds, P.N. (1999). Identification of Regions in Alleles of the Flax Rust Resistance Gene L That Determine Differences in Gene-for-Gene Specificity. The Plant Cell 11, 495-506.

Enkhbayar, P., Kamiya, M., Osaki, M., Matsumoto, T., and Matsushima, N. (2004). Structural principles of leucine-rich repeat (LRR) proteins. Proteins: Structure, Function, and Bioinformatics 54, 394-403.

Feehan, J.M., Castel, B., Bentham, A.R., and Jones, J.D.G. (2020). Plant NLRs get by with a little help from their friends. Curr. Opin. Plant Biol. 56, 99-108.

Ferreiro, D.U., Komives, E.A., and Wolynes, P.G. (2018). Frustration, function and folding. Curr. Opin. Struct. Biol. 48, 68-73.

Flor, H.H. (1971). Current Status of the Gene-For-Gene Concept. Annu. Rev. Phytopathol. 9, 275-296.

Förderer, A., Yu, D., Li, E., and Chai, J. (2022a). Resistosomes at the interface of pathogens and plants. Curr. Opin. Plant Biol. 67, 102212.

Förderer, A., Li, E., Lawson, A.W., Deng, Y.-n., Sun, Y., Logemann, E., Zhang, X., Wen, J., Han, Z., Chang, J., Chen, Y., Schulze-Lefert, P., and Chai, J. (2022b). A wheat resistosome defines common principles of immune receptor channels. Nature 610, 532-539.

Fouché, S., Plissonneau, C., and Croll, D. (2018). The birth and death of effectors in rapidly evolving filamentous pathogen genomes. Curr. Opin. Microbiol. 46, 34-42.

Franceschetti, M., Maqbool, A., Jiménez-Dalmaroni Maximiliano, J., Pennington Helen, G., Kamoun, S., and Banfield Mark, J. (2017). Effectors of Filamentous Plant Pathogens: Commonalities amid Diversity. Microbiol. Mol. Biol. Rev. 81, e00066-00016.

Fujisaki, K., Abe, Y., Kanzaki, E., Ito, K., Utsushi, H., Saitoh, H., Białas, A., Banfield, M.J., Kamoun, S., and Terauchi, R. (2017). An unconventional NOI/RIN4 domain of a rice NLR protein binds host EXO70 protein to confer fungal immunity. bioRxiv, 239400.

Fujisaki, K., Abe, Y., Ito, A., Saitoh, H., Yoshida, K., Kanzaki, H., Kanzaki, E., Utsushi, H., Yamashita, T., Kamoun, S., and Terauchi, R. (2015). Rice Exo70 interacts with a fungal effector, AVR-Pii, and is required for AVR-Pii-triggered immunity. The Plant Journal 83, 875-887.

Galhano, R., and Talbot, N.J. (2011). The biology of blast: Understanding how Magnaporthe oryzae invades rice plants. Fungal Biology Reviews 25, 61-67.

Gao, L., Altae-Tran, H., Böhning, F., Makarova, K.S., Segel, M., Schmid-Burgk, J.L., Koob, J., Wolf, Y.I., Koonin, E.V., and Zhang, F. (2020). Diverse enzymatic activities mediate antiviral immunity in prokaryotes. Science 369, 1077-1084.

Gao, L.A., Wilkinson, M.E., Strecker, J., Makarova, K.S., Macrae, R.K., Koonin, E.V., and Zhang, F. (2022). Prokaryotic innate immunity through pattern recognition of conserved viral proteins. Science 377, eabm4096.

Gao, Y., Wang, W., Zhang, T., Gong, Z., Zhao, H., and Han, G.-Z. (2018). Out of Water: The Origin and Early Diversification of Plant R-Genes. Plant Physiol. 177, 82-89.

Ghosh, S., and O'Connor, T.J. (2017). Beyond Paralogs: The Multiple Layers of Redundancy in Bacterial Pathogenesis. Frontiers in Cellular and Infection Microbiology 7.

Giannakopoulou, A., Steele, J.F.C., Segretin, M.E., Bozkurt, T.O., Zhou, J., Robatzek, S., Banfield, M.J., Pais, M., and Kamoun, S. (2015). Tomato I2 Immune Receptor Can Be Engineered to Confer Partial Resistance to the Oomycete Phytophthora infestans in Addition to the Fungus Fusarium oxysporum. Molecular Plant-Microbe Interactions® 28, 1316-1329.

Gilroy, E.M., Breen, S., Whisson, S.C., Squires, J., Hein, I., Kaczmarek, M., Turnbull, D., Boevink, P.C., Lokossou, A., Cano, L.M., Morales, J., Avrova, A.O., Pritchard, L., Randall, E., Lees, A., Govers, F., van West, P., Kamoun, S., Vleeshouwers, V.G.A.A., Cooke, D.E.L., and Birch, P.R.J. (2011). Presence/absence, differential expression and sequence polymorphisms between PiAVR2 and PiAVR2-like in Phytophthora infestans determine virulence on R2 plants. New Phytol. 191, 763-776.

Goff, S.A., Ricke, D., Lan, T.-H., Presting, G., Wang, R., Dunn, M., Glazebrook, J., Sessions, A., Oeller, P., Varma, H., Hadley, D., Hutchison, D., Martin, C., Katagiri, F., Lange, B.M., Moughamer, T., Xia, Y., Budworth, P., Zhong, J., Miguel, T., Paszkowski, U., Zhang, S., Colbert, M., Sun, W.-l., Chen, L., Cooper, B., Park, S., Wood, T.C., Mao, L., Quail, P., Wing, R., Dean, R., Yu, Y., Zharkikh, A., Shen, R., Sahasrabudhe, S., Thomas, A., Cannings, R., Gutin, A., Pruss, D., Reid, J., Tavtigian, S., Mitchell, J., Eldredge, G., Scholl, T., Miller, R.M., Bhatnagar, S., Adey, N., Rubano, T., Tusneem, N., Robinson, R., Feldhaus, J., Macalma, T., Oliphant, A., and Briggs, S. (2002). A Draft Sequence of the Rice Genome (Oryza sativa L. ssp. japonica). Science 296, 92-100.

Grund, E., Tremousaygue, D., and Deslandes, L. (2019). Plant NLRs with Integrated Domains: Unity Makes Strength. Plant Physiol. 179, 1227-1235.

Guo, H., Ahn, H.-K., Sklenar, J., Huang, J., Ma, Y., Ding, P., Menke, F.L.H., and Jones, J.D.G. (2020). Phosphorylation-Regulated Activation of the Arabidopsis RRS1-R/RPS4 Immune Receptor Complex Reveals Two Distinct Effector Recognition Mechanisms. Cell Host & Microbe 27, 769-781.e766.

Guo, L., Cesari, S., de Guillen, K., Chalvon, V., Mammri, L., Ma, M., Meusnier, I., Bonnot, F., Padilla, A., Peng, Y.-L., Liu, J., and Kroj, T. (2018a). Specific recognition of two MAX effectors by integrated HMA domains in plant immune receptors involves distinct binding surfaces. Proceedings of the National Academy of Sciences 115, 11637-11642.

Guo, L.W., Cesari, S., de Guillen, K., Chalvon, V., Mammri, L., Ma, M.Q., Meusnier, I., Bonnot, F., Padilla, A., Peng, Y.L., Liu, J.F., and Kroj, T. (2018b). Specific recognition of two MAX effectors by integrated HMA domains in plant immune

receptors involves distinct binding surfaces. Proceedings of the National Academy of Sciences of the United States of America 115, 11637-11642.

Halterman, D.A., and Wise, R.P. (2004). A single-amino acid substitution in the sixth leucine-rich repeat of barley MLA6 and MLA13 alleviates dependence on RAR1 for disease resistance signaling. The Plant Journal 38, 215-226.

Hanley, M.E., Lamont, B.B., Fairbanks, M.M., and Rafferty, C.M. (2007). Plant structural traits and their role in anti-herbivore defence. Perspect. Plant Ecol. Evol. Syst. 8, 157-178.

Harris, C.J., Slootweg, E.J., Goverse, A., and Baulcombe, D.C. (2013). Stepwise artificial evolution of a plant disease resistance gene. Proceedings of the National Academy of Sciences 110, 21189-21194.

Helm, M., Qi, M., Sarkar, S., Yu, H., Whitham, S.A., and Innes, R.W. (2019). Engineering a Decoy Substrate in Soybean to Enable Recognition of the Soybean Mosaic Virus NIa Protease. Molecular Plant-Microbe Interactions® 32, 760-769.

Henk, A.D., Warren, R.F., and Innes, R.W. (1999). A New Ac-Like Transposon of Arabidopsis Is Associated With a Deletion of the RPS5 Disease Resistance Gene. Genetics 151, 1581-1589.

Hogenhout, S.A., Van der Hoorn, R.A.L., Terauchi, R., and Kamoun, S. (2009). Emerging Concepts in Effector Biology of Plant-Associated Organisms. Molecular Plant-Microbe Interactions® 22, 115-122.

Hohmann, U., Lau, K., and Hothorn, M. (2017). The Structural Basis of Ligand Perception and Signal Activation by Receptor Kinases. Annu. Rev. Plant Biol. 68, 109-137.

Hou, S., Liu, Z., Shen, H., and Wu, D. (2019). Damage-Associated Molecular Pattern-Triggered Immunity in Plants. Frontiers in Plant Science 10.

Hu, Z., and Chai, J. (2016). Structural Mechanisms in NLR Inflammasome Assembly and Signaling. In Inflammasome Signaling and Bacterial Infections, S. Backert, ed (Cham: Springer International Publishing), pp. 23-42.

Huang, C.-C., Yang, J.-i., Chou, K.-L., Lin, C.-H., and Chang, H.-X. (2021). Copy Number Quantification for the Soybean Cyst Nematode Resistance Locus rhg1 in the Soybean Varieties of Taiwan. In Agronomy.

Huang, S., Jia, A., Song, W., Hessler, G., Meng, Y., Sun, Y., Xu, L., Laessle, H., Jirschitzka, J., Ma, S., Xiao, Y., Yu, D., Hou, J., Liu, R., Sun, H., Liu, X., Han, Z., Chang, J., Parker, J.E., and Chai, J. (2022). Identification and receptor mechanism of TIR-catalyzed small molecules in plant immunity. Science 377, eabq3297.

Huh, S.U., Cevik, V., Ding, P.T., Duxbury, Z., Ma, Y., Tomlinson, L., Sarris, P.F., and Jones, J.D.G. (2017a). Protein-protein interactions in the RPS4/RRS1 immune receptor complex. PLoS Path. 13.

Huh, S.U., Cevik, V., Ding, P., Duxbury, Z., Ma, Y., Tomlinson, L., Sarris, P.F., and Jones, J.D.G. (2017b). Protein-protein interactions in the RPS4/RRS1 immune receptor complex. PLoS Path. 13, e1006376.

Hyon, G.-S., Nga, N.T.T., Chuma, I., Inoue, Y., Asano, H., Murata, N., Kusaba, M., and Tosa, Y. (2012). Characterization of interactions between barley and various host-specific subgroups of Magnaporthe oryzae and M. grisea. J. Gen. Plant Pathol. 78, 237-246.

Inoue, Y., Vy, T.T.P., Yoshida, K., Asano, H., Mitsuoka, C., Asuke, S., Anh, V.L., Cumagun, C.J.R., Chuma, I., Terauchi, R., Kato, K., Mitchell, T., Valent, B., Farman, M., and Tosa, Y. (2017). Evolution of the wheat blast fungus through functional losses in a host specificity determinant. Science 357, 80-83.

Inukai, T., Vales, M.I., Hori, K., Sato, K., and Hayes, P.M. (2006). RMo1 Confers Blast Resistance in Barley and Is Located within the Complex of Resistance Genes Containing Mla, a Powdery Mildew Resistance Gene. Mol. Plant-Microbe Interact. 19, 1034-1041.

Jacob, P., Kim, N.H., Wu, F., El-Kasmi, F., Chi, Y., Walton, W.G., Furzer, O.J., Lietzan, A.D., Sunil, S., Kempthorn, K., Redinbo, M.R., Pei, Z.-M., Wan, L., and Dangl, J.L. (2021). Plant "helper" immune receptors are Ca2+-permeable nonselective cation channels. Science 373, 420-425.

Jayakodi, M., Padmarasu, S., Haberer, G., Bonthala, V.S., Gundlach, H., Monat, C., Lux, T., Kamal, N., Lang, D., Himmelbach, A., Ens, J., Zhang, X.-Q., Angessa, T.T., Zhou, G., Tan, C., Hill, C., Wang, P., Schreiber, M., Boston, L.B., Plott, C., Jenkins, J., Guo, Y., Fiebig, A., Budak, H., Xu, D., Zhang, J., Wang, C., Grimwood, J., Schmutz, J., Guo, G., Zhang, G., Mochida, K., Hirayama, T., Sato, K., Chalmers, K.J., Langridge, P., Waugh, R., Pozniak, C.J., Scholz, U., Mayer, K.F.X., Spannagl, M., Li, C., Mascher, M., and Stein, N. (2020). The barley pan-genome reveals the hidden legacy of mutation breeding. Nature 588, 284-289.

Jenner, C., Hitchin, E., Mansfield, J., Walters, K., Betteridge, P., Teverson, D., and Taylor, J. (1991). Gene-for-gene interactions between Pseudomonas syringae pv. phaseolicola and Phaseolus. Mol Plant Microbe Interact 4, 553-562.

Jia, A., Huang, S., Song, W., Wang, J., Meng, Y., Sun, Y., Xu, L., Laessle, H., Jirschitzka, J., Hou, J., Zhang, T., Yu, W., Hessler, G., Li, E., Ma, S., Yu, D., Gebauer, J., Baumann, U., Liu, X., Han, Z., Chang, J., Parker, J.E., and Chai, J. (2022). TIR-catalyzed ADP-ribosylation reactions produce signaling molecules for plant immunity. Science 377, eabq8180.

Jia, Y., McAdams, S.A., Bryan, G.T., Hershey, H.P., and Valent, B. (2000). Direct interaction of resistance gene and avirulence gene products confers rice blast resistance. The EMBO Journal 19, 4004-4014.

Jones, J.D.G., and Dangl, J.L. (2006). The plant immune system. Nature 444, 323-329.

Jones, J.D.G., Vance, R.E., and Dangl, J.L. (2016). Intracellular innate immune surveillance devices in plants and animals. Science 354, aaf6395.

Jørgensen, J.H., and Wolfe, M. (1994). Genetics of Powdery Mildew Resistance in Barley. Crit. Rev. Plant Sci. 13, 97-119.

Jumper, J., Evans, R., Pritzel, A., Green, T., Figurnov, M., Ronneberger, O., Tunyasuvunakool, K., Bates, R., Žídek, A., Potapenko, A., Bridgland, A., Meyer, C., Kohl, S.A.A., Ballard, A.J., Cowie, A., Romera-Paredes, B., Nikolov, S., Jain, R., Adler, J., Back, T., Petersen, S., Reiman, D., Clancy, E., Zielinski, M., Steinegger, M., Pacholska, M., Berghammer, T., Bodenstein, S., Silver, D., Vinyals, O., Senior, A.W., Kavukcuoglu, K., Kohli, P., and Hassabis, D. (2021). Highly accurate protein structure prediction with AlphaFold. Nature 596, 583-589.

Kang, S., Sweigard, J.A., and Valent, B. (1995). The *PWL* Host Specificity Gene Family in the Blast Fungus *Magnaporthe grisea*. MPMI 8, 939-948.

Khang, C.H., Berruyer, R., Giraldo, M.C., Kankanala, P., Park, S.Y., Czymmek, K., Kang, S., and Valent, B. (2010). Translocation of Magnaporthe oryzae Effectors into Rice Cells and Their Subsequent Cell-to-Cell Movement. Plant Cell 22, 1388-1403.

Kim, M., Hyten, D.L., Niblack, T.L., and Diers, B.W. (2011). Stacking Resistance Alleles from Wild and Domestic Soybean Sources Improves Soybean Cyst Nematode Resistance. Crop Sci. 51, 934-943.

Kim, Y.J., Lin, N.-C., and Martin, G.B. (2002). Two Distinct Pseudomonas Effector Proteins Interact with the Pto Kinase and Activate Plant Immunity. Cell 109, 589-598.

Kim, Y.K., Shin, J.-S., and Nahm, M.H. (2016). NOD-Like Receptors in Infection, Immunity, and Diseases. Yonsei Med J 57, 5-14.

Kobe, B., and Kajava, A.V. (2001). The leucine-rich repeat as a protein recognition motif. Curr. Opin. Struct. Biol. 11, 725-732.

Kourelis, J., and van der Hoorn, R.A.L. (2018). Defended to the Nines: 25 Years of Resistance Gene Cloning Identifies Nine Mechanisms for R Protein Function. The Plant Cell 30, 285-299.

Kourelis, J., and Adachi, H. (2022). Activation and Regulation of NLR Immune Receptor Networks. Plant and Cell Physiology 63, 1366-1377.

Kourelis, J., Sakai, T., Adachi, H., and Kamoun, S. (2021). RefPlantNLR is a comprehensive collection of experimentally validated plant disease resistance proteins from the NLR family. PLoS Biol. 19, e3001124.

Krasileva, K.V., Dahlbeck, D., and Staskawicz, B.J. (2010a). Activation of an Arabidopsis Resistance Protein Is Specified by the in Planta Association of Its Leucine-Rich Repeat Domain with the Cognate Oomycete Effector The Plant Cell 22, 2444-2458.

Krasileva, K.V., Dahlbeck, D., and Staskawicz, B.J. (2010b). Activation of an Arabidopsis Resistance Protein Is Specified by the in Planta Association of Its Leucine-Rich Repeat Domain with the Cognate Oomycete Effector. The Plant Cell 22, 2444-2458.

Krattinger, S.G., Lagudah, E.S., Wicker, T., Risk, J.M., Ashton, A.R., Selter, L.L., Matsumoto, T., and Keller, B. (2011). Lr34 multi-pathogen resistance ABC transporter: molecular analysis of homoeologous and orthologous genes in hexaploid wheat and other grass species. Plant J. 65, 392-403.

Krattinger, S.G., Sucher, J., Selter, L.L., Chauhan, H., Zhou, B., Tang, M., Upadhyaya, N.M., Mieulet, D., Guiderdoni, E., Weidenbach, D., Schaffrath, U., Lagudah, E.S., and Keller, B. (2016). The wheat durable, multipathogen resistance gene Lr34 confers partial blast resistance in rice. Plant Biotechnol. J. 14, 1261-1268.

Krattinger, S.G., Kang, J., Braunlich, S., Boni, R., Chauhan, H., Setter, L.L., Robinson, M.D., Schmid, M.W., Wiederhold, E., Hensel, G., Kumlehn, J., Sucher, J., Martinoia, E., and Keller, B. (2019). Abscisic acid is a substrate of the ABC transporter encoded by the durable wheat disease resistance gene Lr34. New Phytol. 223, 853-866.

Kroj, T., Chanclud, E., Michel-Romiti, C., Grand, X., and Morel, J.-B. (2016). Integration of decoy domains derived from protein targets of pathogen effectors into plant immune receptors is widespread. New Phytol. 210, 618-626.

Kuang, H., Woo, S.-S., Meyers, B.C., Nevo, E., and Michelmore, R.W. (2004). Multiple Genetic Processes Result in Heterogeneous Rates of Evolution within the Major Cluster Disease Resistance Genes in Lettuce[W]. The Plant Cell 16, 2870-2894.

Lapin, D., Johanndrees, O., Wu, Z., Li, X., and Parker, J.E. (2022). Molecular innovations in plant TIR-based immunity signaling. The Plant Cell 34, 1479-1496.

Lapin, D., Kovacova, V., Sun, X., Dongus, J.A., Bhandari, D., von Born, P., Bautor, J., Guarneri, N., Rzemieniewski, J., Stuttmann, J., Beyer, A., and Parker, J.E. (2019). A Coevolved EDS1-SAG101-NRG1 Module Mediates Cell Death Signaling by TIR-Domain Immune Receptors. The Plant Cell 31, 2430-2455.

Latorre, S.M., Reyes-Avila, C.S., Malmgren, A., Win, J., Kamoun, S., and Burbano, H.A. (2020). Differential loss of effector genes in three recently expanded pandemic clonal lineages of the rice blast fungus. BMC Biol. 18, 88.

Le Roux, C., Huet, G., Jauneau, A., Camborde, L., Trémousaygue, D., Kraut, A., Zhou, B., Levaillant, M., Adachi, H., Yoshioka, H., Raffaele, S., Berthomé, R., Couté, Y., Parker, Jane E., and Deslandes, L. (2015). A Receptor Pair with an Integrated Decoy Converts Pathogen Disabling of Transcription Factors to Immunity. Cell 161, 1074-1088.

Lechtenberg, B.C., Mace, P.D., and Riedl, S.J. (2014). Structural mechanisms in NLR inflammasome signaling. Curr. Opin. Struct. Biol. 29, 17-25.

Lee, T.G., Kumar, I., Diers, B.W., and Hudson, M.E. (2015). Evolution and selection of Rhg1, a copy-number variant nematode-resistance locus. Mol. Ecol. 24, 1774-1791.

Letunic, I., and Bork, P. (2021). Interactive Tree Of Life (iTOL) v5: an online tool for phylogenetic tree display and annotation. Nucleic Acids Res. 49, W293-W296.

Lewis, J.D., Wu, R., Guttman, D.S., and Desveaux, D. (2010). Allele-Specific Virulence Attenuation of the Pseudomonas syringae HopZ1a Type III Effector via the Arabidopsis ZAR1 Resistance Protein. PLoS Genet. 6, e1000894.

Lewis, J.D., Lee, A.H.-Y., Hassan, J.A., Wan, J., Hurley, B., Jhingree, J.R., Wang, P.W., Lo, T., Youn, J.-Y., Guttman, D.S., and Desveaux, D. (2013). The Arabidopsis ZED1 pseudokinase is required for ZAR1-mediated immunity induced by the Pseudomonas syringae type III effector HopZ1a. Proceedings of the National Academy of Sciences 110, 18722-18727.

Li, H., Handsaker, B., Wysoker, A., Fennell, T., Ruan, J., Homer, N., Marth, G., Abecasis, G., and Durbin, R. (2009). The sequence alignment/map format and SAMtools. Bioinformatics 25, 2078-2079.

Li, J., Huang, H., Zhu, M., Huang, S., Zhang, W., Dinesh-Kumar, S.P., and Tao, X. (2019). A Plant Immune Receptor Adopts a Two-Step Recognition Mechanism to Enhance Viral Effector Perception. Molecular Plant 12, 248-262.

Li, Q., Xie, Q.G., Smith-Becker, J., Navarre, D.A., and Kaloshian, I. (2006). Mi-1-mediated aphid resistance involves salicylic acid and mitogen-activated protein kinase signaling cascades. Mol. Plant-Microbe Interact. 19, 655-664.

Lorang, J., Cuesta-Marcos, A., Hayes, P.M., and Wolpert, T.J. (2010). Identification and mapping of adult-onset sensitivity to victorin in barley. Mol. Breed. 26, 545-550.

Lorang, J., Kidarsa, T., Bradford, C.S., Gilbert, B., Curtis, M., Tzeng, S.-C., Maier, C.S., and Wolpert, T.J. (2012). Tricking the Guard: Exploiting Plant Defense for Disease Susceptibility. Science 338, 659-662.

Lorang, J.M., Carkaci-Salli, N., and Wolpert, T.J. (2004). Identification and Characterization of Victorin Sensitivity in Arabidopsis thaliana. Mol. Plant-Microbe Interact. 17, 577-582.

Lorang, J.M., Sweat, T.A., and Wolpert, T.J. (2007). Plant disease susceptibility conferred by a "resistance" gene. Proceedings of the National Academy of Sciences of the United States of America 104, 14861-14866.

Lu, X., Kracher, B., Saur, I.M.L., Bauer, S., Ellwood, S.R., Wise, R., Yaeno, T., Maekawa, T., and Schulze-Lefert, P. (2016). Allelic barley MLA immune receptors recognize sequence-unrelated avirulence effectors of the powdery mildew pathogen. Proceedings of the National Academy of Sciences 113, E6486-E6495.

Lukasik, E., and Takken, F.L.W. (2009). STANDing strong, resistance proteins instigators of plant defence. Curr. Opin. Plant Biol. 12, 427-436.

Ma, S., Lapin, D., Liu, L., Sun, Y., Song, W., Zhang, X., Logemann, E., Yu, D., Wang, J., Jirschitzka, J., Han, Z., Schulze-Lefert, P., Parker, J.E., and Chai, J. (2020). Direct pathogen-induced assembly of an NLR immune receptor complex to form a holoenzyme. Science 370, eabe3069.

Ma, Y., Guo, H.L., Hu, L.X., Martinez, P.P., Moschou, P.N., Cevik, V., Ding, P.T., Duxbury, Z., Sarris, P.F., and Jones, J.D.G. (2018). Distinct modes of derepression

of an Arabidopsis immune receptor complex by two different bacterial effectors. Proceedings of the National Academy of Sciences of the United States of America 115, 10218-10227.

Macho, Alberto P., and Zipfel, C. (2014). Plant PRRs and the Activation of Innate Immune Signaling. Mol. Cell 54, 263-272.

Mackey, D., Holt, B.F., 3rd, Wiig, A., and Dangl, J.L. (2002). RIN4 interacts with Pseudomonas syringae type III effector molecules and is required for RPM1-mediated resistance in Arabidopsis. Cell 108, 743-754.

MacLean, D. (2019). TeamMacLean/besthr: Initial Release (0.1.0) (Zenodo).

Maekawa, T., Kracher, B., Saur, I.M.L., Yoshikawa-Maekawa, M., Kellner, R., Pankin, A., von Korff, M., and Schulze-Lefert, P. (2018). Subfamily-Specific Specialization of RGH1/MLA Immune Receptors in Wild Barley. Molecular Plant-Microbe Interactions® 32, 107-119.

Maekawa, T., Cheng, W., Spiridon, L.N., Töller, A., Lukasik, E., Saijo, Y., Liu, P., Shen, Q.-H., Micluta, M.A., Somssich, I.E., Takken, F.L.W., Petrescu, A.-J., Chai, J., and Schulze-Lefert, P. (2011). Coiled-Coil Domain-Dependent Homodimerization of Intracellular Barley Immune Receptors Defines a Minimal Functional Module for Triggering Cell Death. Cell Host & Microbe 9, 187-199.

Magliery, T.J., and Regan, L. (2005). Sequence variation in ligand binding sites in proteins. BMC Bioinformatics 6, 240.

Mago, R., Zhang, P., Vautrin, S., Šimková, H., Bansal, U., Luo, M.-C., Rouse, M., Karaoglu, H., Periyannan, S., Kolmer, J., Jin, Y., Ayliffe, M.A., Bariana, H., Park, R.F., McIntosh, R., Doležel, J., Bergès, H., Spielmeyer, W., Lagudah, E.S., Ellis, J.G., and Dodds, P.N. (2015). The wheat Sr50 gene reveals rich diversity at a cereal disease resistance locus. Nature Plants 1, 15186.

Maidment, J.H.R., Franceschetti, M., Maqbool, A., Saitoh, H., Jantasuriyarat, C., Kamoun, S., Terauchi, R., and Banfield, M.J. (2021). Multiple variants of the fungal effector AVR-Pik bind the HMA domain of the rice protein OsHIPP19, providing a foundation to engineer plant defense. J. Biol. Chem. 296, 100371.

Maqbool, A., Saitoh, H., Franceschetti, M., Stevenson, C.E.M., Uemura, A., Kanzaki, H., Kamoun, S., Terauchi, R., and Banfield, M.J. (2015). Structural basis of pathogen recognition by an integrated HMA domain in a plant NLR immune receptor. eLife 4, e08709.

Marchal, C., Pai, H., Kamoun, S., and Kourelis, J. (2022a). Emerging principles in the design of bioengineered made-to-order plant immune receptors. Curr. Opin. Plant Biol. 70, 102311.

Marchal, C., Michalopoulou, Vassiliki A., Zou, Z., Cevik, V., and Sarris, Panagiotis F. (2022b). Show me your ID: NLR immune receptors with integrated domains in plants. Essays in Biochemistry 66, 527-539.

Martin, E.C., Sukarta, O.C.A., Spiridon, L., Grigore, L.G., Constantinescu, V., Tacutu, R., Goverse, A., and Petrescu, A.-J. (2020a). LRRpredictor—A New LRR Motif Detection Method for Irregular Motifs of Plant NLR Proteins Using an Ensemble of Classifiers. In Genes.

Martin, R., Qi, T., Zhang, H., Liu, F., King, M., Toth, C., Nogales, E., and Staskawicz, B.J. (2020b). Structure of the activated ROQ1 resistosome directly recognizing the pathogen effector XopQ. Science 370, eabd9993.

Maruta, N., Burdett, H., Lim, B.Y.J., Hu, X., Desa, S., Manik, M.K., and Kobe, B. (2022). Structural basis of NLR activation and innate immune signalling in plants. Immunogenetics 74, 5-26.

Mascher, M., Wicker, T., Jenkins, J., Plott, C., Lux, T., Koh, C.S., Ens, J., Gundlach, H., Boston, L.B., Tulpová, Z., Holden, S., Hernández-Pinzón, I., Scholz, U., Mayer, K.F.X., Spannagl, M., Pozniak, C.J., Sharpe, A.G., Šimková, H., Moscou, M.J., Grimwood, J., Schmutz, J., and Stein, N. (2021). Long-read sequence assembly: a technical evaluation in barley. The Plant Cell 33, 1888-1906.

McHale, L.K., Haun, W.J., Xu, W.W., Bhaskar, P.B., Anderson, J.E., Hyten, D.L., Gerhardt, D.J., Jeddeloh, J.A., and Stupar, R.M. (2012). Structural Variants in the Soybean Genome Localize to Clusters of Biotic Stress-Response Genes Plant Physiol. 159, 1295-1308.

Mcintosh, R.A. (1992). Close genetic linkage of genes conferring adult-plant resistance to leaf rust and stripe rust in wheat. Plant Pathol. 41, 523-527.

Meehan, F., and Murphy, H.C. (1946). A New Helminthosporium Blight of Oats. Science 104, 413-414.

Meyers, B.C., Kozik, A., Griego, A., Kuang, H., and Michelmore, R.W. (2003). Genome-Wide Analysis of NBS-LRR–Encoding Genes in Arabidopsis[W]. The Plant Cell 15, 809-834.

Meyers, B.C., Chin, D.B., Shen, K.A., Sivaramakrishnan, S., Lavelle, D.O., Zhang, Z., and Michelmore, R.W. (1998). The Major Resistance Gene Cluster in Lettuce Is Highly Duplicated and Spans Several Megabases. The Plant Cell 10, 1817-1832.

Michelmore, R.W., and Meyers, B.C. (1998). Clusters of Resistance Genes in Plants Evolve by Divergent Selection and a Birth-and-Death Process. Genome Res. 8, 1113-1130.

Moffett, P., Farnham, G., Peart, J., and Baulcombe, D.C. (2002). Interaction between domains of a plant NBS–LRR protein in disease resistance-related cell death. The EMBO Journal 21, 4511-4519.

Morgounov, A., Tufan, H.A., Sharma, R., Akin, B., Bagci, A., Braun, H.J., Kaya, Y., Keser, M., Payne, T.S., Sonder, K., and McIntosh, R. (2012). Global incidence of wheat rusts and powdery mildew during 1969-2010 and durability of resistance of winter wheat variety Bezostaya 1. Eur. J. Plant Pathol. 132, 323-340.

Mukhi, N., Brown, H., Gorenkin, D., Ding, P., Bentham, A.R., Stevenson, C.E.M., Jones, J.D.G., and Banfield, M.J. (2021). Perception of structurally distinct effectors by the integrated WRKY domain of a plant immune receptor. Proceedings of the National Academy of Sciences 118, e2113996118.

Müller, M.C., Praz, C.R., Sotiropoulos, A.G., Menardo, F., Kunz, L., Schudel, S., Oberhänsli, S., Poretti, M., Wehrli, A., Bourras, S., Keller, B., and Wicker, T. (2019). A chromosome-scale genome assembly reveals a highly dynamic effector repertoire of wheat powdery mildew. New Phytol. 221, 2176-2189.

Murakami, J., Tosa, Y., Kataoka, T., Tomita, R., Kawasaki, J., Chuma, I., Sesumi, Y., Kusaba, M., Nakayashiki, H., and Mayama, S. (2000). Analysis of Host Species Specificity of Magnaporthe grisea Toward Wheat Using a Genetic Cross Between Isolates from Wheat and Foxtail Millet. Phytopathology 90, 1060-1067.

Narusaka, M., Shirasu, K., Noutoshi, Y., Kubo, Y., Shiraishi, T., Iwabuchi, M., and Narusaka, Y. (2009). RRS1 and RPS4 provide a dual Resistance-gene system against fungal and bacterial pathogens. Plant J. 60, 218-226.

Ng, A., and Xavier, R.J. (2011). Leucine-rich repeat (LRR) proteins: integrators of pattern recognition and signaling in immunity. Autophagy 7, 1082-1084.

Nga, N.T.T., Inoue, Y., Chuma, I., Hyon, G.-S., Okada, K., Vy, T.T.P., Kusaba, M., and Tosa, Y. (2012). Identification of a Novel Locus Rmo2 Conditioning Resistance in Barley to Host-Specific Subgroups of Magnaporthe oryzae. Phytopathology 102, 674-682.

Ngou, B.P.M., Ahn, H.-K., Ding, P., and Jones, J.D.G. (2021). Mutual potentiation of plant immunity by cell-surface and intracellular receptors. Nature 592, 110-115.

Nombela, G., Williamson, V.M., and Muniz, M. (2003). The root-knot nematode resistance gene Mi-1.2 of tomato is responsible for resistance against the whitefly Bemisia tabaci. Mol. Plant-Microbe Interact. 16, 645-649.

Oikawa, K., Fujisaki, K., Shimizu, M., Takeda, T., Saitoh, H., Hirabuchi, A., Hiraka, Y., Białas, A., Langner, T., Kellner, R., Bozkurt, T.O., Cesari, S., Kroj, T., Maidment, J.H.R., Banfield, M.J., Kamoun, S., and Terauchi, R. (2020). The blast pathogen effector AVR-Pik binds and stabilizes rice heavy metal-associated (HMA) proteins to co-opt their function in immunity. bioRxiv, 2020.2012.2001.406389.

Ortiz, D., de Guillen, K., Cesari, S., Chalvon, V., Gracy, J., Padilla, A., and Kroj, T. (2017). Recognition of the Magnaporthe oryzae Effector AVR-Pia by the Decoy Domain of the Rice NLR Immune Receptor RGA5. The Plant Cell 29, 156-168.

Ortiz, D., Chen, J., Outram, M.A., Saur, I.M.L., Upadhyaya, N.M., Mago, R., Ericsson, D.J., Cesari, S., Chen, C., Williams, S.J., and Dodds, P.N. (2022). The stem rust effector protein AvrSr50 escapes Sr50 recognition by a substitution in a single surface-exposed residue. New Phytol. 234, 592-606.

Padmanabhan, M., Cournoyer, P., and Dinesh-Kumar, S.P. (2009). The leucine-rich repeat domain in plant innate immunity: a wealth of possibilities. Cell. Microbiol. 11, 191-198.

Pais, M., Yoshida, K., Giannakopoulou, A., Pel, M.A., Cano, L.M., Oliva, R.F., Witek, K., Lindqvist-Kreuze, H., Vleeshouwers, V.G.A.A., and Kamoun, S. (2018). Gene expression polymorphism underpins evasion of host immunity in an asexual lineage of the Irish potato famine pathogen. BMC Evol. Biol. 18, 93.

Paterson, A.H., Bowers, J.E., Bruggmann, R., Dubchak, I., Grimwood, J., Gundlach, H., Haberer, G., Hellsten, U., Mitros, T., Poliakov, A., Schmutz, J., Spannagl, M., Tang, H., Wang, X., Wicker, T., Bharti, A.K., Chapman, J., Feltus, F.A., Gowik, U., Grigoriev, I.V., Lyons, E., Maher, C.A., Martis, M., Narechania, A., Otillar, R.P., Penning, B.W., Salamov, A.A., Wang, Y., Zhang, L., Carpita, N.C., Freeling, M., Gingle, A.R., Hash, C.T., Keller, B., Klein, P., Kresovich, S., McCann, M.C., Ming, R., Peterson, D.G., Mehboob ur, R., Ware, D., Westhoff, P., Mayer, K.F.X., Messing, J., and Rokhsar, D.S. (2009). The Sorghum bicolor genome and the diversification of grasses. Nature 457, 551-556.

Pearce, S., Saville, R., Vaughan, S.P., Chandler, P.M., Wilhelm, E.P., Sparks, C.A., Al-Kaff, N., Korolev, A., Boulton, M.I., Phillips, A.L., Hedden, P., Nicholson, P., and Thomas, S.G. (2011). Molecular Characterization of Rht-1 Dwarfing Genes in Hexaploid Wheat Plant Physiol. 157, 1820-1831.

Pedersen, C., van Themaat, E.V.L., McGuffin, L.J., Abbott, J.C., Burgis, T.A., Barton, G., Bindschedler, L.V., Lu, X., Maekawa, T., Weßling, R., Cramer, R., Thordal-Christensen, H., Panstruga, R., and Spanu, P.D. (2012). Structure and evolution of barley powdery mildew effector candidates. BMC Genomics 13, 694.

Pennington, H.G., Jones, R., Kwon, S., Bonciani, G., Thieron, H., Chandler, T., Luong, P., Morgan, S.N., Przydacz, M., Bozkurt, T., Bowden, S., Craze, M., Wallington, E.J., Garnett, J., Kwaaitaal, M., Panstruga, R., Cota, E., and Spanu, P.D. (2019). The fungal ribonuclease-like effector protein CSEP0064/BEC1054 represses plant immunity and interferes with degradation of host ribosomal RNA. PLoS Path. 15, e1007620.

Periyannan, S., Moore, J., Ayliffe, M., Bansal, U., Wang, X., Huang, L., Deal, K., Luo, M., Kong, X., Bariana, H., Mago, R., McIntosh, R., Dodds, P., Dvorak, J., and Lagudah, E. (2013). The Gene Sr33, an Ortholog of Barley Mla Genes, Encodes Resistance to Wheat Stem Rust Race Ug99. Science 341, 786-788.

Perry, G.H., Dominy, N.J., Claw, K.G., Lee, A.S., Fiegler, H., Redon, R., Werner, J., Villanea, F.A., Mountain, J.L., Misra, R., Carter, N.P., Lee, C., and Stone, A.C. (2007). Diet and the evolution of human amylase gene copy number variation. Nat. Genet. 39, 1256-1260.

Pettersen, E.F., Goddard, T.D., Huang, C.C., Meng, E.C., Couch, G.S., Croll, T.I., Morris, J.H., and Ferrin, T.E. (2021). UCSF ChimeraX: Structure visualization for researchers, educators, and developers. Protein Sci. 30, 70-82.

Ping, J., Fitzgerald, J.C., Zhang, C., Lin, F., Bai, Y., Wang, D., Aggarwal, R., Rehman, M., Crasta, O., and Ma, J. (2016). Identification and molecular mapping of Rps11, a novel gene conferring resistance to Phytophthora sojae in soybean. Theor. Appl. Genet. 129, 445-451.

Pottinger, S.E., and Innes, R.W. (2020). RPS5-Mediated Disease Resistance: Fundamental Insights and Translational Applications. Annu. Rev. Phytopathol. 58, 139-160.

Prigozhin, D.M., and Krasileva, K.V. (2021). Analysis of intraspecies diversity reveals a subset of highly variable plant immune receptors and predicts their binding sites. The Plant Cell 33, 998-1015.

Qi, D., and Innes, R. (2013). Recent Advances in Plant NLR Structure, Function, Localization, and Signaling. Frontiers in Immunology 4.

Qi, D., DeYoung, B.J., and Innes, R.W. (2012). Structure-Function Analysis of the Coiled-Coil and Leucine-Rich Repeat Domains of the RPS5 Disease Resistance Protein. Plant Physiol. 158, 1819.

Qi, T., Seong, K., Thomazella, D.P.T., Kim, J.R., Pham, J., Seo, E., Cho, M.-J., Schultink, A., and Staskawicz, B.J. (2018). NRG1 functions downstream of EDS1 to regulate TIR-NLR-mediated plant immunity in Nicotiana benthamiana. Proceedings of the National Academy of Sciences 115, E10979-E10987.

Qutob, D., Tedman-Jones, J., Dong, S., Kuflu, K., Pham, H., Wang, Y., Dou, D., Kale, S.D., Arredondo, F.D., Tyler, B.M., and Gijzen, M. (2009). Copy Number Variation and Transcriptional Polymorphisms of Phytophthora sojae RXLR Effector Genes Avr1a and Avr3a. PLOS ONE 4, e5066.

Rairdan, G.J., Collier, S.M., Sacco, M.A., Baldwin, T.T., Boettrich, T., and Moffett, P. (2008). The Coiled-Coil and Nucleotide Binding Domains of the Potato Rx Disease Resistance Protein Function in Pathogen Recognition and Signaling The Plant Cell 20, 739-751.

Ravensdale, M., Bernoux, M., Ve, T., Kobe, B., Thrall, P., Ellis, J., and Dodds, P. (2012). Intramolecular Interaction Influences Binding of the Flax L5 and L6 Resistance Proteins to their AvrL567 Ligands. PLoS Path. 8, e1003004.

Risk, J.M., Selter, L.L., Chauhan, H., Krattinger, S.G., Kumlehn, J., Hensel, G., Viccars, L.A., Richardson, T.M., Buesing, G., Troller, A., Lagudah, E.S., and Keller, B. (2013). The wheat Lr34 gene provides resistance against multiple fungal pathogens in barley. Plant Biotechnol. J. 11, 847-854.

Robinson, J.T., Thorvaldsdóttir, H., Winckler, W., Guttman, M., Lander, E.S., Getz, G., and Mesirov, J.P. (2011). Integrative genomics viewer. Nat. Biotechnol. 29, 24-26.

Rocafort, M., Bowen, J.K., Hassing, B., Cox, M.P., McGreal, B., de la Rosa, S., Plummer, K.M., Bradshaw, R.E., and Mesarich, C.H. (2022). The Venturia inaequalis effector repertoire is dominated by expanded families with predicted structural similarity, but

unrelated sequence, to avirulence proteins from other plant-pathogenic fungi. BMC Biol. 20, 246.

Rossi, M., Goggin, F.L., Milligan, S.B., Kaloshian, I., Ullman, D.E., and Williamson, V.M. (1998). The nematode resistance gene Mi of tomato confers resistance against the potato aphid. Proceedings of the National Academy of Sciences 95, 9750-9754.

Sacco, M.A., Mansoor, S., and Moffett, P. (2007). A RanGAP protein physically interacts with the NB-LRR protein Rx, and is required for Rx-mediated viral resistance. The Plant Journal 52, 82-93.

Saile, S.C., Jacob, P., Castel, B., Jubic, L.M., Salas-Gonzáles, I., Bäcker, M., Jones, J.D.G., Dangl, J.L., and El Kasmi, F. (2020). Two unequally redundant "helper" immune receptor families mediate Arabidopsis thaliana intracellular "sensor" immune receptor functions. PLoS Biol. 18, e3000783.

Sánchez-Vallet, A., Fouché, S., Fudal, I., Hartmann, F.E., Soyer, J.L., Tellier, A., and Croll, D. (2018). The Genome Biology of Effector Gene Evolution in Filamentous Plant Pathogens. Annu. Rev. Phytopathol. 56, 21-40.

Sarris, P.F., Cevik, V., Dagdas, G., Jones, J.D.G., and Krasileva, K.V. (2016). Comparative analysis of plant immune receptor architectures uncovers host proteins likely targeted by pathogens. BMC Biol. 14, 8.

Sarris, P.F., Duxbury, Z., Huh, S.U., Ma, Y., Segonzac, C., Sklenar, J., Derbyshire, P., Cevik, V., Rallapalli, G., Saucet, S.B., Wirthmueller, L., Menke, F.L.H., Sohn, K.H., and Jones, J.D.G. (2015). A Plant Immune Receptor Detects Pathogen Effectors that Target WRKY Transcription Factors. Cell 161, 1089-1100.

Sato, K., Inukai, T., and Hayes, P.M. (2001). QTL analysis of resistance to the rice blast pathogen in barley (Hordeum vulgare). Theor. Appl. Genet. 102, 916-920.

Saur, I.M.L., Panstruga, R., and Schulze-Lefert, P. (2021). NOD-like receptor-mediated plant immunity: from structure to cell death. Nature Reviews Immunology 21, 305-318.

Saur, I.M.L., Bauer, S., Kracher, B., Lu, X., Franzeskakis, L., Müller, M.C., Sabelleck, B., Kümmel, F., Panstruga, R., Maekawa, T., and Schulze-Lefert, P. (2019). Multiple pairs of allelic MLA immune receptor-powdery mildew AVRA effectors argue for a direct recognition mechanism. eLife 8, e44471.

Saxena, R.K., Edwards, D., and Varshney, R.K. (2014). Structural variations in plant genomes. Briefings in Functional Genomics 13, 296-307.

Schnable, P.S., Ware, D., Fulton, R.S., Stein, J.C., Wei, F., Pasternak, S., Liang, C., Zhang, J., Fulton, L., Graves, T.A., Minx, P., Reily, A.D., Courtney, L., Kruchowski, S.S., Tomlinson, C., Strong, C., Delehaunty, K., Fronick, C., Courtney, B., Rock, S.M., Belter, E., Du, F., Kim, K., Abbott, R.M., Cotton, M., Levy, A., Marchetto, P., Ochoa, K., Jackson, S.M., Gillam, B., Chen, W., Yan, L., Higginbotham, J., Cardenas, M., Waligorski, J., Applebaum, E., Phelps, L., Falcone, J., Kanchi, K., Thane, T., Scimone, A., Thane, N., Henke, J., Wang, T., Ruppert, J., Shah, N., Rotter, K.,

Hodges, J., Ingenthron, E., Cordes, M., Kohlberg, S., Sgro, J., Delgado, B., Mead, K., Chinwalla, A., Leonard, S., Crouse, K., Collura, K., Kudrna, D., Currie, J., He, R., Angelova, A., Rajasekar, S., Mueller, T., Lomeli, R., Scara, G., Ko, A., Delaney, K., Wissotski, M., Lopez, G., Campos, D., Braidotti, M., Ashley, E., Golser, W., Kim, H., Lee, S., Lin, J., Dujmic, Z., Kim, W., Talag, J., Zuccolo, A., Fan, C., Sebastian, A., Kramer, M., Spiegel, L., Nascimento, L., Zutavern, T., Miller, B., Ambroise, C., Muller, S., Spooner, W., Narechania, A., Ren, L., Wei, S., Kumari, S., Faga, B., Levy, M.J., McMahan, L., Van Buren, P., Vaughn, M.W., Ying, K., Yeh, C.-T., Emrich, S.J., Jia, Y., Kalyanaraman, A., Hsia, A.-P., Barbazuk, W.B., Baucom, R.S., Brutnell, T.P., Carpita, N.C., Chaparro, C., Chia, J.-M., Deragon, J.-M., Estill, J.C., Fu, Y., Jeddeloh, J.A., Han, Y., Lee, H., Li, P., Lisch, D.R., Liu, S., Liu, Z., Nagel, D.H., McCann, M.C., SanMiguel, P., Myers, A.M., Nettleton, D., Nguyen, J., Penning, B.W., Ponnala, L., Schneider, K.L., Schwartz, D.C., Sharma, A., Soderlund, C., Springer, N.M., Sun, Q., Wang, H., Waterman, M., Westerman, R., Wolfgruber, T.K., Yang, L., Yu, Y., Zhang, L., Zhou, S., Zhu, Q., Bennetzen, J.L., Dawe, R.K., Jiang, J., Jiang, N., Presting, G.G., Wessler, S.R., Aluru, S., Martienssen, R.A., Clifton, S.W., McCombie, W.R., Wing, R.A., and Wilson, R.K. (2009). The B73 Maize Genome: Complexity, Diversity, and Dynamics. Science 326, 1112-1115.

Schnippenkoetter, W., Lo, C., Liu, G.Q., Dibley, K., Chan, W.L., White, J., Milne, R., Zwart, A., Kwong, E., Keller, B., Godwin, I., Krattinger, S.G., and Lagudah, E. (2017). The wheat Lr34 multipathogen resistance gene confers resistance to anthracnose and rust in sorghum. Plant Biotechnol. J. 15, 1387-1396.

Schultink, A., Qi, T., Lee, A., Steinbrenner, A.D., and Staskawicz, B. (2017). Roq1 mediates recognition of the Xanthomonas and Pseudomonas effector proteins XopQ and HopQ1. The Plant Journal 92, 787-795.

Schwessinger, B., and Rathjen, J.P. (2017). Extraction of high molecular weight DNA from fungal rust spores for long read sequencing. In Wheat rust diseases (Springer), pp. 49-57.

Seeholzer, S., Tsuchimatsu, T., Jordan, T., Bieri, S., Pajonk, S., Yang, W., Jahoor, A., Shimizu, K.K., Keller, B., and Schulze-Lefert, P. (2010). Diversity at the Mla Powdery Mildew Resistance Locus from Cultivated Barley Reveals Sites of Positive Selection. Mol. Plant-Microbe Interact. 23, 497-509.

Segretin, M.E., Pais, M., Franceschetti, M., Chaparro-Garcia, A., Bos, J.I.B., Banfield, M.J., and Kamoun, S. (2014). Single Amino Acid Mutations in the Potato Immune Receptor R3a Expand Response to Phytophthora Effectors. Molecular Plant-Microbe Interactions® 27, 624-637.

Seo, E., Kim, S., Yeom, S.-I., and Choi, D. (2016). Genome-Wide Comparative Analyses Reveal the Dynamic Evolution of Nucleotide-Binding Leucine-Rich Repeat Gene Family among Solanaceae Plants. Frontiers in Plant Science 7.

Seong, K., and Krasileva, K.V. (2023). Prediction of effector protein structures from fungal phytopathogens enables evolutionary analyses. Nature Microbiology 8, 174-187.

Serrano, M., Coluccia, F., Torres, M., L'Haridon, F., and Métraux, J.-P. (2014). The cuticle and plant defense to pathogens. Frontiers in Plant Science 5.

Seto, D., Koulena, N., Lo, T., Menna, A., Guttman, D.S., and Desveaux, D. (2017). Expanded type III effector recognition by the ZAR1 NLR protein using ZED1-related kinases. Nature Plants 3, 17027.

Shao, Z.-Q., Xue, J.-Y., Wu, P., Zhang, Y.-M., Wu, Y., Hang, Y.-Y., Wang, B., and Chen, J.-Q. (2016). Large-Scale Analyses of Angiosperm Nucleotide-Binding Site-Leucine-Rich Repeat Genes Reveal Three Anciently Diverged Classes with Distinct Evolutionary Patterns. Plant Physiol. 170, 2095-2109.

Shen, Q.-H., Zhou, F., Bieri, S., Haizel, T., Shirasu, K., and Schulze-Lefert, P. (2003). Recognition Specificity and RAR1/SGT1 Dependence in Barley Mla Disease Resistance Genes to the Powdery Mildew Fungus. The Plant Cell 15, 732-744.

Shimizu, M., Hirabuchi, A., Sugihara, Y., Abe, A., Takeda, T., Kobayashi, M., Hiraka, Y., Kanzaki, E., Oikawa, K., Saitoh, H., Langner, T., Banfield, M.J., Kamoun, S., and Terauchi, R. (2022). A genetically linked pair of NLR immune receptors shows contrasting patterns of evolution. Proceedings of the National Academy of Sciences 119, e2116896119.

Singh, R.P. (1992). Association between gene Lr34 for leaf rust resistance and leaf tip necrosis in wheat. Crop Sci. 32, 874-878.

Slootweg, E.J., Spiridon, L.N., Roosien, J., Butterbach, P., Pomp, R., Westerhof, L., Wilbers, R., Bakker, E., Bakker, J., Petrescu, A.-J., Smant, G., and Goverse, A. (2013). Structural Determinants at the Interface of the ARC2 and Leucine-Rich Repeat Domains Control the Activation of the Plant Immune Receptors Rx1 and Gpa2 Plant Physiol. 162, 1510-1528.

Spanu, P.D. (2017). Cereal immunity against powdery mildews targets RNase-Like Proteins associated with Haustoria (RALPH) effectors evolved from a common ancestral gene. New Phytol. 213, 969-971.

Spielmeyer, W., McIntosh, R.A., Kolmer, J., and Lagudah, E.S. (2005). Powdery mildew resistance and Lr34/Yr18 genes for durable resistance to leaf and stripe rust cosegregate at a locus on the short arm of chromosome 7D of wheat. Theor. Appl. Genet. 111, 731-735.

Spielmeyer, W., Mago, R., Wellings, C., and Ayliffe, M. (2013). Lr67 and Lr34rust resistance genes have much in common – they confer broad spectrum resistance to multiple pathogens in wheat. BMC Plant Biol. 13, 96.

Springer, N.M., Ying, K., Fu, Y., Ji, T., Yeh, C.-T., Jia, Y., Wu, W., Richmond, T., Kitzman, J., Rosenbaum, H., Iniguez, A.L., Barbazuk, W.B., Jeddeloh, J.A., Nettleton, D., and Schnable, P.S. (2009). Maize Inbreds Exhibit High Levels of Copy Number Variation (CNV) and Presence/Absence Variation (PAV) in Genome Content. PLoS Genet. 5, e1000734.

Srichumpa, P., Brunner, S., Keller, B., and Yahiaoui, N. (2005). Allelic Series of Four Powdery Mildew Resistance Genes at the Pm3 Locus in Hexaploid Bread Wheat. Plant Physiol. 139, 885-895.

Steinbrenner, A.D., Goritschnig, S., and Staskawicz, B.J. (2015). Recognition and Activation Domains Contribute to Allele-Specific Responses of an Arabidopsis NLR Receptor to an Oomycete Effector Protein. PLoS Path. 11, e1004665.

Stirnweis, D., Milani, S.D., Jordan, T., Keller, B., and Brunner, S. (2013). Substitutions of Two Amino Acids in the Nucleotide-Binding Site Domain of a Resistance Protein Enhance the Hypersensitive Response and Enlarge the PM3F Resistance Spectrum in Wheat. Molecular Plant-Microbe Interactions® 27, 265-276.

Stranger, B.E., Forrest, M.S., Dunning, M., Ingle, C.E., Beazley, C., Thorne, N., Redon, R., Bird, C.P., de Grassi, A., Lee, C., Tyler-Smith, C., Carter, N., Scherer, S.W., Tavaré, S., Deloukas, P., Hurles, M.E., and Dermitzakis, E.T. (2007). Relative Impact of Nucleotide and Copy Number Variation on Gene Expression Phenotypes. Science 315, 848-853.

Studier, F.W. (2005). Protein production by auto-induction in high-density shaking cultures. Protein Expression Purif. 41, 207-234.

Sucher, J., Boni, R., Yang, P., Rogowsky, P., Buchner, H., Kastner, C., Kumlehn, J., Krattinger, S.G., and Keller, B. (2017). The durable wheat disease resistance gene Lr34 confers common rust and northern corn leaf blight resistance in maize. Plant Biotechnol. J. 15, 489-496.

Sugihara, Y., Abe, Y., Takagi, H., Abe, A., Shimizu, M., Ito, K., Kanzaki, E., Oikawa, K., Kourelis, J., Langner, T., Win, J., Białas, A., Lüdke, D., Contreras, M.P., Chuma, I., Saitoh, H., Kobayashi, M., Zheng, S., Tosa, Y., Banfield, M.J., Kamoun, S., Terauchi, R., and Fujisaki, K. (2023). Disentangling the complex gene interaction networks between rice and the blast fungus identifies a new pathogen effector. PLoS Biol. 21, e3001945.

Sun, X., Lapin, D., Feehan, J.M., Stolze, S.C., Kramer, K., Dongus, J.A., Rzemieniewski, J., Blanvillain-Baufumé, S., Harzen, A., Bautor, J., Derbyshire, P., Menke, F.L.H., Finkemeier, I., Nakagami, H., Jones, J.D.G., and Parker, J.E. (2021). Pathogen effector recognition-dependent association of NRG1 with EDS1 and SAG101 in TNL receptor immunity. Nature Communications 12, 3335.

Sweat, T.A., and Wolpert, T.J. (2007). Thioredoxin h5 is required for victorin sensitivity mediated by a CC-NBS-LRR gene in Arabidopsis. Plant Cell 19, 673-687.

Sweigard, J.A., Carroll, A.M., Kang, S., Farrall, L., Chumley, F.G., and Valent, B. (1995). Identification, cloning, and characterization of PWL2, a gene for host species specificity in the rice blast fungus. The Plant Cell 7, 1221-1233.

Swiderski, M.R., and Innes, R.W. (2001). The Arabidopsis PBS1 resistance gene encodes a member of a novel protein kinase subfamily. Plant J. 26, 101-112.

Swiderski, M.R., Birker, D., and Jones, J.D.G. (2009). The TIR Domain of TIR-NB-LRR Resistance Proteins Is a Signaling Domain Involved in Cell Death Induction. Molecular Plant-Microbe Interactions® 22, 157-165.

Takabayashi, N., Tosa, Y., Oh, H.S., and Mayama, S. (2002). A Gene-for-Gene Relationship Underlying the Species-Specific Parasitism of Avena/Triticum Isolates of Magnaporthe grisea on Wheat Cultivars. Phytopathology 92, 1182-1188.

Takken, F.L.W., Albrecht, M., and Tameling, W.I.L. (2006). Resistance proteins: molecular switches of plant defence. Curr. Opin. Plant Biol. 9, 383-390.

Talbot, N.J., Ebbole, D.J., and Hamer, J.E. (1993). Identification and characterization of MPG1, a gene involved in pathogenicity from the rice blast fungus Magnaporthe grisea. The Plant Cell 5, 1575-1590.

Tamborski, J., and Krasileva, K.V. (2020). Evolution of Plant NLRs: From Natural History to Precise Modifications. Annu. Rev. Plant Biol. 71, 355-378.

Tamborski, J., Seong, K., Liu, F., Staskawicz, B., and Krasileva, K.V. (2022). Engineering of Sr33 and Sr50 plant immune receptors to alter recognition specificity and autoactivity. bioRxiv, 2022.2003.2005.483131.

Tameling, W.I.L., Elzinga, S.D.J., Darmin, P.S., Vossen, J.H., Takken, F.L.W., Haring, M.A., and Cornelissen, B.J.C. (2002). The Tomato R Gene Products I-2 and Mi-1 Are Functional ATP Binding Proteins with ATPase Activity. The Plant Cell 14, 2929-2939.

Tameling, W.I.L., Vossen, J.H., Albrecht, M., Lengauer, T., Berden, J.A., Haring, M.A., Cornelissen, B.J.C., and Takken, F.L.W. (2006). Mutations in the NB-ARC Domain of I-2 That Impair ATP Hydrolysis Cause Autoactivation. Plant Physiol. 140, 1233-1245.

Tang, D., Wang, G., and Zhou, J.-M. (2017). Receptor Kinases in Plant-Pathogen Interactions: More Than Pattern Recognition. The Plant Cell 29, 618-637.

Tarr, D.E.K., and Alexander, H.M. (2009). TIR-NBS-LRR genes are rare in monocots: evidence from diverse monocot orders. BMC Research Notes 2, 197.

Tasset, C., Bernoux, M., Jauneau, A., Pouzet, C., Brière, C., Kieffer-Jacquinod, S., Rivas, S., Marco, Y., and Deslandes, L. (2010). Autoacetylation of the Ralstonia solanacearum Effector PopP2 Targets a Lysine Residue Essential for RRS1-R-Mediated Immunity in Arabidopsis. PLoS Path. 6, e1001202.

Thomas, N.C., Hendrich, C.G., Gill, U.S., Allen, C., Hutton, S.F., and Schultink, A. (2020). The Immune Receptor Roq1 Confers Resistance to the Bacterial Pathogens Xanthomonas, Pseudomonas syringae, and Ralstonia in Tomato. Frontiers in Plant Science 11.

Thordal-Christensen, H., Gregersen, P., and Collinge, D. (2000). The barley/ Blumeria (syn. Erysiphe) graminis interaction: a case study, pp. 77-100.

Thordal-Christensen, H., Birch, P.R.J., Spanu, P.D., and Panstruga, R. (2018). Why did filamentous plant pathogens evolve the potential to secrete hundreds of effectors to enable disease? Mol. Plant Pathol. 19, 781-785.

Tian, D., Traw, M.B., Chen, J.Q., Kreitman, M., and Bergelson, J. (2003). Fitness costs of R-gene-mediated resistance in Arabidopsis thaliana. Nature 423, 74-77.

Tian, H., Wu, Z., Chen, S., Ao, K., Huang, W., Yaghmaiean, H., Sun, T., Xu, F., Zhang, Y., Wang, S., Li, X., and Zhang, Y. (2021). Activation of TIR signalling boosts pattern-triggered immunity. Nature 598, 500-503.

Tosa, Y., Tamba, H., Tanaka, K., and Mayama, S. (2006). Genetic Analysis of Host Species Specificity of Magnaporthe oryzae Isolates from Rice and Wheat. Phytopathology 96, 480-484.

Tosa, Y., Osue, J., Eto, Y., Oh, H.-S., Nakayashiki, H., Mayama, S., and Leong, S.A. (2005). Evolution of an Avirulence Gene, AVR1-CO39, Concomitant with the Evolution and Differentiation of Magnaporthe oryzae. Molecular Plant-Microbe Interactions® 18, 1148-1160.

Uehling, J., Deveau, A., and Paoletti, M. (2017). Do fungi have an innate immune response? An NLR-based comparison to plant and animal immune systems. PLoS Path. 13, e1006578.

Upson, J.L., Zess, E.K., Białas, A., Wu, C.-h., and Kamoun, S. (2018). The coming of age of EvoMPMI: evolutionary molecular plant–microbe interactions across multiple timescales. Curr. Opin. Plant Biol. 44, 108-116.

Van de Weyer, A.-L., Monteiro, F., Furzer, O.J., Nishimura, M.T., Cevik, V., Witek, K., Jones, J.D.G., Dangl, J.L., Weigel, D., and Bemm, F. (2019). A Species-Wide Inventory of NLR Genes and Alleles in Arabidopsis thaliana. Cell 178, 1260-1272.e1214.

van der Hoorn, R.A.L., and Kamoun, S. (2008). From Guard to Decoy: A new model for perception of plant pathogen effectors. Plant Cell 20, 2009-2017.

van Ooijen, G., Mayr, G., Kasiem, M.M.A., Albrecht, M., Cornelissen, B.J.C., and Takken, F.L.W. (2008). Structure–function analysis of the NB-ARC domain of plant disease resistance proteins. J. Exp. Bot. 59, 1383-1397.

van Wersch, S., Tian, L., Hoy, R., and Li, X. (2020). Plant NLRs: The Whistleblowers of Plant Immunity. Plant Communications 1, 100016.

Vance, R.E. (2015). The NAIP/NLRC4 inflammasomes. Curr. Opin. Immunol. 32, 84-89.

Vanegas, C.D.G., Garvin, D.F., and Kolmer, J.A. (2008). Genetics of stem rust resistance in the spring wheat cultivar Thatcher and the enhancement of stem rust resistance by Lr34. Euphytica 159, 391-401.

Vogel, J.P., Garvin, D.F., Mockler, T.C., Schmutz, J., Rokhsar, D., Bevan, M.W., Barry, K., Lucas, S., Harmon-Smith, M., Lail, K., Tice, H., Schmutz, J., Grimwood, J., McKenzie, N., Bevan, M.W., Huo, N., Gu, Y.Q., Lazo, G.R., Anderson, O.D.,

Vogel, J.P., You, F.M., Luo, M.-C., Dvorak, J., Wright, J., Febrer, M., Bevan, M.W., Idziak, D., Hasterok, R., Garvin, D.F., Lindquist, E., Wang, M., Fox, S.E., Priest, H.D., Filichkin, S.A., Givan, S.A., Bryant, D.W., Chang, J.H., Mockler, T.C., Wu, H., Wu, W., Hsia, A.-P., Schnable, P.S., Kalyanaraman, A., Barbazuk, B., Michael, T.P., Hazen, S.P., Bragg, J.N., Laudencia-Chingcuanco, D., Vogel, J.P., Garvin, D.F., Weng, Y., McKenzie, N., Bevan, M.W., Haberer, G., Spannagl, M., Mayer, K., Rattei, T., Mitros, T., Rokhsar, D., Lee, S.-J., Rose, J.K.C., Mueller, L.A., York, T.L., Wicker, T., Buchmann, J.P., Tanskanen, J., Schulman, A.H., Gundlach, H., Wright, J., Bevan, M., Costa de Oliveira, A., da C. Maia, L., Belknap, W., Gu, Y.Q., Jiang, N., Lai, J., Zhu, L., Ma, J., Sun, C., Pritham, E., Salse, J., Murat, F., Abrouk, M., Haberer, G., Spannagl, M., Mayer, K., Bruggmann, R., Messing, J., You, F.M., Luo, M.-C., Dvorak, J., Fahlgren, N., Fox, S.E., Sullivan, C.M., Mockler, T.C., Carrington, J.C., Chapman, E.J., May, G.D., Zhai, J., Ganssmann, M., Guna Ranjan Gurazada, S., German, M., Meyers, B.C., Green, P.J., Bragg, J.N., Tyler, L., Wu, J., Gu, Y.Q., Lazo, G.R., Laudencia-Chingcuanco, D., Thomson, J., Vogel, J.P., Hazen, S.P., Chen, S., Scheller, H.V., Harholt, J., Ulvskov, P., Fox, S.E., Filichkin, S.A., Fahlgren, N., Kimbrel, J.A., Chang, J.H., Sullivan, C.M., Chapman, E.J., Carrington, J.C., Mockler, T.C., Bartley, L.E., Cao, P., Jung, K.-H., Sharma, M.K., Vega-Sanchez, M., Ronald, P., Dardick, C.D., De Bodt, S., Verelst, W., Inzé, D., Heese, M., Schnittger, A., Yang, X., Kalluri, U.C., Tuskan, G.A., Hua, Z., Vierstra, R.D., Garvin, D.F., Cui, Y., Ouyang, S., Sun, Q., Liu, Z., Yilmaz, A., Grotewold, E., Sibout, R., Hematy, K., Mouille, G., Höfte, H., Michael, T., Pelloux, J., O'Connor, D., Schnable, J., Rowe, S., Harmon, F., Cass, C.L., Sedbrook, J.C., Byrne, M.E., Walsh, S., Higgins, J., Bevan, M., Li, P., Brutnell, T., Unver, T., Budak, H., Belcram, H., Charles, M., Chalhoub, B., Baxter, I., The International Brachypodium, I., Principal, i., sequencing, D.N.A., assembly, Pseudomolecule, a., sequencing, B.A.C.e., Transcriptome, s., analysis, Gene, a., annotation, Repeats, a., Comparative, g., Small, R.N.A.a., Manual, a., and gene family, a. (2010). Genome sequencing and analysis of the model grass Brachypodium distachyon. Nature 463, 763-768.

Vos, P., Simons, G., Jesse, T., Wijbrandi, J., Heinen, L., Hogers, R., Frijters, A., Groenendijk, J., Diergaarde, P., Reijans, M., Fierens-Onstenk, J., Both, M.d., Peleman, J., Liharska, T., Hontelez, J., and Zabeau, M. (1998). The tomato Mi-1 gene confers resistance to both root-knot nematodes and potato aphids. Nat. Biotechnol. 16, 1365-1369.

Wagner, S., Stuttmann, J., Rietz, S., Guerois, R., Brunstein, E., Bautor, J., Niefind, K., and Parker, Jane E. (2013). Structural Basis for Signaling by Exclusive EDS1 Heteromeric Complexes with SAG101 or PAD4 in Plant Innate Immunity. Cell Host & Microbe 14, 619-630.

Walker, B.J., Abeel, T., Shea, T., Priest, M., Abouelliel, A., Sakthikumar, S., Cuomo, C.A., Zeng, Q., Wortman, J., Young, S.K., and Earl, A.M. (2014). Pilon: An Integrated Tool for Comprehensive Microbial Variant Detection and Genome Assembly Improvement. PLOS ONE 9, e112963.

Wan, L., Essuman, K., Anderson, R.G., Sasaki, Y., Monteiro, F., Chung, E.-H., Osborne Nishimura, E., DiAntonio, A., Milbrandt, J., Dangl, J.L., and Nishimura, M.T. (2019). TIR domains of plant immune receptors are NAD+-cleaving enzymes that promote cell death. Science 365, 799-803.

Wang, G., Roux, B., Feng, F., Guy, E., Li, L., Li, N., Zhang, X., Lautier, M., Jardinaud, M.-F., Chabannes, M., Arlat, M., Chen, S., He, C., Noël, Laurent D., and Zhou, J.-M. (2015). The Decoy Substrate of a Pathogen Effector and a Pseudokinase Specify Pathogen-Induced Modified-Self Recognition and Immunity in Plants. Cell Host & Microbe 18, 285-295.

Wang, J., Hu, M., Wang, J., Qi, J., Han, Z., Wang, G., Qi, Y., Wang, H.-W., Zhou, J.-M., and Chai, J. (2019a). Reconstitution and structure of a plant NLR resistosome conferring immunity. Science 364, eaav5870.

Wang, J., Wang, J., Hu, M., Wu, S., Qi, J., Wang, G., Han, Z., Qi, Y., Gao, N., Wang, H.-W., Zhou, J.-M., and Chai, J. (2019b). Ligand-triggered allosteric ADP release primes a plant NLR complex. Science 364, eaav5868.

Wang, J., Chen, T., Han, M., Qian, L., Li, J., Wu, M., Han, T., Cao, J., Nagalakshmi, U., Rathjen, J.P., Hong, Y., and Liu, Y. (2020). Plant NLR immune receptor Tm-22 activation requires NB-ARC domain-mediated self-association of CC domain. PLoS Path. 16, e1008475.

Wang, S., Li, W., Liu, S., and Xu, J. (2016). RaptorX-Property: a web server for protein structure property prediction. Nucleic Acids Res. 44, W430-W435.

Wang, W., Chen, L., Fengler, K., Bolar, J., Llaca, V., Wang, X., Clark, C.B., Fleury, T.J., Myrvold, J., Oneal, D., van Dyk, M.M., Hudson, A., Munkvold, J., Baumgarten, A., Thompson, J., Cai, G., Crasta, O., Aggarwal, R., and Ma, J. (2021). A giant NLR gene confers broad-spectrum resistance to Phytophthora sojae in soybean. Nature Communications 12, 6263.

Waterhouse, R.M., Seppey, M., Simão, F.A., Manni, M., Ioannidis, P., Klioutchnikov, G., Kriventseva, E.V., and Zdobnov, E.M. (2018). BUSCO Applications from Quality Assessments to Gene Prediction and Phylogenomics. Mol Biol Evol 35, 543-548.

Weber, E., Engler, C., Gruetzner, R., Werner, S., and Marillonnet, S. (2011). A Modular Cloning System for Standardized Assembly of Multigene Constructs. PLOS ONE 6, e16765.

Wei, F., Wing, R.A., and Wise, R.P. (2002). Genome Dynamics and Evolution of the Mla (Powdery Mildew) Resistance Locus in Barley. The Plant Cell 14, 1903-1917.

Wei, F., Gobelman-Werner, K., Morroll, S.M., Kurth, J., Mao, L., Wing, R., Leister, D., Schulze-Lefert, P., and Wise, R.P. (1999). The Mla (Powdery Mildew) Resistance Cluster Is Associated With Three NBS-LRR Gene Families and Suppressed Recombination Within a 240-kb DNA Interval on Chromosome 5S (1HS) of Barley. Genetics 153, 1929-1948.

Welsh, J.N., Peturson, B., and Machacek, J.E. (1954). Associated inheritance of reaction to races of crown rust, *Puccinia coronata avenae* erikss., and to victoria blight, *Helminthosporium victoriae* m. and m., in oats. Canadian Journal of Botany 32, 55-68.

Were, V.M. (2018). Investigating the role of effector proteins in the rice blast fungus Magnaporthe oryzae. In College of Life and Environmental Sciences (University of Exeter).

Wicker, T., Oberhaensli, S., Parlange, F., Buchmann, J.P., Shatalina, M., Roffler, S., Ben-David, R., Doležel, J., Šimková, H., Schulze-Lefert, P., Spanu, P.D., Bruggmann, R., Amselem, J., Quesneville, H., Ver Loren van Themaat, E., Paape, T., Shimizu, K.K., and Keller, B. (2013). The wheat powdery mildew genome shows the unique evolution of an obligate biotroph. Nat. Genet. 45, 1092.

Williams, S.J., Sornaraj, P., deCourcy-Ireland, E., Menz, R.I., Kobe, B., Ellis, J.G., Dodds, P.N., and Anderson, P.A. (2011). An Autoactive Mutant of the M Flax Rust Resistance Protein Has a Preference for Binding ATP, Whereas Wild-Type M Protein Binds ADP. Molecular Plant-Microbe Interactions® 24, 897-906.

Williams, S.J., Sohn, K.H., Wan, L., Bernoux, M., Sarris, P.F., Segonzac, C., Ve, T., Ma, Y., Saucet, S.B., Ericsson, D.J., Casey, L.W., Lonhienne, T., Winzor, D.J., Zhang, X., Coerdt, A., Parker, J.E., Dodds, P.N., Kobe, B., and Jones, J.D.G. (2014). Structural Basis for Assembly and Function of a Heterodimeric Plant Immune Receptor. Science 344, 299-303.

Win, J., Kamoun, S., and Jones, A.M.E. (2011). Purification of Effector–Target Protein Complexes via Transient Expression in Nicotiana benthamiana. In Plant Immunity: Methods and Protocols, J.M. McDowell, ed (Totowa, NJ: Humana Press), pp. 181-194.

Win, J., Chaparro-Garcia, A., Belhaj, K., Saunders, D.G., Yoshida, K., Dong, S., Schornack, S., Zipfel, C., Robatzek, S., Hogenhout, S.A., and Kamoun, S. (2012). Effector biology of plant-associated organisms: concepts and perspectives. Cold Spring Harb Symp Quant Biol 77, 235-247.

Wingen, L.U., Münster, T., Faigl, W., Deleu, W., Sommer, H., Saedler, H., and Theißen, G. (2012). Molecular genetic basis of pod corn (Tunicate maize). Proceedings of the National Academy of Sciences 109, 7115-7120.

Wolpert, T.J., and Lorang, J.M. (2016). Victoria Blight, defense turned upside down. Physiol. Mol. Plant Pathol. 95, 8-13.

Wu, C.-H., Abd-El-Haliem, A., Bozkurt, T.O., Belhaj, K., Terauchi, R., Vossen, J.H., and Kamoun, S. (2017). NLR network mediates immunity to diverse plant pathogens. Proceedings of the National Academy of Sciences 114, 8113-8118.

Wu, Z., Li, M., Dong, O.X., Xia, S., Liang, W., Bao, Y., Wasteneys, G., and Li, X. (2019). Differential regulation of TNL-mediated immune signaling by redundant helper CNLs. New Phytol. 222, 938-953.

Wyand, R.A., and Brown, J.K. (2003). Genetic and forma specialis diversity in Blumeria graminis of cereals and its implications for host-pathogen co-evolution. Mol. Plant Pathol. 4, 187-198.

Yaegashi, H. (1988). Inheritance of blast resistance in two-rowed barley. Plant Dis. 72, 608-610.

Yan, X., Tang, B., Ryder, L.S., MacLean, D., Were, V.M., Eseola, A.B., Cruz-Mireles, N., Ma, W., Foster, A.J., Osés-Ruiz, M., and Talbot, N.J. (2023). The transcriptional landscape of plant infection by the rice blast fungus Magnaporthe oryzae reveals distinct families of temporally co-regulated and structurally conserved effectors. The Plant Cell, koad036.

Yoshida, K., Saunders, D.G.O., Mitsuoka, C., Natsume, S., Kosugi, S., Saitoh, H., Inoue, Y., Chuma, I., Tosa, Y., Cano, L.M., Kamoun, S., and Terauchi, R. (2016). Host specialization of the blast fungus Magnaporthe oryzae is associated with dynamic gain and loss of genes linked to transposable elements. BMC Genomics 17, 370.

Yu, D.S., Outram, M.A., Smith, A., McCombe, C.L., Khambalkar, P.B., Rima, S.A., Sun, X., Ma, L., Ericsson, D.J., Jones, D.A., and Williams, S.J. (2022). The structural repertoire of Fusarium oxysporum f. sp. lycopersici effectors revealed by experimental and computational studies. bioRxiv, 2021.2012.2014.472499.

Yu, P., Wang, C., Xu, Q., Feng, Y., Yuan, X., Yu, H., Wang, Y., Tang, S., and Wei, X. (2011). Detection of copy number variations in rice using array-based comparative genomic hybridization. BMC Genomics 12, 372.

Yuan, M., Ngou, B.P.M., Ding, P., and Xin, X.-F. (2021a). PTI-ETI crosstalk: an integrative view of plant immunity. Curr. Opin. Plant Biol. 62, 102030.

Yuan, M., Jiang, Z., Bi, G., Nomura, K., Liu, M., Wang, Y., Cai, B., Zhou, J.-M., He, S.Y., and Xin, X.-F. (2021b). Pattern-recognition receptors are required for NLR-mediated plant immunity. Nature 592, 105-109.

Zdrzalek, R. (2021). Exploring the potential of a rice NLR pair to engineer novel effector recognition specificities ([Great Britain]: University of East Anglia).

Zdrzałek, R., Kamoun, S., Terauchi, R., Saitoh, H., and Banfield, M.J. (2020). The rice NLR pair Pikp-1/Pikp-2 initiates cell death through receptor cooperation rather than negative regulation. PLOS ONE 15, e0238616.

Zhang, S., and Xu, J.-R. (2014). Effectors and Effector Delivery in Magnaporthe oryzae. PLoS Path. 10, e1003826.

Zhang, Z.-M., Ma, K.-W., Gao, L., Hu, Z., Schwizer, S., Ma, W., and Song, J. (2017). Mechanism of host substrate acetylation by a YopJ family effector. Nature Plants 3, 17115.

Zhao, Y.-B., Liu, M.-X., Chen, T.-T., Ma, X., Li, Z.-K., Zheng, Z., Zheng, S.-R., Chen, L., Li, Y.-Z., Tang, L.-R., Chen, Q., Wang, P., and Ouyang, S. (2022). Pathogen effector AvrSr35 triggers Sr35 resistosome assembly via a direct recognition mechanism. Science Advances 8, eabq5108.

Zheng, L.-Y., Guo, X.-S., He, B., Sun, L.-J., Peng, Y., Dong, S.-S., Liu, T.-F., Jiang, S., Ramachandran, S., Liu, C.-M., and Jing, H.-C. (2011). Genome-wide patterns of genetic variation in sweet and grain sorghum (Sorghum bicolor). Genome Biology 12, R114.

Zheng, Y., Zheng, W., Lin, F., Zhang, Y., Yi, Y., Wang, B., Lu, G., Wang, Z., and Wu, W. (2010). AVR1-CO39 Is a Predominant Locus Governing the Broad Avirulence of Magnaporthe oryzae 2539 on Cultivated Rice (Oryza sativa L.). Molecular Plant-Microbe Interactions® 24, 13-17.

Zhu, M., Jiang, L., Bai, B., Zhao, W., Chen, X., Li, J., Liu, Y., Chen, Z., Wang, B., Wang, C., Wu, Q., Shen, Q., Dinesh-Kumar, S.P., and Tao, X. (2017). The Intracellular Immune Receptor Sw-5b Confers Broad-Spectrum Resistance to Tospoviruses through Recognition of a Conserved 21-Amino Acid Viral Effector Epitope. The Plant Cell 29, 2214-2232.

Zimin, A.V., Marçais, G., Puiu, D., Roberts, M., Salzberg, S.L., and Yorke, J.A. (2013). The MaSuRCA genome assembler. Bioinformatics 29, 2669-2677.

Zipfel, C. (2014). Plant pattern-recognition receptors. Trends Immunol. 35, 345-351.

Zipfel, C., Robatzek, S., Navarro, L., Oakeley, E.J., Jones, J.D.G., Felix, G., and Boller, T. (2004). Bacterial disease resistance in Arabidopsis through flagellin perception. Nature 428, 764-767.